Investigating a role for linker histone H1 in quiescent cells of *Saccharomyces cerevisiae*

A dissertation presented for the degree of Doctor of Philosophy, in the Faculty of Science, Trinity College Dublin by

Reham Hussain Al-Najjar

2024

Moyne Institute of Preventive Medicine

Department of Microbiology

School of Genetics and Microbiology

Trinity College Dublin

Declaration

I declare that this thesis has not been submitted as an exercise for a degree at this or any other university and it is entirely my own work, except where it is duly acknowledged in the text.

I agree to deposit this thesis in the University's open-access institutional repository or allow the library to do so on my behalf, subject to Irish Copyright Legislation and Trinity College Library conditions of use and acknowledgement.

I consent to the examiner retaining a copy of the thesis beyond the examining period, should they wish (EU GDPR May 2018).

Reham Al-Najjar

Summary

The aim of this study was to determine whether either Hho1p or Hmo1p can be considered the best candidate to function as linker histone H1 in *Saccharomyces cerevisiae*. The hypothesis was that yeast linker histone H1 would function to compact chromatin and repress gene transcription in the quiescent cell population that forms during yeast stationary phase. The *hho1*Δ and *hmo1*Δ deletion mutants were therefore characterised to understand the role of Hmo1p and Hho1p in chromatin function, cellular physiology, and transcription during quiescent cell development in stationary phase.

Initial analysis revealed that the *hho1*Δ mutant did not show many growth defects during exponential phase. On the other hand, the *hmo1*Δ mutant had a longer lag phase and entered stationary phase at a low cell density. Microscopy also revealed that the *hmo1*Δ mutant cells had an elongated cell morphology suggesting a role for Hmo1p in cell structure regulation. Stress response tests indicated that during exponential growth, while the *hho1*Δ mutant was more sensitive to both acetic acid and hydrogen peroxide, the *hmo1*Δ mutant had improved growth on acetic acid. Thus, both mutants displayed distinct phenotypes during exponential phase and in early stationary phase.

Chromatin sensitivity assays of exponentially growing cells showed an increase in micrococcal nuclease sensitivity in both mutants, pointing towards roles for both Hmo1p and Hho1p in chromatin compaction in actively growing cells. Interestingly, the level of phosphorylated H2A at serine 129 in the exponential *hho1*Δ mutant was higher than wt suggesting this mutant accrued greater DNA damage indicating a probable role for Hho1p in DNA repair. Neither deletion mutant had a large effect on thermotolerance of stationary phase cells. However, overexpression of both Hmo1p and Hho1p yielded cells in stationary phase with increased thermotolerance compared to wt, indicating a protective role for Hmo1p and Hho1p during stationary phase. Together, this supports a role for Hmo1p and Hho1p in influencing chromatin structure in exponential phase and stationary phase cells.

Analysis of the quiescent and non-quiescent cell populations formed in stationary phase wt, *hho1*Δ and *hmo1*Δ mutant cells showed aberrant cell development occurred in both mutants. Less quiescent (Q) cells were formed in the *hho1*Δ mutant, and these cells lost viability over time. Furthermore, the viability of the *hho1*Δ mutant non-quiescent (NQ) population increased over time. This suggests Hho1p has an anti-apoptotic effect in Q cells, and is pro-apoptotic in NQ cells.

In the *hmo1*Δ mutant, correct quiescent cell development was delayed with viability of the mutant Q cells taking longer to increase than that seen in wt. Similar to what was seen in *hho1*Δ, the viability of *hmo1*Δ NQ cells increased as stationary phase developed. Thus, both Hho1p and Hmo1p are important for correct Q and NQ cell development during stationary phase, but may play different roles in this process.

Global transcriptome analyses revealed different gene expression changes in *hho1*Δ and *hmo1*Δ mutants. *HHO1* did not influence transcription widely in exponential phase cells, although the influence of *HHO1* upon transcription increased during growth into SP. Gene repression by both *HMO1* and *HHO1* increased during quiescent cell development, and co-repression by *HMO1* and *HHO1* acting on the same genes also increased over time. However, the *hmo1*Δ mutant had the greatest defect in gene activation in quiescent cells suggesting the dominant role for Hmo1p in quiescent cells was to promote transcription as opposed to bringing about gene repression, as was the original hypothesis if Hmo1p acted as linker histone H1.

The analysis of global occupancy of Hho1p and Hmo1p revealed that occupancy by Hho1p increased as cells grew into stationary phase and showed that genome-wide Hho1p occupancy was greater than Hmo1p occupancy in quiescent cells. By correlating Hmo1p and Hho1p occupancy with the gene transcription changes in the respective mutants, the data showed that the number of genes directly repressed by Hmo1p and Hho1p increased during quiescent cell development. Although the genes subject to direct repression by Hmo1p and Hho1p were largely independent of each other, a few genes were subject to direct co-repression by both Hmo1p and Hho1p, with the greatest number of these directly co-repressed genes evident in quiescent cells.

Together, these data suggest Hmo1p and Hho1p have independent and overlapping roles in both the positive and negative regulation of gene transcription as quiescence develops. Thus, neither Hho1p of Hmo1p fulfilled our predicted role for linker histone in yeast which would be to definitively repress gene transcription and compact chromatin in the quiescent cell population. Instead, these data suggest that linker histone H1 function in yeast may be fulfilled by a combination of Hho1p and Hmo1p activity acting at all stages of yeast cell growth.

Acknowledgements

In the name of God, the Most Merciful, the Most Compassionate, I would like to thank my God ‘Allah’ for all of the blesses that he gave me. Sometimes a person cannot find appropriate words to express their gratitude to the wonderful people who have passed through their life, but I will try as much as I can to do so, as what my heart has is much greater than what is translated from my tongue.

I will begin by expressing my thanks and gratitude to my professor, supervisor, mentor, friend and leader, Prof. Alastair Fleming. This is a person whom I have never and will never do enough to thank as he has been there with me since the beginning of my Ph.D. journey and continues to be my support and motivation. He provided me with information, advice, and support. He thanked me and praised me when I succeeded, and he was patient and guided me when I made mistakes. If he sees me sad, he consoles me, and if he sees me happy, he smiles and rejoices at my happiness. His expertise and dedication were pivotal in shaping this work and helping me navigate the challenges along the way.

I would also thank the wonderful Dr. Karsten Hokamp, Dr. Yousif Gusti, and Dr. Suliman Gedair for helping me with analyzing the data and providing useful advice and guidance. there assistance was instrumental in the completion of my experiments and data analysis, and they did not refuse any request related to my project, even when they was very busy.

I would also like to thank the members of my thesis committee, Dr. Carsten Kröger, Dr. Gary Moran, Dr. Kim Roberts, and Dr. Ursula Bond, for their constructive criticism and suggestions, which greatly enhanced the quality during the last four years of my research. Thanks also to the Head of Department, Dr. Marta Martins, for all her support.

Special thanks to the wonderful to the Moyne departmental office and technical staff Dr.Ciaran, Jayne, Noreen, Connie, Dee, Meriam, Stephen, Ronan, Dave, and Margaret. A huge thank you, to those who contributed so much to the smooth running of the department, and who were always happy to support and help me with anything I needed and high-quality services to keep everything organized.

I Also, thank you to the Biology Teaching Centre Dr. Audrey Carroll and Dr. Glynis Robinson and all staff for their advice, support and help in the teaching lab, which gave me more experience in my future work.

Thanks to all Fleming lab members past and recent, for their help throughout this work in the lab. My sincere thanks go to Microbiology department current and past members of the Moyne Institute. Thank you to my friends Dr. Ali Bakheet, Kevin Mercurio, Zain Baazeem, and Pranay Agarwal who always make me feel like we are one family.

There is a person I always called my best friend in Dublin, Dr. Ghayah Al-Sulaim, whose encouragement and advice had a profound impact on my work on this journey. We shared many moments of joy and fun outside and inside home in Dublin. Thank you, my best friend.

On my personal life, I am eternally grateful to my family, particularly my parents, my father Hussain Al-Najjar, (passed away), may ALLAH be merciful, and my mother Sabah Al-Najjar for all their support and love. You are the reason that keeps me always pushing to be the best. Thank you for having my back since the day I was born until now.

Thank you my Mam Sabah for your prayers, which kept me safe and successful. Saying ‘thank you’ will never be enough to repay a fraction of what you have done, and still do for me, and who encouraged me to continue my studies in Canada when my father was in hospital. When I heard my father passed away she supported me and my sisters and brothers. When I felt sad to not see him again, she encouraged me to come to Dublin to continue my dad’s dream to get a Ph.D. despite my insistence on staying by her side to take care of her. Thank you, mam, you are a great woman.

My dad Hussain who passed away in 2015, may ALLAH be merciful, before I began my Ph.D. journey and he could not see me earn my doctorate, a dream he wished me to achieve. he always encouraged me to continue my studies and supported me with hir prayers. And he was help me some support and strong words when I had problem in master’s degree. I still feel like you are here by my side. Now, I am fulfilling that dream he eagerly awaited. I had hoped for his presence on this significant day. Thank you, dad, you great man. May ALLAH be merciful on you, the most precious person in my life.

Thank you to my sisters Roaa, Rasha, Reem, Rana, and our little one Raneem, and my brothers Raid, Ahmad, Abdulrahman, for their unwavering support, love, and patience. You gave me endless and unconditional love. Your belief in me has been my greatest strength. Thank you my brothers Abdulrahman, and Ahmad my Partners in crime throughout my postgraduate journey since Canada, Victoria and Ireland, Dublin. You are my soulmate.

Final part from my family, I also thank my nieces, nephews, and their spouses Ibrahem, Abdulaziz, Hoor, Seba, Yosef, Mohammed, Nouf, and Almaha for your love, kindness, and support always.

Big thanks to acknowledgements my special friends, Mariam Al-Mutairi, and Muhannad Al-Rasheed, your camaraderie and intellectual discussions were a constant source of inspiration motivation and personal growth. Thank you for being there during the highs and lows of this journey. When I always said ‘I don’t need to complete my PhD and cry’ you have encouraged and believed me I can do it. ‘Thank you very much’

I would like to thank the Education Ministry High in Saudi Arabia for their financial support, which enabled me to pursue this research without financial burden and made my dream possible. Also, thank all the members of the Royal Embassy of Saudi Arabia in Dublin, headed by the Saudi Ambassador, Dr. Nail Al-Jubeir, and I thank the Saudi Cultural bureau in Dublin and all its members.

Lastly, thank you all my friends in my life and this thesis reflects the collective support of many remarkable individuals, I deeply appreciate everyone who supported me throughout this journey.

Dedication

This thesis is dedicated to:

My parents: my late father, Hussain Al-Najjar, whom I will pray for always, and my mother, Sabah Al-Najjar, may Allah keep her safe.

My sisters: Roaa, Rasha, Reem, Rana, and our little one Raneem, and my brothers: Raid, Ahmad, Abdulrahman and their children and spouses.

My special friends: Muhannad Al-Rasheed.

My supervisor: Prof. Alastair Fleming.

Conferences

1. Al-Najjar RH. and Fleming AB. 2021, (June 22nd). Attended the IFS (Irish Fungal Society) Annual Conference (Virtual).
2. Al-Najjar RH. and Fleming AB. 2022, (December 8th). Investigating the roles of Hho1p and Hmo1p during the stationary phase in *Saccharomyces cerevisiae.* Poster presentation SGM Xmas social at the Atrium of the Smurfit Institute of Genetics at Trinity College Dublin (TCD) in Ireland.
3. Al-Najjar RH. and Fleming AB. 2023, (April 17th – 20th). Investigating the roles of Hho1p and Hmo1p during the stationary phase in *Saccharomyces cerevisiae.* Poster presentation at Microbiology Society Annual Conference 2023 at the International Convention Centre (ICC) in Birmingham, UK.
4. Al-Najjar RH. and Fleming AB. 2023, (June 1st). Investigating the roles of Hho1p and Hmo1p during the stationary phase in *Saccharomyces cerevisiae.* Poster Presentation and Oral flash talk at DAPI at University College Dublin (UCD) in Ireland.
5. Al-Najjar RH. and Fleming AB. 2023, (June 22nd). Investigating the roles of Hho1p and Hmo1p during the stationary phase in *Saccharomyces cerevisiae.* Poster Presentation at the IFS (Irish Fungal Society) Annual Conference at Dublin College University (DCU) in Ireland.
6. Al-Najjar RH. and Fleming AB. 2023, (August 20th – 25th). Investigating the roles of Hho1p and Hmo1p during the stationary phase in *Saccharomyces cerevisiae.* Poster presentation at ICYGMB 31 (International Conference on Yeast Genetic and Molecular Biology) at the Innovation Centre in Florence, Italy.
7. Al-Najjar RH. and Fleming AB. 2024, (June 19th – 20th). Investigating the roles of Hho1p and Hmo1p during the stationary phase in *Saccharomyces cerevisiae.* Poster Presentation at the IFS (Irish Fungal Society) Annual Conference at the School of Biological Sciences at Queen's University Belfast, UK.

Table of Contents

List of Tables

Index of Figures

Chapter 1

Introduction

1.1 Chromatin

Saccharomyces cerevisiae, also known as baker's yeast, has been widely used for genetic research since the mid-twentieth century. Investigation of gene regulation in this organism has greatly helped our understanding of the mechanisms of eukaryotic cell function. The experimental value of this single-celled eukaryote organism rests in its simple life cycle, short generation time and the ease by which it can be genetically modified (Johnston, 1987; Mell and Burgess, 2001).

Within the eukaryotic cell, DNA is tightly associated with proteins to form a structure called chromatin. The fundamental subunit of chromatin is the nucleosome consisting of two each of the core histone proteins, H2A, H2B, H3 and H4, around which is wrapped 146bp of DNA (Fig 1.1A) (Andrews and Luger, 2011). This basic structure then repeats and folds upon itself to package the eukaryotic DNA genome within the confines of the nucleus. The DNA connecting nucleosomes can be associated with the 'linker' histone H1, which can act to further compact DNA within the nucleus (Fig. 1.1B).

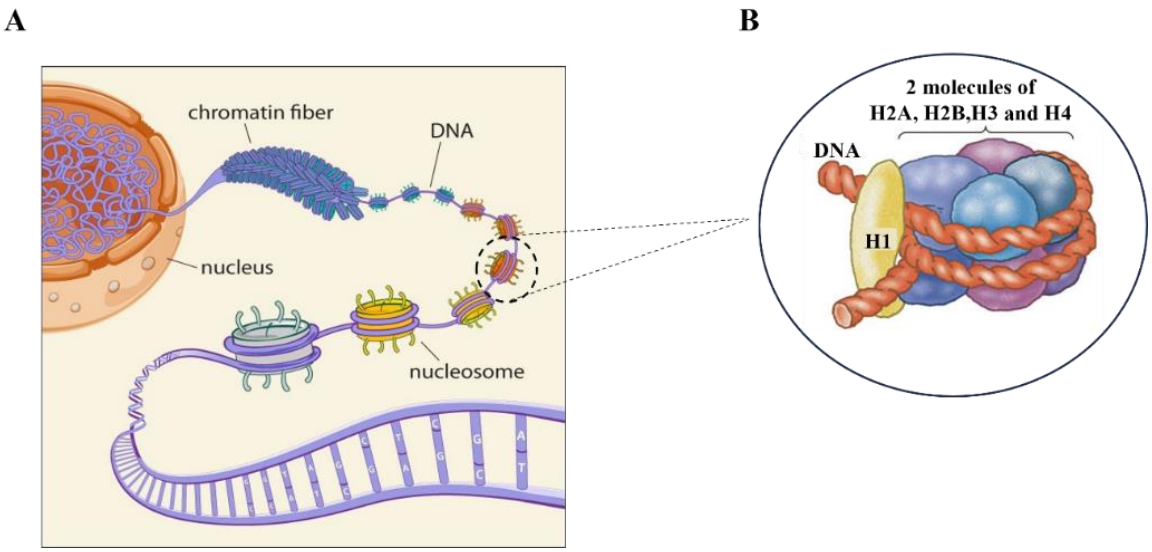

Figure 1.1: Diagram depicting chromatin-organized DNA. (A) Shows nucleosomes, each consisting of two copies of the core histone proteins H3, H4, H2A and H2B and DNA, and the N-terminal histone tails. **(B)** Demonstrates that the DNA linker region connecting nucleosomes is where histone H1 binds to form the chromatosome and further compacts DNA within the nucleus. This figure was adapted from (Baker, 2011).

1.2 The core histones

The four core histones making up the nucleosome octamer are known as H2A, H2B, H3 and H4 (Table 1.1). They all share the same fundamental structure comprising a structured globular domain and a flexible N-terminal tail. Studies have shown that the core histones are well conserved in all the eukaryotes (Baxevanis and Landsman, 1998). Together, these small, basic histones combine into an octamer of a single (H3-H4)2 tetramer and two H2A-H2B dimers. There are approximately fourteen regions of contact with the histone proteins and DNA causing the nucleosome to form a very stable DNA-protein complex (Luger *et al.*, 1997).

Histone Protein	Size (Mol. weight)/kDa
H2A	15.3
H2B	14
H3	15.3
H4	11.3

Table 1.1: The core histone proteins. The table lists the four core histone proteins, H2A, H2B, H3 and H4, and gives their size (in kDa).

1.2.1 The linker histone binds to the nucleosome

Histone H1, also known as 'linker histone' binds to the DNA linker region where the DNA enters and exits the nucleosome (the dyad) (Fig. 1.2) (An *et al.*, 1998; Sivolob & Prunell, 2003; Syed *et al.*, 2010; Bednar *et al.*, 2016). Unlike core histones, which are stable components of the nucleosome, linker histones are mobile, with residence times measured in minutes (Lever *et al.*, 2000; Misteli *et al.*, 2000; Flanagan & Brown, 2016). In mammalian cells, H1 has an average stoichiometry of about 0.8 molecules per nucleosome, with variations depending on the type of cell (Woodcock *et al.*, 2006). Histone H1 interacts with about 20bp of DNA to form the chromatosome consisting of ~167bp of DNA, the core histone octamer, and one molecule of H1(Allan *et al.*, 1980) (Fig. 1.2).

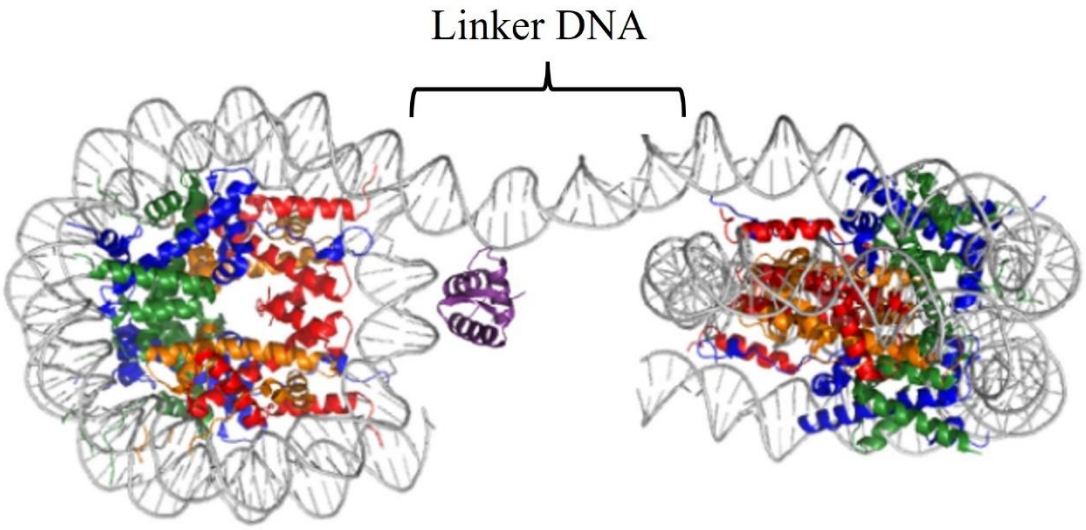

Figure 1.2: Histone H1 is associated with the DNA linker and the nucleosome to form the 'chromosome'. The globular domain of histone H1 (purple) binds the nucleosome at the dyad. This figure was derived from (Zhou *et al.*, 2015).

1.3 Histone H1 in yeast

Linker histones are the most disparate class of histone proteins (Kasinsky *et al.*, 2001). For example, while the sequence of the core histone H4 is 92 per cent identical between yeasts and humans, the degree of sequence identity between human H1 and the proposed yeast linker histone called Hho1p is only 31 per cent. In addition, whereas yeast only has Hho1p, the majority of eukaryotes have multiple different H1 subtypes (Millán-Ariño *et al.*, 2016)**.** Histone H1 plays a role in stabilizing nucleosomes and maintaining higher-order chromatin structures, which control gene expression and cellular responses (Miloshev *et al.*, 2019).

Although the linker histone H1's structure and function are well characterized in higher eukaryotes, the yeast equivalent's identity and role remains controversial. It is commonly accepted that the yeast-linker histone H1 is encoded by the *HHO1* gene. The *HHO1* gene was identified by a scan of the yeast genome sequence for homologues of the conserved histone H1 globular domain (Landsman, 1996; Ushinsky *et al.*, 1997). However, the yeast Hho1p protein's structure is distinct from the canonical linker histone H1 (Fig. 1.3), and its role in yeast has proved elusive. Indeed, the deletion of *HHO1* in vegetatively growing yeast shows no striking phenotype (Patterton *et al.*, 1998). However, it has been proposed to operate during the stationary phase of yeast, where it may promote chromatin compaction and contribute to DNA damage repair (Schäfer *et al.*, 2008). Disrupting *HHO1* leads to chromatin structure changes in replicatively old yeast cells, further indicating it does have a role in chromatin structure and function (Uzunova *et al.*, 2013).

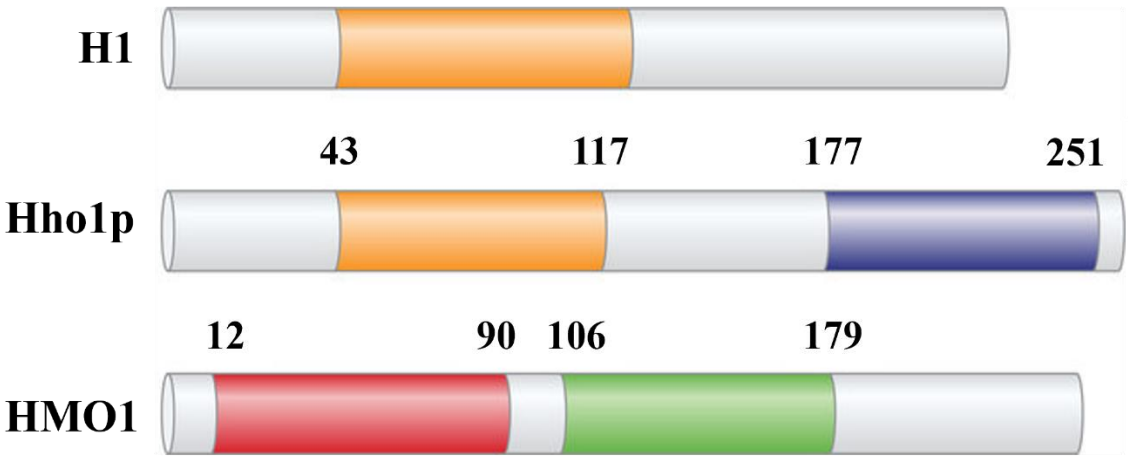

Figure 1.3: Metazoan H1 and yeast Hho1p, and Hmo1p domain organization. Metazoan H1 typically contains a N-terminal extension of 40-amino-acids followed by a globular domain of 80 amino acids (orange) and a long CTD characterized by S / TPXK-like repetitions. Yeast Hho1p contains a lysine-rich N-terminal segment followed by a globular domain similar to that of H1 (orange). Another lysine-rich section links this planetary domain to the second (purple) globular domain. Yeast Hmo1p consists of box A (red), which has little resemblance to HMG consensual domains, followed by a lysine-rich linker, box B (green) domain, and a lysine-rich CTD. This figure was adapted from (Panday and Grove, 2017).

1.4 High-mobility group box protein (HMGB)

Recently, another candidate has been identified that may function as the yeast H1 protein called Hmo1p. Hmo1p is an abundant high mobility group box (HMGB) protein (Ghaemmaghami *et al.*, 2003; Kulak *et al.*, 2014). Hmo1p has two globular domains of around 80 amino acids each, called box A and box B (Fig. 1.3), and is thus more like its mammalian H1 counterpart in structure. Box A has a low DNA binding affinity but exhibits preferable binding to four-way junction DNA. Box B has a higher DNA affinity but a lower structural specificity (Kamau *et al.*, 2004; Albert *et al.*, 2013). Hmo1p has a C-terminal domain that is distinguished by a stretch of essential amino acids in addition to the A and B domains (Bauerle *et al.*, 2006; Xiao *et al.*, 2010). *HMO1* gene deletion is not lethal, however deletion results in significant growth defects and decreased plasmid stability (Ray & Grove, 2009; Xiao *et al.*, 2011).

In the nucleolus, the 25 kDa Hmo1p accumulates on ribosomal RNA genes (Kamau *et al.*, 2004; Albert *et al.*, 2013). Maintenance of a novel chromatin structure at this site (Lu *et al.*, 1996; Bermejo *et al.*, 2009) and facilitation of ribosomal RNA transcription are *in vivo* roles of Hmo1p (Gadal *et al.*, 2002). HMGB proteins like Hmo1p have been shown to have binding sites that overlap with H1, potentially resulting in mutually exclusive associations with DNA entry/exit points on the nucleosome (Thomas & Stott, 2012; Nalabothula *et al.*, 2014). Like H1, HMGB proteins bend DNA (Lee & Thomas, 2000; Watson *et al.*, 2014). It has also been stated that the C-terminal extension of HMGB proteins interact specifically with the H3 histone N-terminal tail (Ueda *et al.*, 2004).

Although there are some indications that Hmo1p could function as a linker histone in yeast, little research has been carried out to confirm whether Hmo1p could be the yeast functional equivalent of the mammalian H1 protein or whether it functions together with Hho1p.

1.5 Chromatin Remodelling

Although chromatin is generally considered to be repressive to processes like transcription, this repressive structure can be altered or 'remodelled' by **(i)** post-translational modifications to the histone proteins, and **(ii)** ATP-dependent chromatin remodelling complexes. Each of these processes can alter chromatin structure and function to switch genes on or off.

(i) Histone post-translational modifications (PTMs)

Histone post-translational modifications (PTMs) play a crucial role in regulating chromatin structure and gene expression in eukaryotic organisms. *S. cerevisiae* has been extensively studied to understand the molecular mechanisms of action of histone PTMs. Indeed, many of the histone modifications and the enzymes responsible for their regulation were first identified from studies in yeast.

The N-terminal tails of the core histones protrude from the nucleosomes and are subject to many of the various chemical modifications, such as acetylation, methylation, phosphorylation, ubiquitination, and sumoylation (Fig. 1.4) (Oliveira and Sauer, 2012; Jezek *et al.*, 2017; Separovich and Wilkins, 2021). These modifications dynamically regulate chromatin compaction and accessibility, influencing gene transcription, DNA repair, and replication (Oliveira and Sauer, 2012; Jezek *et al.*, 2017; Separovich and Wilkins, 2021).

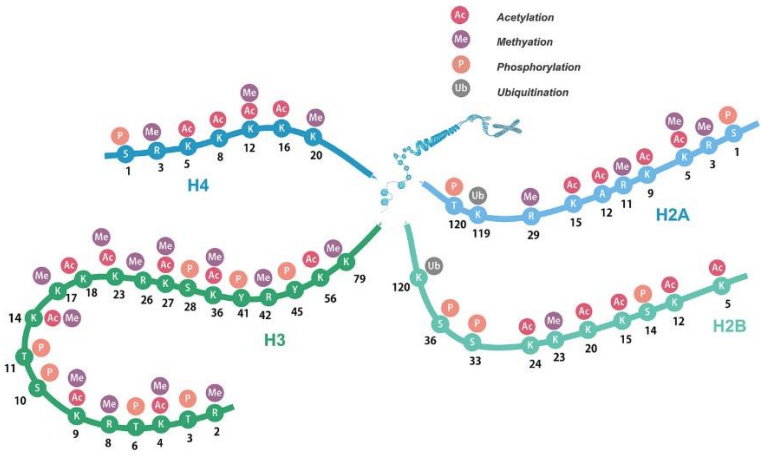

Figure 1.4: Schematic showing examples of various histone PTMs, including acetylation (Ac), phosphorylation (P), methylation (Me), and ubiquitylation (Ub) of the core histone proteins indicated. This figure was adapted from (Liu *et al.*, 2023).

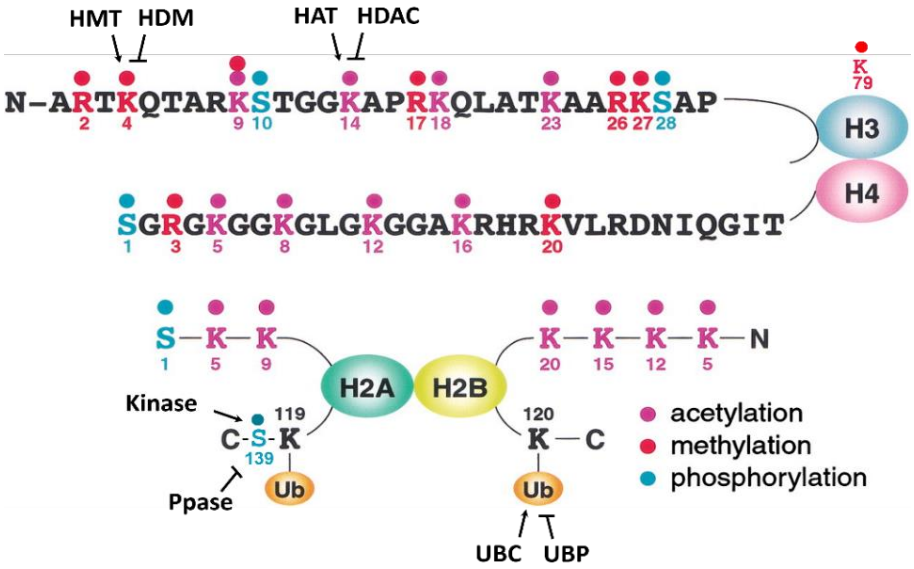

Figure 1.5: Schematic showing regulation of histone post-translational modifications. The modifications shown include acetylation (purple), methylation (red), phosphorylation (green), and ubiquitination (orange). Most of these PTMs are dynamic; there is machinery such as histone acetyltransferases (HATs), methyltransferases (HMTs), and ubiquitin conjugating enzymes (UBCs) to add these marks. Other enzymes can remove them such as histone demethylases (HDMs), histone deacetylases (HDACs), phosphatases (Ppases) and ubiquitin proteases (UBPs). This figure was adapted from (Zhang and Reinberg, 2001).

1. Histone Acetylation

Histone acetylation of lysine (K) residues, catalyzed by histone acetyltransferases (HATs) and reversed by histone deacetylases (HDACs), is a well-studied modification associated with transcriptional activation in *S. cerevisiae* (Kuo *et al.*, 1996) (Fig. 1.5). The HATs Gcn5p and Esa1p are known to acetylate histones H3 and H4, and this modification is associated with promoting gene expression by relaxing chromatin structure (Suka *et al.*, 2002).

2. Histone Methylation

Histone methylation (me) occurs on lysine (K) and arginine (R) residues and can lead to both transcriptional activation and repression in *S. cerevisiae*. The three best characterised sites of histone methylation in yeast are methylation of histone H3 at lysine's 4, 36 and 79 (H3K4me, H3K36me, and H3K79me, respectively). These modifications are added by *SET1*, *SET2* and *DOT1* respectively. Significantly, each site can be mono-, di-, or trimethylated, with each type of modification potentially having a unique role. Cells use enzymes to regulate these methylation states: lysine methyltransferases (KMTs) add methyl groups, while lysine demethylases (KDMs), such as Jhd1, remove them from specific lysine residues on histone H3 (Shilatifard, 2006). The role of histone methylation can be diverse. However, a well characterised role for H3K36me has been shown to be required for nucleosome reassembly after RNA polymerase II elongation across gene coding regions whereby it promotes subsequent histone deacetylation. Thus, although this modification correlates with actively transcribed regions, its role is arguably repressive (Venkatesh and Workman, 2015).

3. Histone Phosphorylation

Histone phosphorylation, regulated by various kinases and phosphatases, occurs on serine and threonine residues and is crucial for chromatin dynamics and gene expression in *S. cerevisiae*. For example, phosphorylation of histone H3 serine 10 (H3S10) by the cyclin-dependent kinase Cdk1 is involved in mitotic chromosome condensation and gene activation (Hsu *et al.*, 2000).

4. Histone Ubiquitination and Sumoylation

Histone ubiquitination and sumoylation are reversible modifications that regulate chromatin structure and transcriptional activity in *S. cerevisiae*. The E3 ubiquitin ligase Bre1p and the E2 conjugating enzyme, Rad6p, mediates histone H2B ubiquitination at lysine 123 in the C-terminal tail (Henry *et al.*, 2003).

This modification is associated with transcriptional elongation and DNA repair processes (Fleming *et al.*, 2008; Li *et al.*, 2008). Similarly, sumoylation of histones by the SUMO ligase Siz1 influences transcriptional repression and DNA damage response pathways (Nathan *et al.*, 2006).

These histone post-translational modifications are generally thought to function via the histone code hypothesis in which 'Writers', such as the HAT, Gcn5p, write the code, 'Readers', which are other non-chromatin proteins, then read the code to bring about an effect. Finally, 'Erasors', such as HDACs, remove the code, to set the default chromatin state (Jenuwein and Allis, 2001).

(ii) ATP-dependent chromatin remodelling

The first example of an ATP-dependent chromatin remodelling complex was the Swi-Snf complex which was discovered in *Saccharomyces cerevisiae* (Becker and Hörz, 2002; Mohrmann and Verrijzer, 2005). Subsequent work showed that the yeast Swi-Snf complex was evolutionary conserved from yeasts to human cells (Wang *et al.*, 1996). This complex can slide, disassemble, or even evict nucleosomes in an ATP-dependent manner thereby 'opening' up access to the underlying DNA for the transcription machinery to enable gene transcription. The Swi-Snf complex consists of 12 subunits, each with a unique role. These complexes can have abnormalities in human cells and mutants of this complex are believed to be responsible for approximately 25% of all human cancers (Roberts and Orkin, 2004). Other ATP-dependent remodelling complexes in yeast are INO80 and RSC (Clapier *et al.*, 2017).

1.6 Gene transcription

Once the yeast is optimally growing it has the potential to synthesize up to 13,000 proteins per second (von der Haar, 2008; Dever *et al.*, 2016). A key stage in this process is gene transcription initiation, wherein RNA polymerase II (Pol II) starts the process of transcribing RNA from DNA (Fig. 1.6). This process involves Pol II binding to a specific region of the gene known as the promoter, often containing a TATA box, typically located within a nucleosome-free region (NFR) flanked by well-positioned nucleosomes referred to as -1 and +1 nucleosomes (Sekinger *et al.*, 2005). The initiation of transcription begins with the recognition of specific DNA sequences, known as promoters, by transcription factors (Fig. 1.1). Promoters typically contain core promoter elements, such as the TATA box, initiator (Inr), and downstream promoter element (DPE), which serve as binding sites for general transcription factors (GTFs). The assembly of the pre-initiation complex (PIC) at the promoter is facilitated by the sequential recruitment of GTFs, including TFIID, TFIIA, TFIIB, TFIIF, TFIIE, and TFIIH. TFIID, composed of the TATA-binding protein (TBP) and TBP-associated factors (TAFs), plays a central role in promoter recognition and serves as a scaffold for the assembly of other GTFs (Thomas and Chiang, 2006; Juven-Gershon and Kadonaga, 2010). In addition to the core promoter elements and GTFs, other gene-specific transcription factors can recruit co-activators like Mediator to facilitate PIC assembly (Spitz and Furlong, 2012; Allen and Taatjes, 2015).

Following pre-initiation complex (PIC) formation, RNA synthesis is initiated (Smolle and Workman, 2013). Subsequent to initiation, the transcription process progresses into elongation, during which RNA polymerase moves along the gene until transcription termination (Nechaev and Adelman, 2011). Following transcription, mRNA is transported from the nucleus to the cytoplasm, where it is translated into proteins (Dever *et al.*, 2016).

1.6.1 Chromatin structure and regulation of transcription

The accessibility of gene promoters to transcription factors and the transcriptional machinery is influenced by chromatin structure and histone modifications. Nucleosomes can occlude transcription factor binding sites and thereby block transcription initiation. As described previously, chromatin-modifying enzymes such as histone acetyltransferases (HATs), histone deacetylases (HDACs), histone methyltransferases (HMTs), and histone

demethylases (HDMs), regulate the post-translational modifications (PTMs) of histone proteins to regulate chromatin structure and function. Furthermore, remodelling complexes like Swi-Snf can remove nucleosomes at promoters. Thus, either way of altering chromatin structure, or both together, can make chromatin either permissive or repressive for transcriptional initiation (Kouzarides, 2007; Li *et al.*, 2007).

In summary, transcriptional initiation in eukaryotic cells is a tightly regulated process involving the coordinated interaction of promoter regulatory elements with gene-specific transcription factors, GTFs, and chromatin-modifying enzymes.

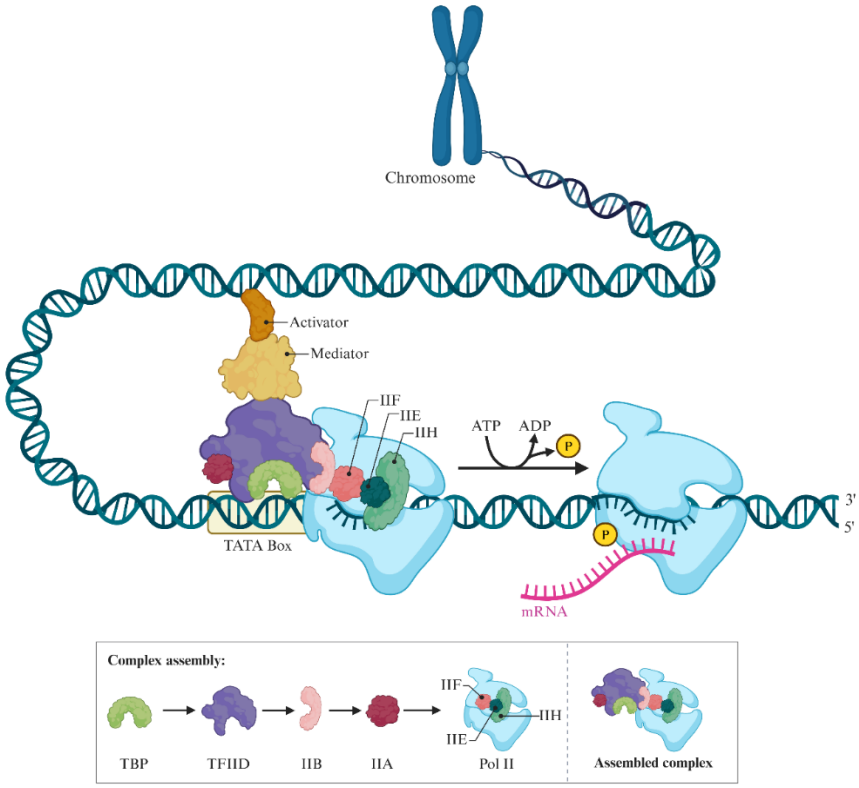

Figure 1.6: Eukaryotic Gene Regulation - Transcriptional Initiation. A depiction of the pre-initiation complex (PIC) structure reveals the positioning of RNA polymerase II (Pol II) along with general transcription factors (GTFs) such as TFIIA, TFIIB (C-terminal domain), the TBP subunit of TFIID, TFIIE, and TFIIK subunits Ssl2 (helicase module) and TFIIK (kinase module) at a TATA box within a gene promoter. The TATA box spans positions from -63 to -56 upstream of the transcription start site (TSS), while the dashed box indicates the transcription bubble formed upon initial promoter melting. This figure was created using BioRender.

1.7 Yeast Stationary Phase

Starvation is one of the most common stresses encountered by living organisms and it is estimated that most of the microorganism biomass on earth today exists in nutrient limiting environments (Herman, 2002). *S. cerevisiae* responds to nutrient starvation by ceasing growth and entering a non-proliferating state known as stationary phase (SP), which can be considered similar to mammalian G0. G0 is a unique phase during which cells exit the mitotic cell cycle following arrest at the G1 phase and become quiescent. Quiescence is a survival strategy during which transcription and translation are reduced to save energy. Importantly, quiescence is a reversible state as these cells can re-enter the cell cycle when nutrients become available.

During the growth of *S. cerevisiae* in glucose-based nutrient-rich media, several distinct phases are observed as the cells enter the stationary phase (Fig. 1.7). In the logarithmic phase of rapid growth, *S. cerevisiae* metabolizes glucose through fermentation. Once glucose is depleted, the cells temporarily cease growth and switch to respiration to derive energy from the previously produced ethanol. This transition from fermentation to respiration is known as the diauxic shift. The cells undergo a comprehensive transcriptional reprogramming during this shift to sustain growth, albeit at a slower pace. Upon depletion of all available carbon sources, yeast cells reach true stationary phase, typically between days 4-7 of growth. Additionally, yeast can also enter a G0-like phase or stationary phase when deprived of other essential nutrients such as nitrogen, phosphorous, and sulphur (Werner-Washburne *et al.*, 1993; Herman, 2002).

Little is known about the fate of chromatin during stationary phase except the long-established observation that chromosomes become condensed and there is an overall shutdown in transcription (Pi∼ non, 1978; Choder, 1991). Transcription rates have been shown to be 6-fold lower in SP when compared to actively growing cells, with global translation occurring at about 0.3% that of actively growing cells in the logarithmic phase of growth. Global studies have shown that while there is an overall reduction in transcription during SP, a subset of SP specific transcripts consisting of about 700 gene products or about 13% of the ORFs within the yeast genome remain active (Fuge *et al.*, 1994; van de Peppel *et al.*, 2003).

Furthermore, many histone PTMs associated with active transcription are retained in quiescent yeast cells despite the general shut down in transcription (Young *et al.*, 2017). The retention of these 'markers' of active transcription were proposed to poise the genome for rapid transcriptional reactivation upon nutrients becoming available in the environment.

Other characteristics associated with SP cells include the accumulation of the storage carbohydrates glycogen and trehalose, and an increased resistance to a variety of environmental stresses. Together, these changes increase the ability of yeast cells to survive extended periods of starvation (Herman, 2002; Gray *et al.*, 2004).

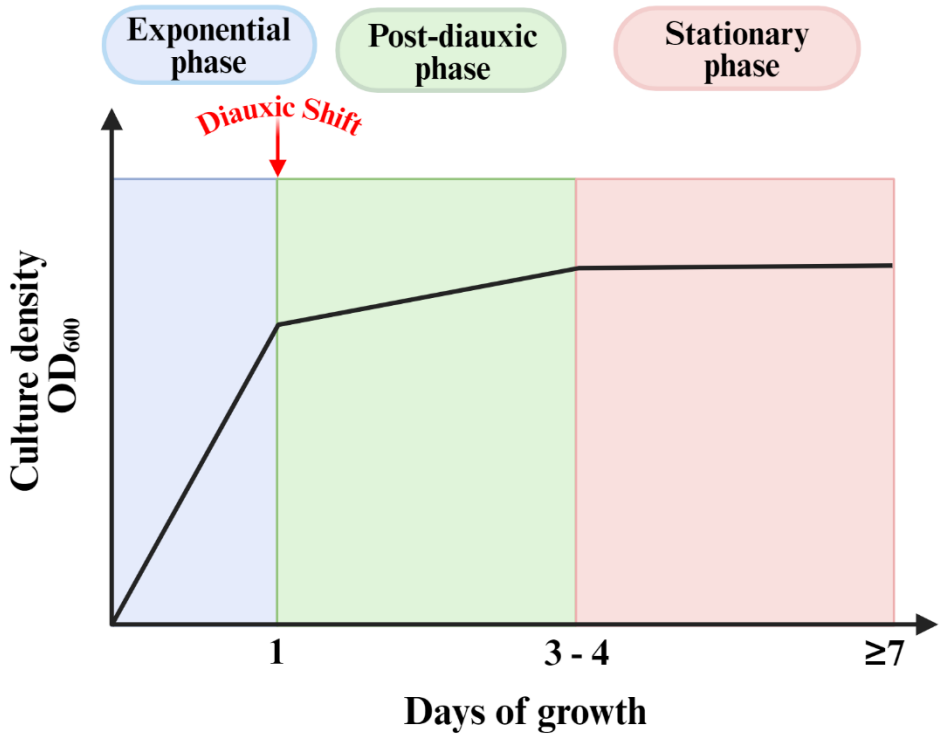

Figure 1.7: The transition to the stationary phase involves distinct growth phases. Initially, during the logarithmic phase characterized by rapid growth (depicted in light blue), yeast cells metabolize glucose through fermentation. Upon depletion of glucose, a global reprogramming event called the diauxic shift occurs, marking a shift to slower growth as yeast cells utilize fermentation by-products via respiration (shown in light green). Eventually, when all carbon sources in the media are depleted, cells arrest and enter true stationary phase (illustrated in light brown). Entry into stationary phase typically occurs after 4 to 7 days of growth. This figure was created using BioRender.

1.7.1 Yeast stationary phase cultures form two cell populations

Previous work has identified that *Saccharomyces cerevisiae* stationary-phase (SP) cultures comprise two cell populations (Allen *et al.*, 2006) (Fig. 1.8A). During yeast SP, the younger daughter cells form a quiescent (Q) cell population, whilst the older mother cells form a non-quiescent population (NQ) of cells that undergo apoptosis and necrosis. It is the quiescent cell population that will remain viable during SP, and it is these cells that will re-enter the cell cycle upon nutrient addition to the media.

Quiescence, or G0, is important in the growth and reproduction of all organisms, in addition to being the most frequent cell condition on earth (Kasinsky *et al.*, 2001; Gray *et al.*, 2004). Quiescent cells are also involved in the establishment and survival of infectious microbial diseases such as tuberculosis (Alexander & Perfect, 1997; Parrish *et al.*, 1998). Quiescence is important in complex eukaryotes for the survival of stem cells and plays an important role in diseases such as cancer (Suda *et al.*, 2005).

The yeast quiescent cells are characterised as having low metabolic activity and reduced transcription and translation, as well as being more resistant to various stresses. Importantly, the two cell populations in yeast SP can be separated by a Percoll-density gradient centrifugation process (Fig. 1.8B). This is because the two cell populations have different cell densities; the quiescent cells are denser than the non-quiescent cells. Evidence suggests that the difference in cell density is due to accumulation of trehalose in the (Q) cells which is used as a storage carbohydrate (Svenkrtova *et al.*, 2016).

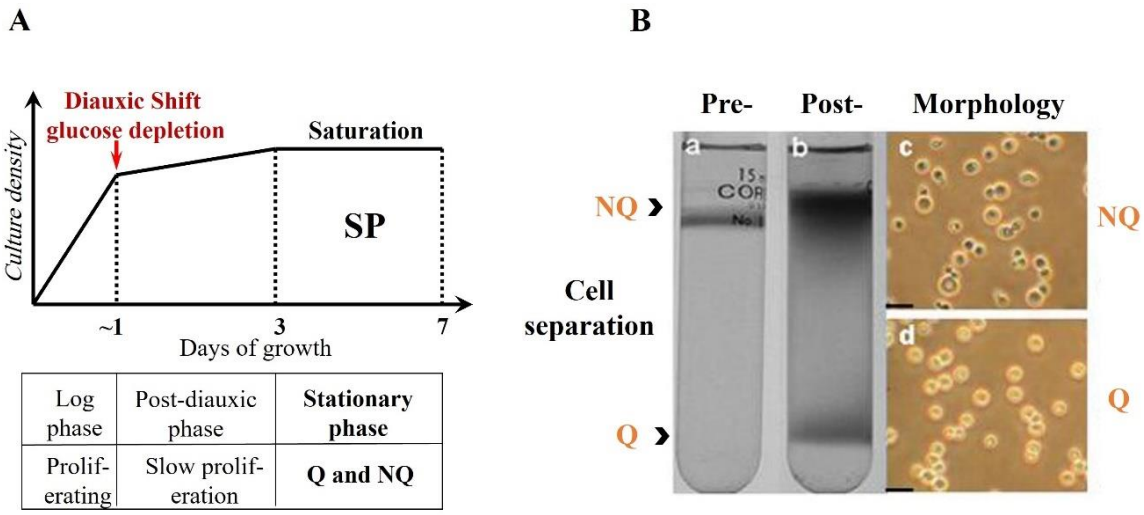

Figure 1.8: Diagram depicting growth of yeast into stationary phase (SP) and the cell separation technique to isolate quiescent (Q) and non-quiescent (NQ) cell populations. **(A)** Yeast growth events during entry into yeast stationary phase **(B)** Percoll density gradient centrifugation to separate (Q) and (NQ) cell populations from stationary phase cultures. Cells are shown pre- and post-centrifugation. Cell morphology is shown of the separated (Q) and (NQ) cells isolated after the density gradient centrifugation. This figure was adapted from (Allen *et al.*, 2006).

1.7.2 The transition to quiescence is highly regulated and is dependent on several steps

The study by (Allen *et al.*, 2006) described the isolation of two distinct populations from yeast SP cultures after separation by density centrifugation. The less-dense upper population of cells was heterogeneous and mostly made up of non-quiescent (NQ), budded mother cells. These NQ cells, although maintaining the ability to remain viable for a period of time, rapidly lost the ability to re-enter the cell cycle. In fact, after 14 days, many of these cells showed characteristic markers of apoptotic and necrotic cell death. The denser, lower population of cells was found to have characteristics of quiescent (Q) cells. This population was comprised mostly of unbudded daughter cells that retained viability and had the ability to synchronously re-enter the cell cycle upon glucose replenishment.

The quiescent (Q) daughter cells and the NQ mother cells were morphologically and physiologically distinct from each other. For example, the Q population had increased thermo-tolerance when compared to the NQ population, and increased levels of reactive oxygen species were detected in the NQ cells (Allen *et al.*, 2006). Initial models suggested that the cell division that occurred following glucose depletion led to production of Q and NQ cells (Allen *et al.*, 2006; Aragon *et al.*, 2008). However, follow-up studies have led to another model of Q and NQ cell formation. It has been suggested that cell-fate commitment occurs prior to glucose depletion and that Q cells are formed during an elongated cell cycle that occurs during the post diauxic phase of growth (Davidson *et al.*, 2011). Interestingly, another observation from this same study showed that the Q cells exhibit high rates of respiration. It had previously been suggested that Q cells were metabolically quiet, but this study proposed that decreased respiration might not always be characteristic of the quiescent state and, in fact, maintaining respiration may be necessary for survival of Q cells (Davidson *et al.*, 2011). Microarray analysis revealed more than 1300 mRNAs that distinguished Q cells from NQ cells. Transcripts specific to Q cells included mRNAs that encode proteins with a role in membrane maintenance, the oxidative stress response, and signal transduction. Many of the proteins encoded by these transcripts have roles in genome stability, whereas NQ cell-specific mRNAs encode proteins involved in Ty-element transposition and DNA recombination (Aragon *et al.*, 2008). Interestingly, Q cells were shown to contain nearly 2000 unique protease released transcripts, i.e., transcripts that were only released and detected upon addition of a protease step during the RNA extraction procedure. This

discovery, alongside that showing the retention of PTMs associated with active transcription, suggests that Q cells are poised to rapidly respond to environmental changes and may do so by maintaining large numbers of relevant mRNAs in processing bodies and stress granules (Giménez-Barcons and Díez, 2011; Shah *et al.*, 2013; Young *et al.*, 2017).

Several events have been implicated in controlling the development of the Q population of cells. It is thought that during the post diauxic cell division, the cells undergo asymmetric divisions and build protective cell walls around the daughter cells that become quiescent. These Q cells accumulate storage carbohydrates and contain abundant highly functional mitochondria that allow for long-term viability (Davidson *et al.*, 2011a). Many regulatory factors have been implicated in the successful transition to quiescence. Two recently published examples are the mRNA binding protein Ssd1p that plays a role in Q-cell wall assembly, and a global transcriptional repressor, Xbp1p, which represses genes involved in the regulation of cell growth, cell division and metabolism (Li *et al.*, 2008b; Miles *et al.*, 2013). Both of these regulatory events play a part in what seems to be the complex and highly regulated progression to quiescence. Overall, a tightly regulated programme of events that is not yet fully understood plays a role in the formation of the long-lived Q cells that maintain the ability to synchronously re-enter the cell cycle when a favourable environment returns.

1.8 Chromatin remodelling during yeast stationary phase

1.8.1 Changes in histone modifications

During the stationary phase, yeast cells undergo alterations in histone post-translational modifications (PTMs) that regulate chromatin structure and gene expression. Studies have shown a general reduction in histone acetylation patterns during the stationary phase, which contributes to the transcriptional regulation of genes involved in stress response and metabolic adaptation (Weinberger *et al.*, 2007; McKnight *et al.*, 2015). Most interestingly, quiescent cells have been shown to retain the PTM signature associated with actively growing cells despite the general shut-down in transcription in these cells (Young *et al.*, 2017).

1.8.2 Chromatin remodelling complex activity during stationary phase

Chromatin remodelling complexes, such as the SWI/SNF and INO80 complexes, play crucial roles in reorganizing chromatin structure during the stationary phase. These complexes are involved in ATP-dependent nucleosome remodelling, allowing access to transcription factors and RNA polymerase machinery for the activation of stress-responsive genes (Vinayachandran *et al.*, 2018). Interestingly, Hmo1p and Hho1p have been shown to interact with ATP-dependent chromatin remodelling complexes RSC, ISW1a, and SWI/SNF (Amigo *et al.*, 2022).

Furthermore, the Tup1-Cyc8 complex was also shown to be required for the repression of a particular set of genes upon glucose depletion, a condition that stimulates cells to enter a quiescent state. Upon glucose starvation, Tup1 relocates to new genomic targets associated with sugar transport and carbohydrate metabolism, maintaining this binding into the stationary phase. The absence of Tup1 results in the differential expression of thousands of genes, mostly those involved in nutrient transport and metabolism, and leads to abnormal cell morphology and multiple DAPI-stained nuclear puncta, indicative of mitotic irregularities. Furthermore, Tup1 interacts with chromatin-modifying complexes such as Rpd3L for histone deacetylation and Isw2 for nucleosome positioning, which are vital for maintaining repressed chromatin states during quiescence (Bailey *et al.*, 2022).

1.8.3 Histone Variant Deposition

The deposition of histone variants also contributes to chromatin remodelling during the stationary phase. For example, the incorporation of the histone variant H2A.Z into nucleosomes is regulated by the SWR1 complex and is associated with the activation of stress-responsive genes in yeast during the stationary phase (Kobor *et al.*, 2004).

1.9 The aim of this research

The aim of this project was to study the roles of Hho1p and Hmo1p in yeast cells to determine which, if any, is the yeast linker histone H1 equivalent. I will investigate the role of these two histone H1 candidates in exponential and separated quiescent cells isolated from yeast stationary phase cultures. I will test the hypothesis that yeast H1 functions specifically in the quiescent population of yeast cells formed during SP to repress transcription. If the hypothesis is correct, it will be predicted that gene transcription will be elevated in one or other of the mutant quiescent cell populations.

All previous investigations into yeast Hho1p function have been performed in unseparated SP cultures. Thus, the role of Hho1p in stationary phase may have been missed due to the 'noise' generated from the non-quiescent cell population undergoing apoptosis and necrosis. Furthermore, investigation into the role of Hmo1p during yeast stationary phase in separated quiescent cells has not been carried out at all.

Chapter 2

Materials & Methods

2.1 Yeast strains and growth conditions

Cells were cultivated using yeast extract peptone (YP) broth and agar {All Fore medium}. YP, broth was composed of 1% (w/v) yeast extract, 2% (w/v) peptone, and 2% (w/v) dextrose (glucose [D]). The cells were grown at 30°C with a shaking speed of 200g, unless otherwise specified. Overnight starter cultures were created by inoculating 10 ml of YPD with a single yeast colony. The next day, this culture was used to inoculate a larger volume of YPD. The culture was allowed to grow until the desired OD_{600} was reached, which was determined by a spectrophotometer. A volume of this starter culture was sub-inoculated into a greater volume of YPD broth and grown under the same conditions until the log phase was attained {Optical density between 0.6 - 0.8 nm on the spectrophotometer}. The experiment showed the presence of diauxic shift and stationary phase-specific quiescent cells.

The strains containing autotrophic markers were cultured in a synthetic complete (SC) medium. The SC medium was made by combining 0.19% yeast nitrogen base, 0.059% complete supplement medium, and 0.5% $[NH_4]_2SO_4$. In the case of solid media, 2% agar was added to the solution which was then autoclaved. Glucose was later added to the medium to achieve a final concentration of 2%. Finally, amino acids were included or excluded based on the requirement.

S. cerevisiae strains were in the BY4741 background and were obtained from the gene deletion library (Table 2.1).

Strain	Genotype	Source	comment
BY4741 (WT)	*Mata; his3Δ1; leu2Δ0; met15Δ0; ura3Δ0*	ResGen library	Background strainfor deletion mutants used in this study
*hho1*Δ	*Mata; his3Δ1; leu2Δ0; met15Δ0; ura3Δ0, hho1*Δ*::KAN*	ResGen library	Background strain for *hho1*Δ
*hmo1*Δ	*Mata; his3Δ1; leu2Δ0; met15Δ0; ura3Δ0, hmo1*Δ*::KAN*	ResGen library	Background strain for *hmo1*Δ
Y258 (WT)	*MATa pep4-3, his4-580, ura3-53, leu2-3,112* (pRS416)	This study	Over-expression strain (empty vector control)
pGAL-*HHO1*	*MATa pep4-3, his4-580, ura3-53, leu2-3,112* (BG1805-URA3: pGAL- *HHO1*)	Thermo Scientific	Over-expression strain
pGAL-*HMO1*	*MATa pep4-3, his4-580, ura3-53, leu2-3,112* (BG1805-URA3: pGAL- *HMO1*)	Thermo Scientific	Over-expression strain
Hho1-9myc	*Mata; his3Δ1; leu2Δ0; met15Δ0; ura3Δ0*; *HHO1*::HIS3-9myc	This study	9-myc tagging of Hho1p in BY4741 (wt)
Hmo1-9myc	*Mata; his3Δ1; leu2Δ0; met15Δ0; ura3Δ0*; *HMO1*::HIS3-9myc	This study	9-myc tagging of Hmo1p in BY4741 (wt)
Hho1-9myc	*Mata; his3Δ1; leu2Δ0; met15Δ0; ura3Δ0*; *hmo1*Δ::KAN, *HHO1*::HIS3-9myc	This study	9-myc tagging of Hho1p in *hmo1*Δ::KAN
Hmo1-9myc	*Mata; his3Δ1; leu2Δ0; met15Δ0; ura3Δ0*; *hho1*Δ::KAN, *HMO1*::HIS3-9myc	This study	9-myc tagging of Hmo1p in *hho1*Δ::KAN

Table 2.1: Yeast strains used in this research

2.2 Growth Curve and Final Cell Density

The YPD liquid medium was used for growing cells, and ThermoSpectronic {Genesys 10UV} was used to measure OD_{600}. The measurements were taken every 2 hours by combining a 90 µl sample with 10 µl H_2O. The final cell density was determined after 24 and 48 hours of growth in YPD using a haemocytometer.

2.3 Microscope images of the yeast cells

Cells were grown in YPD at 30°C overnight to the mid-log and stationary phases {day 7}. The cells were then washed with distilled water, and 10µl was spotted onto a glass slide. They were viewed using a Leica DM500 microscope at x100 magnification with an oil immersion lens. Photographs were taken using Leica Application Suite (LAS) software to capture the images, which were enlarged using Microsoft PowerPoint.

2.4 Growth 'Spot' Tests

Cultures were grown to the mid-exponential stage and stationary phase {day 7} and equal cell densities; $1x10^7$ cells/ ml were resuspended in YPD. The cultures were spotted in serial 10-fold dilutions and grown at 30°C unless otherwise stated. Cell sensitivity to cell wall damaging agents was verified by spot tests on YPD media containing the indicated concentrations of caffeine. The cultures were grown at different temperatures, 15°C, 30°C, and 37°C to verify sensitivity to temperature. Sensitivity to osmotic and oxidative stress was verified by spot tests on YPD media containing different concentrations of hydrogen peroxide (H_2O_2) and sodium chloride (NaCl). The cultures were grown at a non-fermentable carbon source, Acetic Acid.

2.5 Cell transformation (High-efficiency LiAc transformation)

Gene disruption and gene tagging were performed using PCR-mediated approaches with modified protocols. (Wach *et al.*, 1997; Longtine *et al.*, 1998). The transformation protocol was based on the high-efficiency protocol from (Gietz and Schiestl, 2007). The cells were cultured overnight in 10 ml culture and counted using a haemocytometer. A pre-warmed 50 ml culture of YPD was inoculated to a final cell density of ~$5x10^6$/ml. The cells were grown until a cell density of ~$2x10^7$ (~2 doubling) was reached. The cells were centrifuged for 5 minutes at 1500g, and the supernatant was discarded. The cells were resuspended in 25 ml of sterile water and centrifuged again for 5 minutes at 1500g. The supernatant was once again discarded, and the cells were resuspended in 1 ml of sterile 100 mM LiAc. This suspension was then transferred to a 1.5 ml microcentrifuge tube, and the cells were pelleted at top speed for 30 seconds before removing the LiAc.

The cells were then resuspended in 400µl of 100 mM LiAc, giving a final cell density of approximately ~$2x10^9$ cells/ml. This suspension was vortexed and divided into 50µl aliquots. The cells were pelleted, and a transformation mix was added to each cell pellet. The essential transformation mix consisted of 240µl PEG (50% w/v PEG 3350), 36µl 1M LiAc, and 25µl of 10 mg/ml single-stranded DNA from salmon testes (Sigma), which had been boiled for 5 minutes at 95°C and then placed on ice, and ~1 µg DNA. The mixture was made up to 360µl with sterile water and vortexed vigorously for 1 minute. The mix was incubated in a water bath at 42°C for 40 minutes. Cells were then centrifuged at 7000 g for 30 seconds, and the transformation mix was gently removed with a micropipette. The pellet was gently resuspended in 1 ml of sterile water. The cells were plated directly onto the relevant selective media for transformants using auxotrophic markers. When antibiotic markers were used, the cells were incubated in 5 ml of YPD and grown overnight at 30°C, 200g. The following day, the cells were centrifuged for 5 minutes at 453g, the supernatant was removed, and the cells were plated onto the selective media. The transformation was confirmed by PCR and western blot analysis where appropriate.

2.6 Chromosomal gene epitope tagging

Epitope tagging was performed as described by (Janke *et al.*, 2004). Epitope tag sequences were introduced into the C-terminal end of genes such that the resultant protein product contained nine copies of the myc epitope (E Q K L I S E E D L). For tagging Hho1p and Hmo1p, the nine myc-tag nucleotide sequence was first PCR amplified from the template plasmid pYM19 (Fig. 2.1). PCR primers were designed such that the resultant PCR products contained 46 bp overhangs complementary to the 24 bp immediately upstream of *HHO1* and *HMO1* stop codon at the 5' end, and the first 18 bp immediately downstream of the *HMO1* and *HHO1* stop codons (and including the stop codon) at the 3' end. PCR products were transformed into the appropriate yeast strain and introduced into the chromosome by homologous recombination.

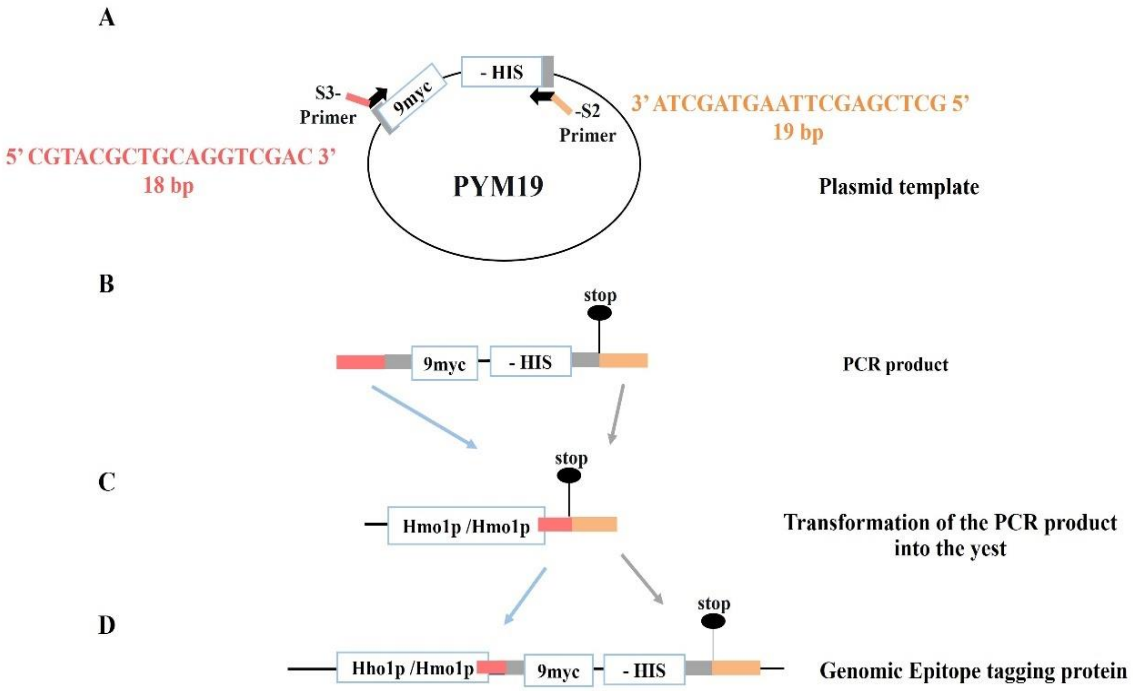

Figure 2.1: Overview of the epitope tagging process. (A) Plasmid pYM19, which contains the 9x myc epitope sequence and the -HIS resistance cassette, was used as template DNA for PCR **(B and C)** The sequences of primers contain regions homologous to pYM19 and the amplification yields a product with homology immediately upstream and downstream of the *HHO1* and *HMO1* stop codon (read and yellow boxes) **(D)** By taking advantage of homologous recombination pathways the PCR product is integrated into the genome resulting in an epitope-tagged *HHO1* and *HMO1* combined with a -HIS resistance cassette to allow for selection. Figure adapted from (Janke *et al.*, 2004).

Name	Sequence	comment
***ACT1*-F**	CTGAATTAACAATGGATTCTGG	Strain Confirmation
***ACT1*-R**	AGATACCTCTCTTGGATTGAGC	
Kan-B-F	CTGCAGCGAGGAGCCGTAAT	Strain Confirmation
Kan-B-R	TGATTTTGATGACGAGCGTAAT	
***HHO1* conA-F**	GTTTGCTTTGATGAAATGCTATTCT	Strain Confirmation
***HHO1* conD-R**	TCAGATTTTAAAGCCTTTTCTTCAA	
***HMO1* conA-F**	TATTACCCGACTCGATTATCTACCA	Strain Confirmation
***HMO1* conD-R**	TGTTTTGCTTCCTTCTTTTTCTCTA	
***HMO1*- S2**	TATTTATTTTAGAAAGACAGTAGAGTAAT AGTAACGAGTTTGT CGTC	Tagging Hmo1 with 9myc
***HMO1*- S3**	AGAAGAAGAAGAAGAAGGATAAGAAGAA GGACAAATCCAACTCTTCTA	
***HHO1*- S2**	GATAGTATTGCTATCACCATTGACATTCTC GTTTGGATATTCACTTTTTA	Tagging Hho1 with 9myc
***HHO1*- S3**	GCCCCTCCGGCATTATTAAACTAAACAAG AAGAAGGTCAAACTCTCCACG	
***TEL* VI-R 121 F**	CGTGTGTAGTGATCCGAACTCAGT	Control for ChIP qPCR
***TEL* VI-R 121 R**	GACCCAGTCCTCATTTCCATCAATAG	
***FLO1* RT-F**	TACCACCACAGACGGGTTCT	*FLO1* Transcription/ChIP
***FLO1* RT-R**	CAACAGTTGAACGCGGTTGC	
***PMA1* ORF-F**	GAAAAAGAATCTTTAGTCGTTAAGTTCGTT	Control for ChIP qPCR
***PMA1* ORF-R**	AATTGGACCGACGAAAAACATAA	

Table 2.2: Primers used in strain construction and confirmation in this study

Name	Selectable marker	Source	Comment
pYM19	HIS3	(Janke *et al.*, 2004)	Tagging template
pYM27	KanMX4	(Janke *et al.*, 2004)	Confirmation of *HHO1*/ *HMO1*:: KAN Mutant
pRS416	URA3	Fleming lab	Over-expression control
pRS413	HIS3	(Christianson *et al.*, 1992)	Transformation control

Table 2.3: Plasmids used in this study

2.7 DNA Extraction

The DNA extraction procedure started with centrifuging an overnight 10 ml cell culture at 1500g for 5 minutes. After discarding the supernatant, the cells were resuspended in 1 ml of water and transferred to a 1.5 ml microcentrifuge tube. Further pelleting was done by centrifugation at 6000g for 5 minutes, followed by discarding the supernatant. Next, the pellets were resuspended in 200µl of breaking buffer (containing 2% Triton X-100, 1% SDS, 100mM NaCl, 10mM Tris-Cl [pH8.0], 1mM EDTA [pH8.0]), and ~500µl of glass beads (400-600µm) {Sigma} were added. To the suspension, 200µl of phenol/chloroform/isoamyl alcohol was added and mixed by vortexing for 5 minutes. After that, 200µl of TE (pH 7.5) was added and briefly vortexed, followed by centrifugation at 13,400g for 5 minutes. The upper aqueous layer was transferred to a new 1.5ml microcentrifuge tube, and 400µl of chloroform was added. This was centrifuged at 14,600g for 5 minutes, and the upper layer was transferred to a new 1.5ml tube. For precipitation, 1 ml of 100% ethanol was added, and DNA was pelleted by centrifugation at 13,400g for 5 minutes. After discarding the supernatant, the pellet was resuspended in 500µl of 70% ethanol. The DNA was again pelleted by centrifugation, and the resulting pellet was dried and resuspended in 400µl of TE (pH 7.5), and 25 µg of RNase A was added. The mixture was incubated at 37°C for 1 hour, and then DNA was ethanol precipitated.

2.8 Ethanol Precipitation

To precipitate DNA, 0.3 volumes (30µl) of 4 M Lithium Chloride, 0.3 volume (30µl) of molecular water {nuclease-free} and 2 volumes of 100% ethanol were added. The mixture was stored at -20°C overnight or for 1 hour. The precipitated DNA was pelleted by centrifugation at 14,600g for 10 minutes, followed by resuspension in 1 ml 70 % ethanol. After further centrifugation at 14,600g for 10 minutes, the pellet was dried in a heat block at 37°C. The dried pellet was then resuspended in either nuclease-free water or TE buffer, pH 8.0, to the desired volume. Then add the tube in a heat block at 37°C for 2 min and stored at -20°C until next experiment.

2.9 End-point polymerase chain reaction (PCR)

PCR was carried out using the MyTaq HS {Bioline} DNA polymerase mix as per the manufacturer's instructions. The PCR reaction conditions included an initial denaturation step at 95°C for 1 minute, followed by 30 cycles of denaturation at 95°C for 15 seconds, annealing for 15 seconds, and extension at 72°C for 10 seconds. A final extension step was then conducted at 72°C for 2 minutes. The annealing temperature was determined based on the primers used.

2.10 Thermotolerance assay

As described in (Allen *et al.*, 2006) this assay has been performed with minor modifications. Cells were grown overnight in a 50 ml culture to mid-log phase (OD_{600} 0.6-0.8 nm) and stationary phase {day 7}. The cultures were counted using a haemocytometer and collected samples to a final cell density of ~ $4x10^7$ then placed in either two tubes. (each tube should contain $4x10^7$ cells). After that, incubate one tube at 30°C and the other tube at 52°C for 1 hour in a shaker and then add in ice for 10 min. For cell viability analysis, prepare a 10-fold serial dilution for each tube (30°C and 52°C). Spread 100µl of the 10^4x and 10^5x dilutions into YPD plates per sample and incubate at 30°C until colonies can be counted. The percentage of cells able to form colonies after incubation at 52°C was calculated relative to the number of colonies formed after incubation of the cells at 30°C (Fig. 2.2).

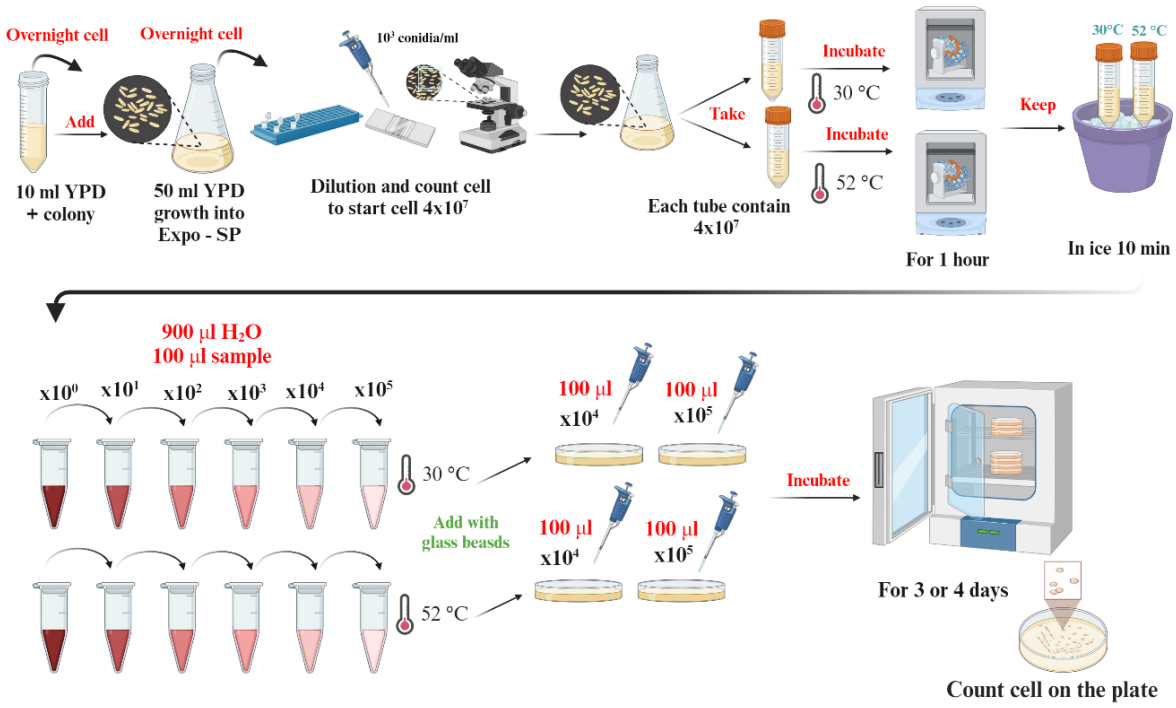

Figure 2.2: Schematic of thermotolerance assay. This figure was created using BioRender.

2.11 Fractionation of stationary phase {day 7} cultures

2.11.1 Preparation of Percoll density gradient

As described in (Allen *et al.*, 2006) fractionation of stationary phase cultures has been performed with minor modifications. To prepare a solution with a final NaCl concentration of 167mM, Percoll {GE Healthcare} was diluted 9:1 (v/v) with 1.5 M NaCl. To create density gradients, 15 ml of glass Corex tubes were filled with 10 ml of Percoll solution and centrifuged in a Sorvall centrifuge using an SS-34 rotor (10,500g for 15 min, 20°C). The density gradients were created beforehand and kept at 4 °C for up to 24 hours until needed.

2.11.2 Density gradient separation of yeast cultures

To fractionate the cultures, Centrifuge 6.5 ml of cells at 1500g for 5 minutes and remove the supernatant. Next, resuspended the cell pellets in 650µl of Tris buffer (50 mM Tris-Cl, pH 7.5) and carefully layered pre-made gradients drop-by-drop with the entire 650µl of resuspended cells. The gradients were centrifuged at 2000g for 60 minutes at 20°C, resulting in two distinct bands. Then, collected the upper fraction (non-quiescent cells, NQ) by gently pipetting some of the band (< 50 % per gradient) from two gradients to a 15 ml centrifuge tube. The cells were washed once in 5x volume Tris buffer and pelleted by centrifugation at 1500g for 5 minutes at 18°C. The number of cells recovered was measured by spectrophotometry and removed 10 OD_{600} unit samples for protein extraction, which we washed in 1 ml of 20% trichloroacetic acid (TCA) and stored at -80°C until required (Section 2.10.1). The lower fraction (quiescent, Q) was collected and washed in 5x volume Tris buffer and pelleted by centrifugation at 1500g for 5 minutes at 18°C. The pellet was resuspended in 350µl Tris buffer, loaded onto another gradient, and centrifuged as before to purify the lower band. After centrifugation, harvested the lower band and washed it in 5x volume Tris buffer. Then resuspended the cell pellet in 10 ml of Tris buffer and measured the optical density of the purified cells was.10 OD_{600} unit samples were taken for protein (Section 2.11.1) and RNA (Section 2.13.1), whereas 75 OD_{600} units of cells were immediately cross-linked for ChIP analysis (Section 2.15).

2.12 Western blot analysis

2.12.1 Protein Extraction

The 20% TCA Protocol (Szymanski and Kerscher, 2013) was adapted to extract protein. Cells were grown overnight in a 50 ml culture to mid-log phase (OD_{600} 0.6 - 0.8 nm), the diauxic shift (DX), and stationary-phase{day 7} specific quiescent cell (Q). A volume equivalent to 10 OD_{600} units was removed and centrifuged at 1500g for 5 minutes. After removing the supernatant, the cell pellet was resuspended in 1 ml of 20% trichloroacetic acid (TCA) and transferred to a 1.5 ml microcentrifuge tube. It was then centrifuged at 13,200g for 1 minute, and the supernatant was removed. The pellet was resuspended in 250µl 20% TCA, and ~500µl of glass beads (400 - 600µm) were added. The samples were vortexed for 30 seconds using a high-speed benchtop homogenizer and kept on ice for 1 minute, repeated thrice. The cell lysate was transferred to a 1.5 ml microcentrifuge tube.

The glass beads were washed using 500µl 5% TCA, and the wash was added to the cell lysate and kept on ice for 3 minutes. The cell lysate was centrifuged at 13,200g for 1 minute, and the supernatant was discarded. The pellet was resuspended in 300µl 1x Laemmli (0.1% 2-mercaptoethanol, 10% glycerol, 2% SDS & 63 mM unbuffered Tris-Cl) and incubated at 95°C for 5 minutes. After centrifuging for 1 minute at 13,200g, the supernatant was transferred to a new 1.5 ml microcentrifuge tube and stored at -20°C.

2.12.2 Bradford Assay

This method was used for protein quantification of cell lysates and was performed according to instructions provided by Sigma. Bovine Serum Albumin (BSA) standards, ranging from 1 to 10 µg/ml, and diluted protein samples in H_2O. Next, added the Bradford Reagent {Sigma} and measured the absorbance (A_{595}) with a spectrophotometer. By comparing the absorbance values to a standard curve, were able to calculate the protein concentration accurately. To ensure consistency, adjusted the protein sample concentrations to 2 mg/ml using 1x Laemmli buffer and stored them at -20°C.

2.12.3 SDS-Polyacrylamide gel electrophoresis (PAGE)

To prepare for protein examination, it's important to first clean the glass plates. Depending on the specific protein being analysed, 10 ml of either 10% or 15% (v/v) acrylamide-resolving gel solution should be made per gel. Assemble 1mm thick plates and clamp them tightly, then pour the gel solution between the plates until 1cm below the comb top when inserted. Immediately overlay the gel with 1 ml of isopropanol to allow for polymerization, and let it set for 20 minutes. Remove the isopropanol layer and prepare 10 ml of 5% (v/v) acrylamide stacking gel to be layered on top of the resolving gel. Immerse plastic combs containing 15 wells into the stacking gel and allow the gels to set before using them for SDS-PAGE. See the recipes below for details on the resolving and stacking gels:

15 % resolving gel (10 ml): 2.3 ml H_2O, 2.5 ml 1.5 M Tris-HCl (pH 8.8), 5 ml 30% acrylamide, 100µl 10 % (w/v) SDS, 100µl 10 % (w/v), ammonium persulfate (APS), 4µl TEMED.

10 % resolving gel (10 ml): 3.8 ml H_2O, 2.6 ml 1.5 M Tris-HCl (pH 8.8), 3.4 ml 30% acrylamide, 100µl 10 % (w/v) SDS, 100µl 10 % (w/v), ammonium persulfate (APS), 2µl TEMED.

Stacking gel (10 ml): 6.4 ml H_2O, 1.65 ml 1 M Tris-HCl (pH 6.8), 1.65 ml 30% acrylamide, 100µl 10 % (w/v) SDS, 100µl 10 % (w/v), ammonium persulfate (APS), 10µl TEMED.

For precise protein analysis, it is highly recommended to heat the protein for 5 minutes at 95°C before loading 40µg into each well. Additionally, to include the EZ-Run™ Prestained *Rec* Protein Ladder {Fisher} was loaded as a size reference sample. The gels should be run for 3 hours at 100V in running buffer (25 mM Tris, 190 mM glycine, 0.1% w/v SDS) to ensure optimal results.

2.12.4 Western Blot

In this study, the western blotting protocol was adapted from Current Protocols in Molecular Biology (Gallagher *et al.*, 2011). To transfer the protein to a polyvinylidene fluoride (PVDF) membrane {Immobilon}, a transfer buffer consisting of (25 mM Tris, 190 mM glycine, and 20% v/v methanol) was used. The transfer process was carried out at 300 mA for 90 minutes using Bio-Rad equipment {Mini trans-blot 153BR} surrounded by ice. Before use, the PVDF membrane was activated by soaking in 100% methanol for 20 seconds, followed by water for 2 minutes. Additionally, two sponges and four pieces of blotting paper were soaked in a transfer buffer. After transfer, the membrane was incubated in 20 ml of blocking buffer at room temperature for 1 hour to prevent non-specific binding of the primary antibody. The primary antibody was then added and incubated overnight at 4 °C to allow for specific binding to the target protein. The next day, the membrane was washed four times for 5 minutes in TBST (Tris-buffered saline, 0.05% Tween 20) to remove any unbound primary antibody. The secondary antibody was then added and incubated in 20 ml of blocking buffer at room temperature for 90 minutes or 2 hours to bind to the primary antibody. The membrane was washed once for 10 minutes in TBST and three times for 10 minutes in TBS {Sigma} to remove any unbound secondary antibodies. Finally, the bound antigens were visualized using image quant {LAS4000} imager after preparing the Enhanced chemiluminescent (ECL). Western blotting substrate {Pierce} according to the manufacturer's instructions.

N.B. For H3K79m^3 and H3H79m^2, I used similar steps above except the step for washes used Tris-buffered saline, 0.1% Tween 20.

The (table 2.4) below provides information on the antibodies used in the western blot analysis, including their dilution in the blocking buffer:

Marvel blocking buffer: 5 % (w/v) Marvel non-fat dry milk in TBS with 0.05 % Tween 20 (v/v).

BSA blocking buffer: 5 % bovine serum albumin (Sigma) (w/v) in TBS with 0.1 % Tween 20 (v/v).

Proteins	Concentration	Species	Source	Blocking buffer
β-actin	1:3000	Mouse	Abcam (8224)	5% Milk/TBST
Pol II-ser2	1:2000	Rabbit	Abcam (5095)	5% Milk/TBST
Pol II-ser5	1:1000	Rabbit	39750	5% Milk/TBST
Hho1	1:1000	Rabbit	Abcam (71833)	5% Milk/TBST
Gcn5	1:500	Rabbit	Santa Cruz (Sc-9078)	5% Milk/TBST
Had1	1:500	Rabbit	Santa Cruz (Sc-9077)	5% Milk/TBST
Cyc8 (Ssn6)	1:500	Goat	Santa Cruz (Sc-11955)	5% Milk/TBST
Snf5	1:1000	Rabbit	07-320	5% Milk/TBST
Snf2 -N	1:2000	Rabbit	J-Reese	5% Milk/TBST
Tup1	1:10,000	Rabbit	J-Reese	5% Milk/TBST
Anti-myc	1:5000	Mouse	Millipore (05-724)	5% Milk/TBST
H3	1:5000	Rabbit	39163	5% Milk/TBST
H4	1:1000	Rabbit	Abcam (7311)	5% Milk/TBST
H2A	1:3000	Rabbit	39236	5% Milk/TBST
H2B	1:2500	Rabbit	39239	5% Milk/TBST
H3K14ac	1:5000	Rabbit	07-353	5% Milk/TBST
$H4ac^4$	1:6000	Rabbit	06-866	5% Milk/TBST
$H3K4me^3$	1:3000	Rabbit	39-159	5% Milk/TBST
$H3K36me^3$	1:3000	Rabbit	Ab 9050	5% BSA/TBST
$H3K79me^2$	1:3000	Rabbit	04-835	5% BSATBST
$H3K79me^3$	1:10,000	Rabbit	Ab 2621	5% Milk/TBST
H2A.Z / HtZ1	1:1000	Rabbit	39648	5% Milk/TBST
H2A S129- phosphor	1:1000	Rabbit	39271	5% Milk/TBST
H3 S10- phosphor	1:5000	Rabbit	39253	5% Milk/TBST

Table 2.4: Antibodies used in western immunoblotting

2.13 RNA Protocols

2.13.1 RNA Extraction

RNA was extracted using the hot phenol method adapted from Current Protocols (Collart and Oliviero, 1993). First, 50 ml cultures were grown to the mid-exponential growth (OD_{600} 0.6 - 0.8 nm) phase of the diauxic shift (DX), and stationary-phase {day 7} specific quiescent cell (Q). A 50 ml sample was centrifuged for 5 minutes at 1500g. The pellet was resuspended into 1 ml of sterile water and transferred to a 1.5 ml tube. The cells were then pelleted by centrifugation. At this point, the cell pellets were either stored at -80°C or RNA was immediately extracted. The cell pellet was resuspended in 400µl TES (10 mM Tris-Cl pH=7.5, 10 mM EDTA pH=8, 0.5% w/v SDS) and 400µl saturated phenol to extract RNA. This was incubated at 65°C for 1 hr with occasional vortexing for 10-15 seconds. The sample was then placed on ice for 5 minutes and centrifuged for 5 minutes at 13,500g. The upper layer was transferred to a new 1.5 ml tube, and 400µl of saturated phenol was added. The sample was vortexed, kept on ice for 5 minutes, and then centrifuged for 5 minutes at 14,600g. The upper aqueous layer was transferred to a new 1.5 ml tube, and 400µl of chloroform was added, followed by centrifugation for 5 min at 14,600g. The upper aqueous layer was transferred to a new 1.5 ml tube, and 40µl of sodium acetate (4M, pH=5.3) was added, followed by 1 ml of ice-cold 100% v/v ethanol. This was kept at -20 °C for one hour and then centrifuged for 10 minutes at 14,600 g at 4°C. The pellet was then washed with ice-cold 70% v/v ethanol and centrifuged for 5 minutes at 14,600g at 4°C. Finally, the pellet was completely dried and then resuspended in nuclease-free water. The RNA concentration was quantified utilizing a Nano-drop ND-100 spectrophotometer {Thermo Scientific}, with measurements taken at an absorbance wavelength of 260nm.

2.13.2 RNA-Seq

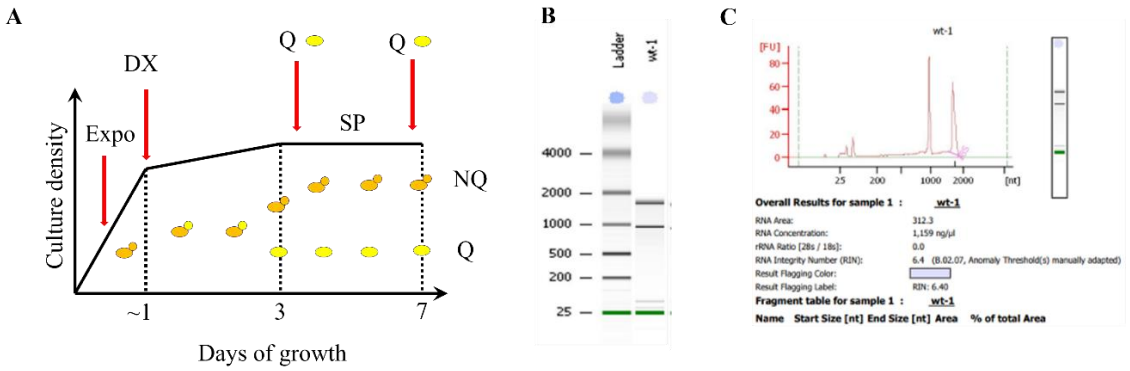

Figure 2.3: RNA sample preparation for RNA-Seq analysis. (A) Schematic to show times of RNA extraction at exponential phase (Expo), at the diauxic shift (DX), and in purified day 7 lower (Q) cells. **(B)** 1% Agarose formaldehyde gel showing the 28S and 18S rRNA bands from total RNA prepared from a representative wt sample (exponential phase) indicated. **(C)** Chromatogram of representative exponential wt sample showing RNA integrity (RIN) using RNA nano bioanalyzer 2100.

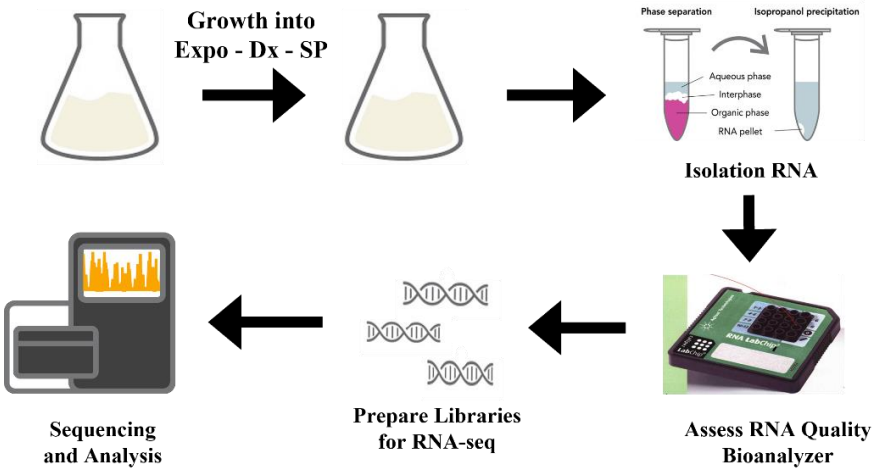

Figure 2.4: Schematic to illustrate the major steps in RNA-Sequencing. Yeast cells were grown to mid-log phase (Expo) of growth at the diauxic shift (DS), and in purified day 7 lower (Q) cells and total RNA was isolated, DNase treated and purified before being sent for sequencing. The RNA sequencing process involved depletion of ribosomal RNA (rRNA), fragmentation of RNA, and preparation of cDNA, which was subsequently sequenced. The bioinformatics analysis entailed mapping the reads to a reference genome, followed by differential gene expression (DGE) analysis. Figure adapted from (Carsten Kröger & Ali Bakheet, 2023).

To perform RNA-Seq, the total RNA was extracted as per the standard protocol. Next, DNase treatment and purification of the extracted RNA were carried out using the {RNeasy Minelute Cleanup Kit from Qiagen}, following the manufacturer's guidelines. The quality of the RNA was assessed using the {2100 Bioanalyzer system} before sequencing, which is illustrated in (Fig. 2.3C). The sequencing process involved three major steps: rRNA depletion, cDNA library preparation, and sequencing on the Illumina Platform. For analysing differential gene expression {DGE} for each RNA-Seq dataset, was carried out using the {DESeq2 Bioconductor} package in (Fig. 2.4). This package normalized the raw count reads using the median of ratios method for each sample. Calculated the fold change from these normalized counts and determined the Log2 of this number using the formula Log2 {Group2 mean normalized counts/ Group 1 mean normalized counts}. The RNA-Seq data was presented visually using J-Browse 2 2.4.2, which was prepared by Dr Karsten Hokamp {Trinity College Dublin, Ireland}. Following RNA-seq, the R2 (square) regression coefficient {Quality control} analysis on the data. It recognizes the percentage of variation of the dependent variable and showed that the data was of good quality.

2.14 Chromatin comet assay (ChCA)

Yeast cells grown to logarithmic phase (10 x10^6 cell/ml) were subjected to Comet Assay according to (Georgieva *et al.*, 2012). 1.5 ml aliquots from the yeast cultures were prepared and centrifuged at 10,000 r.p.m for 5 minutes. The cells were then resuspended in S buffer consisting of [1 M Sorbitol and 25 mM NaH_2PO_4 with a pH of 6.5]. Aliquots of yeast cells were mixed with 0.7% low-gelling agarose (type VII) and 5 mg/ml of Zymolyase. The agarose-cell mixture was layered on glass slides coated with normal agarose {Type II-A} and covered with coverslips. After incubation at 4°C for 5 minutes, the microgels solidified and the cover glasses were removed. Spheroplasting of yeast cells was done by Zymolyase for 10 minutes at 37°C, followed by in situ treatment with different concentrations of micrococcal nuclease (MNase) or deoxyribonuclease I {DNase I} for 1 minute at 37°C. The enzyme action was stopped by placing the slides into a lysis solution containing [1 M NaCl, 50 mM EDTA, 30 mM NaOH, and 0.1% N-lauroylsarcozine with a pH of 10]. All successive steps were performed in a cold room at 10°C. Lysis of the spheroplasts was carried out for 1 hour by submerging the slides into the lysis solution.

DNA was denatured for 3x 20 minutes in a buffer containing [10 mM EDTA and 30 mM NaOH with a pH of 12.6]. Subsequent electrophoresis was conducted for 15 minutes at 0.45 V/cm in the same buffer. After successive dehydration in 75% and 100% ethanol for 5 minutes each, the slides were left to air-dry. Comets were observed under a Leitz epi-fluorescence microscope {Orthoplan, VARIO ORTHOMAT 2} using a 450 - 490 nm band-pass filter following the staining of DNA with the fluorescent dye SYBR green I {Molecular Probes Inc, Eugene, OR, USA}. Pictures were taken with a digital camera, Olympus μ800, at a resolution of 8 mpx. Three independent repetitions of the experiments were performed, and in each experiment, 150 randomly chosen comets per nuclease concentration were taken for quantification.

2.14.1 Quantification of chromatin comet assay the "r" parameter

According to (Olive *et al.*, 1990) the parameter "r" was defined as the distance {in arbitrary units} between the centre of mass of the comet head and the centre of mass of the comet tail. The tail moment [TM] was calculated by multiplying the percentage of DNA in the tail {measured as the integrated optical density of the tail, or I OD tail} by the parameter "r" (Olive and Banánth, 1993). The percentage of DNA in the tail {also known as the DNA percentage} was calculated as a part of the whole DNA content in the comet, which was assumed to be 100%.

2.15 Chromatin Immunoprecipitation (ChIP) protocol

2.15.1 Cell growth and formaldehyde crosslinking

To initiate the process, a single colony was added to 10 ml of YPD and incubated overnight at 30°C and 200g. The following day, the starter culture was transferred to 300 ml of YPD and allowed to grow until it reached a plate number of 0.6 – 1 nm {50 OD_{600} units for mid-log and 75 OD_{600} units for separated Q cells}. This volume was then divided into 5 x 50 ml cultures, each in a 250 ml flask, to prepare for crosslinking (Fig. 2.5).

The next step was to add Formaldehyde {Sigma, 37%} to a final concentration of 1% in the cultures. The cultures were left to shake for 20 minutes at room temperature. To stop the cross-linking reaction, 3 ml of 2.5 M glycine was added for 5 minutes at room temperature.

After crosslinking, the cultures were transferred to a 50 ml falcon tube and centrifuged at 1500g for 5 minutes at 4°C. The supernatant was carefully removed, and the cell pellet was resuspended in 25 ml of ice-cold TBS. The cells were centrifuged once again at 1500g at 4 °C, and the supernatant was discarded. Washed twice with ice-cold TBS and resuspended the pellets in 1 ml ice-cold TBS and transferred to a new 1.5 ml tube then centrifuged 1300g for 3 min at 4°C and the cell pellets were stored at -80°C until required.

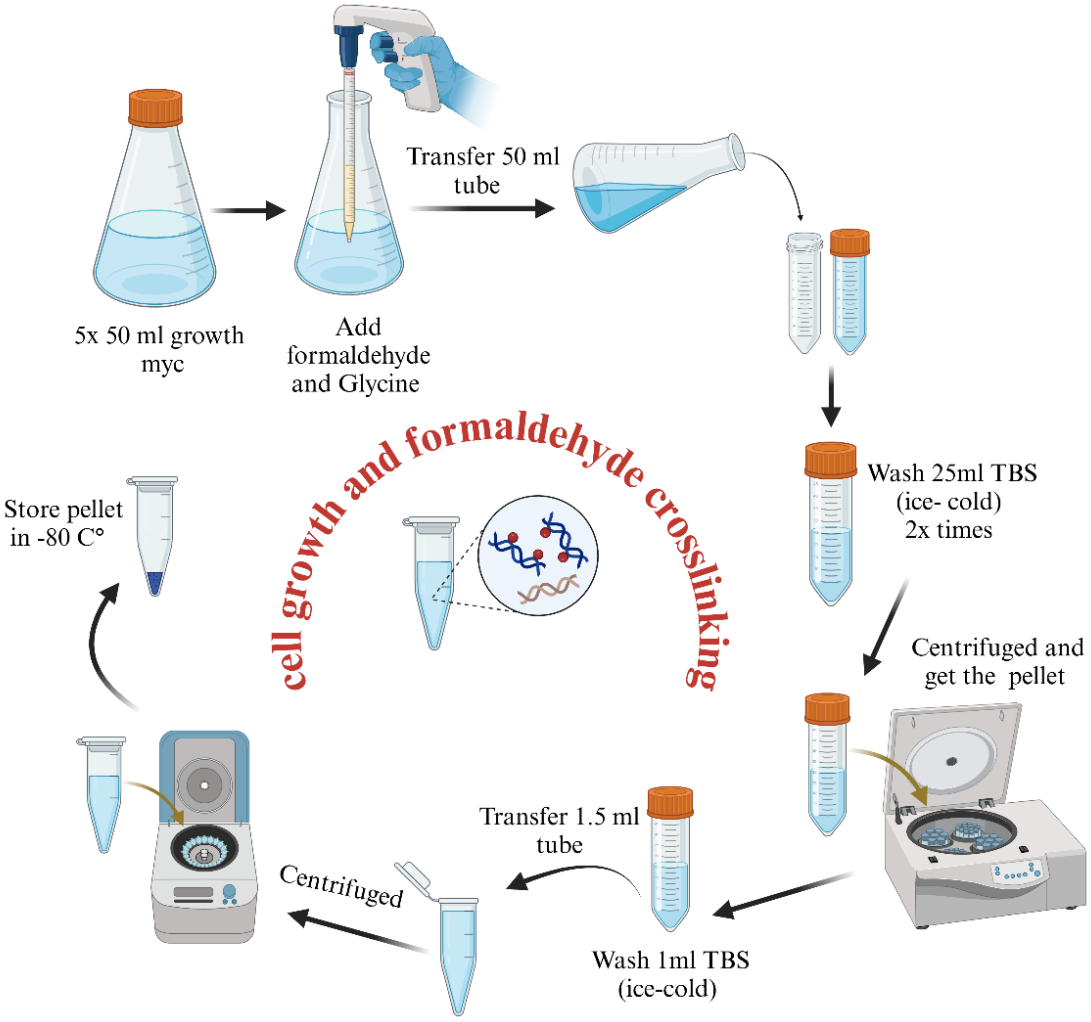

Figure 2.5: Schematic of cell growth and formaldehyde crosslinking. This figure was created using BioRender.

2.15.2 Cell lysis and sonication

The cells that had been cross-linked were resuspended in 400 µl of FA lysis buffer, which contained [50 mM HEPES, 140 mM NaCl, 1 mM EDTA, 1% Triton X-100, and 0.1% sodium deoxycholate]. Additionally, a protease inhibitor cocktail (Sigma) diluted at a ratio of 1:100 and 2 mM PMSF (Sigma) was also added. Then, around ~500µl of zirconia beads {BioSpec Products, Inc} were added to each tube. The samples were vortexed for 30 seconds using a high-speed benchtop homogenizer and then kept on ice for 1 minute. This process was repeated up to four more times. The samples were checked manually under a microscope to ensure that most cells had been lysed. The cell lysate was then transferred to a new 1.5 ml tube. The lysate was topped up to 1 ml with ice-cold FA lysis buffer and sonicated using a {Sanyo Soniprep 150 sonicator}. Take 80μl from the lysate in a new tube to check the sample in the gel before sonication (Fig. 2.7). Then, samples were sonicated in 1.5 ml tubes on ice at 8 amplitude microns and subjected to 12 pulses of 11 seconds duration. Samples were stored on ice for 1 minute between pulses to avoid overheating. The lysates were then clarified by centrifugation for 30 seconds at 13,200 g at 4°C. Take 80μl from the lysate in a new tube to check the sample in the gel after sonication (Fig. 2.7). The supernatant was then separated into 5 or 7.5 OD_{600} unit aliquots and stored at -80°C until used. All chromatin immunoprecipitation experiments used 5 and 7.5 OD_{600} units of mid-log cells, diauxie shift (Dx) and quiescent cells (Q), respectively.

The DNA for fragment length was taken from the pre-and post-sonication samples. 80µl of lysate was added to 100µl ChIP elution buffer, 20µl protease {20mg/ml}, and 1µl $CaCl_2${1M}, then the solution was incubated at 42°C for 2 hours. Cross-links were reversed by incubation at 65°C for 6 hours. 25µl of sodium acetate (3M, pH=5.3) was added, followed by 25µl of distal water, and 250µl then phenol/chloroform/isoamyl alcohol was added and mixed by vortexing for 3 minutes. This was centrifuged at 13,200g for 5 minutes, and the upper layer was transferred to a new 1.5ml tube then 500µl of ice-ethanol 100% was added. This was kept at -20 °C for one hour. After that, DNA was pelleted by centrifugation at 13,200g for 5 minutes. After discarding the supernatant, the pellet was resuspended in 200µl of TE (pH 8), 1.5µl of RNase A {25 µg}, was added and briefly vortexed. The mixture was incubated at 37°C for 2 hours, and then DNA was ethanol precipitated.

The optimal fragment size for ChIP is usually between 300 – 500 bp. To verify this, each sample of sonicated DNA was visualised using a 1.5% agarose gel (Fig. 2.14).

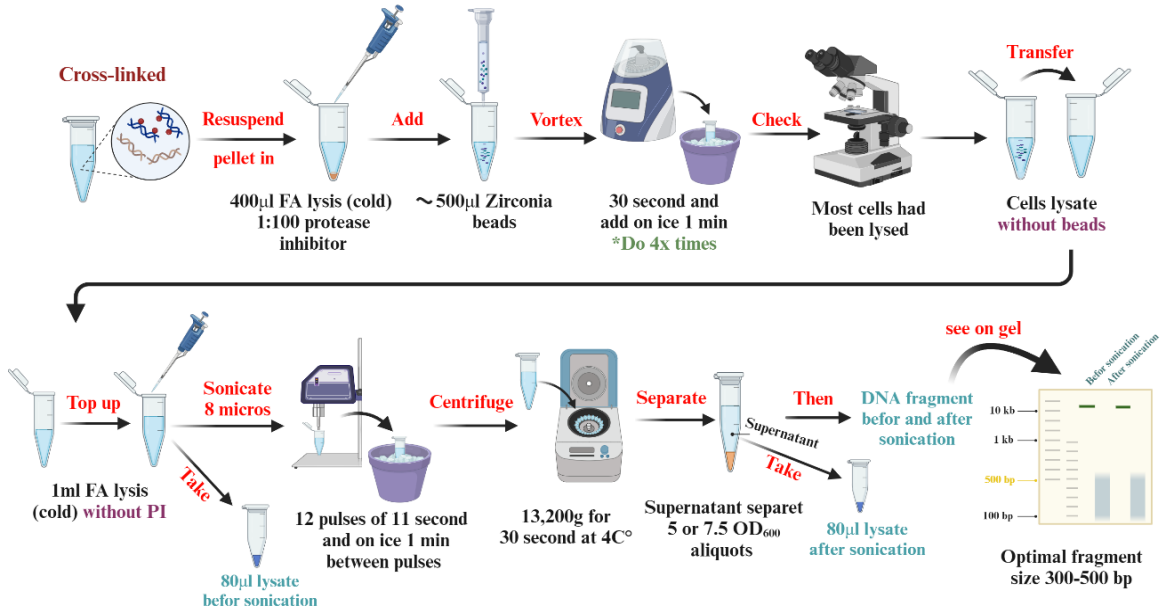

Figure 2.6: Schematic for Cell lysis and sonication. This figure was created using BioRender.

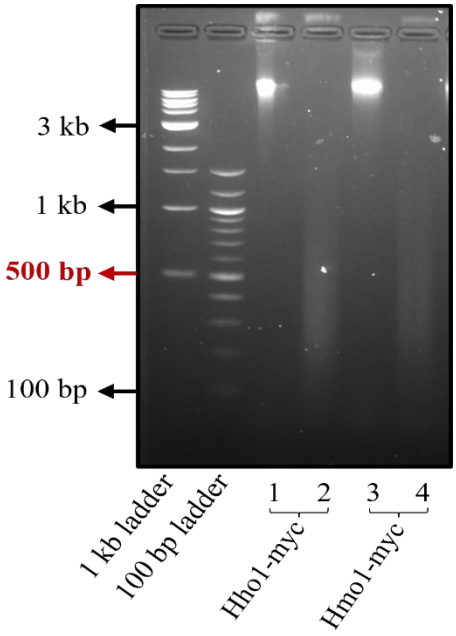

Figure 2.7: Verification of DNA fragment length after sonication. **Agarose gel to show fragment size of sonicated DNA.** A 1 kb DNA ladder and a 100 bp ladder (both NEB), were added as indicated; the gel shows results from two wt samples. For each sample, the DNA included was **1-** un-sonicated genomic for Hho1-myc DNA, **2-** sonicated genomic DNA that had been RNase treated, for Hho1-myc **3-** un-sonicated for Hmo1p-myc, and **4-** sonicated DNA which had been RNase treated for Hmo1-myc.

2.15.3 Immunoprecipitation

Cross-linked lysates were thawed on ice and made up to 500µl with FA lysis buffer containing protease inhibitor. 20µl was taken from each as input (IN). The IN samples were protease treated by adding 100µl ChIP elution buffer (25 m Tris Cl [pH 7.5], 5 m EDTA, 0.5 % SDS), 1 M $CaCl_2$ and 2 mg/ml protease type XIV (Sigma) to each 20µl IN sample and bringing the mixture to 200µl with 60µl TE (pH 7.5). These samples were incubated at 42°C for 2 hours and cross-links were reversed by incubating at 65°C for 6 hours. The IN samples were purified using a {Qiagen QiaQuick} PCR purification kit as per manufacturer's instructions. The appropriate antibody was added to the remaining 480µl lysate and incubated with rotation at 4°C overnight. The following morning the appropriate magnetic Dynabeads {Life Technologies} were washed three times for 5 minutes in 1ml FA lysis buffer. Washed beads were resuspended in FA lysis buffer and distributed evenly between lysates containing the antibody. This mixture was incubated for 2 hours at 4°C (Table 2.5).

The antibody-bead complexes were washed in 1ml FA lysis buffer for 5 minutes, followed by two washes in 1 ml ChIP wash buffer #1 (50 mM HEPES [pH 7.5], 0.5 M NaCl, 1 mM EDTA, 1 % Triton X-100, 0.1 % Sodium deoxycholate), two washes in 1 ml ChIP wash buffer #2 (10 mM Tris-Cl [pH 8.0], 0.25 M LiCl, 1 mM EDTA, 0.5 % NP-40, 0.5 % Sodium deoxycholate) and a single wash in 1 ml TE (pH 7.5). Beads were bound to a magnet and supernatant was discarded between washes. After the final wash, beads were resuspended in 250µl ChIP elution buffer (25 mM Tris-Cl [pH 7.5], 5 mM EDTA, 0.5 % SDS) and mixed. The suspension was incubated at 65°C for 20 minutes and rotated for 10 minutes at room temperature. Samples were centrifuged at 1300g for 2 minutes and supernatant was transferred to a new 1.5 ml tube. To protease-treat IP samples, 20 mg/ml protease and 1 M $CaCl_2$ were added, and the solution was incubated at 42°C for 2 hours. Cross-links were reversed by incubation at 65°C for 6 hours. IPs were purified using a {Qiagen QiaQuick} PCR purification kit according to manufacturer's instructions. In the final elution step samples for ChIP-qPCR were dissolved in 50µl of Buffer EB {Qiagen}, and samples for ChIP-Seq were dissolved IN / IP in Buffer EB {Qiagen}(Fig. 2.8).

Antibody	OD Units per IP	Number of washes	Amount of antibody	Invitrogen Dynabeads	Source	Comment
Myc	10 OD 5x units	2	2.5 µl / IP	Protein G slurry 50 µl per IP	Millipore 05-724	ChIP-seq for Expo and DX
Myc	15 OD 5x units	2	2.5 µl / IP	Protein G slurry 75 µl per IP	Millipore 05-724	ChIP-seq for Q
Pol II	5 OD 1x units	2	4.5 µl / IP	Protein A/G 30 µl per IP	Covance (MMS126R)	ChIP-qPCR Test

Table 2.5: Antibodies and conditions for chromatin immunoprecipitation and ChIP-seq

For each IP sample for ChIP-seq, 5 individual IPs were performed (10 or 15 OD per IP). After the final wash in TE pH 7.5, the beads-chromatin complex was poolled in a single 1.5ml tube prior to elution and DNA purification (Fig. 2.8).

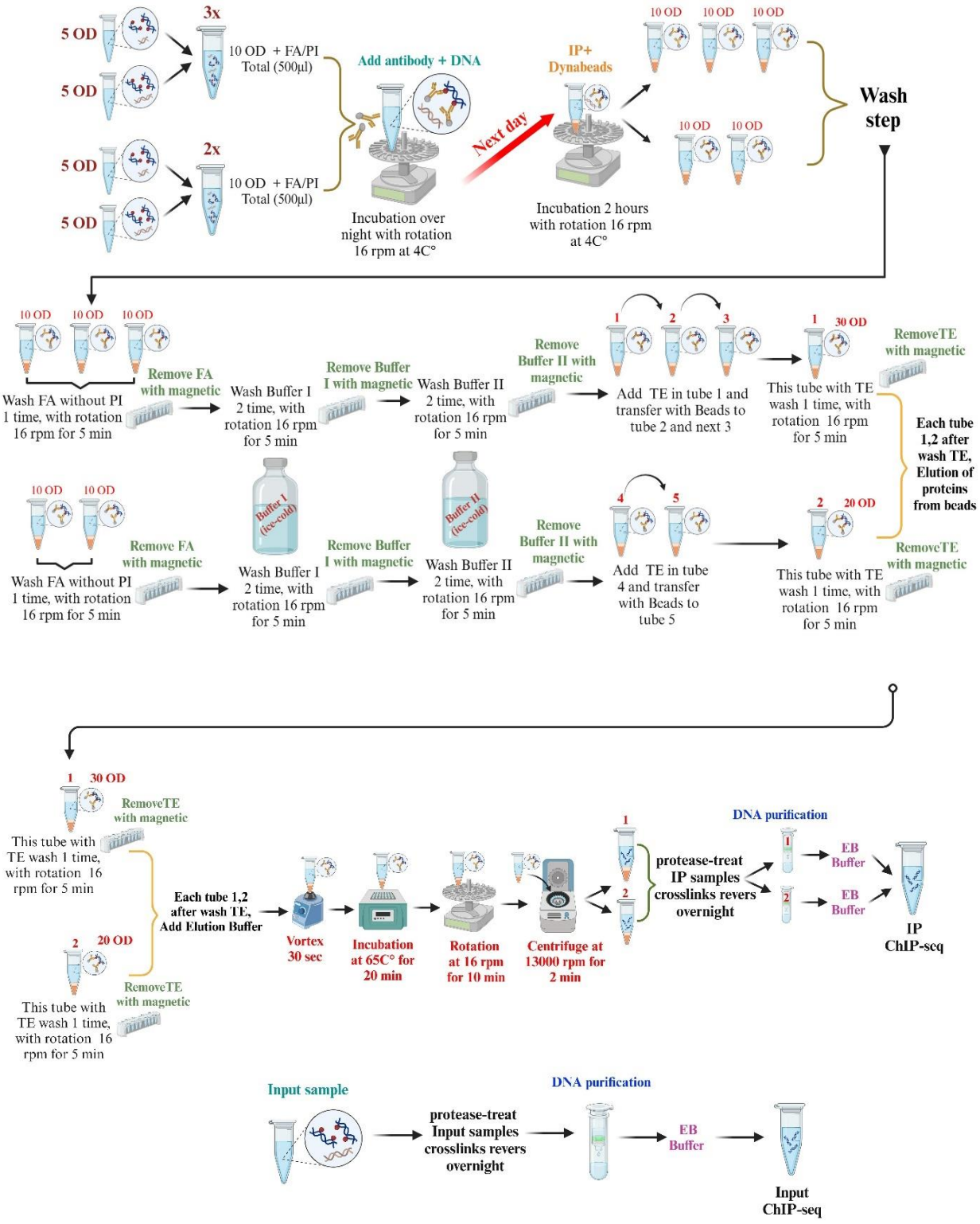

Figure 2.8: Schematic for chromatin immunoprecipitation and ChIP-seq. This figure was created using BioRender.

2.15.4 Two-Step normalization of ChIP-qPCR data

For IP/input ChIP analysis, the template DNA was used for qPCR. A real-time PCR system from {Applied Biosystems} was used for relative quantification based on a standard curve. By using PCR on purified IP and inputs, qPCR was performed following a Pol II ChIP experiment. Comparing IP levels (which refer to protein occupancy in a given region) to input levels (which are indicative of DNA quantities in a given sample) allowed us to determine levels of enrichment. RNAPII levels were determined at *FLO1* (an inactive gene in wt) and *PMA1* (an active gene) as a negative and positive control, respectively. The Tel VI region is used as an internal negative control for Pol II occupancy (Fig. 2.9). The experiment was performed on lysates that I had made {labelled experiment test strain}, and on lysates which had previously supported a successful Pol II ChIP result {labelled as control}.

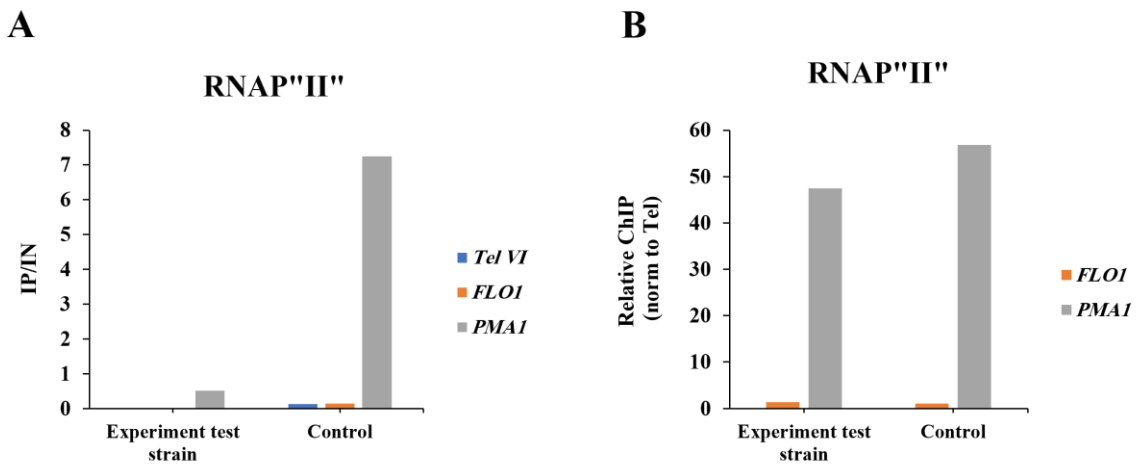

Figure 2.9: Analysis of ChIP DNA concentration using qPCR. **Normalization of RNAP II ChIP data.** In both ChIP experiments, IP /IN DNA was not normalized for sample variability (**A-** left hand-side of plots). RNAP II IP/Input data were further normalized to internal control regions TEL respectively (**B-** right hand-side of plots).

2.15.5 DNA sequencing

ChIP DNA, prepared according to the aforementioned protocol, was submitted to Genewiz {Azenta Germany} for sequencing and subsequent bioinformatic analysis. Sequencing was conducted on the {Illumina NovaSeq (2X150b) platform}. Trimmomatic 0.38 was utilized to remove sequencing adapters and low-quality bases. The resulting reads were aligned to the reference genome using bowtie2, and Samtools 1.9 was employed to filter aligned reads, retaining those with a minimum mapping quality of 30, concordant alignment, and designated as primary-called alignments. Reads mapped to mitochondria and unplaced contigs were excluded from further analysis. {MACs 2.1.2} was employed to identify peaks in the IP samples compared to input (IN) samples, focusing on narrow enrichment peaks typically observed in ChIP-Seq analysis of transcription factor occupancy, such as Hho1p and Hmo1p. Each group comprised two biological replicates, and peaks identified in at least 66% of samples were retained for downstream analysis. Merged peak files were formatted as BED files. Visualization of the data was performed using the Yeast Epigenome Project Browser {YEn} (Rossi *et al.*, 2021) and my data using J-Browser.

2.16 Statistical analysis

Statistical analysis was conducted using {GraphPad Prism 11}. To determine the statistical significance of the results, either a T-test or Two-way ANOVA was employed as appropriate. For multiple comparisons, a Tukey's multiple comparison test was utilized if there was no significant difference {p-value < 0.05} in the standard deviations of the groups, which was assessed by a Brown-Forsythe test. In cases where there was a significant difference in standard deviations, a Games-Howells test was conducted for multiple comparisons. Results were considered statistically significant if the {p-value was less than 0.05}. {Funrich software} was utilized to generate all Venn diagrams, while {Metascape software} was employed to produce all Gene Ontology analyses.

Chapter 3

Characterisation of mutants deficient for *hho1*Δ and *hmo1*Δ

3.1 Introduction

Histone H1 binds to the DNA linker region where the DNA enters and exits the nucleosome (the dyad) (An *et al.*, 1998a; Sivolob and Prunell, 2003a; Syed *et al.*, 2010a; Bednar *et al.*, 2016a). Although the linker histone H1's structure and function are well characterized in higher eukaryotes, the yeast equivalent's identity and role remain controversial. It is commonly accepted that the *HHO1* gene encodes the yeast-linker histone H1 (Brush, 2015). The *HHO1* gene was identified by a scan of the yeast genome sequence for homologs of the conserved histone H1 globular domain (Landsman, 1996; Ushinsky *et al.*, 1997). However, the deletion of *HHO1* in vegetatively growing yeast shows no striking phenotype (Bryant *et al.*, 2012a). Interestingly, Hho1p has been proposed to operate during the stationary phase of yeast where it may promote chromatin compaction and contribute to DNA damage repair (Patterton *et al.*, 1998; Schäfer *et al.*, 2008). However, whether Hho1p is the actual yeast linker histone H1 equivalent remains controversial.

Recently, another candidate has been identified that may function as the yeast H1 protein called Hmo1p. *HMO1* gene deletion is not lethal; however, deletion results in significant growth defects and decreased plasmid stability (Ray and Grove, 2009a; Xiao *et al.*, 2011a). In *vivo,* Hmo1p has been shown to maintain a novel chromatin structure at the rDNA site within the nucleolus and facilitates ribosomal RNA transcription (Gadal *et al.*, 2002). Hmo1p is also associated with DNA entry/exit points on the nucleosome (Lu *et al.*, 1996; Bermejo *et al.*, 2009).

To investigate if either Hmo1p or Hho1p might be the most likely candidate for linker histone H1 function in *Saccharomyces cerevisiae,* I analyzed the phenotypes of *hho1*Δ and *hmo1*Δ gene deletion mutants. The first step in my project was to determine if the *hho1*Δ and *hmo1*Δ deletion mutants displayed similar or different phenotypes in exponential and/or stationary phase. If yeast linker histone H1 is functioning to aid compaction of chromatin in stationary phase, it would be predicted that the best candidate for yeast linker histone H1 would have the greatest severity of phenotypes during stationary phase in the appropriate gene deletion mutant.

3.2 Results

3.2.1 Confirmation of *HHO1* and *HMO1* gene deletions

The first experiments were to confirm that the deletion of the *HHO1* and *HMO1* genes in the strains obtained from the yeast gene deletion library (ResGen) were correct. Each mutant was constructed by replacing their gene coding regions with the *KAN* gene (Baker Brachmann *et al.*, 1998). PCR was performed to confirm the *hho1*Δ and *hmo1*Δ deletion mutants using oligos up and downstream of the expected gene deletion and oligos internal to the selectable marker used in the gene deletion attempt (Fig. 3.1A and 6A, respectively).

3.2.1.1 Confirming the *HHO*1 single gene deletion by PCR analysis

The results showed that the *HHO1* gene deletion was correct (Fig. 3.1B). The expected sized DNA bands of 481 and 880 bp were found within the *hho1*Δ mutant strain in lanes 6 and 8, while the wt result was negative, aside from weak spurious bands found in the wt (lanes 5 and 7).

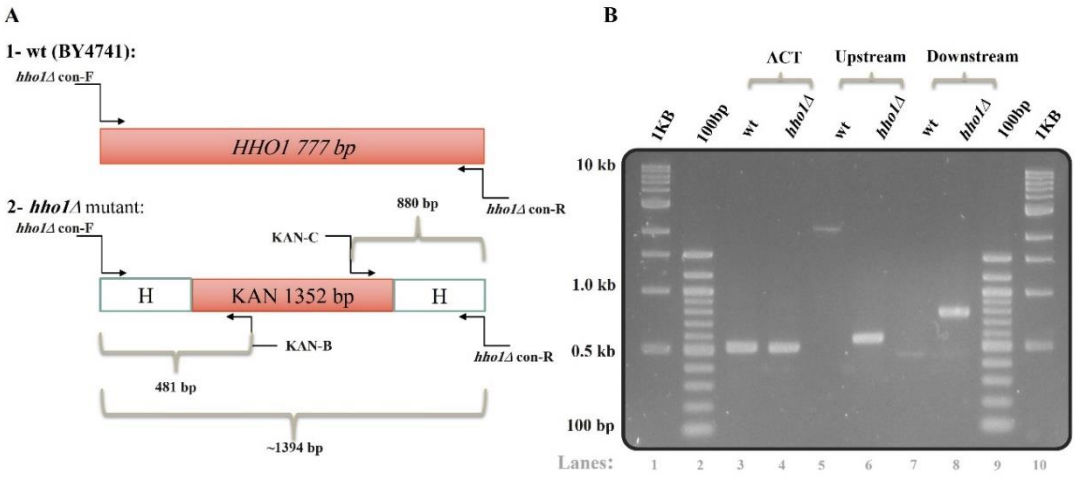

Figure 3.1: PCR confirmation of the *hho1*Δ mutant. (A) Schematic to show PCR design for gene deletion confirmation. **(B)** Result of PCR confirmation reactions. Two areas were amplified to confirm the presence of the *KanMX* gene: upstream *hho1*Δ con-F and Kan-B primers, which are negative in wt and positive in the (lanes 5 and 6), and downstream *hho1*Δ con-R and Kan-C primers, which are negative in wt and positive in the mutant, (lanes 7 and 8). ACT was used as a positive control for the PCR reaction, lanes (3 and 4).

3.2.1.2 Confirming the *HMO1* single gene deletion by PCR analysis

PCR was next performed using oligos up and downstream of the expected gene deletion in the *hmo1*Δ mutant together with oligos internal to the selectable marker used in the gene deletion attempt (Fig. 3.2A). Two areas were amplified to confirm the presence of the *KanMX* gene: upstream *hmo1*Δ con-F and Kan-B primers which are positive in mutant and negative in wt lane (5 and 6) and downstream *hmo1*Δ con-R and Kan-C primers which are positive in mutant and negative in wt, lane (7 and 8).

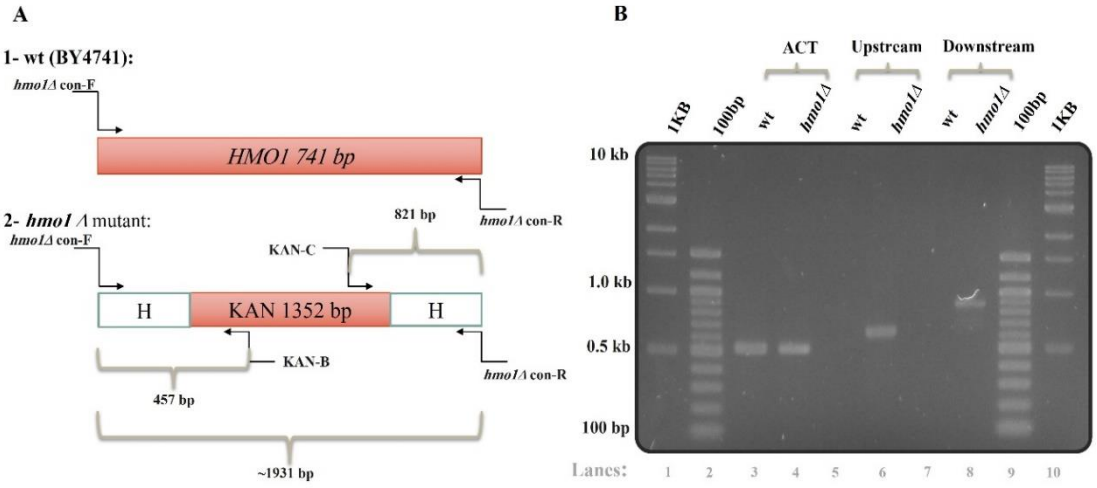

Figure 3.2: PCR confirmation of the *hmo1*Δ mutant. (A) Schematic to show PCR design for gene deletion confirmation. **(B)** Result of PCR confirmation reactions. Two areas were amplified to confirm the presence of the *KanMX* gene: upstream *hmo1*Δ con-F and Kan-B primers which are positive in mutant and negative in wt lane (5 and 6), and downstream *hmo1*Δ con-R and Kan-C primers which are positive in mutant and negative in wt, lane (7 and 8). ACT was used as a positive control for the PCR reaction, lanes (3 and 4).

3.2.2 Mutants deleted for *HHO1* and *HMO1* show distinct phenotypes

I next analysed the phenotypes of the *HHO1* and *HMO1* gene deletion mutants to try to determine which mutant is the best candidate for fulfilling the putative H1 function in yeast.

3.2.2.1 Analysis of growth in liquid media containing glucose

To investigate the growth of the mutants, the strains were individually inoculated into a liquid culture containing glucose (YPD), and the increase in optical density was monitored over time and the doubling time of each strain was calculated (Fig. 3.3). In glucose-containing media, the *hho1*Δ mutant showed no significant defect in growth compared to wt (Fig. 3.3A). Conversely, the *hmo1*Δ mutant showed a delay before the maximum growth rate started, after which it achieved a maximum OD_{600} of less than wt.

I next calculated the doubling time of each mutant following growth in YPD (Fig. 3.3B). Overall, both the *hho1*Δ and *hmo1*Δ mutants showed no significant difference in doubling time compared to each other and to wt. However, as the *hho1*Δ mutant reached a consistently lower cell density than wt after the period of exponential growth, this suggests that the *hmo1*Δ deletion does have a defect in cell growth.

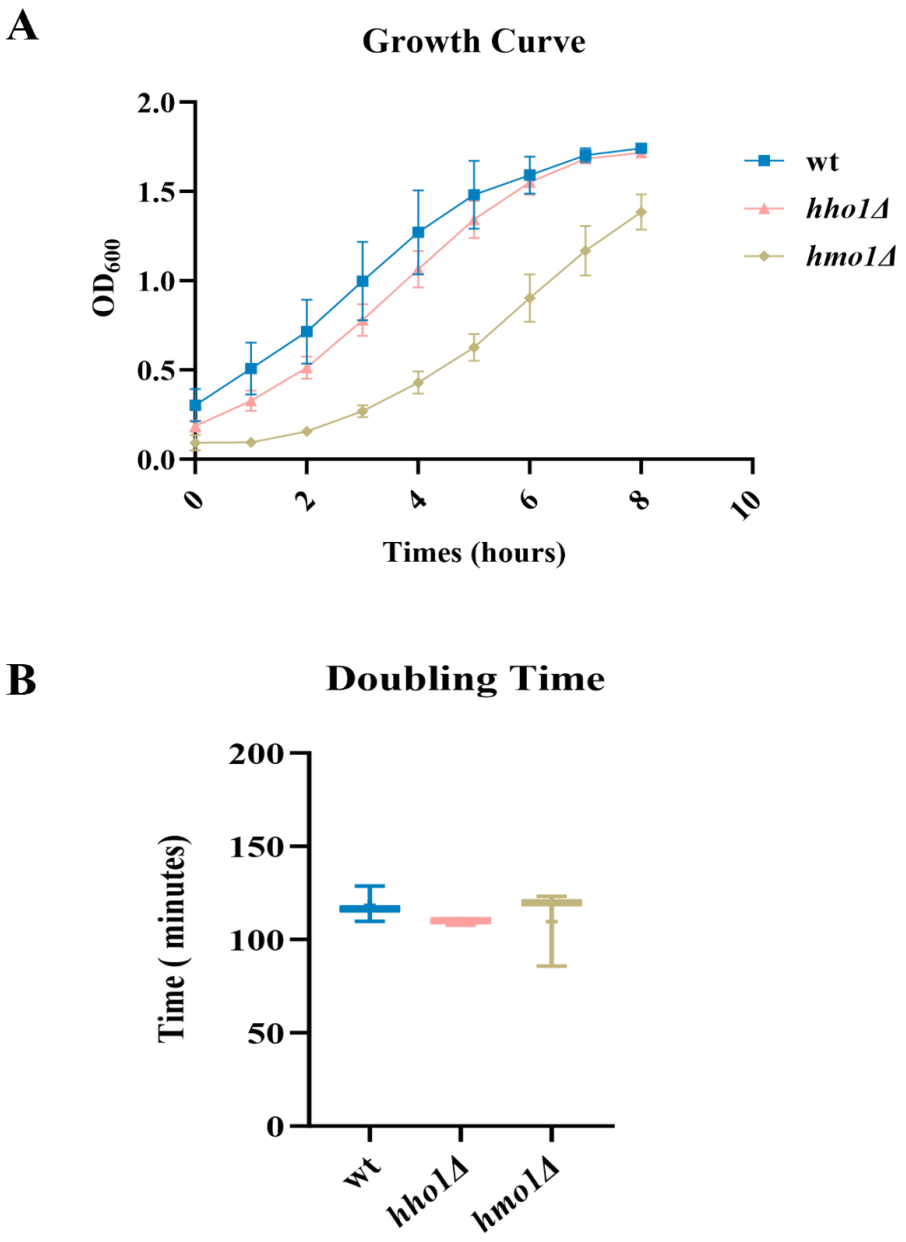

Figure 3.3: Analysing growth of mutants on glucose and doubling time of wt, *hho1*Δ, and *hmo1*Δ deletion strains. (A) Wild type (wt) and single mutants were grown at 30°C in YPD and OD_{600} readings were taken at the time intervals indicated. **(B)** Doubling time of each strain indicated following growth in YPD. For A and B, the experiments were performed in triplicate, and error bars represent standard deviation (SD).

3.2.2.2 Analysis of cell density during entry into stationary phase

I next calculated the final cell density that each strain achieved after 24 hours of growth, which would correspond to the exit of cells from the exponential phase of growth and entry into early stationary phase (Fig.3.4). The wt and *hho1*Δ mutant strain reached a similar final cell density after 24h of growth. However, the cell density reached by the *hmo1*Δ mutant was significantly lower than that reached by wt and the *hho1*Δ deletion strain. Indeed, the *hmo1*Δ mutant cell density at 24h was 36% of that achieved by wt (Fig.3.4). Overall, the *hmo1*Δ mutant exits exponential phase at a lower cell density than wt.

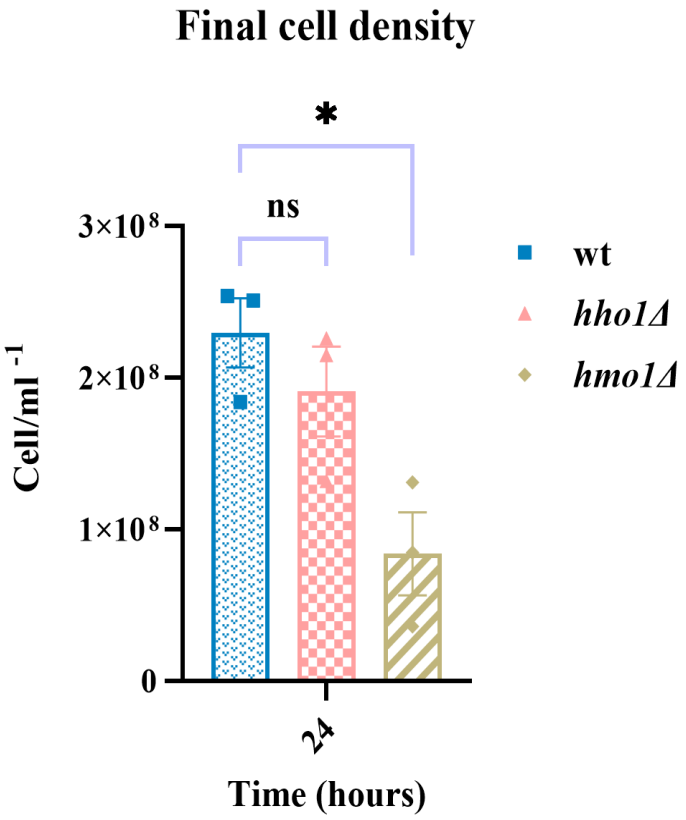

Figure 3.4: Analysis of growth into stationary phase, cell density after 24h growth in YPD. Error bars represent the standard error of triplicate biologically independent experiments' mean (SEM). Standard significance using One-way ANOVA analysis (* p = 0.05, ** p = 0.01, *** p = 0.005).

3.2.2.3 Analysis of cell viability during stationary phase

I next monitored cell viability over a 14-day period (Fig. 3.5). The data revealed that neither mutant lost viability over this time period compared to wt.

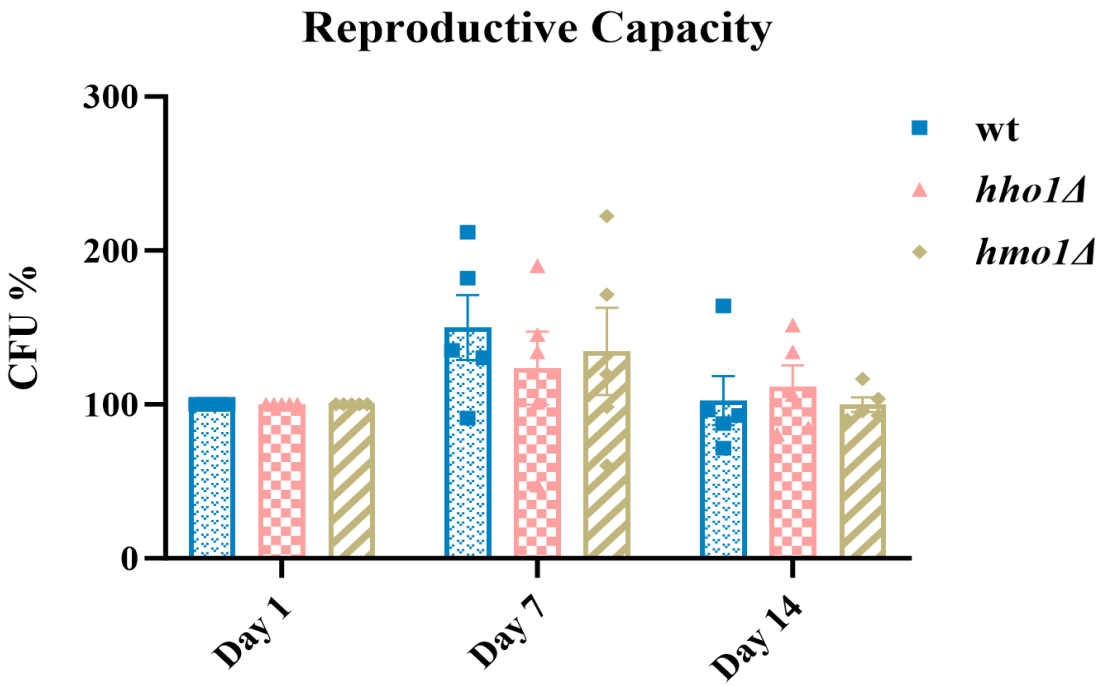

Figure 3.5: Analysis of viability of wt, *hho1*Δ, and *hmo1*Δ deletion strains. Cell viability as measured by colony-forming unit (CFU) capacity of cells at day 1, 7 and 14 of growth in YPD. Error bars represent the standard error of five biologically independent experiments' mean (SEM). Data was normalised to the values for each strain on day 1 (set as 100%).

3.2.2.4 Analyzing *hho1*Δ and *hmo1*Δ mutant cell morphology

I next investigated the cell morphology of each of the mutant strains. Cells were grown to exponential and stationary phases {day 7} and then viewed under a light microscope (Fig. 3.6).

The wt and *hho1*Δ cells show a similar morphology in both exponential and stationary phases. Conversely, the *hmo1*Δ deletion strain displayed a reproducible elongated cell morphology in exponential and stationary phases. Furthermore, the *hmo1*Δ mutant cells looked larger than wt during stationary phase.

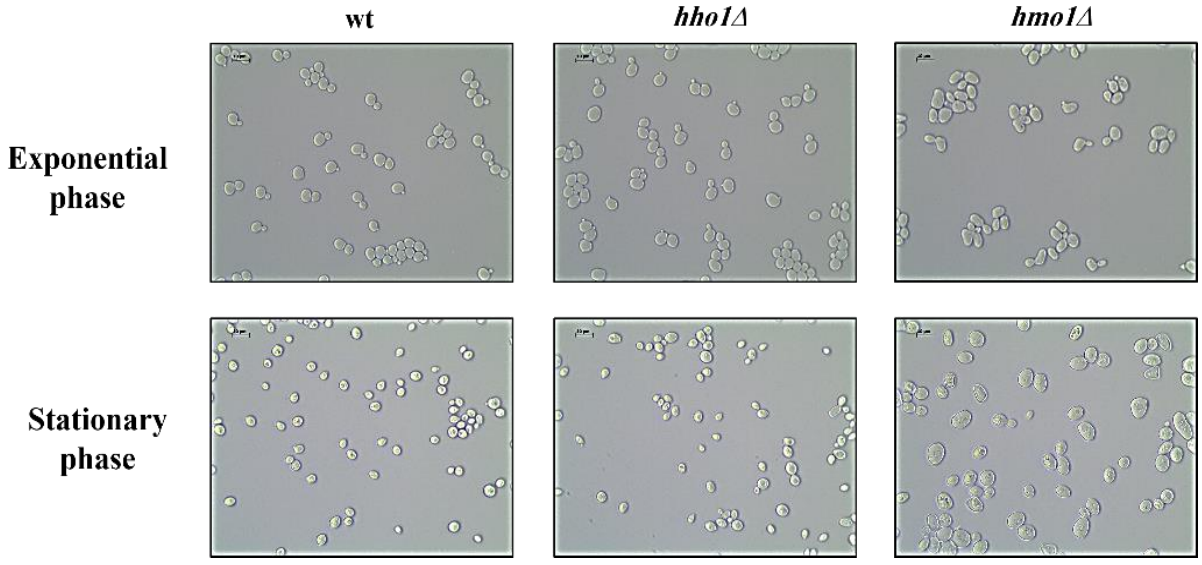

Figure 3.6: Cell images of wt, *hho1*Δ, and *hmo1*Δ mutant cells. The different mutant strains shown were grown in YPD and were examined from exponential and stationary phase (day 7) growing cultures under microscope cells. Microscopy was conducted under a 100x immersion magnification of the oil. The black bar is 10μm.

3.2.3 Testing for phenotypes by challenging cells in various 'spot tests'

In the next series of experiments, I challenged exponential and stationary phase {day 7} cells with various growth conditions or stresses by so-called 'spot tests'. The cells were serially diluted and spotted onto plates containing various carbon sources, reagents, or placed under specific growth conditions. This analysis offers a quick way to rapidly screen for any phenotypes the mutants might display, which may offer insight into the roles of *HMO1* and *HHO1* and indicate whether these roles are stationary-phase specific or not.

3.2.3.1 Analysis of temperature sensitivity

Exponentially growing cells and cells from stationary phase cultures were spotted onto YPD media at the temperature of 15°C and 37℃ (Fig. 3.7). Neither mutant from either growth phase showed a growth defect compared to wt at the high or low temperature tested.

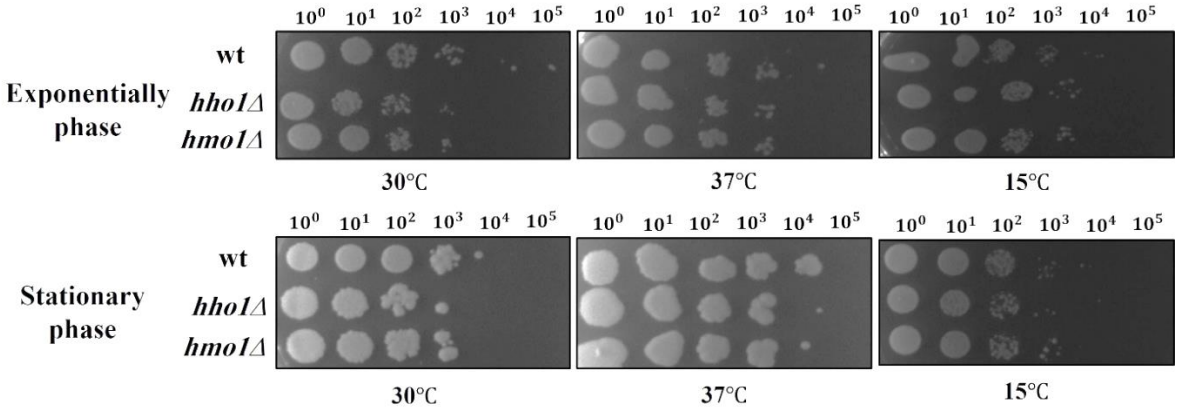

Figure 3.7: Temperature sensitivity growth tests of exponentially and stationary phase growing cultures on plates. Cells were serially diluted, spotted onto YPD plates, and the plates incubated at the indicated temperatures. YPD: control plates. The images were taken after three days of growth.

3.2.3.2 Analysis of the ability to grow on different carbon sources

I next looked at the ability of exponential and stationary phase {day 7} cells to grow on plates containing different carbon sources. The *hmo1*Δ and *hho1*Δ mutant strains showed no differences compared to wt when grown on raffinose, sucrose, galactose, glycerol, or ethanol-containing plates (Fig. 3.8).

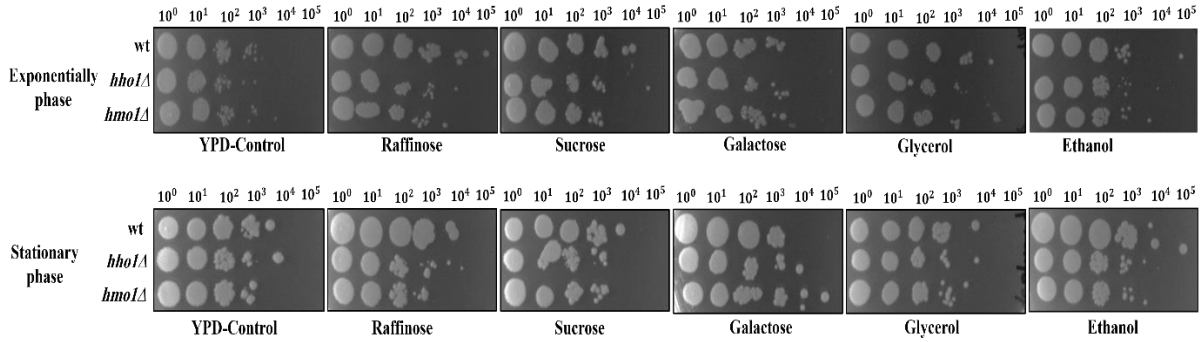

Figure 3.8: Growth tests of exponentially and stationary growing cultures. **on plates with different carbon sources.** YPD: control plates. Cells were grown from different carbon sources. The strain incubated was plated as 10-fold serial dilution starting from 1×10^7 cells/ml. The plates were spotted onto YP-Raffinose (YP-Raff 2%)**,** YP-Sucrose (YP-Suc 2%), YP-Galactose (YP-Gal 2%), YP-Glycerol (YP-Glyc 2%) and YP-Ethanol (YP-Etha 2%). **5µl** of culture was spotted on YPD plates and photographed following 48 hours of growth at 30℃.

3.2.3.3 Analysis for growth on a non-fermentable source

Exponentially growing wt, *hho1*Δ, and *hmo1*Δ cells and cells from stationary phase {day 7} cultures were spotted onto plates containing the non-fermentable carbon source acetic acid (Fig. 3.9). The exponential cells of the *hho1*Δ mutant were more sensitive for growth on acetic acid plates at the concentration of 60 mM, whereas the *hmo1*Δ mutant was better able to grow than wt at this concentration. When stationary phase cells were challenged to grow on acetic acid as the sole carbon source, the *hho1*Δ mutant grew as well as wt, whereas the *hmo1*Δ mutant was able to grow better than wt on the 80mM plate.

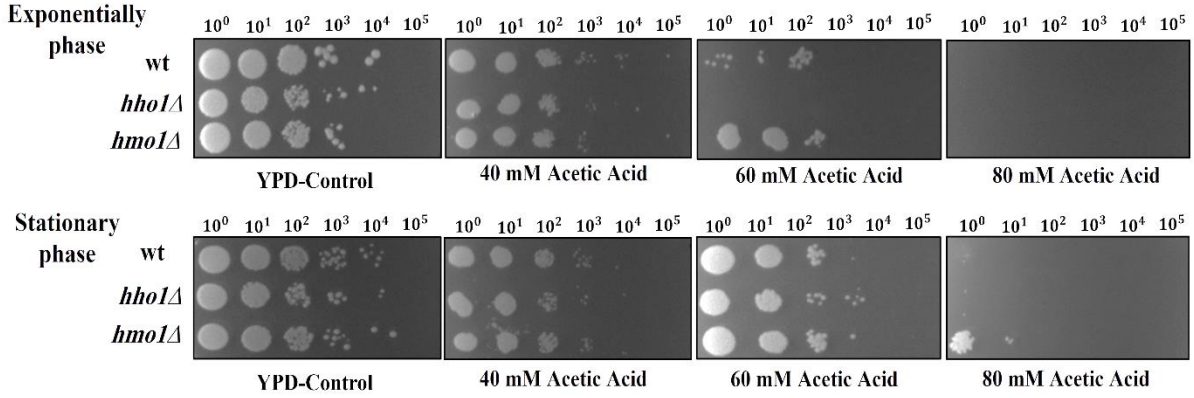

Figure 3.9: Serial ten-fold dilution growth tests a non-fermentable source of exponential and stationary growing cultures. on plates with the indicated compounds or exposures. YPD: control plates. Cells were grown on cultures with known non-fermentable sources of Acetic Acid without glucose (YPD). **5µl** of culture was spotted onto each plate and photographed following 48 hours of growth at 30℃.

3.2.3.4 Analysis of sensitivity to osmotic and oxidative stress

Next, I tested the exponential and stationary phase {day 7} cells for their ability to grow in the presence of high salt concentrations and hydrogen peroxide to test for sensitivity to osmotic and oxidative stress, respectively. Both exponentially and stationary phase mutant strains were unaffected by adding sodium chloride (NaCl) at all concentrations (Fig. 3.10A).

However, when the mutants were challenged to grow in the presence of hydrogen peroxide (H_2O_2), the exponential *hho1*Δ mutant was more sensitive to growth compared to the wt and the *hmo1*Δ mutant (Fig. 3.10B, see exponential 4 and 6mM plates). However, neither of the mutant SP cells showed any sensitivity to growth on hydrogen peroxide compared to wt.

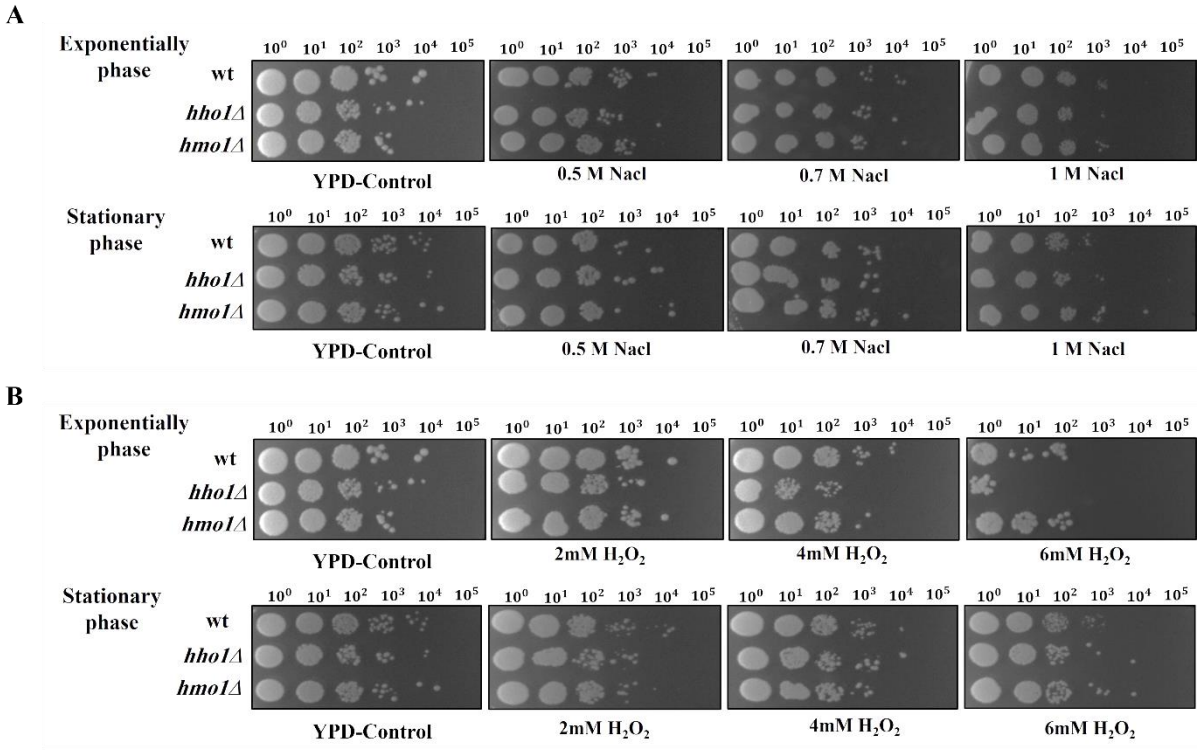

Figure 3.10: Testing cell sensitivity to osmotic and oxidative stress of exponentially and stationary growing cultures. on plates with the indicated compounds or exposures. Cells were grown on plates containing **(A)** Sodium chloride (NaCl) and **(B)** Hydrogen Peroxide (H_2O_2) to test for sensitivity to osmotic stress and oxidative stress, respectively. **5µl** of culture was spotted on YPD plates and photographed following 48 hours of growth at 30℃.

3.2.3.5 Analysis of sensitivity to caffeine

I next tested the mutant cell's ability to grow in the presence of caffeine. Caffeine has pleiotropic effects on yeast but primarily assesses yeast resistance to cell wall stress via the Mpk1p-mediated cell wall integrity pathway (Levin, 2005; Kuranda *et al.*, 2006). Interestingly, both exponential and stationary phase {day 7} cells of each mutant were more resistant to caffeine than wt (Fig. 3.11).

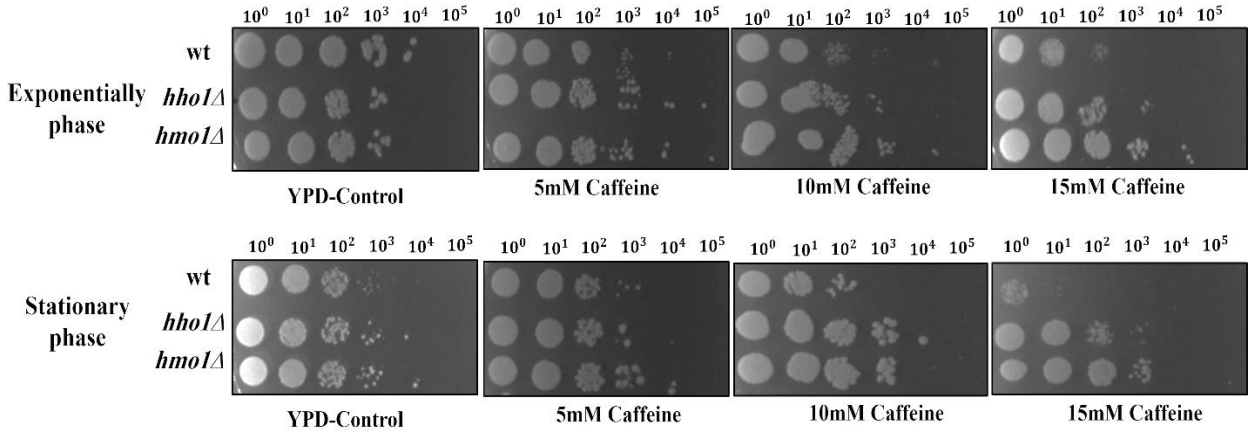

Figure 3.11: Testing cell sensitivity to the caffeine of exponentially and stationary growing cultures, the strains incubated were plated as 10-fold serial dilution starting from 1×10^7 cells/ml. The plates were spotted onto YP-Caffeine (YP-Caff 2%). **5µl** of culture was spotted on YPD plates and photographed following 48 hours of growth at 30℃.

3.2.3.6 Analysis of the growth response to DNA damaging agents

I next analysed the ability of the mutants' exponential and stationary phase {day 7} cells to grow in the presence of the DNA-damaging reagents methyl methane sulfonate (MMS) and hydroxyurea (HU). The DNA alkylating agent, MMS, causes DNA fragmentation following inhibition of DNA replication (Lundin *et al.*, 2005). The enzyme ribonucleotide reductase is inhibited by HU which reduces dNTP levels and inhibits DNA replication resulting in replication fork collapses and double-strand breaks (Koç *et al.*, 2004). However, all strains were unaffected by the presence of MMS and HU to the growth medium in both exponential and stationary growth phases (Fig. 3.12A and B, respectively).

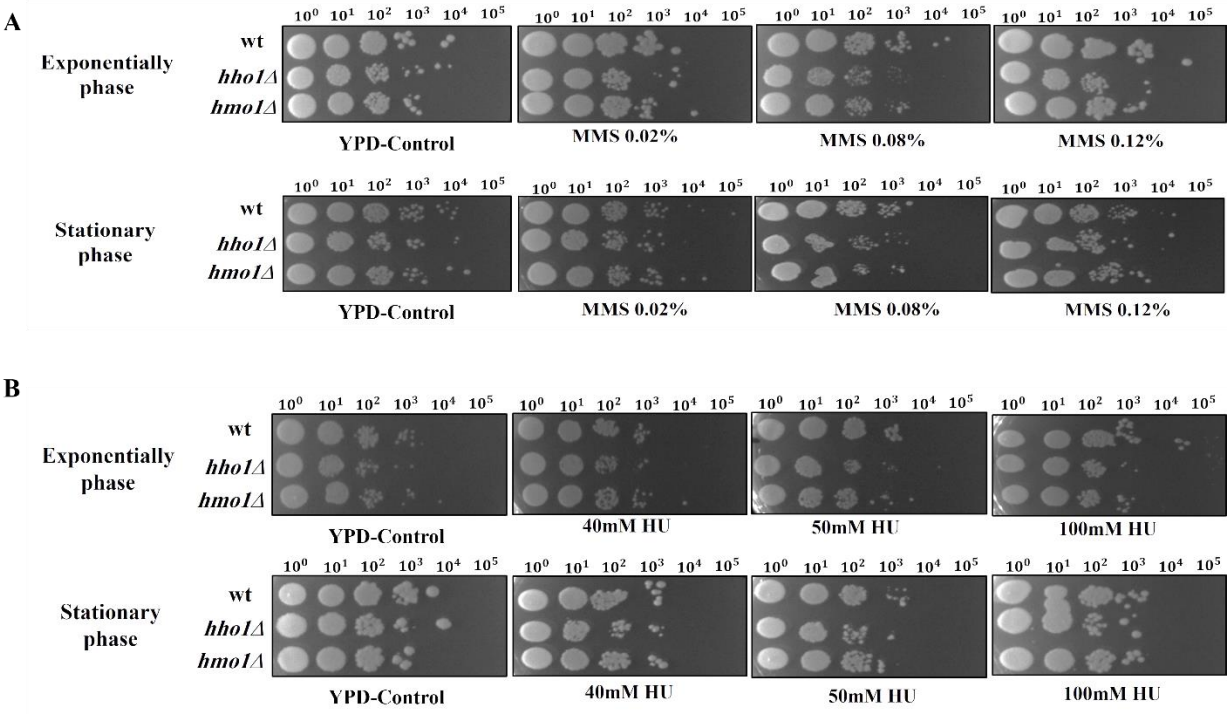

Figure 3.12: Serial ten-fold dilution growth tests to DNA damaging reagent MMS and HU of exponentially and stationary growing cultures, on plates with the indicated compounds or exposures. YPD: control plates. Cells grown on cultures with known DNA damaging agents **(A)** Methyl methane sulfonate (MMS) **(B)** hydroxyurea (HU). **5µl** of culture was spotted on YPD plates and photographed following 48 hours of growth at 30℃.

3.2.4 Analysing *hho1*Δ and *hmo1*Δ mutants for thermosensitivity of cells in liquid culture

I next tested the ability of the exponential and stationary phase {day 7} mutant cells to withstand higher temperatures in liquid culture. This is because one of the hallmarks of yeast cells grown into SP is that the quiescent (Q) cells formed during SP are more thermotolerant than exponentially growing cells (Allen *et al.*, 2006). Cells from exponential and stationary phase cultures were exposed to 30℃ and 52℃ for 1 hour, and the resultant viability of the cells was tested by plating for colony-forming units.

Cells from the exponentially growing wt and mutant cultures equally lost all of their ability to form colonies after heat shock (Fig. 3.13A). However, wt and mutant SP cells were equally resistant to the heat shock, with all strains showing over 50% survival after this heat shock compared to their starting cell viability (Fig. 3.13B). The differences in survival seen between SP cells of wt and the mutants after heat shock were not statistically significant.

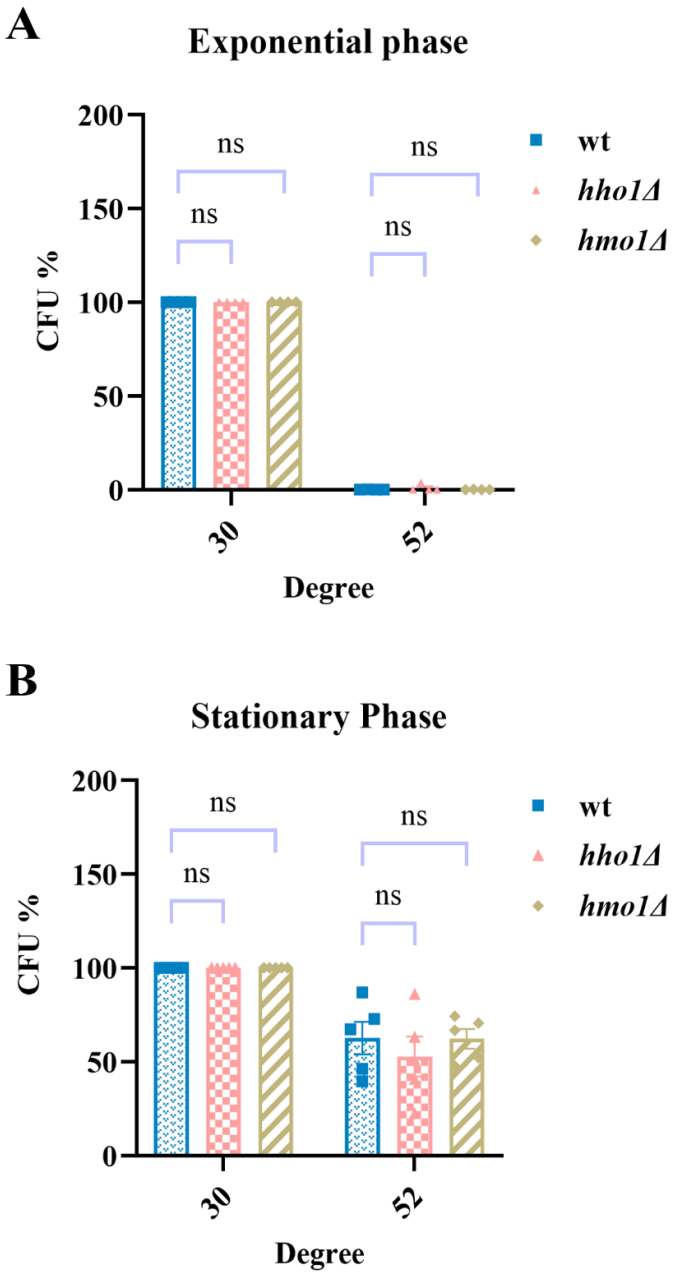

Figure 3.13: Thermotolerance of exponential and stationary phase cells. Cell viability of cells from exponentially growing **(A)** and stationary phase on day 7 cultures **(B)** following exposure to 30°C and 52°C temperatures. The y-axis shows the % of colony-forming units (CFU/ml) after heat shock compared to the CFU/ml before. Error bars represent the standard error of five biologically independent experiments' mean (SEM). Standard significance using Two-way ANOVA analysis.

3.2.5 Examining the consequence of *HMO1* and *HHO1* over-expression

The previous analyses examined *HHO1* and *HMO1* deletion mutants to offer insight into the roles of Hmo1p and Hho1p during the exponential and stationary phases of growth. I therefore decided to examine the consequence of over-expression of the Hmo1p and Hho1p proteins upon exponential and stationary phase cell function by examining strains in which the *HHO1* and *HMO1* genes were placed on a plasmid under the control of a *GAL* promoter which drives over-expression when cells are grown on galactose.

3.2.5.1 Analysis of pGAL-*HHO1* and pGAL-*HMO1* growth characteristics

The strains were incubated in liquid culture in galactose containing minimal media (SC) and growth was monitored by measuring OD_{600} nm over time (Fig. 3.14). The results suggested that both pGAL-*HHO1* and pGAL-*HMO1* strains did show a growth defect compared to wt, whereby the over-expression strains grew slower and to a lower final OD_{600} than wt (containing an empty vector) (Fig. 3.14A). I next measured cell viability by counting the colony-forming capacity of the strains after 1-, 7- and 14-days of growth (Fig.3.14B). The results suggested that there was a loss in viability of the Hmo1p over-expression strain (pGAL-*HMO1*) compared to wt by day 7, while both the pGAL-*HHO1* and pGAL-*HMO1* strains showed an increased loss in viability compared to wt by day 14.

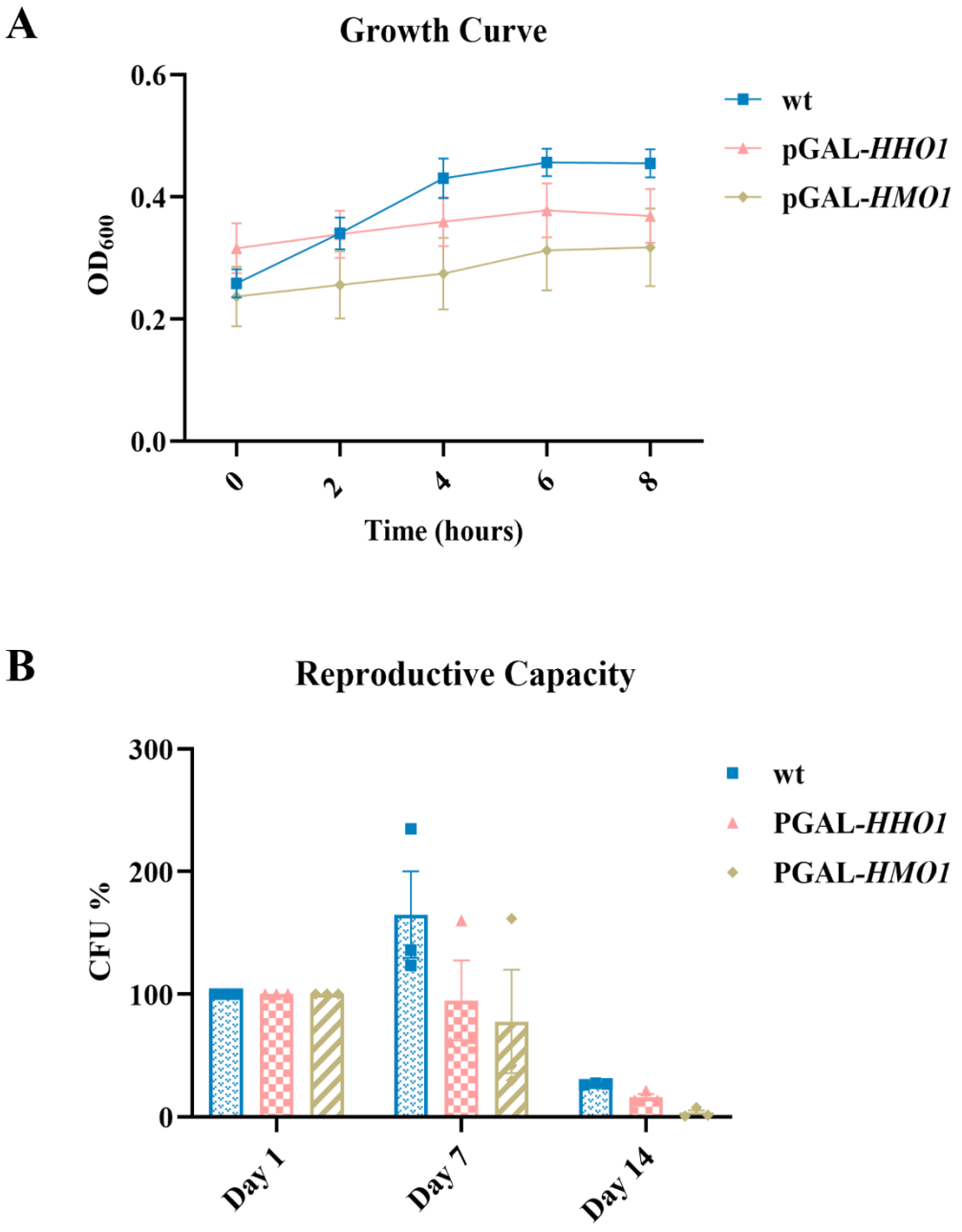

Figure 3.14: Analysis of growth characteristics of *HHO1* and *HMO1* over-expression strains compared to wt. (A) wild type (wt; empty vector) and mutants were grown at 30°C for 8 hours, and OD_{600} readings were taken at regular intervals **(B)** Viability colony-forming capacity of cells day1-7 and 14 cultures. Error bars represent the standard error of triplicate biologically independent experiments' mean (SEM).

3.2.5.2 Cell morphology of exponential and stationary phase over-expression strains

I next examined the cell morphology of the pGAL-*HHO1* and pGAL-*HMO1* strains during exponential growth and in the stationary phase {day 7}. The results showed no differences for either strain compared to wt in either exponential or stationary phase (Fig.3.15). Indeed, it is notable that the elongated cell morphology seen in the *hmo1*Δ gene deletion mutant (see Fig. 3.6) was no longer visible in the Hmo1p over-expression strain.

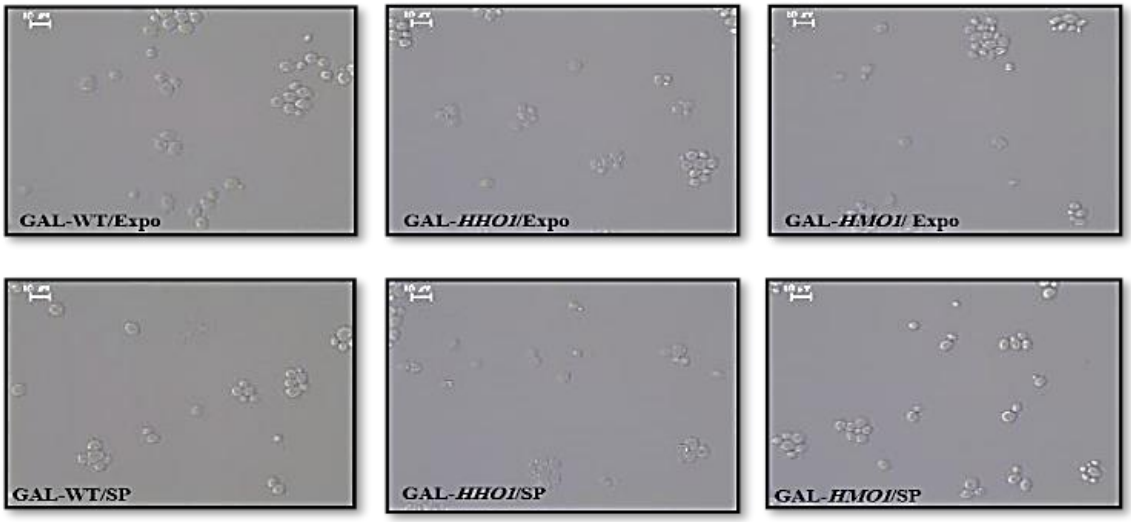

Figure 3.15: pGAL-*HHO1*, pGAL-*HMO1* strains cell morphology. The two mutant strains and wt (empty vector) were grown on SC (-U) and cells from exponential and stationary phase cultures were viewed under the microscope cells. Microscopy was conducted under a 100x immersion magnification of the oil; the white bar is 10μm. The images shown are representative of multiple cell images viewed.

3.2.5.3 Analysing thermosensitivity of cells in liquid culture

I next repeated the thermotolerance test for the over-expression strains grown in liquid culture. Interestingly, both *HHO1* and *HMO1* over-expression strains showed an increase in thermotolerance compared to wt during both exponential growth (Fig. 3.16A) and the stationary phase {day 7}(Fig. 3.16B). Thus, both Hho1p and Hmo1p seem to have a protective effect against heat exposure when the proteins are over-expressed. The differences in survival seen between wt and the mutants after heat shock were statistically significant (Fig. 3.13).

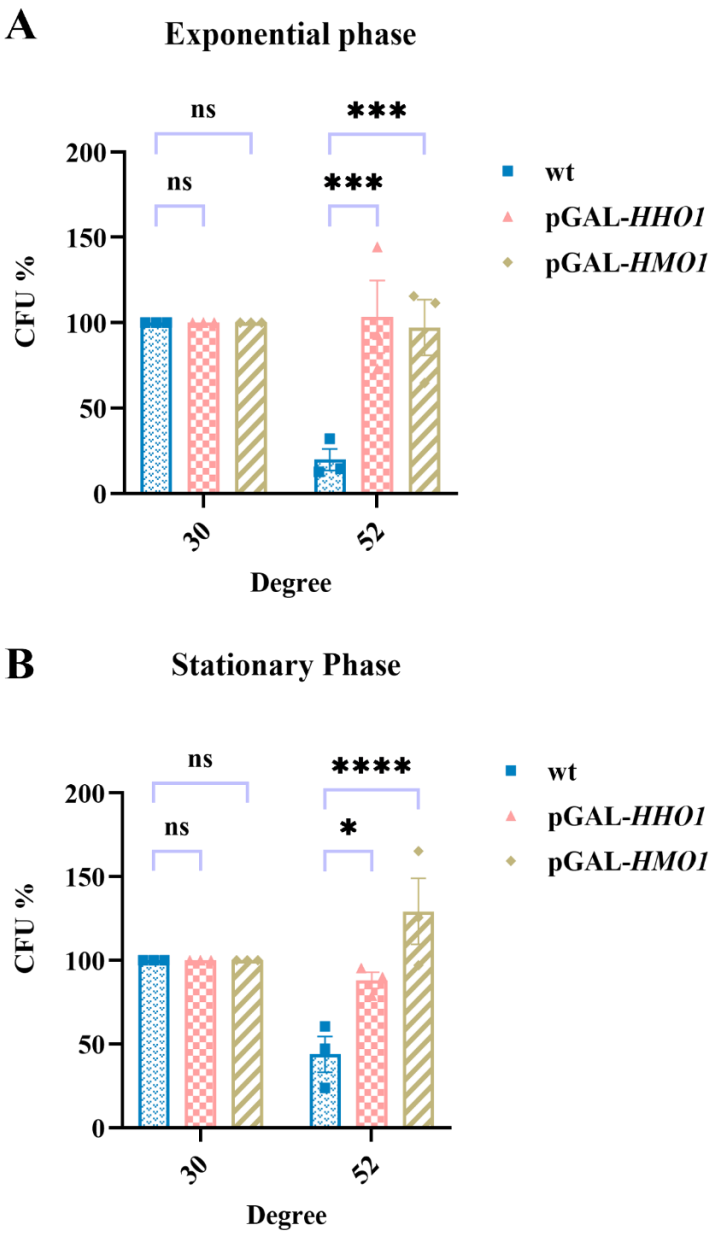

Figure 3.16: Thermotolerance of exponential and stationary phase *HMO1* and *HHO1* over-expression mutants compared to wt. Thermotolerance of cells from exponentially growing **(A)** and stationary phase on day 7 cultures **(B)** grown at 30°C and 52°C. The survival ratio of *BG1805* cells over-expressing Hmo1p and Hho1p after being incubated at the indicated temperatures for 1 hour. The y-axis shows the % of colony-forming units (CFU/ml) after heat shock compared to the CFU/ml before. Error bars represent the standard error of three to triplicate biologically independent experiments' mean (SEM). Standard significance using Two-way ANOVA analysis (* p = 0.05, ** p = 0.01, *** p = 0.005.).

3.2.6 Measuring protein abundance in *hho1*Δ and *hmo1*Δ mutants

3.2.6.1 Investigating Hmo1p and Hho1p abundance during SP

If either Hho1p or Hmo1p are functioning as linker histone during SP, I predicted that there might be an increase in their levels during SP. Following the successful epitope tagging of Hmo1p (Hmo1-myc), I performed Western blot analysis for Hho1p and Hmo1p (Hmo1-myc) on lysates that were prepared from mid-log phase (Expo) cells, cells at the diauxic shift (DX), and in unseparated SP cells that were isolated after day 5 and day 7 of growth (Fig. 3.17).

The results show that in wt cells, Hho1p and Hmo1p show the greatest levels in exponential cells and at diauxie, after which levels decrease during SP. Hho1p levels in the *hmo1*Δ mutant follow a similar profile as that seen in wt. However, Hmo1p levels in the *hho1*Δ mutant are lower in exponential phase cells, and cells at diauxie, compared to what is seen in wt. Thus, in wt cells, Hmo1p and Hho1p show reduced abundance during SP and, interestingly, the data suggests that Hho1p is required to maintain Hmo1p levels prior to entry into SP.

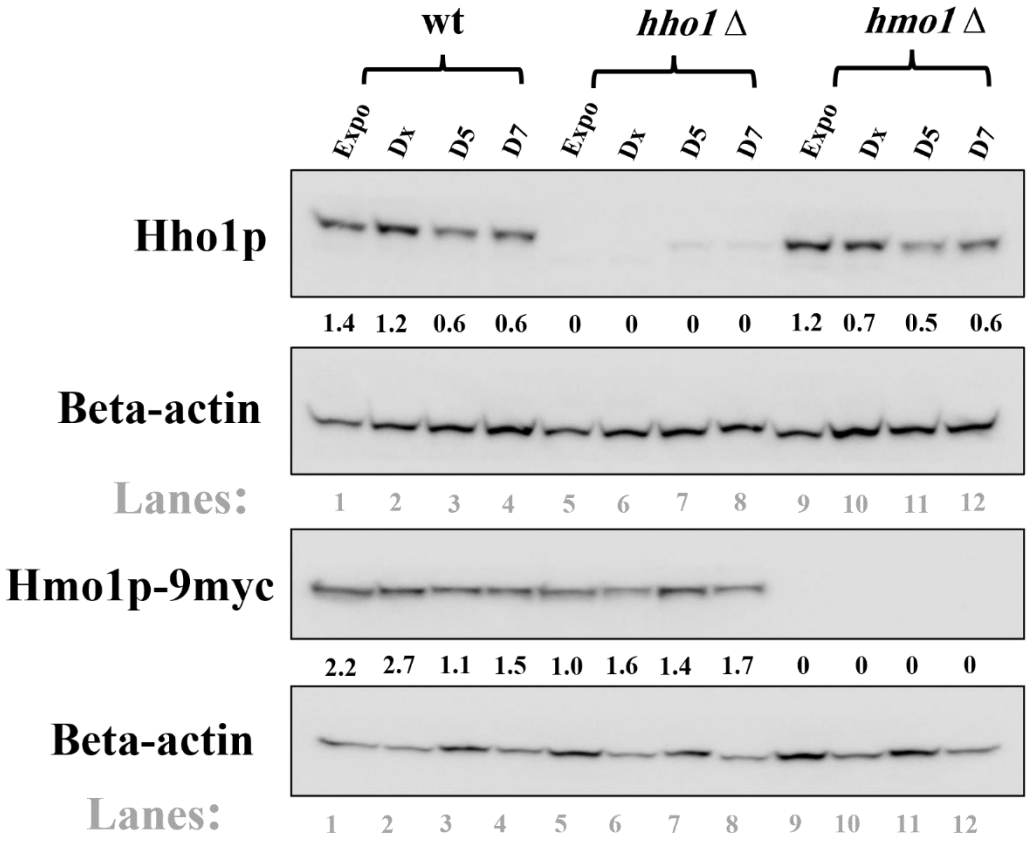

Figure 3.17: Hho1p and Hmo1p abundance. Western blot analysis of TCA extracted proteins from cells in the logarithmic phase of growth (Expo, lanes 1,5 and 9), at the diauxic shift (DX, lanes 2, 6, and 10), and in unseparated cells isolated after 5 and 7 days of growth (D5 and D7, lanes 3-4, 7, -8 and 11, -12 respectively). Antibodies specific to Hho1p and Hmo1-9myc were used for immunoblotting. Equal loading was monitored by measuring beta-actin. Representative images of reproducible data are shown. The numbers under the Hmo1-myc and Hho1p blots represents the ratio of target protein band intensity versus Actin signal intensity to enable quantification and better comparison.

3.2.6.2 Investigating RNA Pol II CTD phosphorylation levels in unseparated mutant cells during SP

RNA polymerase II (RNAP II) drives mRNA transcription in yeast (Nechaev and Adelman, 2011). In its active form, it is phosphorylated on the serine-2 and serine-5 residues in the carboxy-terminal domain (CTD) of the Rpb3 subunit (Nechaev and Adelman, 2011; Fuchs *et al.*, 2009). I wanted to investigate if the active forms of RNAP II were increased in stationary phase cells of the *hmo1*Δ and *hho1*Δ mutant cells, which would be the prediction if Hmo1p and Hho1p were acting to repress transcription during SP. I first examined the abundance of the RNAPII machinery using an antibody that does not distinguish between the active and inactive forms of RNAP II to determine the base levels of RNAP II in wt and mutant cells at mid-log phase (Expo), at the diauxic shift (DX), and at day 5, and day 7 of growth (Fig. 3.18, Pol II). The results showed that in wt cells, RNAP II remains at a constant level at all growth stages tested. RNA Pol II levels showed a similar profile to wt in the *hmo1*Δ mutant. However, levels in the *hho1*Δ mutant were greater in exponential cells, and in cells at diauxic, compared to wt.

I next examined the serine 2 and serine 5 phosphorylated forms of RNAPII in wt and mutant cells throughout growth into SP (Fig. 3.18, Pol II serine 2-P/ Pol II serine-5-P). In wt, levels were high during exponential growth and at diauxie, but dropped in the day 5 and day 7 grown SP cells. A similar profile as that seen in wt was apparent for Pol II ser2-P and Pol II ser-5-P in both mutants, although Pol II Ser-5-P levels in the *hho1*Δ mutant were higher than wt at day 5 before dropping to wt levels.

This suggests that in wt and the *hmo1*Δ mutant, Pol II levels remain constant during exponential growth and during SP, but Pol II is predominantly inactive (low ser-2 and ser-5-P levels) during SP. However, in the *hho1*Δ mutant, Pol II levels are elevated in exponential phase and in cells at diauxie, and Pol II ser-5-P levels remain high in day 5 cells.

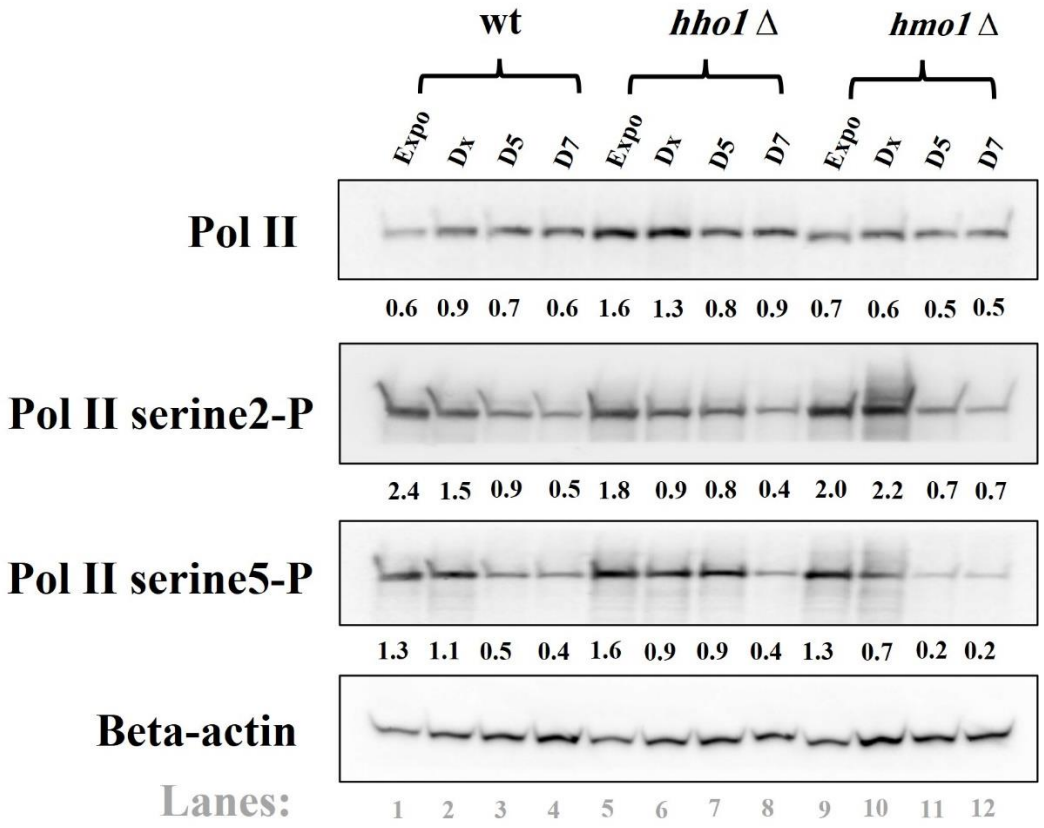

Figure 3.18: RNAP II persists in SP but in a non-initiating and non-elongating form. Western blot analysis of TCA extracted proteins from cells in the logarithmic phase of growth (Expo, lanes 1,5 and 9), isolation of population cells on diauxic shift (DX, lanes 2, 6, and 10), and unseparation cells isolated after 5 and 7 days of growth (D5 and D7, lanes 3-4, 7, -8 and 11, -12 respectively). Antibodies were specific to RNAP II, RNAP II Ser2-P, and RNAP II Ser5-P for immunoblotting. Equal loading was monitored by measuring beta-actin, and representative blots are shown. The numbers under the Pol II blots represents the ratio of target protein band intensity versus actin signal intensity to enable quantification and better comparison.

3.2.6.3 Examination of histone post-translational modifications in mutant cells during growth into SP

Histone methylation (me) at H3K4, H3K36, and H3K79 are all associated with active transcription (Liu *et al.*, 2005; Rando, 2007).

A previous study from our laboratory demonstrated that despite an overall shutdown of transcription in SP cells, H3K4me3, H3K36me3, H3K79me3, and H3K79me2 levels were retained within day 7 SP cells (Young *et al.*, 2017, BMC Genomics). I therefore examined these marks in the *hho1*Δ and *hmo1*Δ mutant cells to determine whether there might be an altered abundance of these transcription-associated modifications in the absence of Hho1p and Hmo1p.

3.2.6.3.1 Histone H3K4 H3K36 and H3K79 methylation levels during growth into SP

Western blot analysis was initially performed using antibodies specific to H3K4me^3 and H3K36me^3 (Figure 3.19). These data revealed that H3K4 methylation marks in wt remained more or less constant throughout the growth period measured. However, H3K4me levels were reduced in the *hho1*Δ and *hmo1*Δ mutant day 5 and day 7 cells (Fig 3.19A).

Interestingly, the levels of H3K36me^3 in wt were undetectable in SP cells but were detectable in *hho1*Δ and *hmo1*Δ mutant SP cells. Thus, whereas H3K36me3 is lost during SP in wt cells, this mark persists in SP cells of the *hho1*Δ and *hmo1*Δ mutants. Conversely, H3K4me3 levels are reduced in mutant SP cells compared to wt, where this mark persists. The levels of both H3K79me3 and H3K79me2 in wild-type (wt) cells remained consistent throughout the measured growth period. However, the quantification of the H3K79me3 data suggested the *hmo1*Δ and *hho1*Δ mutants had higher levels of this modification in exponential phase cells and at diauxie. The levels of H3K79me^2 showed no significant variation across all studied stages of growth in wt and in both mutants (Fig. 3.19B) indicating that its level does not depend on the growth stage or the presence of Hmo1p or Hho1p.

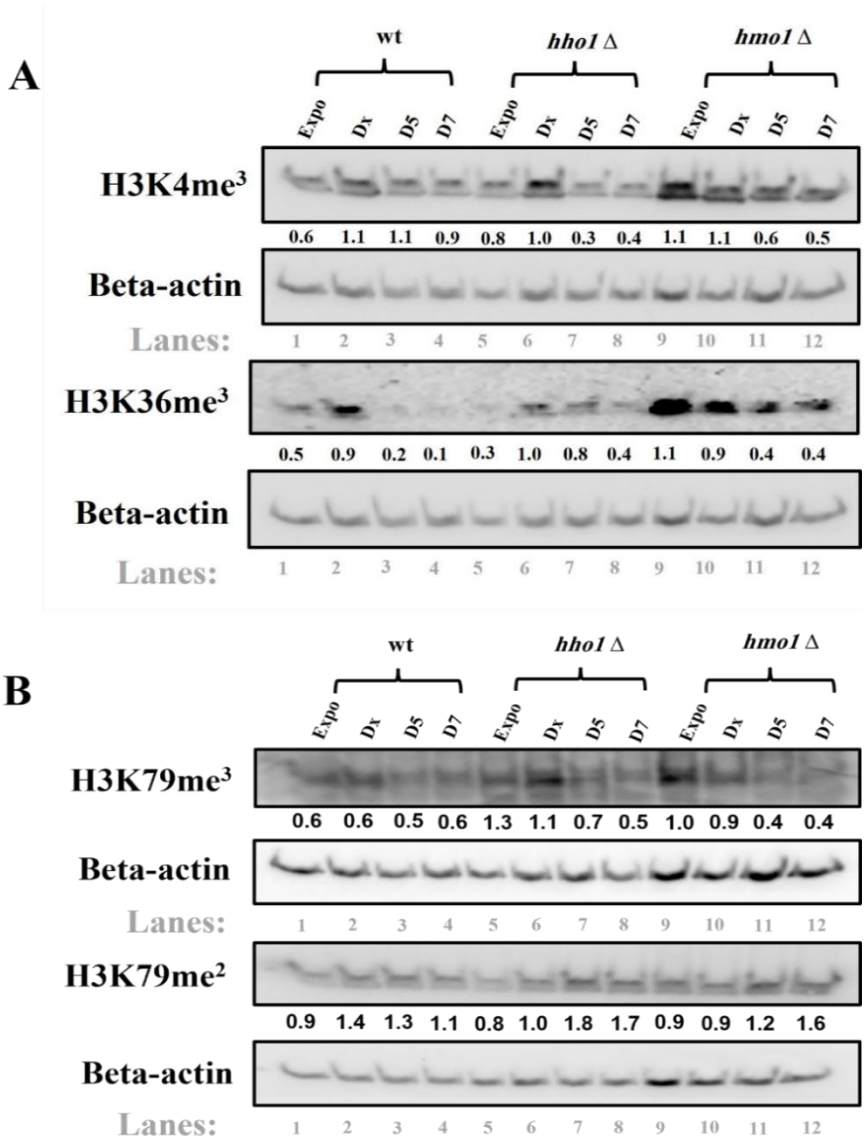

Figure 3.19: Measuring H3K4, H3K36, and H3K79 methylation levels during stationary phase. Western blot analysis of TCA extracted proteins from cells in the logarithmic phase of growth (Expo, lanes 1,5 and 9), isolation of population cells on diauxic shift (DX, lanes 2, 6, and 10), and unseparation cells isolated after 5 and 7 days of growth (D5 and D7, lanes 3-4, 7, -8 and 11, -12 respectively). Antibodies were specific to H3K4me^3, H3K36me^3, H3K79me^3, and H3K79me^2 for immunoblotting. Equal loading was monitored by measuring beta-actin. Representative images of reproducible data are shown. The numbers under the blots represents the ratio of target protein band intensity versus actin signal intensity to enable quantification.

3.2.6.3.2 H2B monoubiquitylation levels during growth into SP

The Rad6/Bre1 ubiquitin-ligase complex catalyzes mono-ubiquitylation of H2B (H2Bub1) which aids in promoting both transcriptional initiation and elongation. (Robzyk *et al.*, 2000; Xiao *et al.*, 2005; Fleming *et al.*, 2008).

H2Bub1 is also essential for the di- and tri-methylation of H3K4 and H3K79 and is thus a key regulator of other histone modifications (Nakanishi *et al.*, 2009). It has been demonstrated that H2Bub1 is induced by carbohydrates in yeast and that H2B ubiquitylation disappears in response to glucose depletion at diauxie (Dong and Xu, 2004). I therefore wanted to test if there would be any difference in the prevalence of H2Bub1 as cells enter into SP in the *hho1*Δ and *hmo1*Δ mutant cells.

As before, western blot analysis was performed on lysates prepared from mid-log phase (Expo) cells, cells at the diauxic shift (DX), and in unseparated stationary phase cells that were isolated at 5- and 7 days of growth to determine the timing of H2Bub1 depletion and to investigate whether the point at which H2Bub1 was lost differed between the *hho1*Δ and *hmo1*Δ mutants. The antibody used in this study was against histone H2B. This enables the detection of unmodified and ubiquitylated H2B due to the difference in their molecular weights; 14 kDa for H2B, and 22 kDa for H2Bub1.

Consistent with published data, H2Bub1 was present in wt mid-log phase cells (Figure 3.20A, lanes 1,5 and 9) but was significantly reduced following glucose depletion (Figure 3.20, lanes 2,3,4,6,7,8,10,11 and 12, respectively) (Dong and Xu, 2004). Interestingly, there was a greater abundance of H2Bub1 in *hho1*Δ and *hmo1*Δ exponential cells compared to wt. Also of note, whereas a small amount of H2Bub was visible in wt day 5 and -7 SP cells, the loss of H2Bub in mutant day 5 and 7 cells seemed almost complete (Fig. 3.20B).

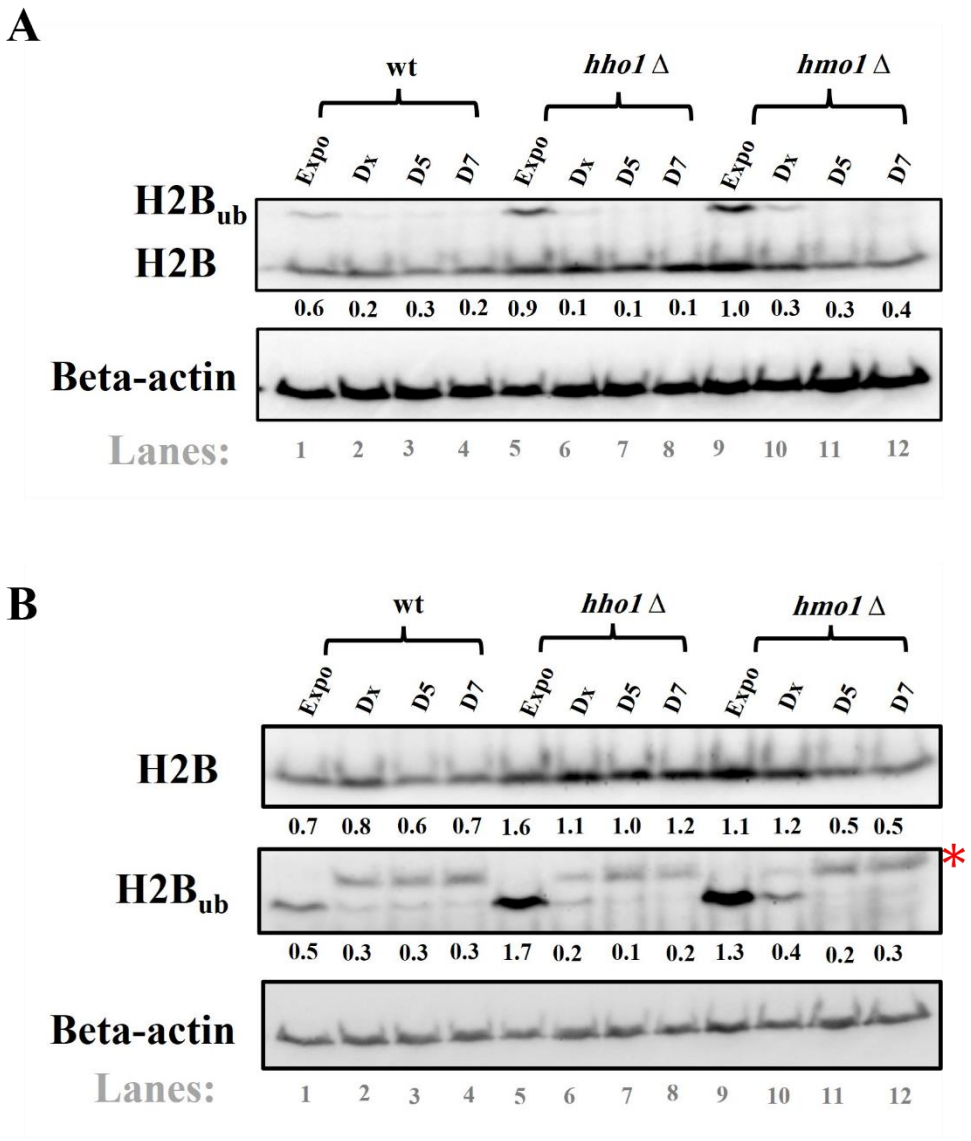

Figure 3.20: H2Bub is lost in both SP populations. Western blot analysis of TCA extracted proteins from cells in the logarithmic phase of growth (Expo, lanes 1,5 and 9), cells at the diauxic shift (DX, lanes 2, 6, and 10), and in unseparated cells isolated after 5 and 7 days of growth (D5 and D7, lanes 3-4, 7, -8 and 11, -12 respectively). Antibodies were specific to H2B. Equal loading was monitored by detection of beta-actin. Representative images of reproducible data are shown. The numbers below each lane correspond to the quantification of each target band (target protein intensity/actin band intensity). **(A)** histone H2B and H2Bub1 detection, **(B)** a biological replicate of histone H2B and H2Bub1 detection. The asterisk represents a non-specific band.

3.2.6.3.3 Investigating histone H2A Ser129 phosphorylation and histone H3 Ser10 phosphorylation during growth of mutants into SP

Protein modification through phosphorylation is a widely known process; however, it occurs infrequently on histones (Fuchs *et al.*, 2009; Lo *et al.*, 2001). Like other mechanisms, histone phosphorylation can be influenced by changes in the extracellular environment. H3S10 phosphorylation promotes transcription, chromatin remodelling and mRNA processing by affecting H3K14 acetylation in response to fluctuations in the carbon source levels (Fuchs *et al.*, 2009; Lo *et al.*, 2001).

H2A phosphorylation at the C-terminus is linked to DNA damage repair, with H2A phosphorylation being one of the first marks occurring on chromatin in response to DNA double strand breaks (Downs *et al.*, 2000).

I therefore examined these histone phosphorylation events in the *hmo1*Δ and *hho1*Δ mutants during growth into SP to determine if Hmo1p and Hho1p might influence these modifications (Figure 3.21).

Examination of H3 serine 10 phosphorylation showed that in wt this modification was present in exponential cells and cells at diauxic but was absent in SP cells. The *hho1*Δ mutant cells showed a similar profile as wt of this modification during growth into SP, but levels of this mark were reduced at both early cell growth stages compared to wt. Strikingly, no H3 serine 10 phosphate could be detected in the *hmo1*Δ mutant at any of the times tested.

Analysis of H2A-ser129 phosphorylation in wt showed a strong signal in exponential cells and a signal which was 2-fold less than that in exponential cells in the diauxic cells, whilst the modification was largely absent during SP. However, the levels of this modification in the *hho1*Δ mutant were higher than wt levels in the diauxic cells and, most strikingly, the modification was still present in SP *hho1*Δ mutant cells. The *hmo1*Δ mutant showed a profile for this modification across the growth stages tested more similar to wt. Together, the *hho1*Δ mutant showed aberrant H2A ser 129 and H3 ser 10 phosphorylation levels, whilst H3 ser 10 levels were undetectable in *hmo1*Δ at all stages of growth.

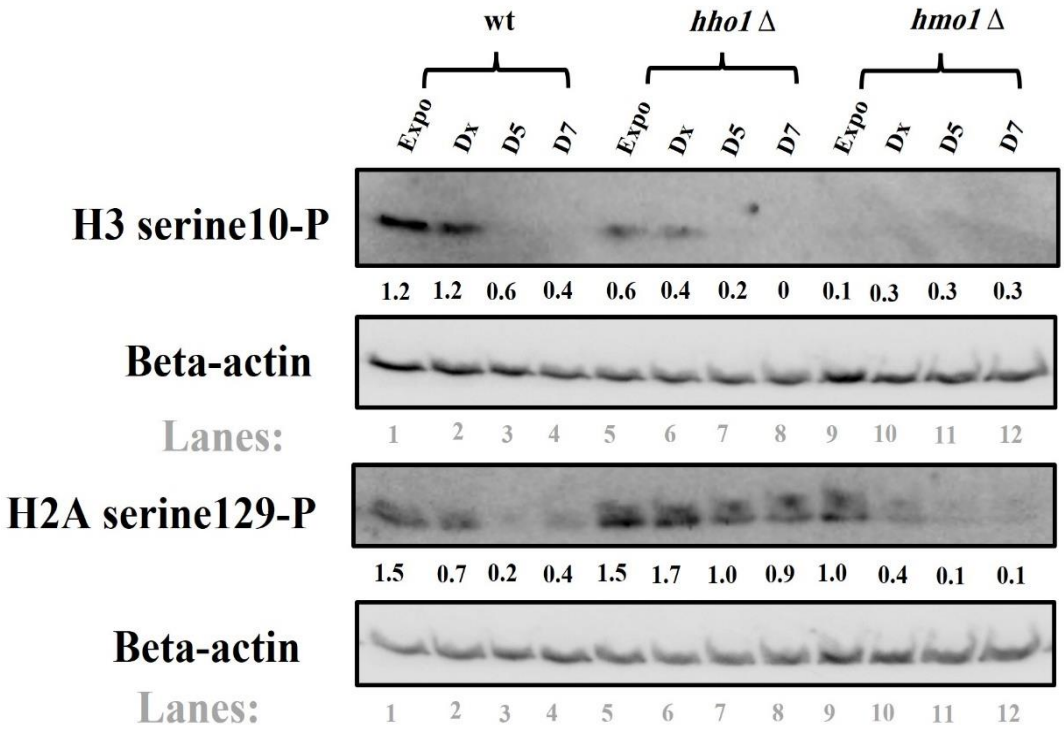

Figure 3.21: Measuring H3 and H2A phosphorylation levels during SP. Western blot analysis of TCA extracted proteins from mid-log phase cells (Expo, lanes 1, 5, and 9), Diauxic shift (DX, lanes 2, 6, and 10), and from stationary phase unseparation cells isolated after 5, 7 days of growth (D5 and D7, lanes 3, 4, 7, 8, 11 and 12). Antibodies specific to H3-ser10 and H2A-ser-129 were used for immunoblotting. Beta-actin loading controls are shown. Representative images of reproducible data are shown. The numbers below each lane correspond to the quantification of each target band (target protein intensity/actin band intensity).

3.2.6.3.4 Histone acetylation levels during growth of the mutants into SP

Histone acetylation is another transcription-related PTM that has been linked to active transcription, DNA replication (H3K56ac) and chromatin compaction (H4K16ac) (Dang *et al.*, 2009). The activity of various histone acetylases and histone deacetylase enzymes (HATs) antagonistically regulate this highly dynamic modification which is known to be largely reduced in SP cells (Young *et al.*, 2017; Bailey *et al.*, 2022).

Western blot analysis was performed using antibodies against H3K14ac and tetra-acetylated H4 ($H4ac^4$) (Figure 3.22). Consistent with published data, both acetylation marks were dramatically reduced in wt day 5 and 7 SP cells. The same result was seen for the *hho1*Δ mutant. However, although the marks were lost in *hmo1*Δ mutant SP cells, the abundance of these marks in the *hmo1*Δ mutant exponential and diauxic cells was higher than that seen in wt.

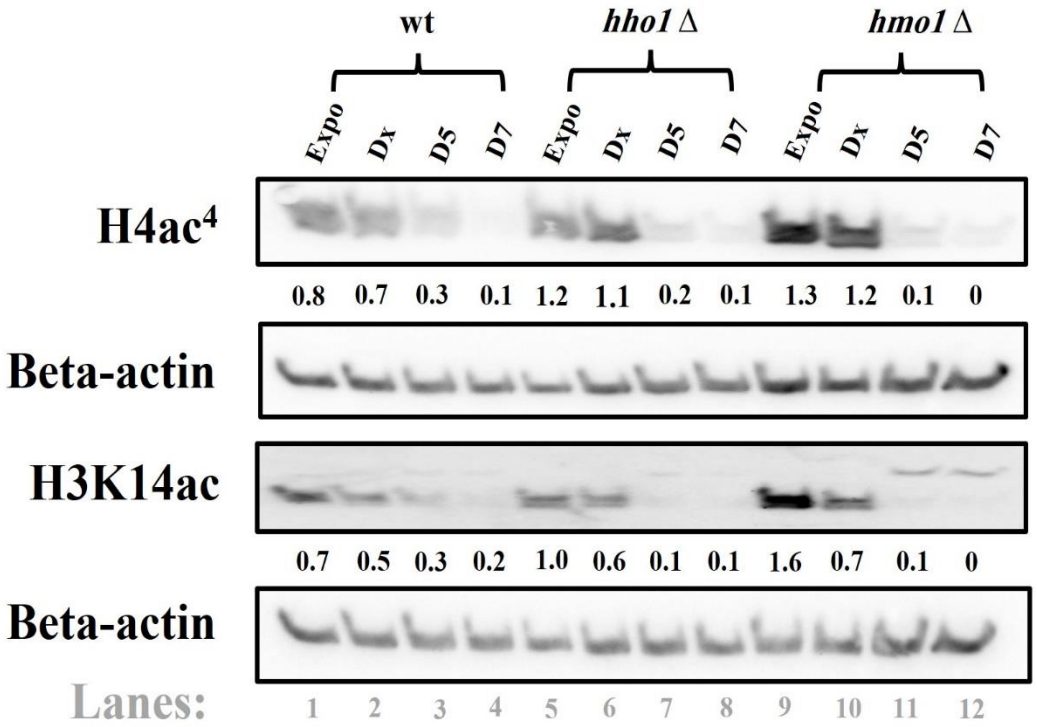

Figure 3.22: Histone acetylation is depleted during entry into SP. Western blot analysis of TCA extracted proteins from cells in the logarithmic phase of growth (Expo, lanes 1,5 and 9), isolation of population cells on diauxic shift (DX, lanes 2, 6, and 10), and unseparation cells isolated after 5 and 7 days of growth (D5 and D7, lanes 3-4, 7, -8 and 11, -12 respectively). Antibodies were specific to H3K14ac and acetylated H4 (H4ac4) for immunoblotting. Equal loading was monitored by measuring beta-actin. Representative images of reproducible data are shown. The numbers below each lane correspond to the quantification of each target band (target protein intensity/actin band intensity).

3.2.6.4 Examining the regulators of histone acetylation as cells enter into SP

The addition of acetyl moieties to lysine residues of both H3 and H4 is catalyzed by histone acetyltransferases (HATs) and is antagonized by histone deacetylases (HDACs) (Grant *et al.*, 1997; Allard *et al.*, 1999). Gcn5p, the catalytic subunit of the SAGA complex, is a HAT known to catalyze the acetylation of both H3K9 and H3K14 (Robert *et al.*, 2004; Pokholok *et al.*, 2005).

We sought to determine whether the loss of both H4ac^4 and H3K14ac during SP correlated with a decrease in Gcn5p levels, and if this expected relationship might be altered in the mutants. Western blot analysis using a Gcn5p-specific antibody revealed that the Gcn5p levels detectable in wt exponential cells were decreased in the diauxic cells and were largely absent in wt SP cells. This Gcn5p profile observed in wt was also seen in both mutants (Figure 3.23).

I next examined the HDAC, Rpd3p. As can be seen, Rpd3p levels were equally high in wt cells at every stage of growth tested. The mutants both showed a similar Rpd3p abundance profile as wt. Thus, Gcn5p and Rpd3p, which together can regulate histone acetylation levels are unaffected by loss of either *HMO1* or *HHO1*.

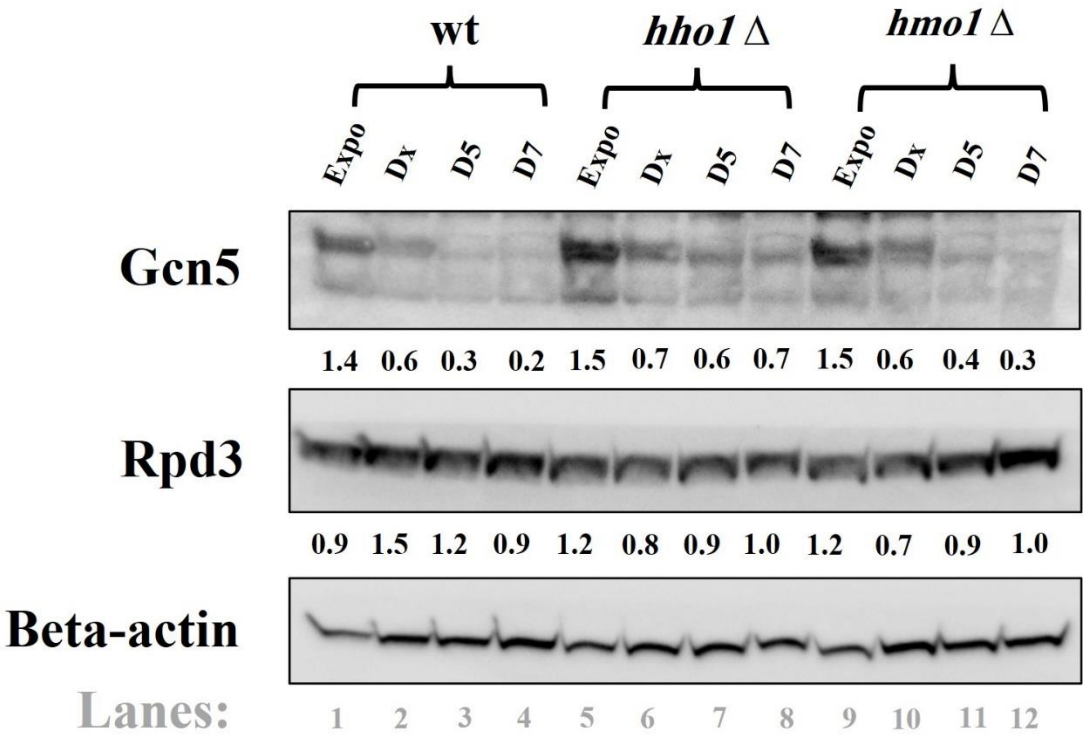

Figure 3.23: HAT and HDAC levels during SP. Western blot analysis of TCA extracted proteins from cells in the logarithmic phase of growth (Expo, lanes 1,5 and 9), isolation of population cells on diauxic shift (DX, lanes 2, 6, and 10), and unseparation cells isolated after 5 and 7 days of growth (D5 and D7, lanes 3-4, 7, -8 and 11, -12 respectively). Antibodies were specific to the HAT (Gcn5) and HDACs (Rpd3) for immunoblotting. Equal loading was monitored by measuring beta-actin. Representative images of reproducible data are shown. The numbers below each lane correspond to the quantification of each target band (target protein intensity/actin band intensity).

3.2.6.5 Analysing core histone levels as cells grow into SP

To investigate the structure of SP chromatin in the mutants, the initial step was to measure core histone protein levels during growth into SP using commercially available antibodies for histones H3, H4, H2A, and H2B. As before, Western blot analysis on lysates from cells at mid-log phase (Expo), at the diauxic shift (DX), and in cells that were isolated after 5 and 7 days of growth during stationary phase, was performed. The results showed that H2A and H2B levels remained at a constant level in wt cells at each stage of growth tested. However, H2A and H2B levels in the *hho1*Δ mutant were higher than wt in the diauxic cells, and in the SP cells. Conversely, the data suggested that the H2A and H2B levels in the *hmo1*Δ mutant were higher than wt in exponential phase and at diauxie. (Figure 3.24A).

Histone H3 levels in wt remained constant throughout the growth period tested. However, H3 levels were higher in the *hho1*Δ mutant diauxic and SP cells compared to wt and *hmo1*Δ mutants (Figure 3.24B). Conversely, H3 levels were higher in the pre-SP *hmo1*Δ cells compared to wt.

Interestingly, histone H4 levels in wt were highest in exponential cells, and sequentially dropped lower as cells entered into SP. This profile was also seen in the *hmo1*Δ mutant cells. However, in the *hho1*Δ mutant cells, histone H4 levels were greater than that seen in wt at diauxic and beyond (Figure 3.24B). Thus, overall, these data suggest that the *hho1*Δ mutant has greater levels of the core histones in post exponential cells compared to what was seen in wt and the *hmo1*Δ mutant, whereas the *hmo1*Δ mutant has greater histone levels than wt prior to entry into SP.

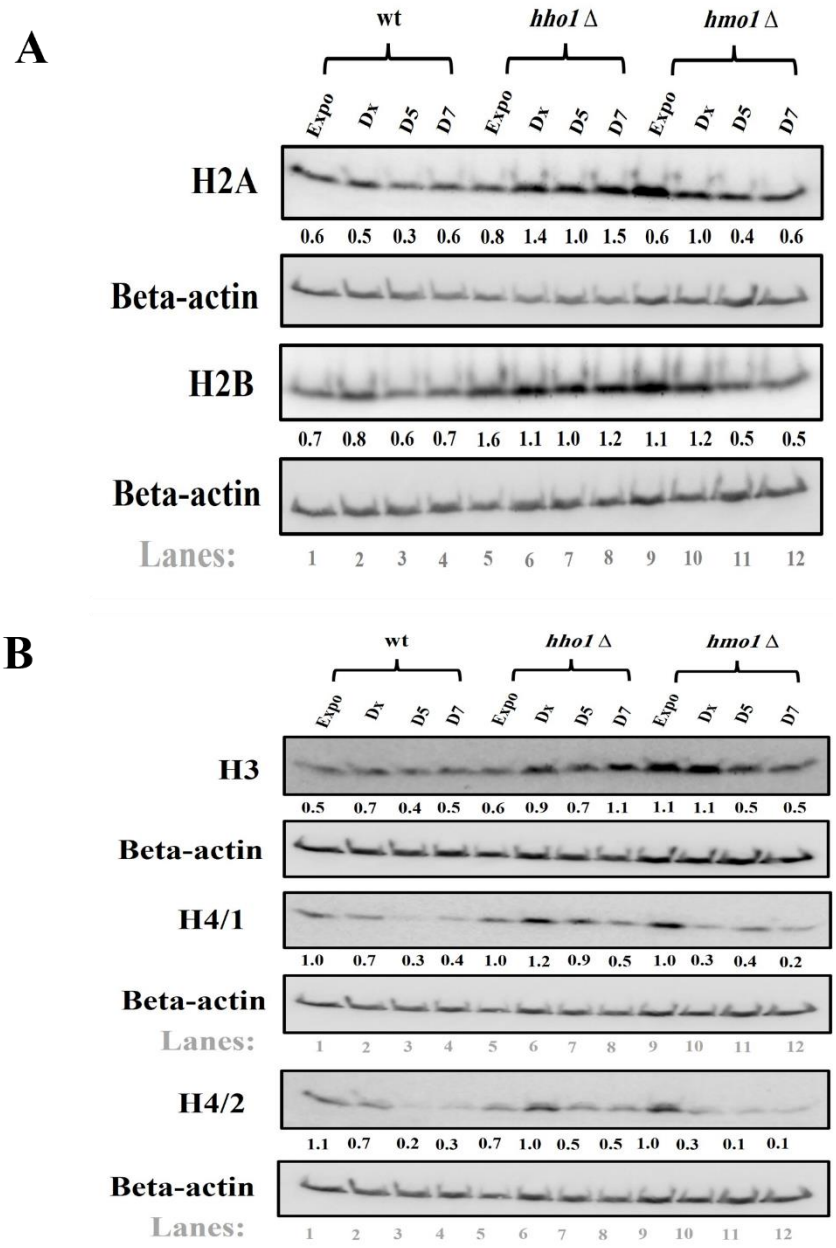

Figure 3.24: Core histone protein abundance during growth into stationary phase. (A) Western blot analysis of TCA extracted proteins from mid-log phase cells (Expo, lanes 1, 5, and 9), Diauxic shift (DX, lanes 2, 6, and 10), and from stationary phase unseparated cells isolated after 5, 7 days of growth (D5 and D7, lanes 3, 4, 7, 8, 11 and 12). Antibodies specific to H2A and H2B were used for immunoblotting. **(B)** Western blot analysis of TCA lysates using antibodies specific to H3 and H4. Beta-actin loading controls are shown (A and B). Representative images of reproducible data are shown. Results from two biological replicates are shown for the histone H4 blot; labelled as H4/1 and H4/2.

3.2.6.5.1 Levels of the non-canonical histones variant, H2A.Z (Htz1)

Apart from the four core histones (H2A, H2B, H3, and H4), there are a few variants of these histones in yeast that can perform alternate functions (Redon *et al.*, 2002). In yeast, H2A.Z (Htz1) and Cse4p (also known as CENP-A in metazoans) are two such variants which can replace histone H2A and H3, respectively (Stoler *et al.*, 1995; Meluh *et al.*, 1998).

Htz1p can be found in the promoter regions of genes instead of H2A, and nucleosomes containing Htz1p are considered less stable than those containing H2A suggesting they may have a role in marking gene promoters for rapid activation (Keogh *et al.*, 2006; Millar *et al.*, 2006).

It was hypothesized that Htz1p abundance might increase during SP in wt cells to facilitate a quick response back into vegetative growth in response to appropriate environmental changes. The western blot analysis showed that the abundance of Htz1p protein in wt remained fairly constant over the sampling period as cells grew into SP (Figure 3.25, respectively, lanes 3-4, 7-8 and 11-12). Interestingly however, the data suggests that Htz1p levels increased in both mutant cells after exponential phase.

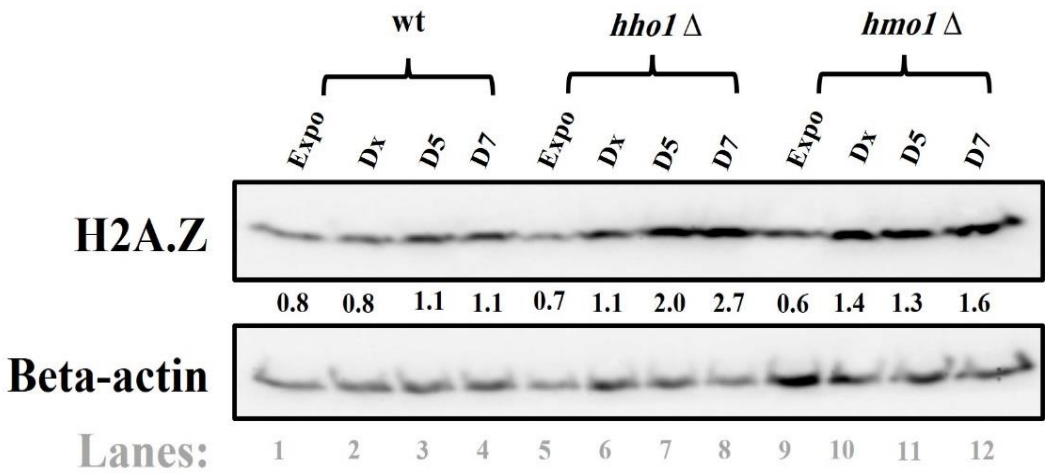

Figure 3.25: The non-canonical histone H2A.Z levels during SP. Western blot analysis of TCA extracted proteins from mid-log phase cells (Expo), at the diauxic shift (DX), and from unseparated stationary phase cells isolated after 5 and 7 days of growth (D5 and D7). Antibodies specific to H2A.Z (Htz1p) were used for immunoblotting. Beta-actin loading controls are shown. Representative images of reproducible data are shown.

3.2.6.6 Investigating chromatin remodelling complexes during growth into SP

Chromatin structure and function can be regulated by various chromatin remodelling complexes. For example, ATP-dependent remodellers such as Swi-Snf can 'open' chromatin up to activate gene transcription, whilst remodellers such as Tup1-Cyc8 complex can 'close' chromatin to repress gene transcription (Nagy and Tora, 2007).

I therefore analysed Tup1-Cyc8 co-repressor complex levels in wt and mutant cells during growth into SP as this complex is normally required for chromatin compaction and gene repression; two processes which have been proposed to occur in SP (Schäfer *et al.*, 2008). I wanted to determine whether the abundance of Tup1-Cyc8, and hence its activity, might be disrupted in the absence of Hho1p and Hmo1p during SP. This was pertinent to investigate, considering Tup1-Cyc8 has recently been shown to function during SP (Bailey *et al.*, 2022).

Interestingly, in wt cells, Tup1p and Cyc8p levels decreased after exponential growth despite recent data showing a role for Tup1-Cyc8 in gene repression during SP. However, there was no significant difference in Tup1p and Cyc8p levels in either of the mutants compared to wt at any of the growth stages tested (Figure 3.26).

I then examined levels of the Swi-Snf subunit, Snf2p, in wt and mutant cells as they grew into SP. Opposite to expectation, in wt, Snf2p levels remained at a constant level in all stages of growth into SP; a profile unaltered in both of the mutants (Figure 3.26). Thus, the Tup1-Cyc8 repressor seems to lose abundance during SP, whereas the Swi-Snf co-activator persists at an equal level throughout exponential phase and into SP. Importantly, there is no difference in either Swi-Snf or Tup1-Cyc8 abundance in either of the mutants compared to wt.

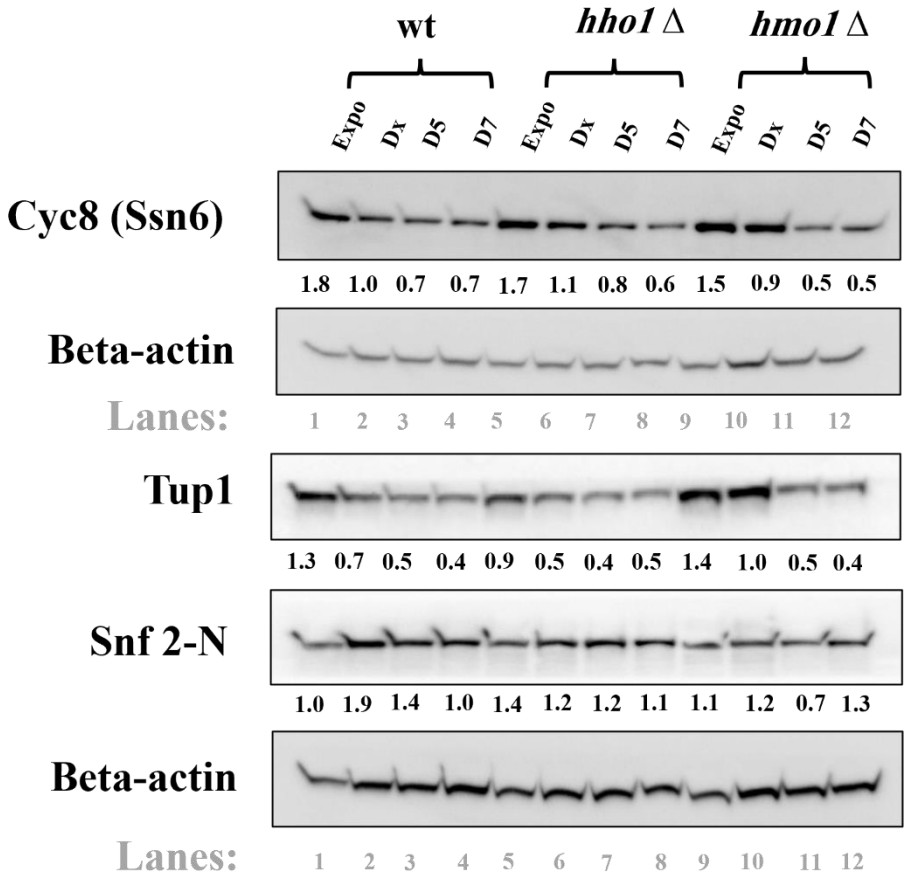

Figure 3.26: Chromatin remodelling levels during SP. Western blot analysis of TCA extracted proteins from mid-log phase cells (Expo, lanes 1, 5, and 9), Diauxic shift (DX, lanes 2, 6, and 10), and from stationary phase unseparation cells isolated after 5, 7 days of growth (D5 and D7, lanes 3, 4, 7, 8, 11 and 12). Antibodies specific to Tup1, Snf2-N, and Cyc8 (Ssn6) were used for immunoblotting. Beta-actin loading controls are shown. Representative images of reproducible data are shown. The number for Quantification to quantify, analyze, and detect bands in western blots and other gel images.

3.2.7 Chromatin Structure Analysis

Previous work had suggested that chromatin is compacted during SP and that Hho1p plays a role in this process (Georgieva *et al.*, 2012). In conjunction with our collaborator, I performed a preliminary analysis of chromatin structure in exponentially growing wt and *hho1*Δ mutant cells using the Comet assay (Fig. 3.27).

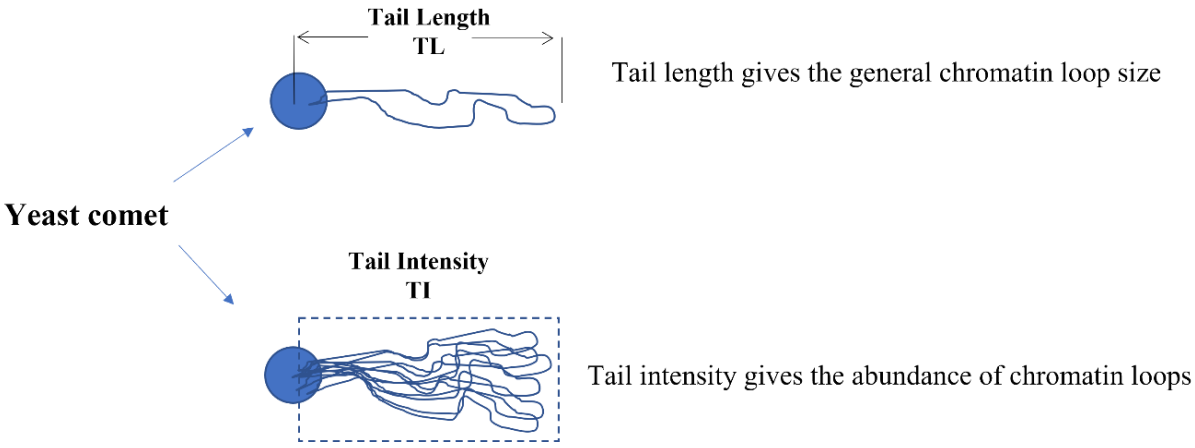

Figure 3.27: The Chromatin Comet Assay (ChCA). DNA loops protruding from the comet head are schematically drawn. Chromatin loops can have their tail length (TL) and intensity (TI) quantified by the comet assay to offer insight into higher order chromatin structure (Georgieva et al., *BBA Gen Reg Mechanisms*, 1819 (5): 366-374).

The 'Comet Assay' is a test of the sensitivity of chromatin in cells to digestion by Micrococcal Nuclease A (MNase). High chromatin compaction is resistant to digestion, resulting in shorter chromatin tails. Decreased compaction increases sensitivity to digestion, giving longer tails. Overall, using this technique, we can assess the relative size and abundance of chromatin loops within cell nuclei which can inform us of higher order chromatin structure.

The aim was to test the hypothesis that Hho1p (and/or Hmo1p) promotes chromatin compaction in cells. If the hypothesis is true, chromatin should be less compacted in the *hho1*Δ and *hmo1*Δ cells, and more sensitive to digestion with MnaseA.

In my initial analysis using this assay I only investigated chromatin structure in the exponentially growing *hho1*Δ mutant and wt cells (Fig 3. 28). The results revealed a difference in the accessibility of the yeast chromatin at its higher-order structure in the *hho1*Δ mutant with the comet tail length being longer in the *hho1*Δ mutant compared to wt, at least when treated with a lower concentration of MNase (Fig 3.28 B, C 10u). The trend of tail shortening was also different for the two strains; the wt had some pausing (increased resistance to digestion) at the MNase concentration of 25 -50 u/ml, whereas this trend was absent in the *hho1*Δ mutant (Fig 3.28 D). Together, these data suggest nuclear chromatin in the *hho1*Δ mutant was more susceptible to Mnase digestion indicating a potentially less compacted structure in this mutant.

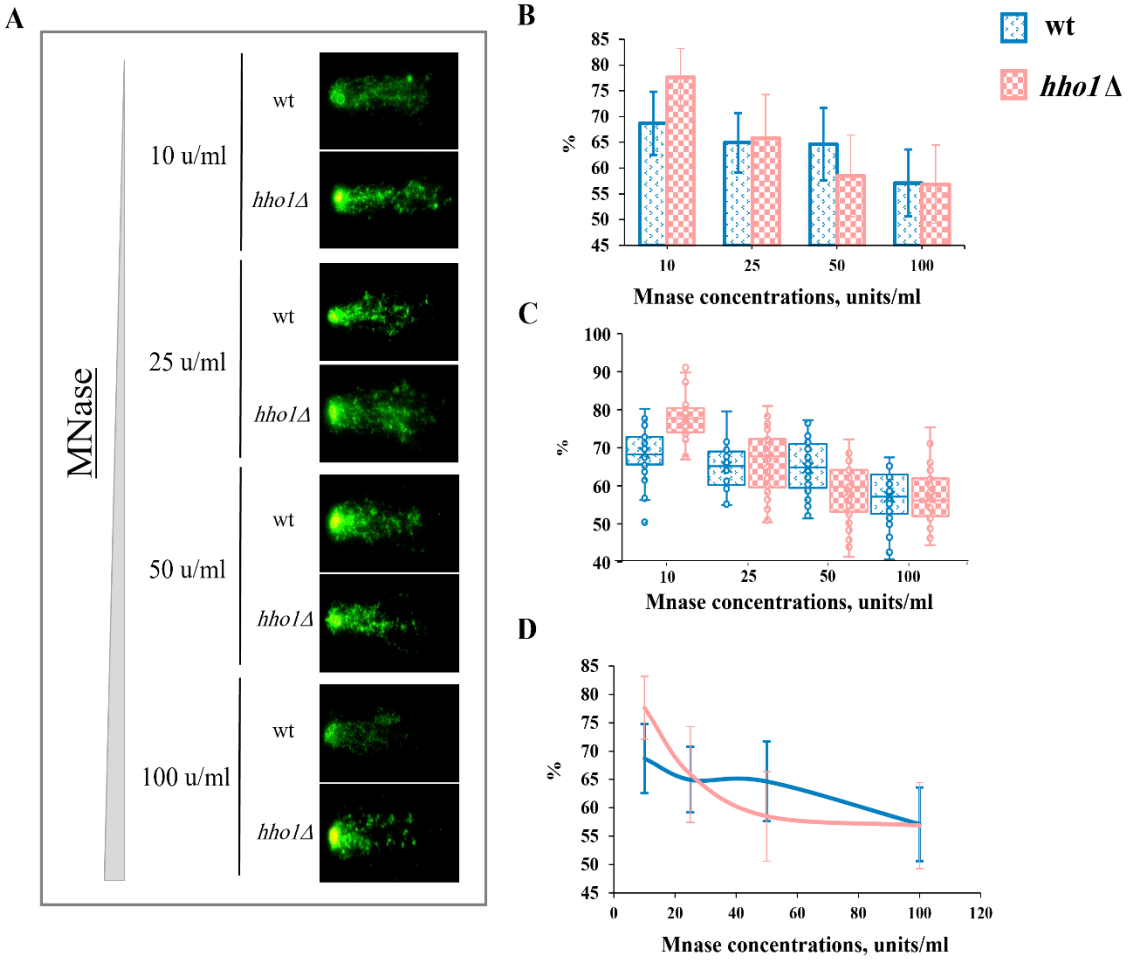

Figure 3.28: Comet assay to test chromatin compaction. (A) Images of comets formed following MNase digestion of exponentially growing wt and *hho1*Δ. Approximately 20 images were taken from every single slide from every MNase concentration. The specialized software Comet Score assessed the comets in these images (Georgieva et al., *BBA Gen Reg Mechanisms*, 1819 (5): 366-374). **(B)** Comet tail length. **(C)** Comet tail length size distribution. **(D)** The trend of comet tail shortening.

When the experiment was repeated for exponentially growing *hmo1*Δ mutant cells, the results revealed that, although tail length in the *hho1*Δ and *hmo1*Δ mutants were similar, there was no difference in tail length for either mutant compared to wt (Fig 3.29A). Although these results contrasted with the previous experiment, the data did show that tail intensity was greater in the *hmo1*Δ mutant than that in the wt and *hho1*Δ mutant (Fig 3.29B).

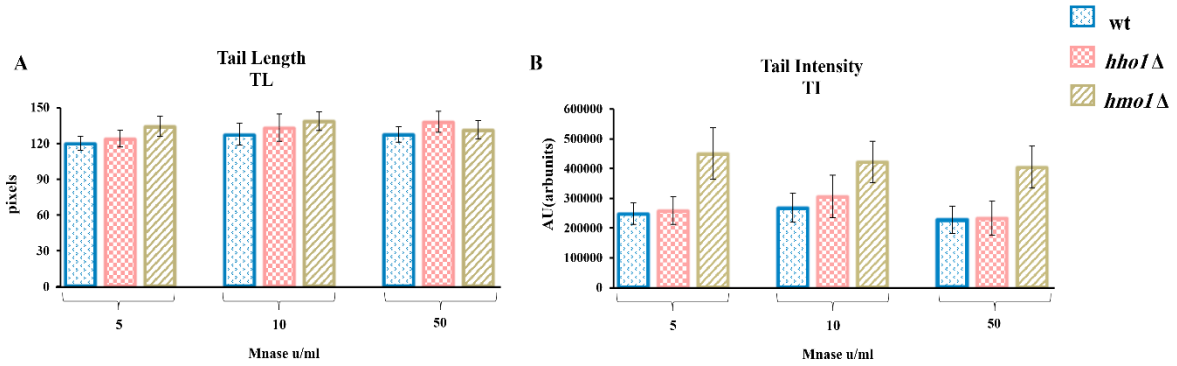

Figure 3.29: Comet assay in wt, *hho1*Δ and *hmo1*Δ mutant cells. Measurement of the parameter of 50 comets for each Mnase concentration differences between wild-type, *HHO1* and *HMO1* cells **(A)** Tail Length **(TL) (B)** Tail Intensity **(TI)**. The measurements were performed manually and calculated by the help of Comet Score software. The specialized software Comet Score assessed the comets in these images (Georgieva et al., *BBA Gen Reg Mechanisms*, 1819 (5): 366-374). Data is from three biological replicates and error bars represent SD.

Together, this suggests that there is evidence of a more open chromatin in both the exponential *hho1*Δ and *hmo1*Δ mutants. The main goal was to repeat the analysis on SP cells, as we had hypothesised that either *hmo1*Δ or *hho1*Δ would be most likely working in SP to compact chromatin. Unfortunately, analysis of chromatin using the comet assay in SP cells was not feasible due to technical difficulties with removing the cell wall to enable Mnase treatment.

3.3 Summary of main findings

3.3.1 *hho1*Δ mutant

- The *hho1*Δ mutant has a reduced capacity to grow on acetic acid in exponential phase.
- *hho1*Δ cells are more sensitive to oxidative stress in exponential phase.
- H2A Ser129 phosphorylation levels are greater throughout SP in the *hho1*Δ mutant suggesting that this mutant is incurring more damage than wt during SP.
- Htz1p levels were increased in the *hho1*Δ mutant after day 5 and 7 of growth.

3.4.2 *hmo1*Δ mutant

- *hmo1*Δ displays an elongated cell shape.
- *hmo1*Δ cells are more resistant to oxidative stress in exponential phase.
- *hmo1*Δ cells enter SP at a lower cell density than wt or *hho1*Δ.
- H3 Ser10 phosphorylation is absent in the *hmo1*Δ mutant in exponential and SP cells suggesting a compromised ability to effectively respond to the environment.
- Over expressing Hmo1p causes a loss in viability during SP.

- Both *hmo1*Δ and *hho1*Δ show evidence of chromatin decompaction during exponential phase.
- Over expression of both Hho1p and Hmo1p increases thermotolerance of SP cells suggesting a protective role for both proteins in SP cells.
- Histone H3 K36 trimethylation levels persist in *hmo1*Δ and *hho1*Δ cells during SP.

3.4 Discussion

The data presented in this chapter described initial experiments looking at the *HHO1* and *HMO1* gene deletion mutants to observe any obvious phenotypes that these mutants might have to give an insight into the role of these proteins.

I therefore tested the mutant strains deleted for the *hho1*Δ and *hmo1*Δ genes to determine if they had distinct phenotypes or showed differing strength of phenotypes during exponential and stationary phases of growth. It was proposed that such analyses would identify whether the different genes made differing contributions to cell function. The hypothesis was that if the proteins were important for stationary phase function, we would expect to see more phenotypes exhibited during stationary phase.

Overall, minimal phenotypes were observed when deletion mutant cells were exposed to a variety of tests. However, there were results showing some differences in cell growth and cell morphology in the single mutants deleted for each *HHO1* and *HMO1*. For example, when these experiments looked at the growth of each individual mutants in the rich media (YPD), the result showed the *hmo1*Δ mutant did show a growth defect compared to wt, whereby the *hmo1*Δ mutant strain showed a longer lag phase and grew to a lower OD_{600} than wt and the *hho1*Δ mutant (Fig. 3.3). The *hmo1*Δ mutant also had a lower cell viability count after 24h of growth compared to the wt and *hho1*Δ mutant. Together the data shows that the *hmo1*Δ mutant displays the greatest growth defect in exponential phase and loses viability in early stationary phase.

Next, we looked at the cell morphology of each mutant using the light microscope. The result showed the *hmo1*Δ mutant cells displayed a reproducible elongated cell morphology in exponential and stationary phase cells, whilst the *hho1*Δ mutant had no such defect (Fig. 3.6). The mutants were also investigated for growth on solid media with different carbon sources and grown in conditions with various external stressors. The results did not show many differences between the exponential and stationary phase mutants compared to wt for most of the conditions tested (Fig. 3.8).

However, testing of the mutants by challenging them to grow on plates containing acetic acid as a sole carbon source revealed opposing phenotypes for the mutants such that exponential grown *hho1*Δ mutants were more sensitive than wt to growth whilst *hmo1*Δ mutants showed better growth than wt (Fig. 3.9). However, when stationary phase cells were spotted onto the acetic acid plates, although the *hmo1*Δ mutant retained the reduced ability to grow on the plates, the *hho1*Δ mutant grew as well as wt. Therefore, these data suggest that the deletion of *HHO1* and *HMO1* genes resulted in minimal phenotypes in most conditions, except for growth and cell morphology defects in *hmo1*Δ mutants, and differential sensitivity to acetic acid in *hho1*Δ and *hmo1*Δ mutants.

When cells were grown on hydrogen peroxide (H_2O_2), the exponential *hho1*Δ mutant was more sensitive for growth compared to the wt. However, when stationary phase cells were spotted onto the hydrogen peroxide (H_2O_2) containing plates, the phenotype in the *hho1*Δ mutant was not apparent, and it grew as well as wt (Fig. 3.10). The results suggest that the *hho1*Δ mutant is more susceptible to oxidative stress induced by hydrogen peroxide during exponential growth, but not during stationary phase. This might suggest that the chromatin structure and function of the *hho1*Δ mutant is differentially affected by the cell cycle stage and the environmental conditions. The *hho1*Δ mutant may have more dynamic and accessible chromatin in exponential phase, which could render it more vulnerable to DNA damage. In contrast, the wild-type cells may have a more stable and compact chromatin, which could protect them from oxidative stress, but also limit their plasticity. Thus, the role of Hho1p in modulating chromatin structure and function may be important for cell survival and longevity under different physiological states.

A key hallmark of the quiescent cells formed during the stationary phase is that these cells display increased thermotolerance (Allen *et al.*, 2006). I therefore tested exponential and stationary phase cells of the mutants and wt to determine if this key characteristic of SP cells was retained in the mutants. The results showed that the mutants behaved the same as wt during exponential phase growth and were sensitive to the high temperature exposure with minimal viable cells remining in either wt or mutants after the heat shock.

Similarly, when the stationary phase cells were exposed to the heat shock, both mutants behaved the same as wt and showed the same amount of resistance to the temperature as the wt cells. Thus, deletion of *hmo1*Δ and *hho1*Δ do not seem to affect the thermotolerance typical of SP cells (Fig. 3.13).

Overall, therefore, although there were several phenotypes associated with *hho1*Δ and *hmo1*Δ mutants, there does not seem to be any dramatic SP-specific defects that were detected by my tests in these mutants.

I therefore chose to examine the consequence of over-expression of the *HHO1* and *HMO1* genes. The rationale was that an overabundance of these proteins might yield phenotypes which might indicate any roles they might have in exponential and stationary phase more clearly than a deletion mutant. The results showed that both the over-expression mutants grew poorly in galactose media compared to wt and lost viability over a 14-day period. Interestingly, the thermotolerance of the mutants in liquid culture was also increased during exponential phase and during stationary phase compared to what was seen in the deletion mutants. Thus, overabundance of the Hmo1p and Hho1p proteins seems to have a greater impact upon cell function during SP than an absence of the proteins which occurs in the deletion mutants (Fig. 3.14).

In summary, the results demonstrate that the chromatin-associated proteins Hmo1p and Hho1p are involved in various aspects of cell physiology, such as growth, viability, and stress response, in both exponential and stationary phases. However, the effects of deleting or overexpressing these genes are not identical, suggesting that they have distinct and complex roles in regulating chromatin structure and function. The deletion mutants show some phenotypes that are consistent with a loss of chromatin compaction and stability, such as increased sensitivity to hydrogen peroxide. The overexpression mutants, on the other hand, show phenotypes that are indicative of a gain of chromatin rigidity and resistance, such as reduced growth and viability, and increased thermotolerance. These results imply that the optimal level of Hmo1p and Hho1p proteins is essential for maintaining a balance between chromatin flexibility and stability, which may be crucial for cell adaptation and survival under different environmental and physiological conditions.

Western blot analysis was performed on lysates from mid-log phase cells (Expo), diauxic shift cells (DX), and stationary phase cells that were isolated after 5 and 7 days of growth. These lysates were tested with a wide panel of different antibodies against core histones, specific histone modifications, regulatory factors, and the Hmo1p and Hho1p proteins themselves. If Hmo1p and Hho1p played role during SP, we predicted that their levels may increase during SP. However, the data showed that in wt, both Hmo1p and Hho1p levels decreased in day 5 and day 7 SP cells. (Fig. 3.17). This is inconsistent with previous studies that showed that Hho1p and Hmo1p can be displaced from chromatin by transcriptional activity (Schäfer *et al.*, 2008; Panday and Grove, 2016). However, the reduced abundance of these proteins in wt during SP does not necessarily mean that they will not have a role in chromatin compaction or gene regulation during SP. Indeed, perhaps these proteins need to deplete in order to promote their activity in SP cells.

The results also showed that Hmo1p levels were lower in exponential phase cells, and cells at diauxie, in the *hho1*Δ mutant compared to that seen in wt. This suggests that Hho1p positively regulates Hmo1p levels prior to entry into SP. Further experiments are needed to elucidate the molecular mechanisms and biological significance of Hho1p and Hmo1p dynamics during SP as Hmo1p and Hho1p might have other functions besides chromatin compaction during SP, such as DNA repair or replication (Bendandi *et al.*, 2020; Sokolova *et al.*, 2023).

RNA Pol II drives mRNA transcription in yeast. In its active form, it is phosphorylated on the serine-2 and serine-5 residues in the carboxy-terminal domain (CTD) of the Rpb3p subunit (Suh *et al.*, 2013). I investigated if the active forms of RNAP II were present at wt levels in stationary phase cells of the *hmo1*Δ and *hho1*Δ mutant cells or not. Indeed, the prediction would be that if Hho1p and Hmo1p were acting to repress transcription in SP, the phosphorylated forms of Pol II might be more abundant in the mutants during SP.

The *hmo1*Δ mutant showed no significant difference in the levels of Pol II or in the phosphorylated forms of Pol II compared to wt during growth into SP (Fig. 3.18). This suggests that the transcription machinery was not more active in the absence of Hmo1p during SP.

However, Pol II levels during exponential phase were higher than wt in the *hho1*Δ mutant. Furthermore, Pol II ser-5-phosphate levels persisted at a higher level than wt by day 5 of growth into SP. The increased abundance of Pol II in the exponential phase *hho1*Δ cells and the retention of the serine-5 phosphorylated form into day 5 of growth in *hho1*Δ suggests the normal regulation of Pol II activity might be aberrant in the absence of Hho1p as cells transition from active growth into SP.

The results therefore indicate that Hho1p may have the more major role in regulating the activity of RNA Pol II during the transition from exponential growth to stationary phase in yeast cells. Conversely, the phosphorylation status of the CTD of Rpb3p, which reflects the transcriptional activity of RNA Pol II, is not altered by the deletion of *HMO1*. This implies that the transcriptional output of the cells is not affected by the absence of Hmo1p during growth into stationary phase. The role of Hmo1p in modulating chromatin structure and function may be independent of the transcription machinery or may involve other factors that compensate for its loss.

All three forms of trimethylation (H3K4me3, H3K36me3, and H3K79me3) were reduced in wt SP cells (Fig. 3.19). The reduction of these tri-methylation marks in stationary phase (SP) cells is consistent with the known lower transcriptional activity of these cells compared to the higher activity in exponential phase (Expo) cells (Lam *et al.*, 2022). This is consistent with the idea that SP cells enter a state of quiescence, where they reduce their metabolic and biosynthetic activities, and conserve their energy and resources for survival (Garay *et al.*, 2014). The deletion of *HHO1* and *HMO1* led to higher levels of H3K36me3 in SP cells compared to wt, indicating that the transcriptional output of the mutants could be aberrant, and potentially upregulated, in this phase. This implies that Hho1p and Hmo1p could have a role in regulating histone methylation during the transition from exponential phase to SP and/ or that transcription is elevated in both mutants during SP.

Consistent with published data, in diauxic and SP cells (Fig. 3.20), there were significant decreases in the levels of all forms of histone acetylation (Jazwinski and Kim, 2019). Specifically, wt SP cells showed significant decreases in acetylation marks which are associated with active transcription (H3K14ac and H4ac4) (Fig. 3.22) (Karmodiya *et al.*,

2012). This drop in cellular levels of histone acetylation during SP occurred against a background of, reduced Gcn5p levels and Rpd3 levels that remained constant throughout exponential growth and into stationary phase. Importantly, both mutants' Gcn5p, Rpd3p, and histone acetylation levels behaved like wt, suggesting *HMO1* and *HHO1* do not contribute to the regulation of histone acetylation levels at any stage of growth (Fig. 3.22). Similarly, there was no difference in the timing of loss of H2Bub at diauxie in the mutants compared to wt (Fig. 3.20).

The nucleosome is composed of 146 bp of DNA wrapped around a histone protein octamer. The canonical histone octamer consists of a single (H3-H4)2 tetramer and two H2A-H2B dimers (Luger *et al.,* 1997). The data presented here showed that this composition was maintained throughout SP in wt cells, with the exception of H4, which was reduced in SP (Fig. 3.24B). Interestingly, the data suggested that Hmo1p and Hho1p had opposing effects upon histone levels. Overall, all 4 core histone levels increased in the *hho1*Δ mutant as cells grew into SP, whereas, on balance, histone levels depleted compared to wt levels in the *hmo1*Δ mutant is it grew into SP. Thus, *HHO1* might negatively influence histone levels during growth into SP whereas *HMO1* seemed to positively influence histone levels as cells grew into SP. Either way, both effects of *HHO1* and *HMO1* upon core histone levels during the development of SP could influence chromatin compaction and subsequent gene transcription.

The data also showed that the abundance of the histone variant, Htz1p, increased during the sampling period in SP cells in wt cells (Fig. 3.25). Htz1p is an important highly conserved histone variant of histone H2A (Redon *et al.*, 2002). The presence of Htz1p in nucleosomes around the TSS in the promoter of genes is inversely proportional to the transcription rate, and it has been suggested that the presence of Htz1p at gene promoters may poise them for activation (Zhang *et al.*, 2005). Thus, increased Htz1p levels in wt SP chromatin might poise the SP genome for rapid activation of transcription upon the presence of glucose being detected in the environment. Interestingly, the data suggested that Htz1p levels were increased in the *hho1*Δ mutant after day 5 and 7 of growth. This might suggest the *hho1*Δ mutant genomes might be more transcriptionally active or at least primed for more rapid activation upon exposure to nutrients.

The phosphorylation of histone H3 Ser10 plays a crucial role in cell cycle progression and in regulating downstream transcription-coupled histone acetylation and was seen to be depleted in wt day 5 and 7 cells (Moore *et al.*, 2007). In the *hmo1*Δ mutant, the complete absence of H3 Ser10 phosphorylation in exponential and SP cells could suggest a compromised ability to effectively respond to the environment and might give altered gene expression patterns.

H2A Ser129 phosphorylation is a PTM which forms around chromatin at DNA double strand breaks to mark these damage points for repair. The greater levels of this modification throughout SP in the *hho1*Δ mutant suggests that this mutant is incurring more damage than wt during SP. This would be consistent with a failure of compaction of chromatin in SP *hho1*Δ mutant cells which might be predicted to allow less protection against DNA damage. Alternatively, it could mean that the DNA damage repair pathways have failed in SP cells in the absence of Hho1p.

The analysis of chromatin structure by using the Comet assay was preliminary and could only be applied to exponentially growing cells. This was because the technique relies upon enzymatic digestion of the yeast cell wall to enable Mnase treatment of the chromatin. Unfortunately, the tougher cell walls of the SP cells meant that sufficient digestion of the cell walls could not be achieved to apply the technique to SP cells. Nevertheless, the data from exponential cells showed that the compaction profiles differed in the presence/absence of Hho1p and Hmo1p. Interestingly, the assay showed that the chromatin of the *hmo1*Δ and *hho1*Δ mutant cells was more sensitive to Mnase than wt chromatin, suggesting a role for Hmo1p and Hho1p in compacting exponential phase chromatin.

In conclusion, the comprehensive analysis of *HHO1* and *HMO1* gene deletion mutants, as well as the examination of *HHO1* and *HMO1* overexpression, has provided valuable insights into the roles of these chromatin-associated proteins in yeast cells during both exponential and stationary phases. While the deletion mutants exhibited minimal defects in certain conditions, significant differences were observed in cell growth, viability, and morphology between *hho1*Δ and *hmo1*Δ mutants. The *hmo1*Δ mutant stood out with a pronounced growth defect in the exponential phase, coupled with reduced viability in the early stationary phase.

The distinct elongated cell morphology of *hmo1*Δ mutants further supported the critical role of *HMO1* in maintaining normal cellular architecture. Additionally, both mutants displayed a potential defect in respiration when exposed to acetic acid, indicating an important role for Hho1p and Hmo1p in metabolism. Contrary to initial expectations, the deletion of *HHO1* or *HMO1* genes did not seem to affect the thermotolerance typical of stationary phase cells. However, overexpression of *HMO1* and *HHO1* did offer these SP cells resistance to high temperature which is consistent with a protective role for these proteins presumably acting at the level of promoting chromatin compaction. The examination of RNA Pol II levels and activity during the transition from exponential to stationary phase revealed a positive influence of Hho1p upon Pol II abundance in exponential phase cells, and showed Pol II ser-5 levels persisted for longer into SP in the *hho1* mutant compared to wt. This suggests a greater role for Hho1p in regulating transcription during growth into stationary phase or at least a greater role for Hho1p in impacting Pol II levels and phosphorylation status.

In summary, the study demonstrates that Hho1p and Hmo1p play complex and distinct roles in modulating chromatin structure and cell function, influencing various aspects of cell physiology such as growth, viability, and stress response. The dynamic regulation of these proteins during different growth phases underscores their importance in cellular adaptation and survival under varying environmental conditions. The intricate balance between chromatin flexibility and stability, influenced by Hho1p and Hmo1p, emerges as a crucial factor for cell physiology and function.

Chapter 4

Analysing the role of *HMO1* and *HHO1* in quiescent and non-quiescent cell development during stationary phase

4.1 Introduction

During its lifetime, a living organism faces many forms of stress, and one of the most common among them is starvation. To ensure long-term survival, organisms must detect and adapt to nutrient scarcity. When confronted with limited nutrients, *Saccharomyces cerevisiae* halts growth and enters a non-proliferating phase referred to as the stationary phase (SP).

When grown in glucose-based, nutrient-rich media, *S. cerevisiae* goes through several growth phases, beginning with a rapid logarithmic growth phase driven by fermentation. This is followed by cell cycle arrest when glucose is depleted. During this cell cycle arrest, there are global reprogramming events that allow for a slower growth phase where fermentation products are used as secondary carbon sources via respiration. This period of transition from fermentation to respiration is known as the diauxic shift (DX). As soon as all available carbon sources are depleted, yeast cells enter the true stationary phase where cell growth and proliferation have ceased (Werner-Washburne *et al.*, 1993; Herman, 2002b).

Although it was previously believed that all cells in SP cultures were quiescent, recent analysis has revealed that this cell population is heterogeneous. Specifically, stationary phase (SP) cultures of *S. cerevisiae* consist of two cell populations: one that is quiescent (Q), and one that is non-quiescent (NQ) (Allen *et al.*, 2006). The Q population is composed of young daughter cells that retain viability for long periods, while the NQ population is mostly composed of mother cells that are older and undergo cell death, either through apoptosis or necrosis. These two cell populations have different physical and behavioural traits, including different levels of stress resistance and thermotolerance. Furthermore, the Q population can re-enter the cell cycle once nutrients are replenished (Allen *et al.*, 2006).

The understanding of stationary phase, and the creation of the distinct Q and NQ populations, has expanded in recent years. However, the function of chromatin and the linker histone H1 in regulating Q and NQ formation is not well understood. I therefore monitored the formation of the quiescent (Q) and non-quiescent (NQ) populations in the *hho1*Δ and *hmo1*Δ mutants during SP to investigate if Hho1p or Hmo1p played any role in Q and NQ cell development in stationary phase (SP).

4.2 Results

4.2.1 Percoll-gradient centrifugation to separate quiescent (Q) and non-quiescent cells (NQ)

Previous studies had shown that stationary phase (SP) quiescent and non-quiescent cell populations can be separated by a Percoll gradient centrifugation procedure since the quiescent (Q) and non-quiescent (NQ) cells have different cell densities (Allen *et al.*, 2006). The quiescent cells are most dense and form a band at the bottom of the gradient following centrifugation. Conversely, the less dense non-quiescent cells form an upper band following centrifugation. I, therefore, grew wt, *hho1*Δ, and *hmo1*Δ cells to day 7 of stationary phase (SP) and performed the Percoll density gradient centrifugation to examine Q and NQ cell development during SP in the mutants compared to wt.

I put an equal number of cells onto separate gradients (Fig. 4.1, pre-centrifugation). Following Percoll-gradient centrifugation, the wt formed two bands consistent with the formation of NQ (upper band) and Q cells (lower band) (Fig. 4.1, wt, post-centrifugation). In wt, a larger proportion of lower Q cells formed compared to the upper NQ cells. Following centrifugation of the day 7 *hho1*Δ mutant cells, although two bands were visible after centrifugation, there were more upper NQ cells and fewer lower Q cells visible (Fig. 4.1, *hho1*Δ, post-). Furthermore, the lower *hho1*Δ band did not progress to the bottom of the gradient as was the case for the wt lower band which formed at the very bottom of the tube.

This result suggested that by day 7 of stationary phase (SP), the development of Q and NQ cells in the *hho1*Δ mutant is different from the normal development seen in wt such that less Q cells (lower band) have formed in the *hho1*Δ mutant.

When the experiment was performed using the *hmo1*Δ day 7 mutant cells, although two bands could be seen in the gradient following centrifugation, there appeared to be more upper NQ cells formed as compared to wt (Fig. 4.1, *hmo1*Δ, post-).

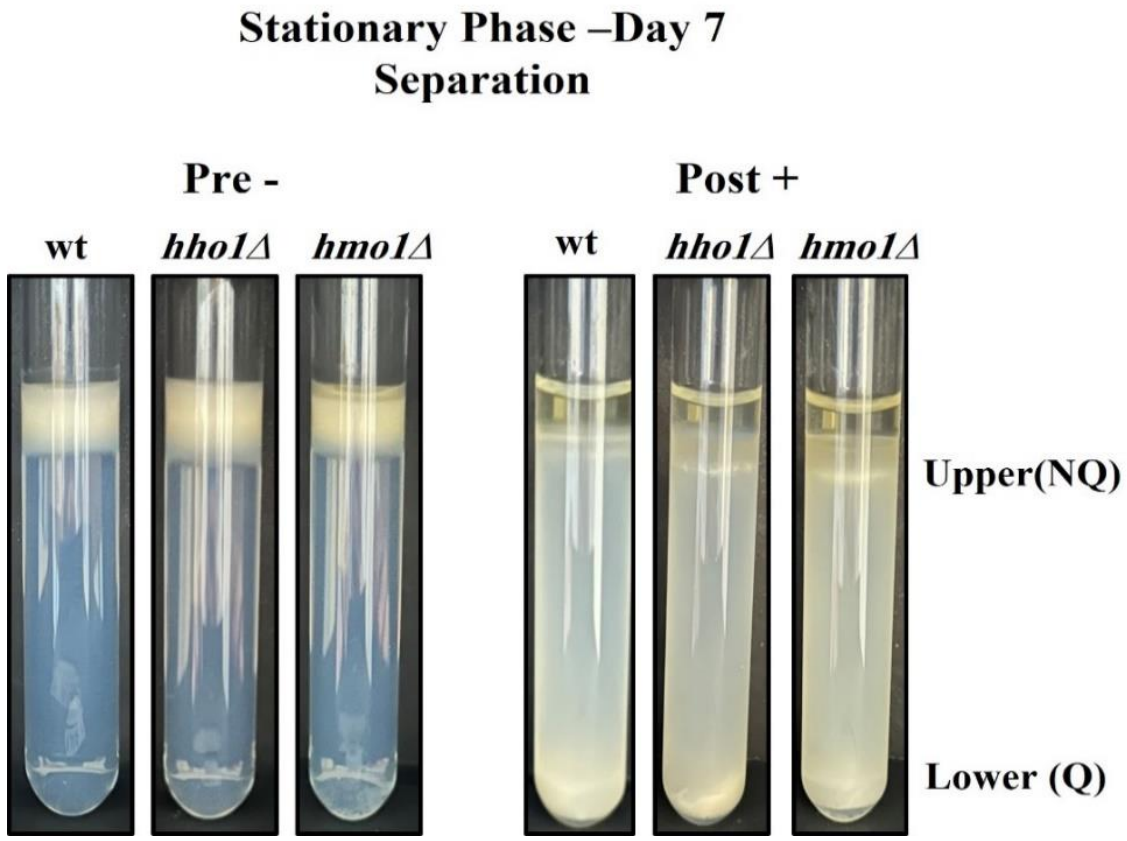

Figure 4.1: Separation of Day 7 cultures into quiescent (Q) and non-quiescent cell (NQ) populations. Images of day 7 wt, *hho1*Δ, and *hmo1*Δ mutant cells before (pre-) and after (post-) centrifugation of percoll density gradients loaded with cells harvested from 6.5 ml of day 7 cultures.

4.2.2 Exponential phase wt and mutants did not form two cell populations

As a control, I performed a percoll density gradient centrifugation upon exponential wt, *hho1*Δ, and *hmo1*Δ mutant cells. The results showed that following centrifugation, the wt, *hho1*Δ, and *hmo1*Δ gradients looked identical, and neither the wt, *hho1*Δ, or *hmo1*Δ cells formed two populations (Fig. 4.2). This means that the two cell populations formed in the wt, *hho1*Δ, and *hmo1*Δ mutant day 7 cells were specific to stationary phase (SP)).

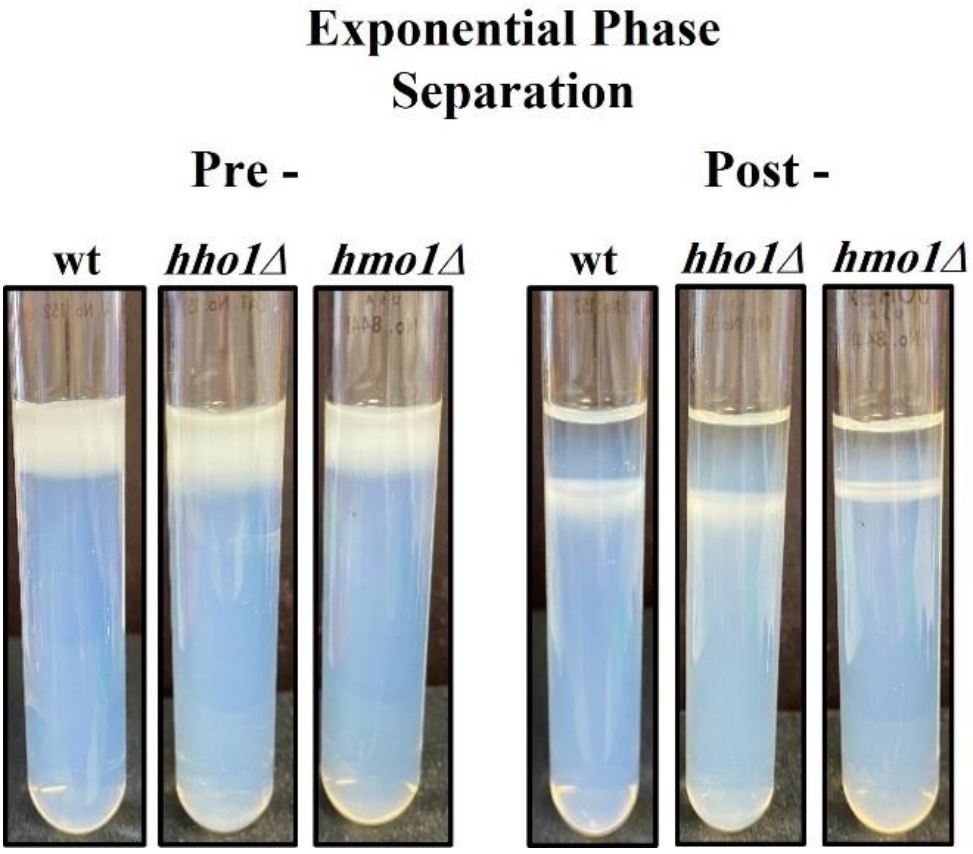

Figure 4.2: Exponential phase cells do not form two populations following Percoll-gradient centrifugation. Images of exponential wt, *hho1*Δ, and *hmo1*Δ cells before (pre) and after (post-) centrifugation of percoll density gradients loaded with equal cell numbers.

4.2.3 The gradients were fractionated to isolate the two populations

I next fractionated the two separated populations of wt, *hho1*Δ, and *hmo1*Δ mutants' day 7 stationary phase (SP) cells formed after the centrifugation (Fig. 4.3A) and counted the total cell number in each of the upper and lower fractions. The result of the cell counts in each fraction were expressed as a % of the total number of cells in both the upper and lower fractions to show the proportion of cells found in the upper (NQ) and lower (Q) cell fractions in the wt, *hho1*Δ, and *hmo1*Δ SP cultures (Fig. 4.3B). Cells from each of the fractions in the wt, *hho1*Δ, and *hmo1*Δ mutants were also diluted and plated out for colony-forming units to determine the number of viable cells in each fraction (Fig. 4.3C).

The results showed that in wt, more lower (Q) cells formed (80%) than upper NQ cells (20%) (Fig. 4.3A, B). Conversely, in the *hho1*Δ mutant a much greater number of NQ cells formed (70%) and less Q cells (30%), compared to wt. The *hmo1*Δ mutant also formed slightly less Q cells (70%) cells compared to wt.

The cell viability results show that almost 55% of the wt lower Q cells retained viability, compared to only 20% of the wt upper NQ cells showing viability (Fig. 4.3C). However, in both the *hho1*Δ, and *hmo1*Δ mutants, over twice as many (~50%) of the lower (NQ) cells retained viability compared to the viability seen in the wt NQ cells.

Thus, after 7 days of growth into stationary phase (SP), the *hho1*Δ mutant formed far fewer lower Q cells than were formed in wt SP cultures and there was a retention in viability of the *hmo1*Δ, and *hho1*Δ mutant upper NQ cell populations compared to wt. This suggests that Hho1p and Hmo1p are required for the normal development of Q and NQ cell formation during SP.

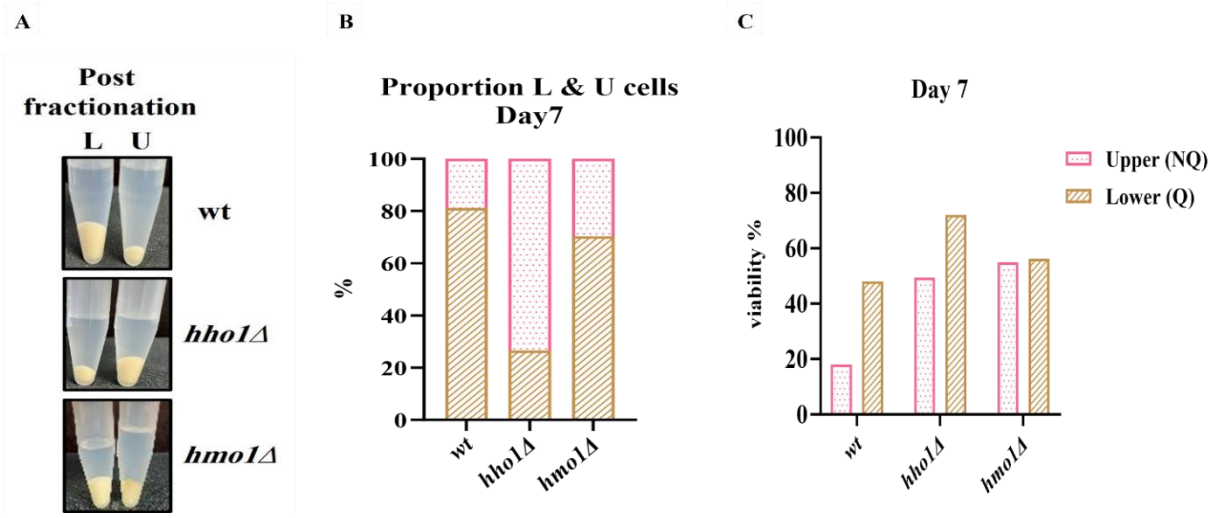

Figure 4.3: The gradients were fractionated to isolate the two populations. Cells were harvested from the fractionated gradients; **(A)** Total cell counts for the upper fraction (NQ) and lower fraction (Q) were calculated using a hemacytometer. **(B)** The cell counts in each fraction were expressed as a % of the total cell numbers from both fractions. **(C)** The % of viable cells from both fractions in wt, *hho1*Δ, and *hmo1*Δ were determined by plating out for colony forming units and viability was shown as a % of the total number of cells counted in each fraction. **(A-B-C).** The data shown is representative of the experiment performed in triplicate.

4.2.4 Cell morphology of unseparated, Q cell And NQ cells in *hho1*Δ and *hmo1*Δ strains during SP

I next examined cell morphology of the wt, *hho1*Δ, and *hmo1*Δ mutants Q cell and NQ cells during stationary phase (SP) (Fig. 4.4). The results showed the wt upper population contained more budded cells than could be seen in the wt lower cell population. This is consistent with the wt day 7 cells forming Q (lower cells) and NQ (upper cells) cell populations. When we looked at the mutants, the separated upper and lower cells looked similar to wt.

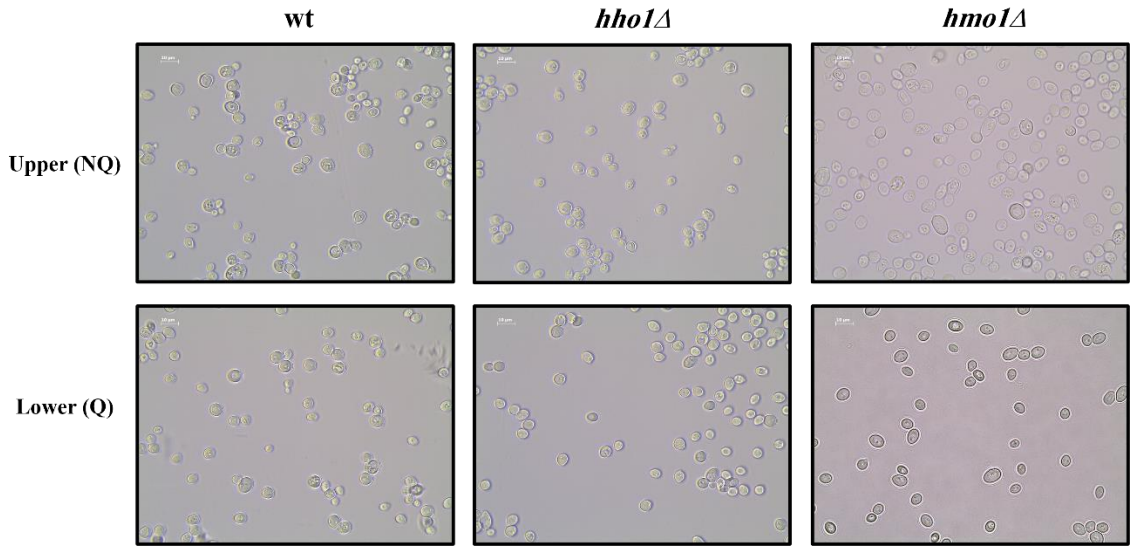

Figure 4.4: Day 7, Q, and NQ cell morphology in wt, *hho1*Δ, and *hmo1*Δ strains. Day 7 wt, *hho1*Δ, and *hmo1*Δ grown day 7, Q, and NQ cells were examined from growing culture under the microscope. Microscopy was conducted under a 100x immersion magnification of the oil. The white scale bar is 10μm.

4.2.5 Time course cell separation analysis

To get more insight into how the upper (NQ) and lower (Q) cell populations develop during the stationary phase (SP) I did a finer time-course cell separation analysis by monitoring wt, *hho1*Δ, and *hmo1*Δ cells during the exponential phase, at diauxie (24 hour), and at days 3, 5, and 7 of stationary phase (Fig 4.5).

In all strains, the Q and NQ cell populations were not visible until day 3 of growth (Fig. 4.5A, D and G). In wt cells, 10% of the cells form in the upper (NQ) cell population by day 3, after which this number increases slowly over time to reach ~20% by day 7 (Fig. 4.5B).

In *hho1*Δ cells, much less lower (Q) cells are formed by day 3 than in wt, and the lower Q cell population decreases further over time to reach a final value of about 25% of the total cell population by day 7 (Fig. 4.5E). In the *hmo1*Δ cells, the lower (Q) population is smaller than in wt by day 3, but remains at this level throughout the period tested to yield a final Q population of about 70% of the total cell population by day 7, which is just 10% lower than the day 7 Q cell population formed in wt (Fig. 4.5H).

I next assessed viability in the separated cell populations by plating out for colony forming units (Fig. 4.5C, F and I). In wt at day 3, the upper (NQ) cells show a lower percentage (~25%) of viability compared the viability in the lower Q cells (40%) (Fig. 4.5C). The NQ population then loses viability over time to achieve ~20% viability by day 7, whilst the viability in the lower (Q) population increases slightly over time to reach a level of -50 % viability by day 7. This is consistent with Q and NQ cell formation expected during SP such that, overall, the Q cells retain viability whilst the NQ cells undergo cell death (Fig. 4.5C) (Allen *et al.*, 2006).

In the *hho1*Δ mutant, the viability of the lower (Q) cells was almost 60% at day 3 but decreased over time to a level of 30% by day 7 (Fig. 4.5F). Conversely, the viability of the NQ cell population increased over time going from about 40% viability at day 3 to almost 80% viability at day 7.

Thus, the *hho1*Δ mutant is forming less Q cells than wt during SP, and these Q cells are losing viability over time. Furthermore, the *hho1* mutant NQ cells are showing an increase in viability over time in contrast to the expected loss in viability expected for this population of cells.

In the *hmo1*Δ mutant, the viability of day 3 lower (Q) and upper (NQ) cell populations were between around 20%. However, viability of both of the Q and NQ cells increased over time to achieve a similar level of ~60% viability by day 7.

This suggests that the *hmo1*Δ mutant shows delayed Q and NQ cell development during SP and, whereas the eventual Q cell population subsequently behaves like wt in terms of viability, the *hmo1*Δ NQ cells are showing an increase in viability over time.

Overall, Q and NQ cell development is aberrant in both the *hmo1*Δ and *hho1*Δ mutants, although the defects in SP cell development in the mutants are distinctly different.

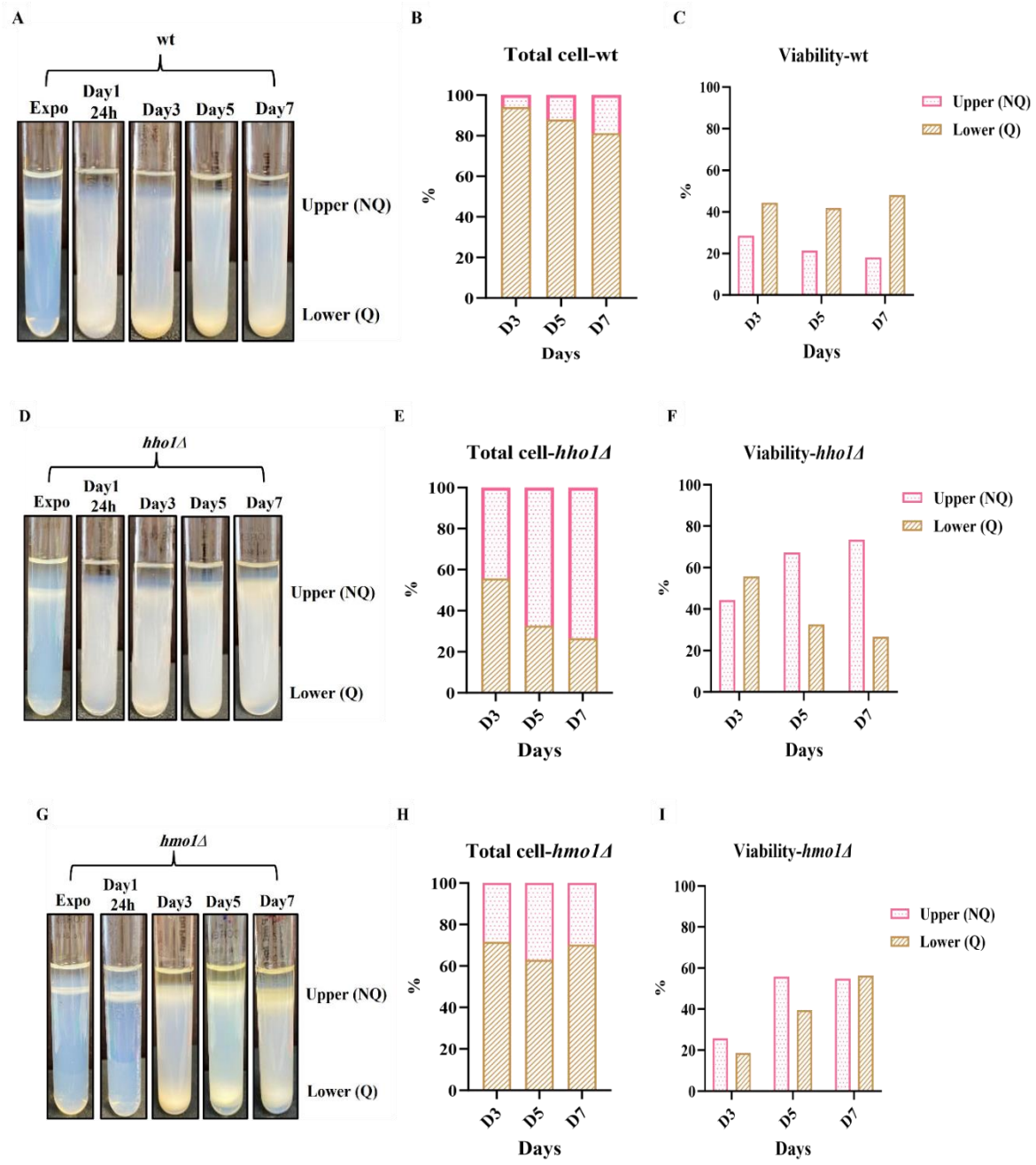

Figure 4.5: Time course cell separation analysis. (A, D, and G) Cell separation of the cells formed in the exponential phase, day 1, and at days 3, 5, and 7 of the stationary phases, Upper (NQ) and Lower (Q) populations are indicated. **(B, E, and H)** Total cell counts for the upper fraction (NQ) and lower fraction (Q) were calculated using a hemacytometer. The cell counts in each wt, *hho1*Δ, and *hmo1*Δ were expressed as a % of the total cell numbers. **(C, F, and I)** The % of viable cells from upper and lower cell populations in wt, *hho1*Δ, and *hmo1*Δ were determined by plating out for colony-forming units and viability was shown as a % of the total number of cells counted in each strain. The data shown are representative of the experiment performed in triplicate.

4.3 Summary of main findings

• *hho1*Δ and *hmo1*Δ mutant cells show aberrant development during SP.

4.3.1 *hho1*Δ mutant

• Less Q cells form in the *hho1*Δ mutant.

• Viability of the *hho1*Δ Q cells decreases over time.

• Viability of the NQ cells increases over time.

4.3.2 *hmo1*Δ mutant

• Retention of viability is delayed in *hmo1*Δ Q cells.

• Viability of *hmo1*Δ NQ cells increases.

4.4 Discussion

The main hypothesis of the thesis was that the role of yeast linker histone H1 will function in the quiescent cells formed during the yeast stationary phase when the chromatin is known to be compacted and gene transcription is significantly reduced (Gray *et al.*, 2004). Thus, in this chapter I examined if the *hho1*Δ and *hmo1*Δ mutant SP cultures actually formed a quiescent (Q) cell population or not by performing the percoll density gradient separation on wt and both mutants.

Firstly, the results suggested that the percoll density gradient could separate Q and NQ cells from an SP population. Separation of day 7 wt cell cultures revealed the cell morphology and viability of the wt upper cell band to show large, budded cells and only 20% viability consistent with these cells being the NQ population. The wt lower cells on the other hand were largely small and unbudded and showed a 50% level of viability consistent with these cells largely being Q cells.

However, the proportion of upper and lower cells differed in the *hho1*Δ and *hmo1*Δ mutants such that less lower quiescent cells were formed in the *hho1*Δ mutant than in wt, and that these *hho1*Δ mutant Q cells lost viability over time. This suggests that Q cell formation was decreased in the *hho1*Δ mutant, and that maintenance of viability within these cells fails over time. Thus, *HHO1* is acting to prevent cell death in these cells during SP, suggesting it could have an anti-apoptotic role in the Q cell population.

Further experiments will need to be performed to characterize the *hho1*Δ upper and lower cell populations to confirm if they are indeed NQ and Q cells, or that the upper and lower populations have not formed correctly and are perhaps mixed NQ and Q cells.

The *hmo1*Δ mutant separation experiment also showed that less lower (Q) cells were forming in this strain during SP. The viability in the *hmo1*Δ Q cells was also low by day 3 but then increased. Most interestingly, viability in the upper NQ *hmo1*Δ cell population increased over time. Thus, the *hmo1*Δ mutant shows delayed Q and NQ cell development during SP and the results show that the *hmo1*Δ NQ cell viability increases over time.

Together, this suggests a potential pro-apoptotic role for *HMO1* in the NQ cell population formed during SP. Further experiments will need to be performed to characterize the upper and lower *hmo1*Δ cell populations in more detail to confirm the predicted loss in apoptotic markers in the *hmo1*Δ mutant NQ cells.

In summary the data suggests that *HHO1* is having an anti-apoptotic role in the Q cells such that, in the *hho1*Δ mutant, the Q cells show increased death. Conversely, *HMO1* could be having a pro-apoptotic role in the NQ cells such that, in the *hmo1*Δ mutant, the NQ cells show decreased death.

Chapter 5

Analysis of global transcription during development of cellular quiescence in *hmo1*Δ and *hho1*Δ mutants

5.1 Introduction

In the previous chapters, I have identified phenotypic differences in an *hho1*Δ and *hmo1*Δ mutant compared to wt. The most striking feature revealed by the Percoll gradient separation of stationary phase (SP) cultures was that the quiescent (Q) cell formation was decreased in the *hho1*Δ mutant and that viability of the *hho1*Δ cells decreased over time. Conversely, the *hmo1*Δ mutant shows delayed Q cell development during SP.

This raises the question of whether it is defects in global gene transcription in the mutants during development of stationary phase that causes these problems. I therefore planned to identify the genes under the transcriptional regulation of Hmo1p and Hho1p in exponential phase, at the diauxic shift, and in purified day-7 quiescent cells (Q) formed during stationary phase by comparing the global RNA transcriptome data of each mutant with each other and versus wt.

RNA-seq is a commonly used method for analysing differential gene expression (DGE). The essential stages of a DGE assay have remained relatively unchanged since the earliest publications (Stark *et al.*, 2019). An RNA extraction is the first step, followed by mRNA enrichment or ribosomal RNA depletion. Next, cDNA synthesis and preparation of an adaptor-ligated sequencing library are carried out. The library is then sequenced, usually on an Illumina high-throughput platform, with a read depth of 10–30 million reads per sample. Finally, the computational steps of aligning and/or assembling the sequencing reads to a transcriptome, quantifying the reads that overlap transcripts, filtering and normalising between samples, and performing statistical modelling on significant changes in the expression levels of individual genes and/or transcripts between sample groups are carried out (Stark *et al.*, 2019).

For this experiment, I prepared RNA from three biological replicates of wt, *hho1*Δ and *hmo1*Δ mutant strains in exponential phase, at the diauxic shift, and from stationary phase (SP) purified quiescent (Q) cells at day 7. The RNA was then sent to Genewiz (Azenta Life Sciences) to do RNA sequencing. The RNA-Seq data was presented visually using J-Browse 2 2.4.2, which was prepared by Dr Karsten Hokamp (Trinity College Dublin, Ireland).

In this chapter, I have analysed the data to determine how genes are up- and down-regulated in the mutant strains compared to wt in exponential phase (Expo), diauxic shift (DX) and quiescent cells (Q). The prediction was that the mutants would show an altered transcription profile compared to wt, and perhaps to each other, during development of the Q-cells formed in stationary phase cultures. The main aim was to then infer from the RNA-seq data what the role is of Hho1p and Hmo1p in the development of Q-cells during SP.

To simplify the analysis, I first analysed the data in each mutant compared to wt from each stage of growth (exponential, at diauxie and in day 7 quiescent cells). At the end of each of these sections I compared the profiles of each mutant to each other to test the hypothesis that the Hmo1p and Hho1p might cooperate or have overlapping functions. Finally, I analysed the transcription profiles in each mutant across the growth stages in an attempt to visualise and reveal any obvious differences in transcription profiles in the *hmo1*Δ and *hho1*Δ mutants that might occur during development and maintenance of the quiescent population of cells that form during stationary phase (SP).

5.2 Results of RNA-seq analysis of *hmo1*Δ and *hho1*Δ mutants in exponential phase

5.2.1 The biological replicates show a high level of reproducibility

I began by assessing the quality of my RNA-Seq data from the exponential phase cells by determining the reproducibility among biological replicates from each strain. The compiled R^2 values of the replicates showed a high correlation, suggesting the data was reproducible and of high quality (Fig. 5.1A). Subsequent visualisation of the mapped reads via J-Browse again highlighted the data was of good quality and offered a versatile tool for the analysis of the transcription data (Fig. 5.1B). To confirm the strains used for RNA-Seq were correct, I looked at the mRNA levels of both *HHO1* and *HMO1* in each strain used (Fig. 5.1C and D). These images confirmed the deletion of *HMO1* in the *hmo1Δ* deletion mutant, with no reads assigned to the *HMO1* ORF and confirmed the deletion of *HHO1* in the *hho1*Δ deletion mutant, with no reads assigned to the *HHO1* ORF. Furthermore, the data revealed that transcription of *HMO1* was unaffected in the *hho1*Δ mutant and vice-versa, suggesting that Hmo1p and Hho1p are not regulating each other's transcription.

I next analysed the total genes that were significantly up and downregulated during the exponential phase (Log 2 ≥1, adjusted p-value of $p \leq 0.05$) in each mutant compared to wt. My results identified a total of 395 genes that were significantly up or downregulated in a *hmo1*Δ mutant compared to wt. However, only 67 genes were significantly up or downregulated in the *hho1*Δ mutant compared to wt (Table 5.1).

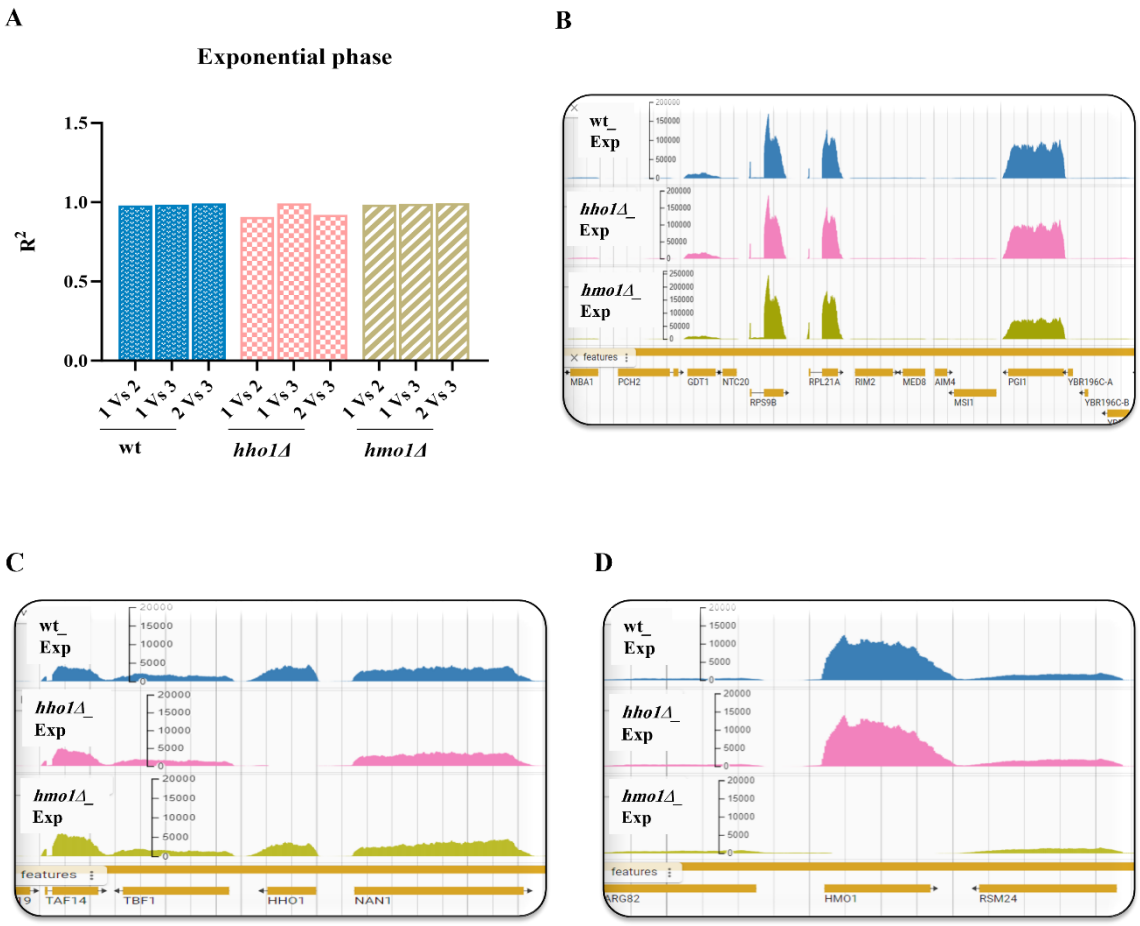

Figure 5.1: Assessing RNA-Seq data quality and strain confirmation. (A) A graph has been created by plotting the normalised counts of each sample against each other during three the exponential phase (Exp) The graph depicts the compiled R^2 values obtained during these stages 1, 2 and 3 there is samples replicate of wt, *hho1*Δ and *hmo1*Δ. **(B)** Screen shot to show average profiles the biological replicates of wt, *hho1*Δ and *hmo1*Δ mutants on J-Browse images of RNA-Seq. (C) Confirmation of *HHO1* and (D) *HMO1* gene deletions.

Of the 395 genes whose transcription was altered in the *hmo1*Δ mutant, 218 genes were downregulated more than 2-fold compared to wt, and 177 genes were upregulated compared to wt. Similarly, the *hho1*Δ mutant had 21 genes that were down-regulated more than 2-fold compared to wt and 46 genes that were up-regulated (Table 5.1).

Thus, we can see significant differences in the number of up or down-regulated genes in each mutant; the *hmo1*Δ mutant showed the largest impact upon gene transcription compared to the *hho1*Δ mutant. The *hmo1*Δ mutant had a similar number of up and downregulated genes (177 and 218 respectively), whereas the *hho1*Δ mutant showed upregulation of 46 genes and down regulation of only 21 genes. This suggests that the *hmo1*Δ mutant has the greatest impact upon transcription during exponential phase and confirms that *HHO1* regulates very few genes during exponential phase. Furthermore, the data shows that the majority of the genes regulated by *HHO1* are negatively influenced by Hho1p, whilst *HMO1* mutant plays a more significant role in positively regulating gene transcription.

A heat map was next used to visualise the total number of genes which were up- and down-regulated in each mutant to show the differential transcription levels in each mutant (Fig. 5.2B-C). The heatmap also groups genes together by their similarity in gene expression patterns (Wickham, 2009; Galili *et al.*, 2018). The red on the heat map indicates the upregulated genes, while the blue indicates the down-regulated genes.

In the case of the *hho1*Δ mutant, most of the genes displayed high levels of up-regulation, as indicated by red colour. On the other hand, the *hmo1*Δ mutants displayed down-regulation in most of their genes compared to the wt, as indicated by the blue colour. This suggests a greater role for *HHO1* in gene repression in the exponential phase, whilst *HMO1* has a greater role in gene activation.

Strain	The number of genes Up-regulated	The number of genes Down-regulated	Total
*hho1*Δ	46	21	67
*hmo1*Δ	177	218	395

Table 5.1: Genes up-regulated and down-regulated by more than two-fold in each strain compared to wt in exponential phase.

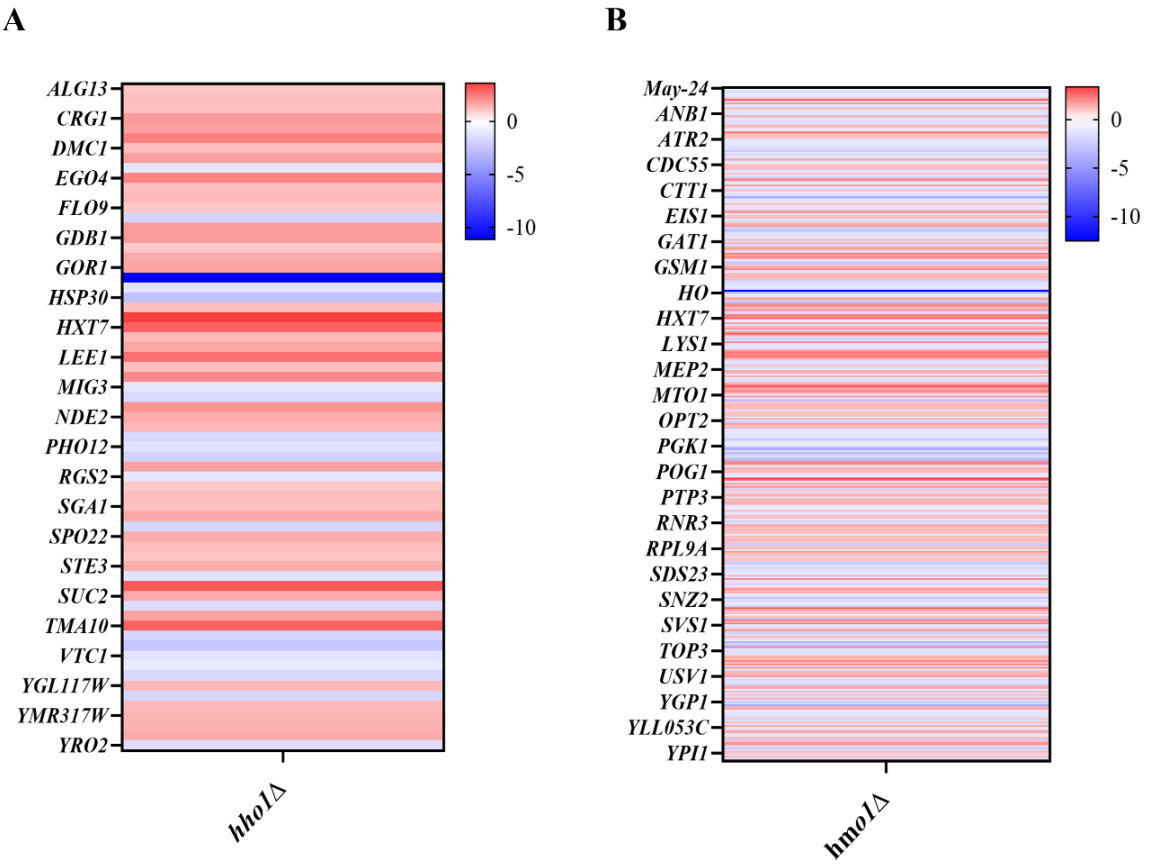

Figure 5.2: Total number of genes up- or down-regulated more than two-fold in each strain compared to wt during exponential phase. The cluster heat maps represents genes in rows and mutants in columns (A and B). Each cell is colour-coded based on the comparative expression level; the down-regulated genes are indicated in blue, while the up-regulated genes are indicated in red, and a p-value of <0.05 for these genes. **(A)** The top 23 of the 67 genes differentially regulated in *hho1*Δ and **(B)** the top 25 of the 395 genes differentially regulated in *hmo1*Δ are indicated to the left of each plot.

5.2.2 Total genes up-regulated in each mutant strain compared to wt during exponential phase

As the linker histone is thought to act predominantly as a repressor to transcription, due to its proposed role in compacting chromatin, it is a reasonable prediction that many target genes would be strongly upregulated when *HMO1* and *HHO1* genes are deleted. Therefore, I first looked at the genes that were significantly upregulated in the *hho1*Δ and *hmo1*Δ mutant strains compared to wt, setting the parameters of at least a two-fold increase (Log2≥ 1, adjusted p-value of p≤0.05). The results showed that although the *hmo1*Δ deletion strain had the most genes that were at least twofold upregulated compared to wt, (177 genes upregulated in this strain), the average transcription levels of the 46 genes upregulated in the *hho1*Δ deletion strain, were de-repressed to the greatest extent compared to the 177 genes de-repressed in the *hmo1*Δ mutant (Fig. 5.3). Thus, although *HMO1* is responsible for repression of the most genes in exponential phase cells compared to *HHO1*, the strength of repression by *HHO1* at its target genes is the strongest.

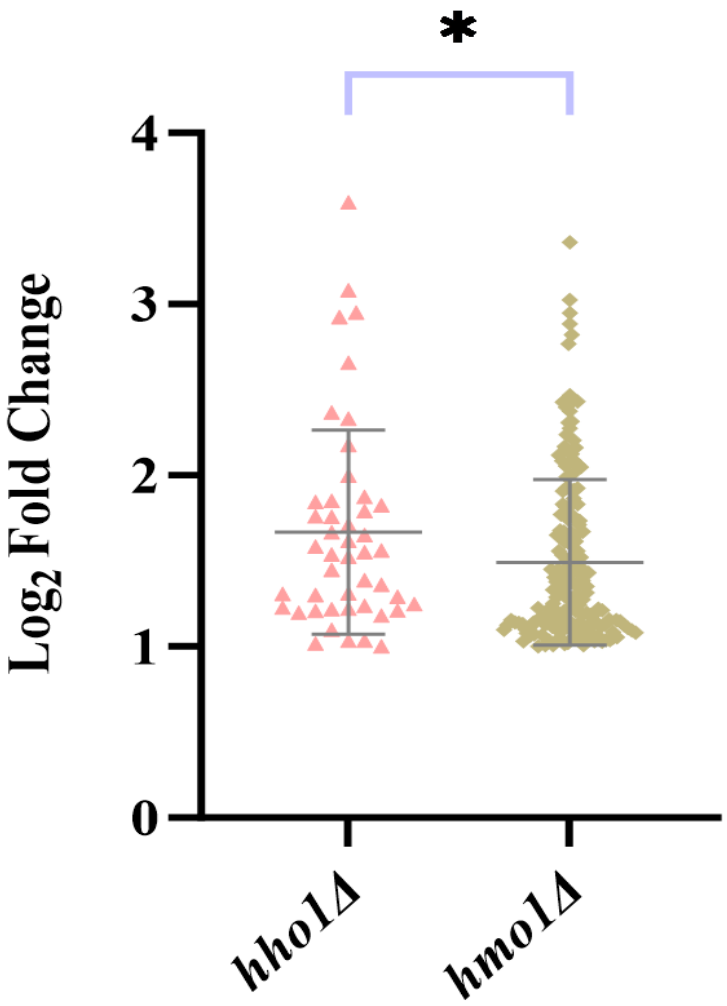

Figure 5.3: Genes significantly up-regulated in each mutant compared to wt. A scatter graph is presented which displays the Log2-fold change values of the genes that are at least two-fold up-regulated (Log2 ≥1, adjusted p-value of p≤0.05) in *hho1*Δ (46 genes) and *hmo1*Δ (177 genes) compared to wt. The graph also indicates the mean and standard deviation. Significance using T-test analysis (* p = 0.05, ** p = 0.01, **** p = <0.0001).

5.2.2.1 Gene ontology analysis of up-regulated genes in each mutant compared to wt

I wanted to investigate the gene ontology (GO) terms associated with the upregulated genes in each mutant strain compared to wt during exponential phase. Using Gene Ontology Metascape, the genes were divided into three sub-ontologies: Metabolic Process, which describes broad biological processes; Molecular Function, which refers to basic activities of the gene products; and Cellular Component, which refers to the location of the gene product.

Firstly, focussing on the gene ontology analysis in *hho1*Δ, in the Biological process category, 8 genes were identified as involved in 'monoatomic cation transport' (GO:0006812), including the *HXT7*, *HXT6*, and *HXT11* genes which encode hexose sugar transporter (Harmonizing model organism data in the Alliance of Genome Resources, 2022) (Fig. 5.4A). The major *HXT* genes (*HXT1 to HXT7*) are clustered in internal small regions of chromosomes, whereas most of the minor *HXT* genes (*HXT8 to HXT17*) are scattered in or near the sub-telomeric region (Boles and Hollenberg, 1997).

In the Molecular function category, 4 genes were identified in the 'glucosidase activity' category (GO:0015926), including *SUC2*, a gene located near the telomere of chromosome II. *SUC2* encodes a protein involved in the catalysis of the hydrolysis of glucosyl compounds like sucrose (Alliance of Genome Resources, 2022).

8 genes were identified in the cellular component category and further classified within the 'Extracellular Region' category (GO:0005576), including the *FLO9* gene, which encodes a flocculin involved in cell substrate adhesion and flocculation, and the *FIT* genes (*FIT1*, *FIT3*) involved in siderophore transport. *FIT1*, is located near the centromere of chromosome IV. (Harmonizing model organism data in the Alliance of Genome Resources, 2022)

Gene ontology analysis in the *hmo1*Δ mutant identified 31 genes as having a role in 'cell communication' (GO:0007154). This cohort of genes included *TPS1* and *NTH1*, located near the telomere (Chromosome XV) and centromere (chromosome IV) respectively. Interestingly, they are both involved in the synthesis and degradation of trehalose.

Trehalose is important for the stress resistance and survival of yeast cells under various environmental conditions, such as heat, cold, dehydration, oxidation, and of course, during quiescence. (Wu *et al.*, 2014; Magalhães *et al.*, 2018; Chen and Lin, 2022) (Fig. 5.4B).

In the Biological process category, the most significant number of genes included members of the *MAL* gene family, located on chromosome VII, near the right telomere (Orikasa *et al.*, 2018) (*MAL32, MAL31, MAL33, MAL11, MAL12*) which are involved in maltose transport, trehalose transport, and regulation of transcription.

A group of 3 genes in Molecular Functions were associated with the GO term 'peroxidase activity' (GO:0004601). This included the genes *PRX1, CTT1, and GPX1*, located on chromosome II (near telomere), chromosome III (near centromere) and chromosome XII (near telomere) respectively, which encode Peroxiredoxin 1, Catalase T and Glutathione Peroxidase 1 respectively. These enzymes are crucial for maintaining cellular redox balance and protecting cells from oxidative damage, which can lead to various diseases and aging processes if left unchecked.

Overall, these data confirm a role for Hmo1p and Hho1p during exponential phase in repressing the expression of genes involved in a diverse array of cellular functions, including repression of many sugar metabolism and stress response genes and include transcription factor encoding genes.

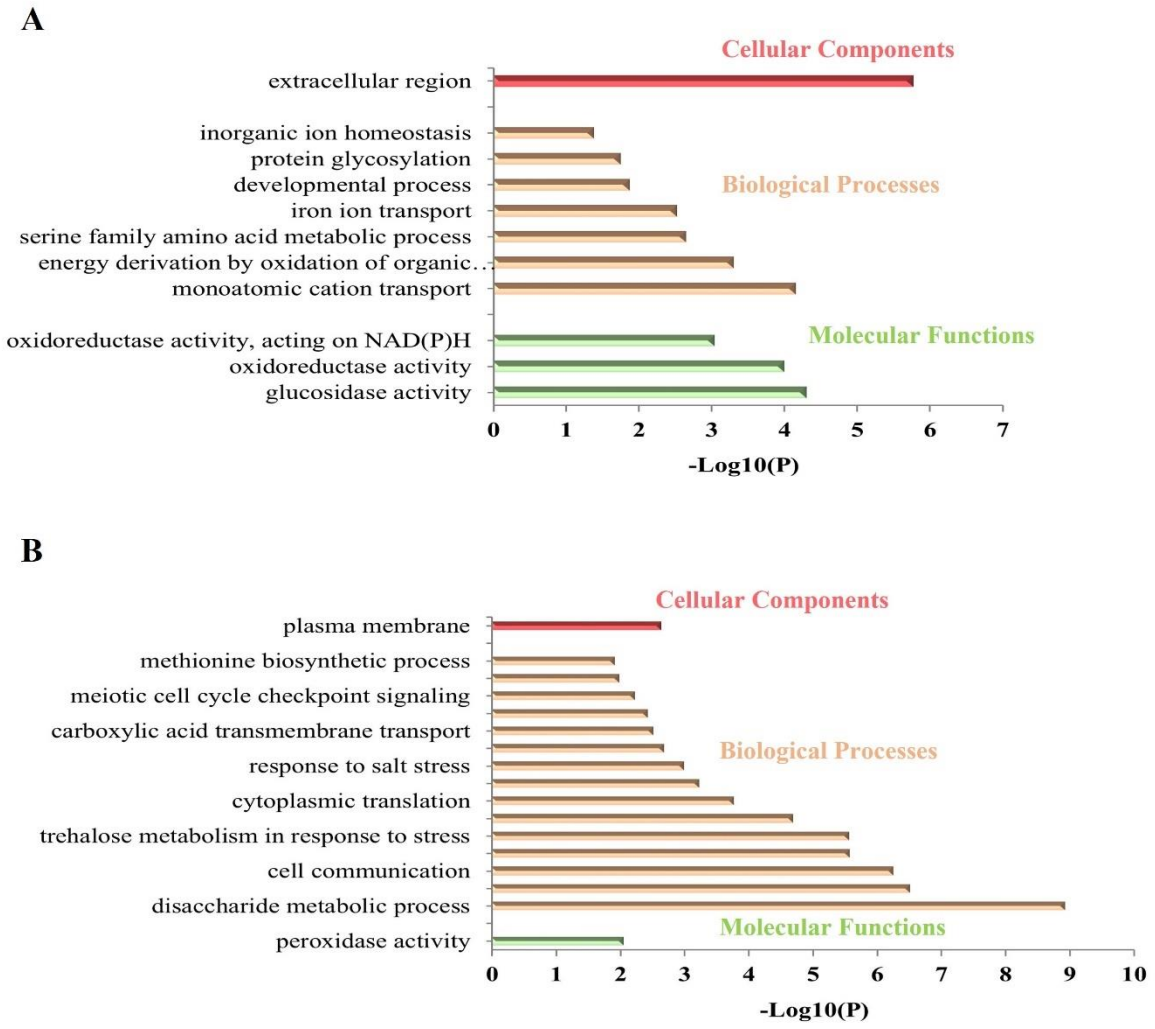

Figure 5.4: Gene ontology analysis of up-regulated genes compared to wt. The significant GO terms from the molecular function category are represented by the light green, biological process category is depicted by the light orange, and the dull red represents significant GO terms from the Cellular Component category according to the Metascape. The X-axis shows the - Log (corrected P-value< 0.05); higher values indicate more statistical significance, and the Y-axis shows the GO term. **(A)** genes up-regulated in *hho1*Δ compared to wt **(B),** genes up-regulated in *hmo1*Δ compared to wt.

5.2.2.2 Identifying genes commonly up-regulated in *hho1*Δ, and *hmo1*Δ deletion strains compared to wt

I next looked to see if there was any overlap in those genes upregulated in the *hho1*Δ and *hmo1*Δ mutants compared to wt (Fig. 5.5A). This might inform us as to whether Hmo1p and Hho1p might cooperate in their repressive regulatory role during exponential phase.

Comparing the total number of genes upregulated in the *hho1*Δ mutant (46 genes) with those upregulated in the *hmo1*Δ mutant (177 genes), we find that only 14 genes overlap. This suggests that only a minimal subset of genes are subject to repression by both Hmo1p and Hho1p suggesting these proteins play largely distinct roles in gene repression during exponential phase.

When I looked at the 14 genes potentially repressed by both *HMO1* and *HHO1* (Table 5.2), I found these genes to be involved in variety of cellular functions such as carbon source transport *(HXT6, HXT7, JEN1*), metabolism (*CRG1*, *GIP2*, *MET28, STR3*), autophagy (*EGO4*), cell wall structure (*PIR3*), gene regulation (*SPO22, SRL3*) and stress response (*LEE1, TMA10*).

Gene	Function
CRG1	S-adenosylmethionine-dependent methyltransferase; implicated in lipid homeostasis.
EGO4	Subunit of the EGO complex, which is involved in the regulation of micro-autophagy.
GIP2	Regulatory subunit of the heterotrimeric Glc7p protein phosphatase, which is involved in glycogen metabolism.
HXT6	Low-affinity glucose transporter of the major facilitator superfamily.
HXT7	High-affinity glucose transporter of the major facilitator superfamily.
JEN1	Monocarboxylate/proton symporter of the plasma membrane, transports lactate, pyruvate, acetate, propionate, and butyrate
LEE1	Zinc-finger transcription factor, involved in the regulation of stress response genes.
MET28	Transcription factor involved in sulphur metabolism.
MRK1	Serine/threonine protein kinase involved in regulating Msn2p and Msn4p.
PIR3	O-glycosylated protein required for cell wall stability.
SPO22	Meiosis-specific protein essential for chromosome synapsis, involved in the assembly and organization of the synaptonemal complex.
SRL3	Subunit of the tRNA splicing endonuclease.
STR3	Cystathionine gamma-lyase, involved in the biosynthesis of methionine from homocysteine
TMA10	Protein of unknown function that associates with ribosomes; protein abundance increases in response to DNA replication stress.

Table 5.2: List of 14 genes commonly up-regulated during exponential phase in both *hho1*Δ and *hmo1*Δ compared to wt.

I next compared the average fold-up regulation of the 14 commonly repressed genes in the two mutants (Fig. 5.5B). Interestingly, unlike the data which showed that on average *HHO1* exerted the greatest repressive effect on those genes upregulated in the *hho1*Δ mutant, the genes commonly repressed by both *HHO1* and *HMO1* were subject to similar levels of repression by *HMO1* and *HHO1*. Example of genes subject to repression by *HMO1* only, by both *HMO1* and *HHO1*, and by *HHO1* only, and are shown in (Fig. 5.5.C, D and E).

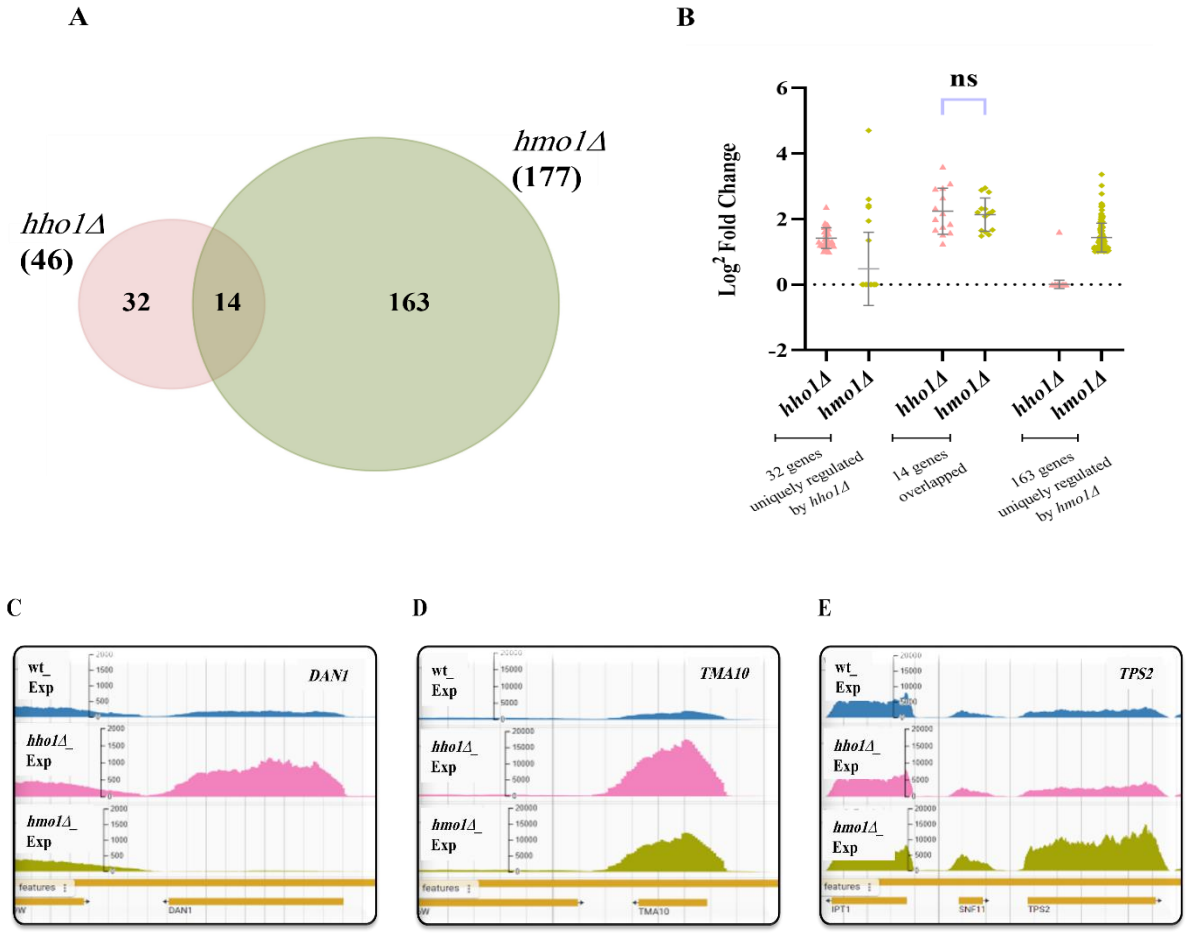

Figure 5.5: Identification of genes commonly and uniquely up-regulated in *hmo1*Δ and *hho1*Δ during exponential phase. (A) Venn diagram of genes upregulated more than 2-fold in exponential phase *hmo1*Δ and *hho1*Δ cells compared to wt**. (B)** boxplot showing average transcriptional fold change of up-regulated genes scatter for shear and uniquely gene, there was no significance (ns) after using T-test analysis. Examples of genes subject to repression by **(C)** *HHO1* only, **(D)** both *HMO1* and *HHO1* together, and **(E)** *HMO1* only.

5.2.2.3 Summary

This section identified and analysed the genes upregulated in the log phase *hmo1*Δ and *hho1*Δ mutants compared to wt. These are the genes at which *HHO1* and *HMO1* are having a negative effect upon transcription. The analysis showed that *HMO1* repressed more genes (177 genes) than *HHO1* did (46 genes).

However, those genes repressed by *HHO1* were, on average, subject to greater repression than that exerted by *HMO1*. Gene ontology analysis of these genes revealed a diverse array of types of genes subject to *HMO1* and *HHO1* repression. Only 14 of the genes repressed by *HMO1* and *HHO1* overlapped, suggesting regulation of gene repression by Hmo1p and Hho1p during exponential phase was functioning largely independently of each other.

5.2.3 Genes down-regulated during the exponential phase in each mutant strain compared to wt

Although the linker histone in yeast has been proposed to function primarily as a repressor of gene transcription, it is possible that it could also be functioning as an activator of transcription. I therefore examined the genes that were at least two-fold downregulated in the mutant strains compared to wt, where it could be inferred that *HHO1* and *HMO1* were required to promote transcription of these genes (Fig. 5.6).

Using the parameters of at least a twofold decrease compared to wt (Log2 ≤-1), the results showed that in the *hmo1*Δ mutant, 218 genes were downregulated. Conversely, in the *hho1*Δ mutant, only 21 genes were downregulated compared to wt (Fig. 5.6). On average, there was no significant difference between the Log2 mean fold change values between each of the deletion mutant strains, suggesting *HMO1* and *HHO1* exerted similar levels of activation at target genes under their positive control.

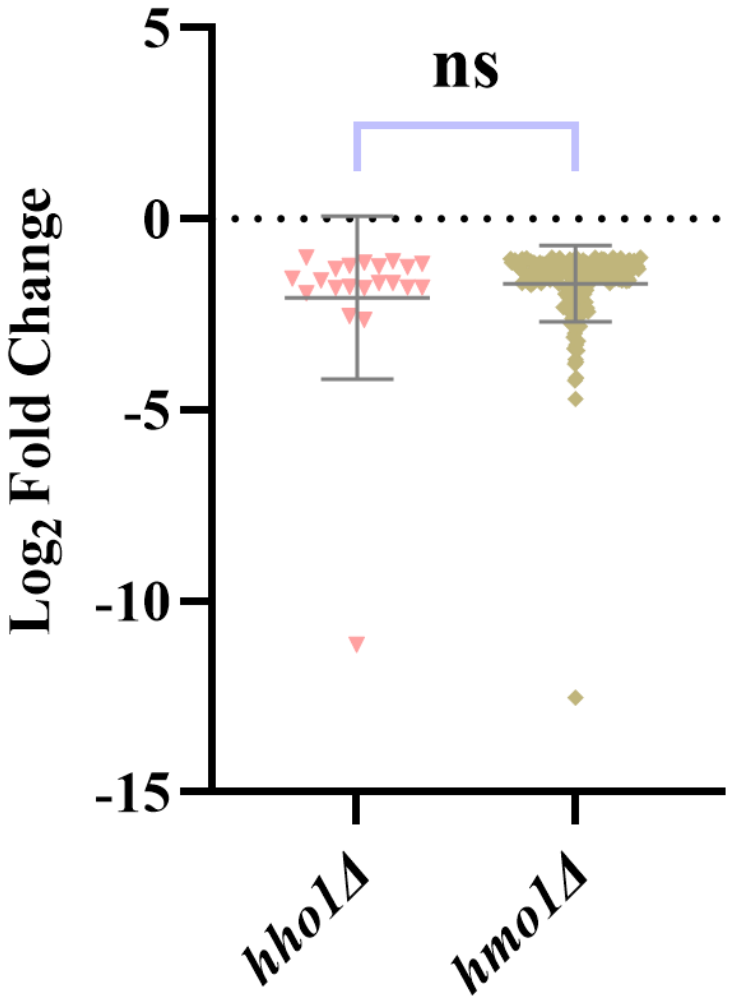

Figure 5.6: Total numbers of genes significantly down-regulated in each mutant compared to wt during exponential phase. A scatter graph is presented which displays the Log2-fold change values of the genes that are at least two-fold down-regulated (Log2 ≥1, adjusted p-value of p≤0.05) in each *hho1*Δ (21 genes) and *hmo1*Δ (218 genes) as compared to wt. The graph also indicates the mean and standard deviation. There is no significance (ns) between the data sets using T-test analysis.

gene name	log2foldChange	Function
HSP30	-2.640025958	Chaperone that protects proteins from stress-induced aggregation
TPO2	-2.545215204	Biological processes, such as polyamine transport, response to oxidative stress, response to acid stress, and regulation of cell cycle
PHO5	-1.945921988	Hydrolyzes phosphate esters and nucleotides in the extracellular region
YKR075C	-1.804537543	Unknown function that is induced by DNA damage and glucose limitation
TMA23	-1.802677139	Involved in ribosomal small subunit biogenesis in yeast
FMP48	-1.798307496	Involved in protein phosphorylation; localizes to mitochondria in yeast
SPL2	-1.794057889	Involved in vacuolar protein targeting in yeast
PHO11	-1.780902681	An acid phosphatase involved in phosphate-containing compound metabolism in extracellular regions
YFL066C	-1.669524028	Helicase-like protein encoded within the telomeric Y' element; induced by DNA damage and UVA irradiation
MNN4	-1.667030205	Mannosyltransferase involved in the biosynthesis of cell wall mannoproteins in yeast
TDA6	-1.612312481	Putative aminotransferase involved in pyridoxine biosynthesis in yeast
YRO2	-1.552522436	Plasma membrane protein that may act as a sensor of cell wall integrity in yeast
PHO12	-1.301676054	Involved in phosphate-containing compound metabolism in extracellular regions
VTC1	-1.25036088	Mediates the transport of polyphosphate into the vacuole in yeast
HIM1	-1.237949884	Involved in meiotic recombination and chromosome segregation in yeast
STP4	-1.228312273	Transcription factor that regulates amino acid permease genes in response to amino acid starvation in yeast
EAF7	-1.175819651	Part of histone acetyltransferase complex that acetylates histone H4 and H2A in yeast
MIG3	-1.138307713	Transcription factor that mediates glucose repression of expression of genes involved in respiration and gluconeogenesis in yeast
RGS2	-1.107865462	Regulator of G protein signaling
VTC3	-1.003503934	Mediates the transport of polyphosphate into the vacuole in yeast

Table 5.3: List of 21 genes down-regulated in *hho1*Δ compared to wt in exponential phase.

Gene ontology analysis of the 21 genes downregulated in *hho1*Δ (see table 5.3) (Fig. 5.7A) revealed six genes involved in vacuolar transport and polyphosphate metabolism including *VTC1,* and *VTC3* which encode proteins involved in the transport of polyphosphate into the yeast vacuole (Kulakovskaya *et al.*, 2021). Three genes (*PHO12*, *PHO11,* and *PHO5)* were identified as being involved in the hydrolysis of phosphoric monoesters.

In the biological process category, the *MIG3* gene was identified, which responds to various stressors, including UV and ethanol.

Gene ontology analysis of the 218 genes downregulated in the *hmo1*Δ mutant (Fig. 5.7B) showed that the most significant number of genes (46 genes) were classified as having a role in 'small molecule metabolic process' (GO:0044281). This cohort family of genes included the *PHOI1, PHO12, PHO5, PHO8,* and *PHO84* genes, which are involved phosphate transport and metabolism.

8 genes were classified as having 'siderophore transport', and included the *ARN1, ARN2* and *SIT1* genes all located in telomere of chromosome IV, involved in cellular iron ion homeostasis, siderophore transport, and transmembrane transport, respectively (Harmonizing model organism data in the Alliance of Genome Resources, 2022).

In the cellular component category, there were 18 'fungal-type cell wall' genes, which included *DAN1,* which encodes a cell wall mannoprotein involved in thermoregulation, *TIR1* and *TIR3* which are both induced by anaerobic conditions, and *SVS1* which encodes a cell wall serine protease that is induced by high salt and alkaline pH conditions. The *TDH1* and *TDH2* genes, involved in gluconeogenesis, were also downregulated.

A group of 3 genes were associated with the GO term 'peroxidase activity ferric-chelate reductase (NADPH) activity'. This included *SSU1*, which encodes a protein involved in sulphite transport (Alliance of Genome Resources, 2022)

These data confirm a significant role for Hmo1p, and to a lesser extent, Hho1p, in being required for activation of gene transcription of diverse types of genes during exponential phase which included many genes involved in the response to stress, metabolism, and the regulation of the cell wall.

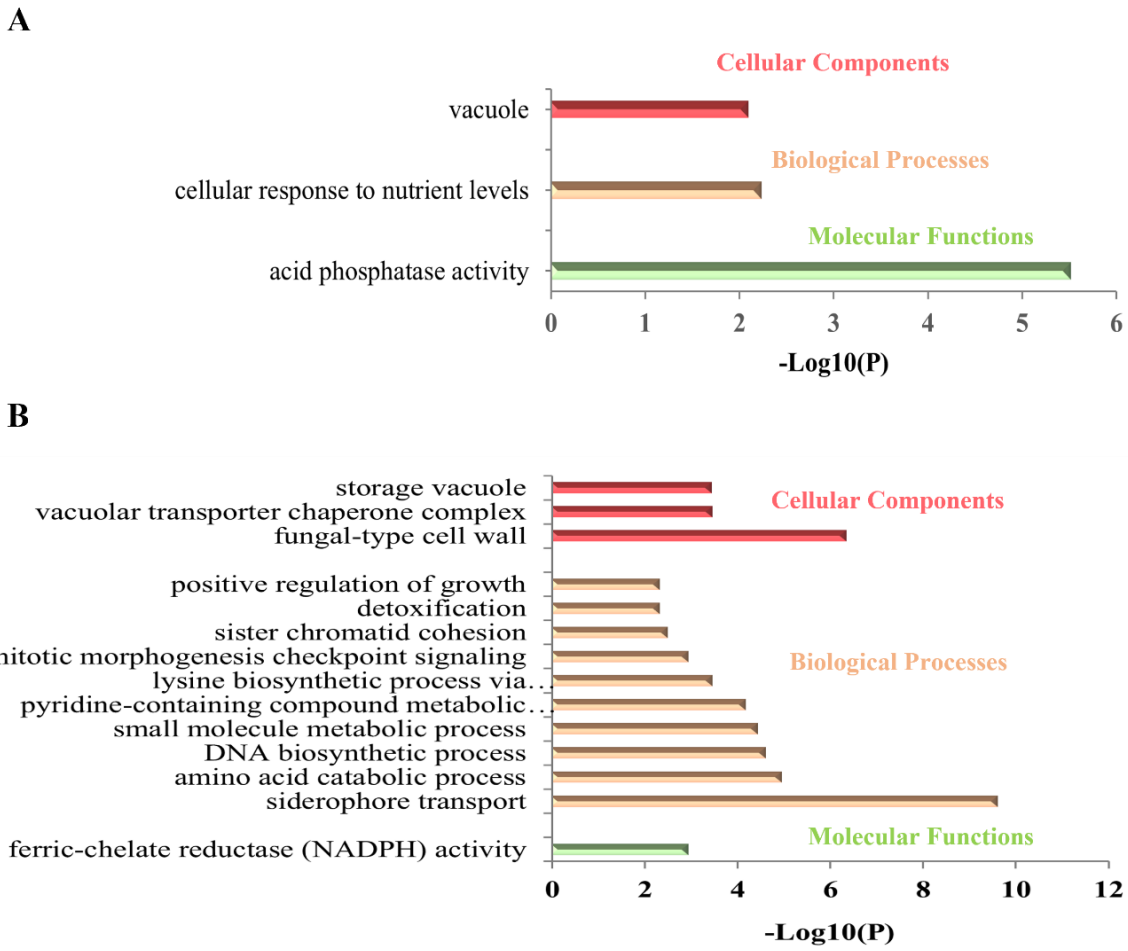

Figure 5.7: Gene Ontology analysis of genes down-regulated in *hmo1*Δ and *hho1*Δ compared to wt during exponential phase. (A) genes down-regulated in *hho1*Δ **(B),** genes down-regulated in *hmo1*Δ. The significant GO terms from the molecular function category are represented by the light green, biological process category is depicted by the light orange, and the dull red represents significant GO terms from the Cellular Component category according to the Metascape. The X-axis shows the - Log (corrected P-value< 0.05); higher values indicate more statistical significance, and the Y-axis shows the GO term.

5.2.3.1 Identification of genes commonly down-regulated in exponential *hho1*Δ and *hmo1*Δ deletion strains compared to wt

I next compared the genes downregulated in the *hho1*Δ and *hmo1*Δ mutants to see if there was much of an overlap in these genes which might suggest co-activation of genes by both Hmo1p and Hho1p (Fig. 5.8A). This analysis showed that only eight genes overlapped as being subject to activation by both *HMO1* and *HHO1*.

When I compared the average fold-down regulation of the shared genes in the two mutants, I found that the 8 genes subject to activation by both *HMO1* and *HHO1* were subject to the most robust activation by *HMO1* (i.e., were most downregulated in *hmo1*Δ) (Fig. 5.8B). Examples of genes subject to activation by *HHO1* only, by both *HMO1* and *HHO1*, and by *HMO1* only, and are shown in (Fig. 5.8C, D and E, respectively).

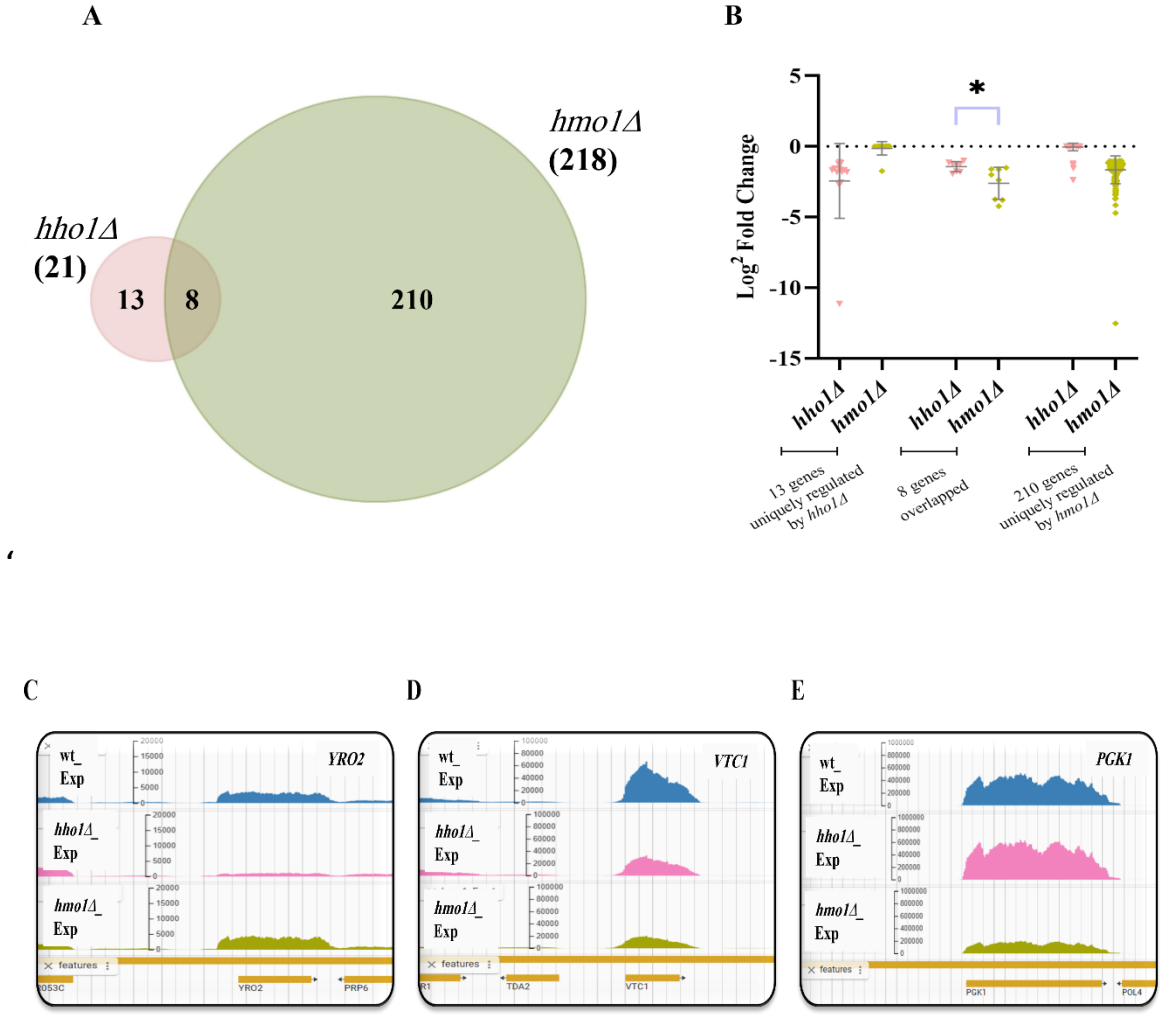

Figure 5.8: Identification of genes commonly and uniquely down-regulated in *hmo1*Δ and *hho1*Δ mutants during exponential phase. (A)Venn diagram of genes more than 2-fold down-regulated in *hho1*Δ and *hmo1*Δ vs wt in exponential phase**. (B)** Scatterplot to show transcription levels of genes commonly and uniquely regulated by *HHO1* and *HMO1*. Significance using T-test analysis (* p = 0.05, ** p = 0.01, **** p = <0.0001). Examples of genes subject to activation by **(C)** *HHO1* only, **(D)** both *HMO1* and *HHO1* together, and **(E)** *HMO1* only.

5.2.3.2 Summary

Different numbers of genes were downregulated in each mutant strain compared to wt during exponential phase; 218 genes were downregulated in *hmo1*Δ, and 21 genes were downregulated in *hho1*Δ. A cohort of 8 genes were commonly downregulated in all mutant strains compared to wt.

This indicates that *HMO1* was dominant in the positive regulation of genes during exponential phase including many genes involved in the stress response and cell wall remodelling.

5.3 Results of RNA-seq analysis of *hmo1*Δ and *hho1*Δ mutants at the diauxic shift

5.3.1 The biological replicates show a high level of reproducibility

I began by confirming the high quality of my RNA-Seq data from the cells at diauxie (Dx) by determining the reproducibility among biological replicates from each strain (Fig. 5.9A). Subsequent visualisation of the mapped reads via J-Browse again highlighted the data was of good quality (Fig. 5.9B). To confirm the strains used for RNA-Seq were correct, I looked at the mRNA levels at diauxie of both *HHO1* and *HMO1* in each strain. These images confirmed the deletion of *HMO1* in the *hmo1*Δ deletion mutant and confirmed the deletion of *HHO1* in the *hho1*Δ deletion mutant (Fig. 5.9C). Furthermore, the data revealed that transcription of *HMO1* at diauxie was unaffected in the *hho1*Δ mutant and vice-versa, suggesting that Hmo1p and Hho1p are not regulating each other's transcription at this stage of growth.

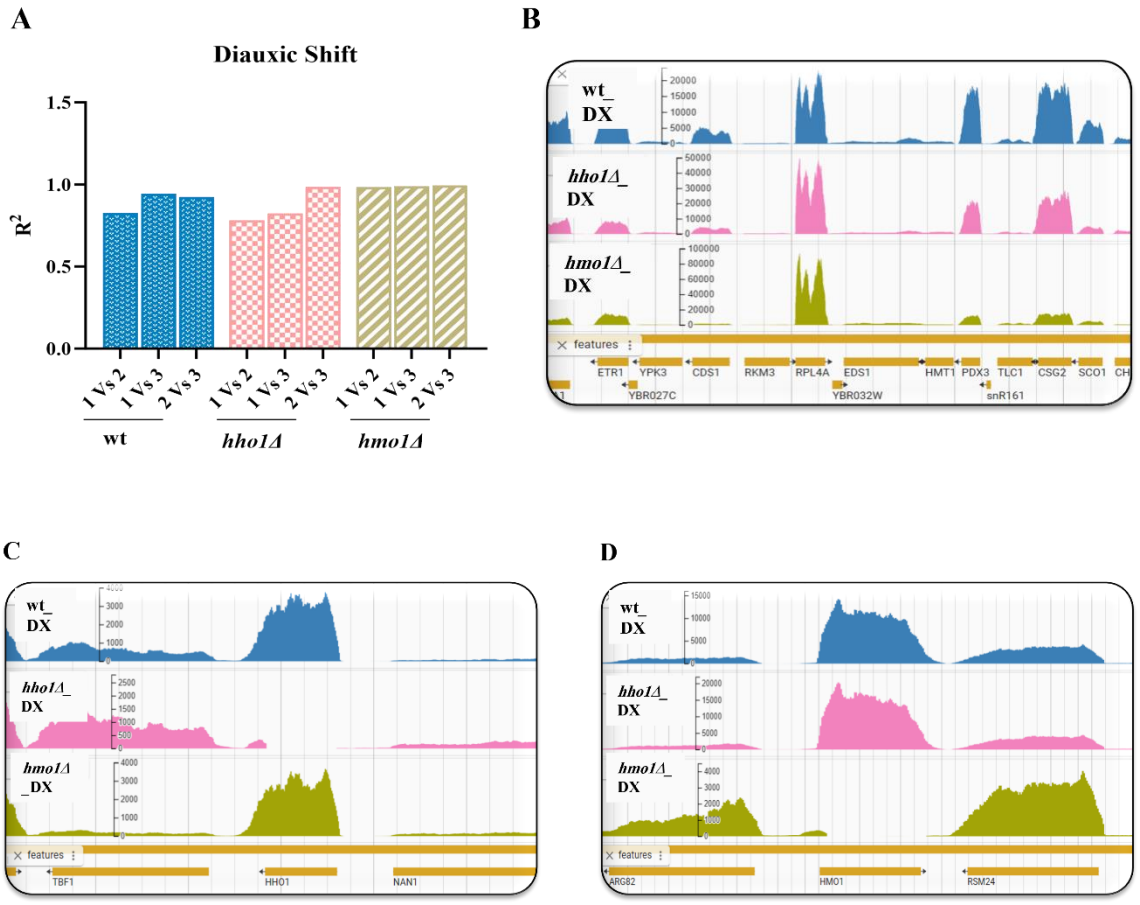

Figure 5.9: A strong correlation between biological replicates and confirmation of the deletion mutants used for RNA-Seq analysis at the diauxic shift. (A) A graph has been created by plotting the normalised counts of each sample against each other during three the diauxic shift (DX) The graph depicts the compiled R^2 values obtained during these stages. 1, 2 and 3 refer to the three different biological replicates that were used for RNA-Seq analysis during the diauxic shift (DX). These replicates are represented in the graph for each of the three conditions: wt, *hho1*Δ, and *hmo1*Δ mutants. **(B)** A screenshot will show the average profiles of the biological replicates of wt, *hho1*Δ, and *hmo1*Δ mutants on J-Browse images of RNA-Seq. **(C)** Confirmation of *HHO1* and **(D)** *HMO1* gene deletions.

5.3.2 The gene transcription profiles at the diauxic shift in *hmo1*Δ and *hho1*Δ mutants compared to wt

I next analysed the total number of genes that were significantly up and downregulated at the diauxic shift (Log 2 ≥1, adjusted p-value of p≤0.05) in each mutant compared to wt (Table 5.4). My results identified a total of 1457 genes were significantly up or downregulated in a *hmo1*Δ mutant compared to wt. However, only 409 genes were significantly up or downregulated in the *hho1*Δ mutant compared to wt. Of the 1457 genes whose transcription was altered in the *hmo1*Δ mutant, 598 genes were down regulated more than 2-fold compared to wt and 859 genes were upregulated compared to wt. Similarly, the *hho1*Δ mutant had 122 genes that were down-regulated more than 2-fold compared to wt and 287 genes that were up-regulated. (Table 5.4)

Thus, we can see significant differences in the number of genes up or down-regulated in each mutant at diauxie; the *hmo1*Δ mutant showed the largest impact upon gene transcription compared to the *hho1*Δ mutant. This shows that the *hmo1*Δ mutant has the greatest impact upon transcription at the diauxic shift regulating more genes than *HHO1* during the diauxic shift. Furthermore, the data shows that the majority of the genes regulated by both *HHO1* and *HMO1* at diauxie were subject to negative regulation, consistent with Hmo1p and Hho1p both acting to predominantly repress genes at this stage of growth.

Strain	The number of genes Up-regulated	The number of genes Down-regulated	Total
*hho1*Δ	287	122	409
*hmo1*Δ	859	598	1457

Table 5.4: Table depicting the number of genes up- and down-regulated by more than two-fold in each strain compared to wt at the diauxic shift.

A heat map was next used to visualise the total number of genes which were up- and down-regulated in each mutant to show the overall differential transcription levels in each mutant (Fig. 5.10A-B). The heatmap also groups genes together by their similarity in gene expression patterns (Wickham, 2009; Galili *et al.*, 2018). Overall, the heatmap illustrates that more genes were upregulated (red) in the *hho1*Δ mutant, indicating that Hho1p primarily contributes to gene repression at the diauxic shift compared to Hmo1p. Nevertheless, distinct clusters of downregulated genes (blue) were evident in each mutant, suggesting a positive regulatory role for both *HMO1* and *HHO1* at these gene cohorts during diauxic phase. Interestingly, there were some genes that showed opposite expression patterns in *hho1*Δ and *hmo1*Δ mutants. This suggests that Hho1p and Hmo1p have opposing roles in the regulation of these genes. In summary, the results reveal that *HHO1* and *HMO1* have a predominantly negative influence upon transcription at diauxie, although there are some clusters of related genes which are dependent upon *HHO1* and *HMO1* for activation.

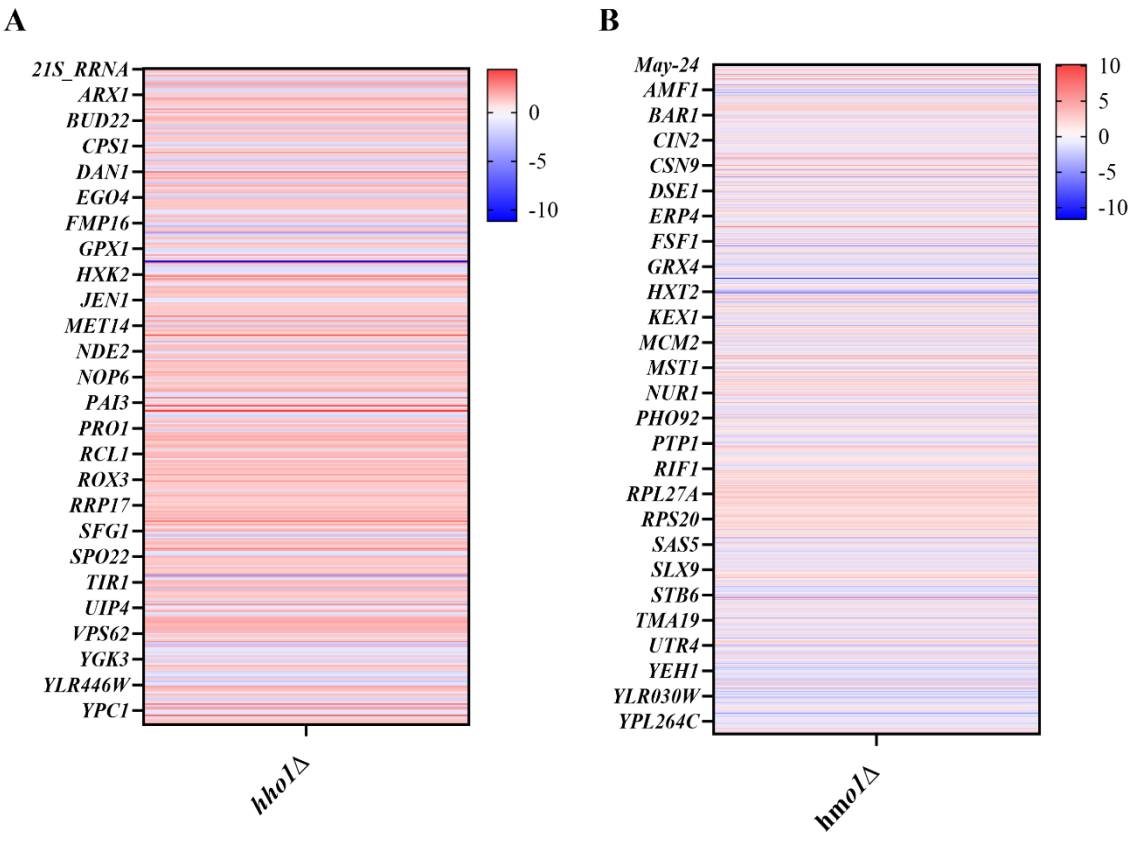

Figure 5.10: Total number of genes up- or down-regulated in *hmo1*Δ and *hho1*Δ mutants compared to wt at diauxie. (A-B) The cluster heat maps represent genes in rows, the strains in columns. Each cell is colour-coded based on the comparative expression level. The down-regulated genes are indicated in blue, while the up-regulated genes are indicated in red, and a p-value of <0.05 for these genes. Only the top 26 of the 409 and 1457 genes differentially regulated in *hho1*Δ and *hmo1*Δ are indicated to the left of each heat map.

5.3.3 Total genes up-regulated in each mutant compared to wt at diauxie

The previous data showed that most genes altered at diauxic in the *hho1*Δ and *hmo1*Δ mutants were upregulated suggesting a predominantly repressive role upon transcription for both *HMO1* and *HHO1* at the diauxic shift. Therefore, I looked more closely at the genes that were significantly upregulated in the *hho1*Δ and *hmo1*Δ mutant strains compared to wt.

The results showed that not only did the *hmo1*Δ deletion strain have the most genes that were at least two-fold upregulated compared to wt and the *hho1*Δ mutant, (859 genes upregulated in the *hmo1*Δ mutant vs 287 gene upregulated in *hho1*Δ), the average transcription levels of these genes were greater than the average upregulation of the 287 genes upregulated in the *hho1*Δ deletion strain (Fig. 5.11). Thus, *HMO1* is responsible for repression of the most genes in diauxic phase cells compared to *HHO1*, and the strength of repression by *HMO1* at its target genes at diauxie is also the strongest.

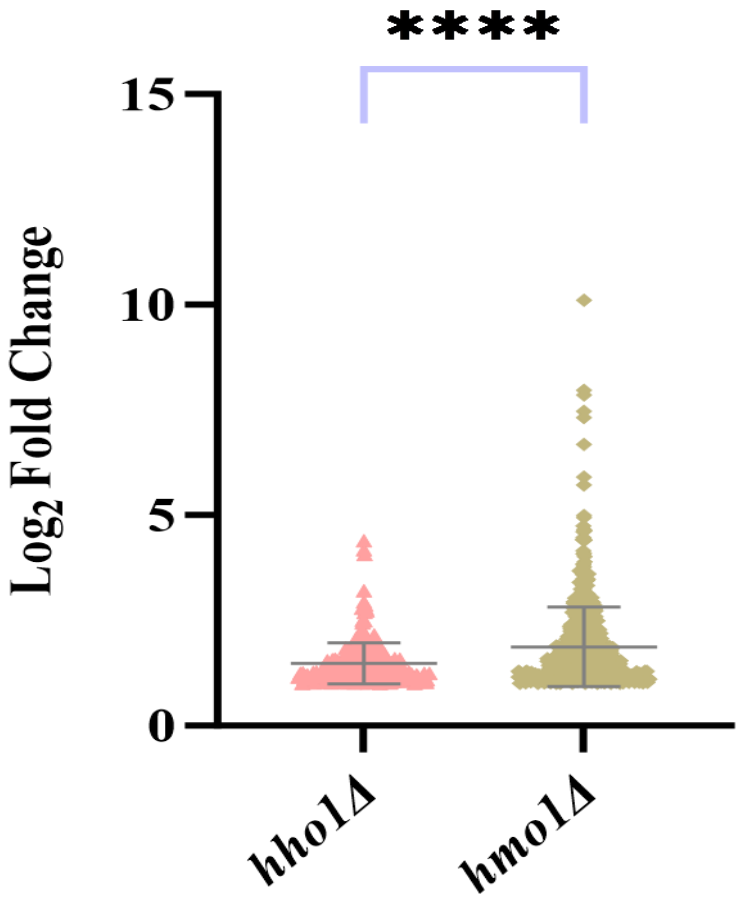

Figure 5.11: Average gene up-regulation in each mutant compared to wt at diauxie. A scatter graph is presented which displays the Log2-fold change values of the genes that are at least two-fold up-regulated (Log2 ≥1, adjusted p-value of p≤0.05) in each strain (*hho1*Δ and *hmo1*Δ) as compared to wt. The graph also indicates the mean and standard deviation. Significance using T-test analysis (* p = 0.05, ** p = 0.01, **** p = <0.0001).

5.3.3.1 Gene ontology analysis of genes up-regulated in each mutant compared to wt at diauxie

I wanted to investigate the gene ontology (GO) terms associated with the upregulated genes in each mutant strain compared to wt. These genes represent where *HMO1* and *HHO1* are acting to negatively influence (repress) gene transcription. Using the Gene Ontology Metascape, the genes were divided into three sub-ontologies, as described before: Metabolic Process, Molecular Function, and Cellular Component, which refers to the location of the gene product.

Firstly, focussing on *hho1*Δ, (Fig. 5.12A) in the Metabolic process category, 96 genes were identified in ribosome biogenesis. This involves the synthesis, processing, and metabolism of ribosomal RNA (rRNA) and other non-coding RNAs (ncRNAs), crucial components of the ribosome. Some of the genes in the category include *DIP2, RIX7, PWP2* and *ARX1*. 26 genes were identified to be involved in tRNA surveillance, catabolism, and modification. Some of the genes in this category include *MTR3, AIR1,* and *CSL4*.

In the Molecular function category, 20 genes were identified in RNA binding and modification, including *DIP2, UTP13, NOP6* and *EMG1*. 36 genes were also revealed to be involved in RNA helicase activity, such as *DRS1* and *FAL1*.

In the cellular component category, 136 genes were found to be associated with the nucleolus, a region found within the nucleus of eukaryotic cells that is primarily involved in the production of ribosomes. Some genes in this category include *NOP56* and *NOP58*, which are core components of the box C/D snoRNP complex, which is involved in the methylation of rRNA. Other genes include *MAK16* which is essential for the assembly of the 60S ribosomal subunit; *NOP14* which is involved in pre-rRNA processing, and *EMG1* which encodes a methyltransferase required for biogenesis of the 40S ribosomal subunit.

Gene ontology analysis in the *hmo1*Δ mutant revealed 331 genes were involved in ribosome biogenesis (Fig. 5.12B). Furthermore, within the cellular components category, the most significant number of genes (228) were classified as being part of ribonucleoprotein complex which included genes such as *KRR1* encoding a protein required for the synthesis of 18S rRNA and for the assembly of 40S ribosomal subunit, *SPB1* a rRNA methyltransferase involved in rRNA processing and maturation of large ribosomal subunit,

MAK31 a subunit of N-terminal acetyltransferase C complex that transfers acetyl groups to N-terminal residues of protein acceptor molecules.

A group of 120 genes in the *hmo1*Δ mutant were involved in Molecular Functions GO term 'structural molecule activity'. Interestingly, this included *TUB4* which is involved in nucleating microtubules from both the cytoplasmic and nuclear faces of the spindle pole body, and *ACT1*, which encodes the key structural protein of the cytoskeleton involved in cell polarization, endocytosis, and other cytoskeletal functions. Other genes upregulated in *hmo1*Δ were *TIM11*, involved in assembly of mitochondrial proton-transporting ATP-synthase complex and in cristae formation and ATP-synthesis coupled proton transport.

Overall, these data confirm a role for Hmo1p and Hho1p in repressing the expression of genes involved in a diverse array of cellular functions. However, a large number of the genes subject to negative regulation by both *HMO1* and *HHO1* were involved in ribonucleoprotein complex structure and RNA metabolism.

This could ultimately suggest a key role for Hmo1p and Hho1p in down regulating protein synthesis at the diauxic shift. Also of note, the key cytoskeleton associated genes *ACT1* and *TUB4* were subject to negative regulation by *HMO1* at the diauxic shift, suggesting a key role for Hmo1p in regulating cell structure dynamics at diauxie.

Furthermore, some key genes involved in mitochondrial structure and function were shown to be subject to *HMO1* negative regulation at the diauxic shift suggesting a role for Hmo1p in regulating the shift from fermentation to respiration which occurs at diauxie.

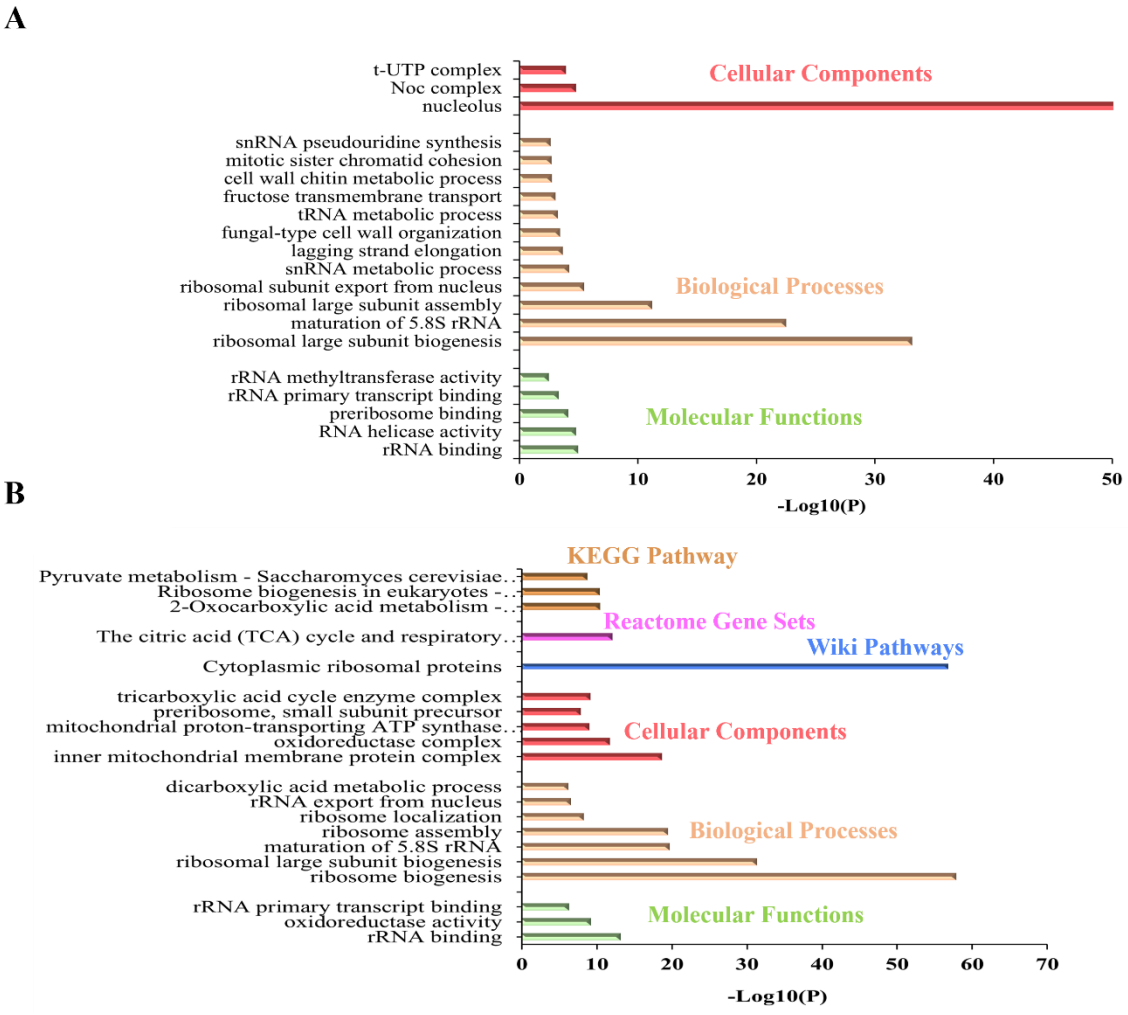

Figure 5.12: Gene Ontology analysis of up-regulated genes compared to wt at diauxie. (A) up-regulated genes of *hho1*Δ **(B),** up-regulated genes of *hmo1*Δ. The significant GO terms from the molecular function category are represented by the light green, biological process category is depicted by the light orange, and the dull red represents significant GO terms from the Cellular Component category according to the Metascape. The X-axis shows the - Log (corrected P-value< 0.05); higher values indicate more statistical significance, and the Y-axis shows the GO term.

5.3.3.2 Identification of genes commonly up-regulated in *hho1*Δ and *hmo1*Δ at diauxie

I next looked to see if there was any overlap in those genes upregulated in the *hho1*Δ and *hmo1*Δ mutants compared to wt at diauxie (Fig. 5.13). This might inform us as to whether *HMO1* and *HHO1* might cooperate in their repressive regulatory role during the diauxic shift.

Comparing the total number of genes upregulated in the *hho1*Δ mutant (287 genes) with those upregulated in the *hmo1*Δ mutant (859 genes), we find that 139 genes overlap. This shows that almost half of the genes negatively regulated by *HHO1* at diauxie are also subject to negative regulation by *HMO1*. This significant subset of genes subject to regulation by both *HMO1* and *HHO1* suggests these proteins play a relatively large overlapping role in gene repression during the diauxic shift (Fig. 5.13A).

Within this *HHO1* and *HMO1* co-repressed gene cohort were genes involved in ribosomal biogenesis and protein synthesis (such as *RPL8A, RPL11B, RPA12, NIP7, FAF1, PWP2, RRT14, RKI1, NOP12, NOP13, RPF1, RPA43, TSR2, MAK16, RPS9B, RPS11A, NOC2, NOC3, NOC4 and RPS9B),* DNA replication and repair (such as *POL1, MCM10, SNM1, RAD27, DIA1* and *FYV7*), and metabolism (such as *ALD5, FDO1 ADH2 ICL2 and FDH2*), and stress response and mitochondrial function (such as *AXL2, PUG1, HCA4* and *NOG1*).

I next compared the average fold-up regulation of the 139 commonly repressed diauxic genes in the two mutants (Fig. 5.13B). Consistent with the data which showed that on average *HMO1* exerted the greatest repressive effect on those genes upregulated in the *hmo1*Δ mutant compared to *hho1*Δ (Fig. 5.13), the genes commonly repressed by both genes were also subject to most repression by *HMO1*. Examples of genes subject to repression by *HHO1* only, a gene repressed by both *HMO1* and *HHO1,* and *HMO1* only, are shown in (Fig. 5.13C, D and E).

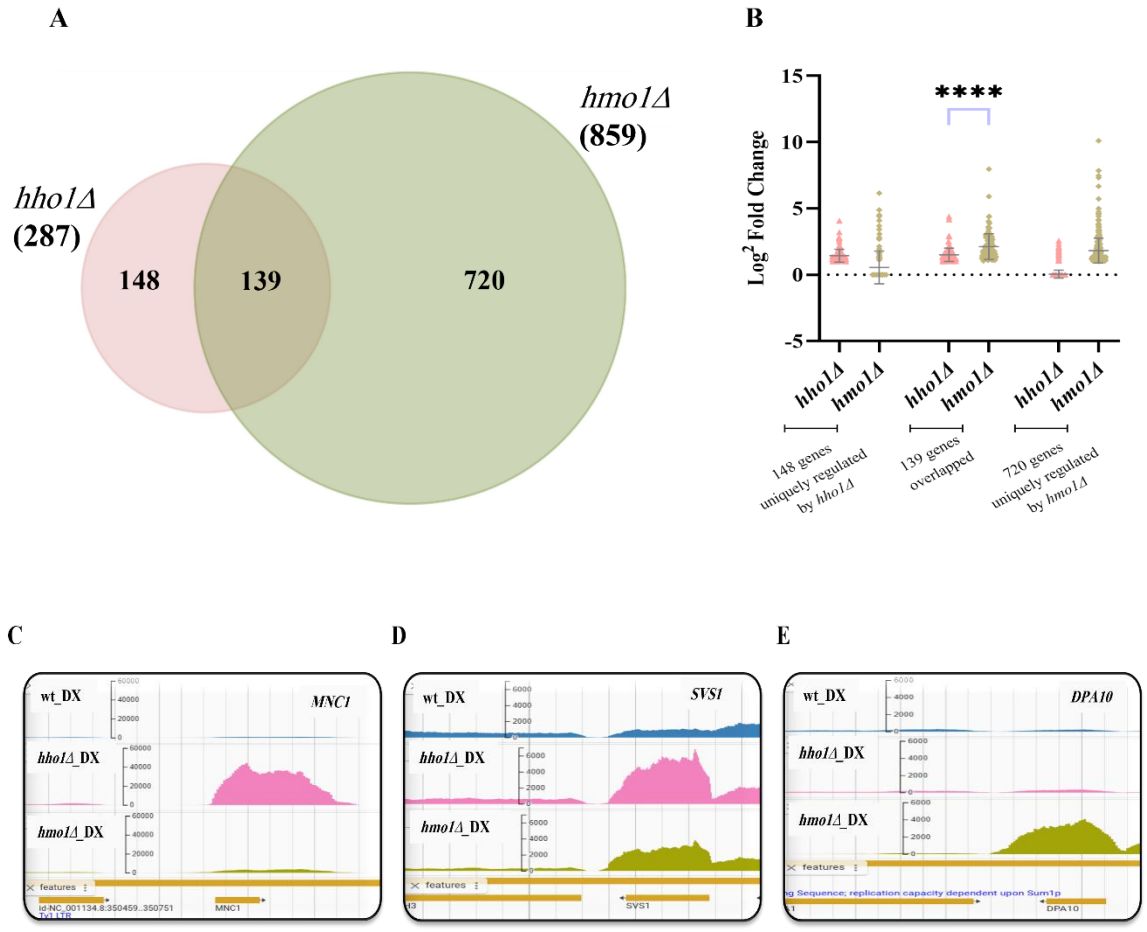

Figure 5.13: Identification of shared and uniquely up-regulated genes in *hmo1*Δ and *hho1*Δ mutated at diauxie. (A) Venn diagram of genes more than 2-fold up-regulated in *hho1*Δ and *hmo1*Δ vs wt at diauxie. **(B)** Scatterplot to show transcription levels of genes commonly and uniquely regulated by *HHO1* and *HMO1*. Significance using T-test analysis (* p = 0.05, ** p = 0.01, **** p = <0.0001). Examples of genes subject to repression by **(C)** *HHO1* only, **(D)** both *HMO1* and *HHO1* together, and **(E)** *HMO1* only.

5.3.3.3 Summary

This section identified and analysed the genes upregulated in the *hmo1*Δ and *hho1*Δ mutants at the diauxic shift compared to wt. These are the genes at which Hho1p and Hmo1p are having a negative effect upon transcription. The analysis showed that Hmo1p repressed more genes (859 genes) than Hho1p did (148 genes). Those genes repressed by Hmo1p were, on average, subject to greater repression than that exerted by Hho1p. Gene ontology analysis of these genes revealed a significant number of genes involved in ribosome structure and RNA function were subject to repression by both Hmo1p and Hho1p. Interestingly, the key cytoskeleton genes, *ACT1* and *TUB4*, were repressed by *HMO1*.

HMO1 also repressed genes involved in respiration. Furthermore, of the 287 genes repressed by *HHO1*, almost half of these were also negatively regulated by *HMO1*. This suggests that *HMO1* plays the dominant role in regulating gene transcription at the diauxic shift and *HMO1* also significantly overlaps with the repression of gene regulation by *HHO1* at diauxie. Finally, *HMO1* contributes the most to the repression of genes repressed by both *HHO1* and *HMO1* at diauxie.

5.3.4 Genes down-regulated in *hho1*Δ and *hmo1*Δ mutants at diauxie

Although the linker histone in yeast has been proposed to function primarily as a repressor of gene transcription, it is possible that it could also be functioning as an activator of transcription. I therefore examined the genes at diauxie that were at least two-fold downregulated in the mutant strains compared to wt, where it could be inferred that Hho1p and Hmo1p were required to promote transcription of these genes (Fig. 5.14).

The results showed that in the *hmo1*Δ mutant, 598 genes were downregulated. Conversely, in the *hho1*Δ mutant, only 122 genes were downregulated compared to wt (Fig.5.6). On average, there was no significant difference between the Log2 mean fold change values between each of the deletion mutant strains, suggesting Hmo1p and Hho1p exerted similar levels of activation at target genes under their positive control at diauxie.

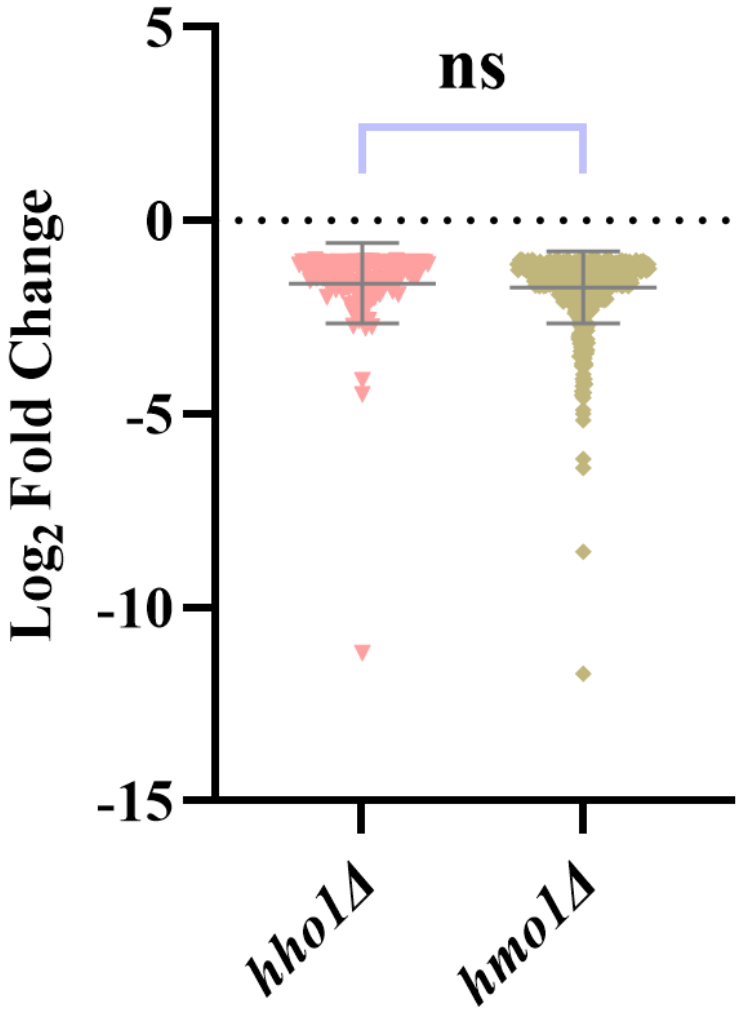

Figure 5.14: Total significantly down-regulated genes in each mutant compared to wt at diauxie. A scatter graph is presented which displays the Log2-fold change values of the genes that are at least two-fold down-regulated (Log2 ≥1, adjusted p-value of p≤0.05) in *hho1*Δ (122 genes) and *hmo1*Δ (598 genes) as compared to wt. The graph also indicates the mean and standard deviation. There was no significant difference (ns) between the average downregulation values in the *hho1*Δ and *hmo1*Δ strains at diauxie using T-test analysis.

5.3.4.1 Gene ontology analysis of down-regulated genes in each mutant at diauxie

Gene ontology analysis of the 122 genes downregulated in *hho1*Δ revealed that 42 genes belonged to the small molecule metabolic process category (Fig. 5.15A). Some genes in this category included *CHA1*, involved in the catabolism of hydroxy amino acids, *AGX1*, which catalyses the conversion of alanine and glyoxylate to pyruvate and glycine, and *NGK1* whose biological role and cellular location are unknown.

18 *HHO1*-influenced genes belong to the carbohydrate metabolic process, genes including *NDE2*, a putative *NADH* dehydrogenase involved in ethanol fermentation, and *TPS2* involved in the synthesis of the storage carbohydrate trehalose.

21 genes belonged to the response to oxidative stress category including *HSP12*, which is induced by heat shock, oxidative stress, and osmo-stress, *YDL124W* which is involved in cellular response to oxidative stress and cellular ketone and amide metabolism, *TSA2*, a stress inducible cytoplasmic thioredoxin peroxidase which cooperates with Tsa1p in the removal of reactive oxygen, and *HSP31* which is induced in response to DNA replication stress.

Gene ontology analysis of the 598 genes downregulated in the *hmo1*Δ mutant (Fig. 5.15B) showed that the most significant number of genes (256 genes) were classified as having a role in 'DNA integration' including *YCL019W*, *YFL002W-A*, *YLR035C-A* and *YLR227W-B*, which are all retrotransposons processed to make a nucleocapsid-like protein (Gag), reverse transcriptase (RT), protease (PR), and integrase (IN), respectively.

100 genes were found to be associated with phosphorus metabolic process including *POF1* which catalyzes the conversion of nicotinamide mononucleotide (NMN) to nicotinamide adenine dinucleotide (NAD+), *PER1*, involved in GPI anchor biosynthesis and manganese homeostasis, and *BST1* which is involved in vesicle organization and ER-to-Golgi vesicle-mediated transport.

In the cellular component category, 94 genes were found to be associated with the plasma membrane. Some prominent genes in this category included *FUS1,* an integral component of the plasma membrane that localizes to the mating projection tip, *AQY3* which encodes a permease involved in passive diffusion of glycerol in the presence of ethanol, *RGD2* which encodes a cytoplasmic GTPase activator involved in signal transduction, and *STE2* which is involved in pheromone-dependent signal transduction involved in cellular conjugation.

In the molecular functions category 121 genes were found to be associated with ribonucleotide binding and 118 genes were found to be associated with purine ribonucleotide binding.

Together these data confirm a significant role *HHO1* in being required for the activation of gene transcription of a wide variety of stress-response genes and genes involved in possible metabolic switching. The data also revealed that *HMO1* was involved in activation of many retrotransposon genes involved in potential genome reorganisation and some key transcription factors and cell signalling proteins. These latter genes suggest a potential central coordination role for Hmo1p in governing large cellular responses at diauxie via the action of downstream proteins, thus potentially acting to amplify Hmo1p's activity.

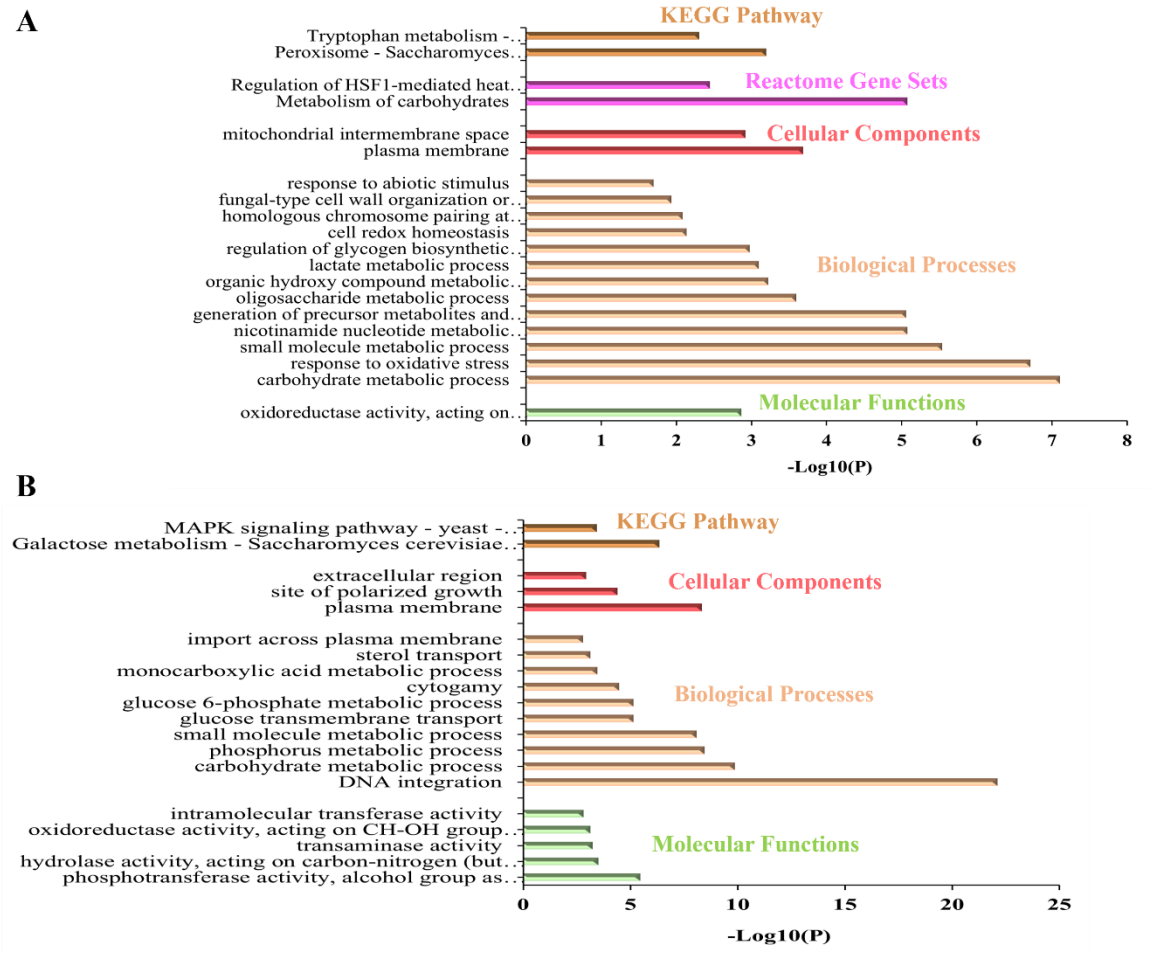

Figure 5.15: Gene Ontology analysis of genes down-regulated in *hmo1*Δ and *hho1*Δ at diauxie compared to wt. (A) down-regulated genes of *hho1*Δ. **(B),** down-regulated genes of *hmo1*Δ. The significant GO terms from the molecular function category are represented by the light green, the biological process category is depicted by the light orange, and the dull red represents significant GO terms from the Cellular Component category according to the Metascape. The X-axis shows the - Log (corrected P-value< 0.05); higher values indicate more statistical significance, and the Y-axis shows the GO term.

5.3.4.2 Identification of common and uniquely down-regulated genes in *hho1*Δ and *hmo1*Δ deletion strains compared to wt at diauxie

I next compared the genes downregulated in the *hho1*Δ and *hmo1*Δ mutants at diauxie to see if there was much of an overlap in these genes which might suggest co-activation of genes by both Hmo1p and Hho1p at the point of glucose depletion (Fig. 5.16A). This analysis showed that only 43 genes overlapped as being subject to activation by both Hmo1p and Hho1p at diauxie.

When I compared the average fold-down regulation of the shared and unique genes in the two mutants, I found that the 43 genes subject to activation by both *HMO1* and *HHO1* were, on average, subject to the most robust activation by *HMO1* (i.e., were most down-regulated in *hmo1*Δ) (Fig. 5.16B). Examples of genes subject to activation by *HHO1* only, a gene activated by both *HMO1* and *HHO1,* and *HMO1* only, are shown in (Fig. 5.16 C, D and E).

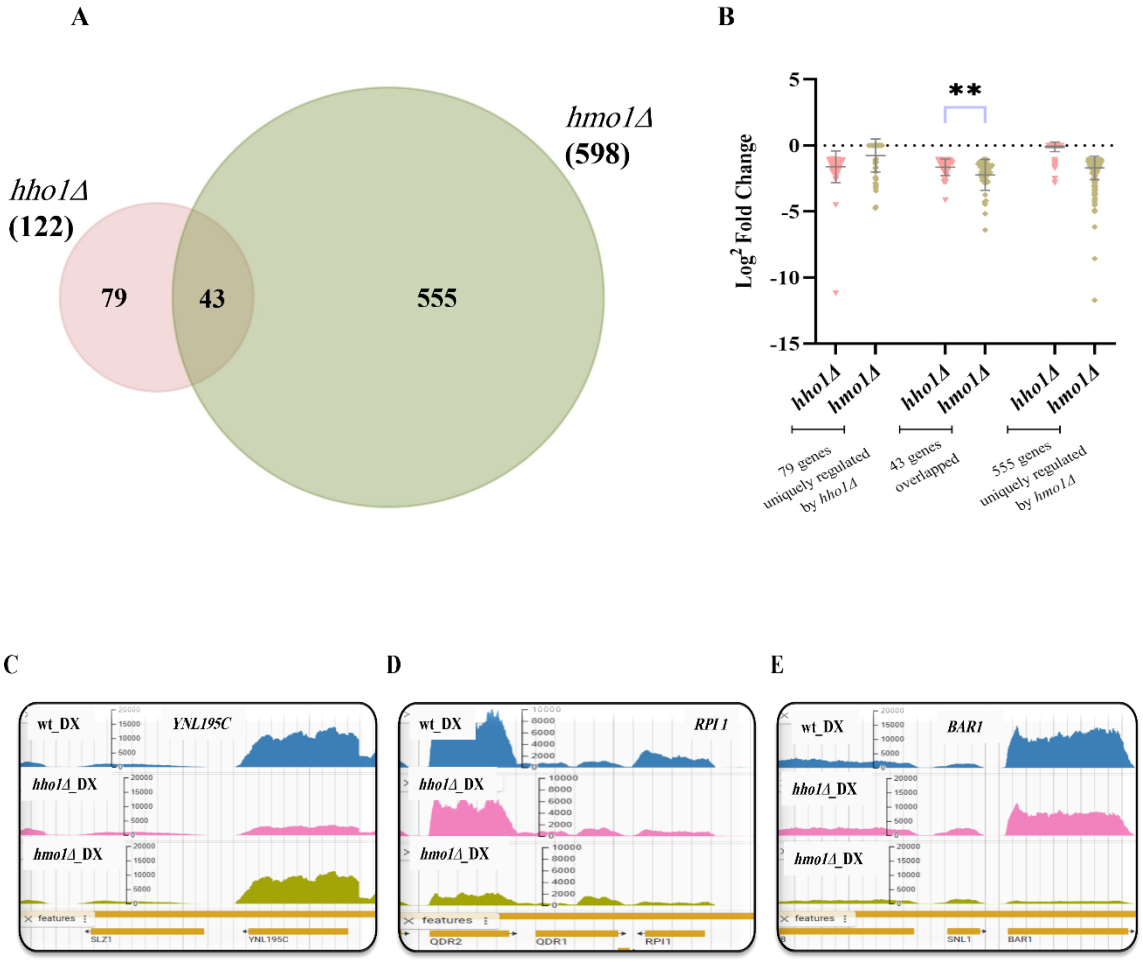

Figure 5.16: Identification of shared and uniquely down-regulated genes in *hmo1*Δ and *hho1*Δ mutants at diauxie. (A) Venn diagram of genes more than 2-fold down-regulated in *hho1*Δ and *hmo1*Δ vs wt at diauxie. **(B)** Scatterplot to show transcription levels of genes commonly and uniquely regulated by *HHO1* and *HMO1*. Significance using T-test analysis (* p = 0.05, ** p = 0.01, **** p = <0.0001). Examples of genes subject to activation by **(C)** *HHO1* only, **(D)** both *HMO1* and *HHO1* together, and **(E)** *HMO1* only.

5.3.4.3 Summary

Different numbers of genes were downregulated in each mutant strain compared to wt at the diauxic shift; 598 genes in *hmo1*Δ and 122 genes in *hho1*Δ. A cohort of 43 genes were commonly downregulated in all mutant strains compared to wt.

This indicates that *HMO1* was dominant in terms of the number of genes subject to positive regulation at diauxie and in terms of the strength of that activation. Interestingly, *HHO1* was responsible for the activation of a wide range of stress-response genes and genes involved in metabolism. *HMO1* was shown to be responsible for the activation of a large number of retrotransposons and genes encoding cell signalling proteins and transcription factors.

5.4 RNA-Seq analysis of purified day-7 quiescent cells (Q) from *hmo1*Δ and *hho1*Δ mutants compared wt

5.4.1 The biological replicates show a high level of reproducibility, and the RNA-Seq analysis confirms the deletion mutants used

For this analysis, wt, *hmo1*Δ and *hho1*Δ mutant quiescent cells were purified from day 7 stationary phase cultures following the percoll gradient separation technique, and RNA was extracted. I then evaluated the RNA-Seq data quality from the day 7 purified quiescent cells by analyzing the R^2 values compiled from these replicates (Fig. 5.17A). This indicated a strong correlation, confirming the data's reproducibility and high quality. Further examination using J-Browse to visualize the mapped reads corroborated the data's quality (Fig. 5.17B).

To confirm the strains utilized for the quiescent cell RNA-Seq analysis, I investigated the mRNA expression levels of *HHO1* and *HMO1* in each strain in the day 7 quiescent cells (Fig. 5.17). The results confirmed the absence of *HMO1* in the *hmo1*Δ deletion mutant and confirmed the absence of *HHO1* in the *hho1*Δ deletion mutant (Fig. 5.17C and D).

Interestingly, the data indicated that the transcription of *HHO1* in the *hmo1*Δ quiescent cells was over 3 times higher than that seen in wt Q cells. Furthermore, *HMO1* transcript levels in the quiescent *hho1*Δ mutant cells was two-fold lower than that seen in wt Q cells. This shows that *HMO1* and *HHO1* are influencing each other's transcription during quiescence. Specifically, it suggests that during quiescence, *HMO1* is having a negative effect upon *HHO1* transcription, whilst *HHO1* is having a positive influence upon *HMO1* transcription.

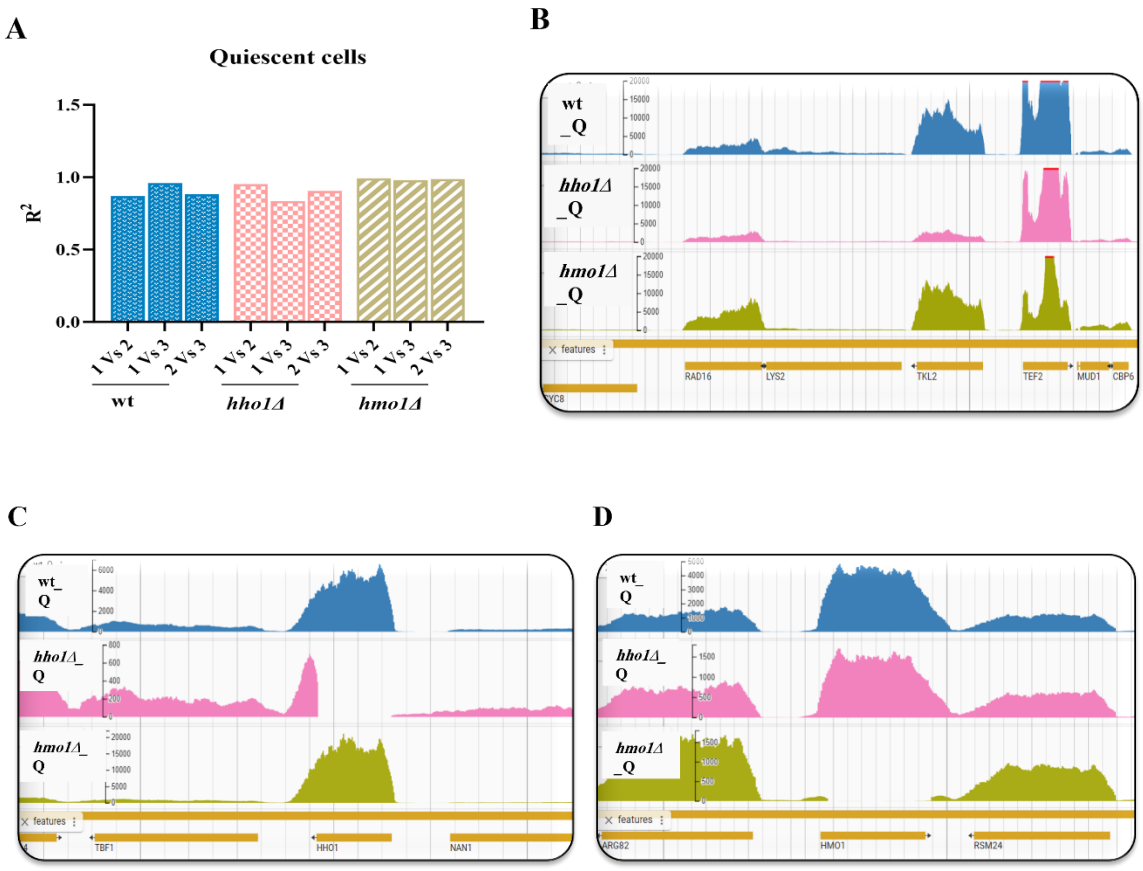

Figure 5.17: Strong correlation between biological replicates and confirmation of the strains employed for RNA-Seq analysis in quiescent cells. (A) A graph depicts the compiled R^2 values obtained by plotting the normalised counts of each sample against each other for the wt, *hmo1*Δ and *hho1*Δ quiescent cells. **(B)** Screen shot to show average profiles the biological replicates of wt, *hho1*Δ and *hmo1*Δ mutants on J-Browse images of RNA-Seq. **(C)** Confirmation of *HHO1* and **(D)** *HMO1* gene deletions.

I next examined the total number of genes that exhibited significant upregulation or downregulation during the quiescent phase in each mutant relative to the wild type (wt) quiescent cells (Table 5.5). This revealed that in the *hmo1*Δ mutant, a total of 2101 genes were significantly altered in expression compared to wt quiescent cells, whereas the *hho1*Δ mutant displayed significant expression changes in 1542 genes compared to wt Q cells.

Out of the 2101 genes with altered transcription levels in the *hmo1*Δ mutant, 1238 genes were downregulated by more than a 2-fold change relative to wt, while 863 genes showed upregulation. In the *hho1*Δ mutant, 854 genes exhibited more than a 2-fold downregulation compared to wt Q cells, and 689 genes showed upregulation compared to wt (Table 5.5).

These findings highlight that the *hmo1*Δ mutant demonstrated a more pronounced effect on gene transcription in Q cells compared to the *hho1*Δ mutant. Specifically, the *hmo1*Δ mutant showed upregulation and downregulation of more genes than the *hho1*Δ mutant. Interestingly, these data show that both *HHO1* and *HMO1* are predominantly exerting a positive regulatory effect on gene expression in the wt day-7 quiescent cell population.

Strain	The number of genes Up-regulated	The number of genes Down-regulated	Total
*hho1*Δ	689	854	1542
*hmo1*Δ	863	1238	2101

Table 5.5: Table depicting the number of genes up- and down-regulated by more than two-fold in each strain compared to wt in separated day 7 quiescent (Q) cells.

A heat map was next used to visualise the genes which were up- and downregulated in each mutant during quiescence to show the differential transcription levels in each mutant compared to wt (Fig. 5.18) (Wickham, 2009; Galili *et al.*, 2018). The heat map analysis for the *HHO1* and *HMO1* mutants indicates some distinct clusters of related genes were down regulated (blue) in each mutant, suggesting a positive role for *HMO1* and *HHO1* at these gene cohorts in the quiescent cells.

For the *HMO1* mutant (B), there was a more varied expression pattern, with several genes displaying both positive (red) and negative (blue) changes in expression. This indicates that the *HMO1* mutation has a more pronounced effect on gene expression, with some genes being upregulated and others downregulated.

Overall, the heat map suggests that the *HMO1* mutation leads to a more diverse alteration in gene expression compared to the *HHO1* mutation. This could imply different roles or regulatory mechanisms for these genes in response to each mutation.

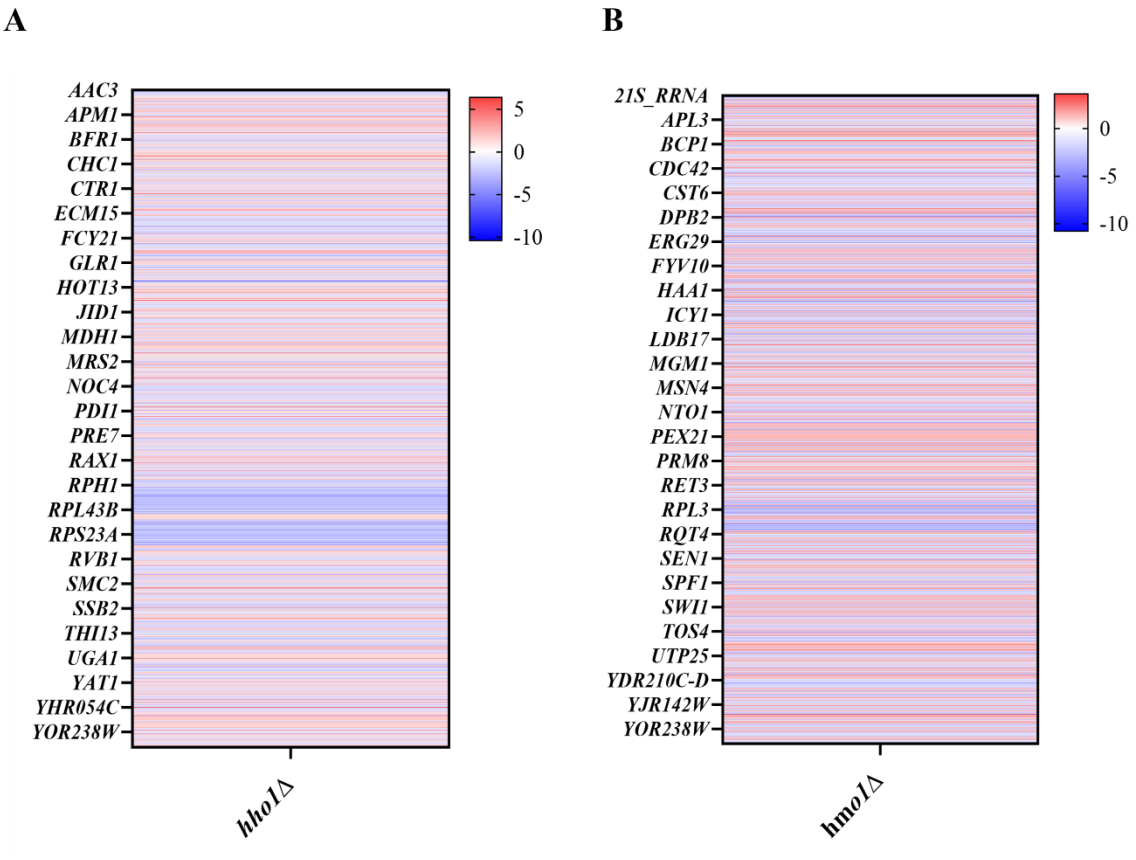

Figure 5.18: Heat map of total genes up- and down-regulated more than two-fold in purified day 7 quiescent cells of each strain. (A-B) The down-regulated genes (compared to wt) are indicated in blue, while the up-regulated genes (compared to wt) are indicated in red (with P values less than 0.05). For clarity, only the top 25 up/downregulated genes have been indicated next to each heat map.

5.4.2 Analysing the genes up-regulated in each mutant strain compared to wt in day-7 quiescent cells

I next analyzed the average levels of transcription of the genes upregulated in the *hho1*Δ and *hmo1*Δ quiescent cells relative to the wild type of quiescent cell levels, focusing on those with at least a two-fold increase (Log2≥ 1, adjusted p-value of p≤0.05) (Fig. 5.19). These upregulated genes should reflect those genes subject to negative regulation by *HMO1* and *HHO1* in quiescent cells. The findings revealed that while the *hmo1*Δ mutant had the highest number of genes upregulated by at least two-fold compared to the wild type Q cells (863 genes), the *hho1*Δ mutant showed a more significant de-repression in the average transcription levels of its 689 upregulated genes.

Therefore, although *HMO1* represses a greater number of genes in quiescent cells than *HHO1*, the intensity of repression exerted by *HHO1* on its target genes during quiescence is more substantial.

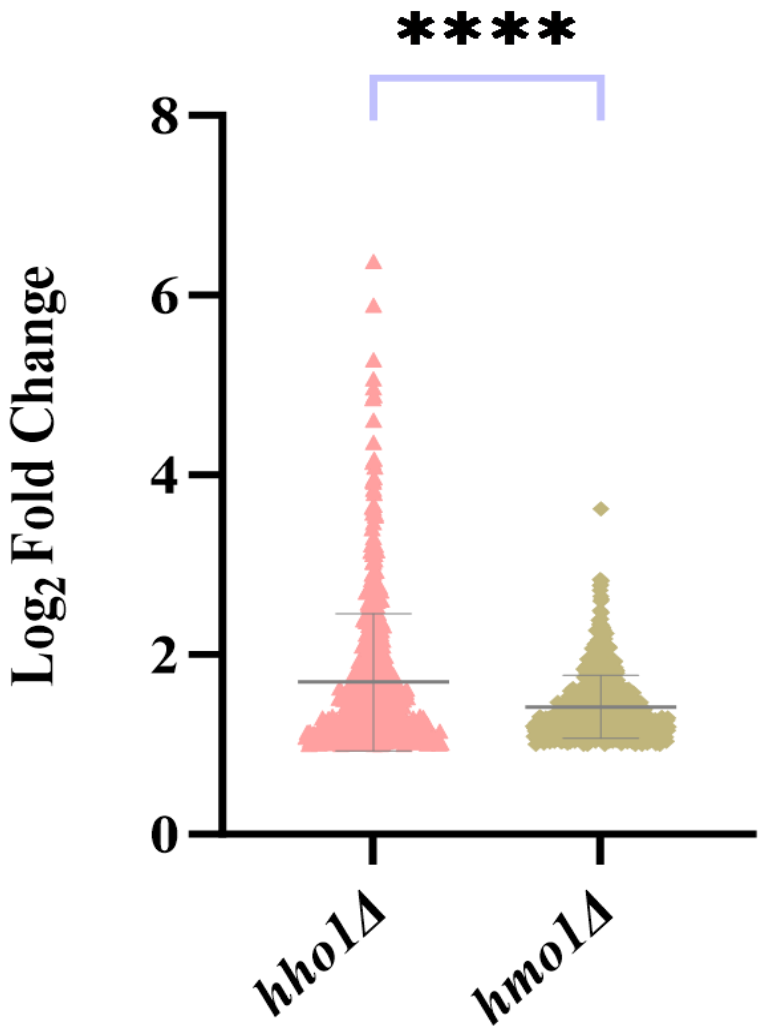

Figure 5.19: Levels of all significantly up-regulated genes in quiescent cells of each mutant compared to wt. A scatter graph is presented which displays the Log2-fold change values of the genes that are at least two-fold up-regulated (Log2 ≥1, adjusted p-value of p≤0.05) in each strain (*hho1*Δ (689 genes) and *hmo1*Δ (863 genes)) compared to wt. The graph also indicates the mean and standard deviation. Significance using T-test analysis (* p = 0.05, ** p = 0.01, **** p = <0.0001).

5.4.2.1 Gene ontology analysis of the genes up-regulated in quiescent cells of each mutant

I next explored the gene ontology (GO) categories linked to the genes that were upregulated in the quiescent mutant strains relative to the quiescent wild type cells. These genes represent the cohort of genes within quiescent cells subject to repressive regulation by *HMO1* and *HHO1*.

Firstly, focusing on the gene ontology analysis in *hho1*Δ (Fig. 5.20A), 50 genes were identified as involved in 'proteasome-mediated ubiquitin-dependent protein catabolic process'. Some genes in this category included *CDC20*, a ubiquitin-protein transferase activator involved in the mitotic spindle assembly checkpoint; *ASI3*, a ubiquitin-protein ligase involved in protein catabolism and response to amino acids; *CUZ1*, a zinc finger protein induced under DNA replication stress; and *NMA111*, a nuclear serine-type endopeptidase involved in heat response, lipid metabolism, protein catabolism, and, interestingly, apoptosis.

In the Molecular Function category, 77 genes were also identified in the 'oxidoreductase activity' category. Some genes in this category include *IMD2*, an inosine monophosphate dehydrogenase involved in GTP biosynthesis; *OYE3*, an NADPH dehydrogenase with a role in apoptosis; *CCP1*, a cytochrome-c-peroxidase of the mitochondrial intermembrane space involved in the response to oxidative stress; and *SRX1*, a sulforedoxin contributing to oxidative stress resistance.

Gene ontology analysis of genes upregulated in the *hmo1*Δ mutant quiescent cells (Fig. 5.20B), identified 208 genes in the Biological Process category described as having a role in 'protein modification by small protein conjugation or removal'. Some prominent genes in this category include *ALD3*, an aldehyde dehydrogenase involved in polyamine catabolism and beta-alanine biosynthesis; *UBP13*, a thiol-dependent deubiquitinase involved in the breakdown of free ubiquitin chains; *YML039W*, a retrotransposon processed to make a nucleocapsid-like protein; and *SCH9*, a protein serine/threonine kinase involved in the regulation of transcription by RNA polymerases I, II, and III.

A group of 39 genes in Molecular Functions included *CDC4*, a subunit of the SCF protein complex which contributes to proteasomal-dependent ubiquitin protein ligase activity involved in protein catabolism; *IRC20*, a ubiquitin transferase and putative helicase involved in double-strand break repair; *DMA2*, a ubiquitin-protein ligase (E3) that controls septin dynamics and the spindle position checkpoint; and *DAS1*, a component of the SCF E3 ubiquitin ligase complex involved in targeting proteins for degradation by the proteasome.

Additionally, 104 genes were identified in the Cellular Component category and further classified within the 'vacuolar membrane' category (GO:0005774). Some examples of genes in this category are *DIP5*, a dicarboxylic acid transmembrane transporter that transfers dicarboxylic amino acids, aspartate, and glutamate, across membranes; *PEP4*, a vacuolar peptidase with a role in autophagy; and *AVT4*, a vacuolar transporter that exports large neutral amino acids from the vacuole.

Overall, these data suggest a role for Hmo1p and Hho1p in repressing the expression of genes involved in a diverse array of cellular functions during quiescence, including repression of many genes involved in proteasome-mediated protein catabolism and stress response genes. Interestingly, the data revealed a role for *HHO1* in repressing some key genes involved in regulating apoptosis, while *HMO1* was required to repress *SCH9*, which encodes a signalling kinase involved in regulating Pol I, II and III transcriptions.

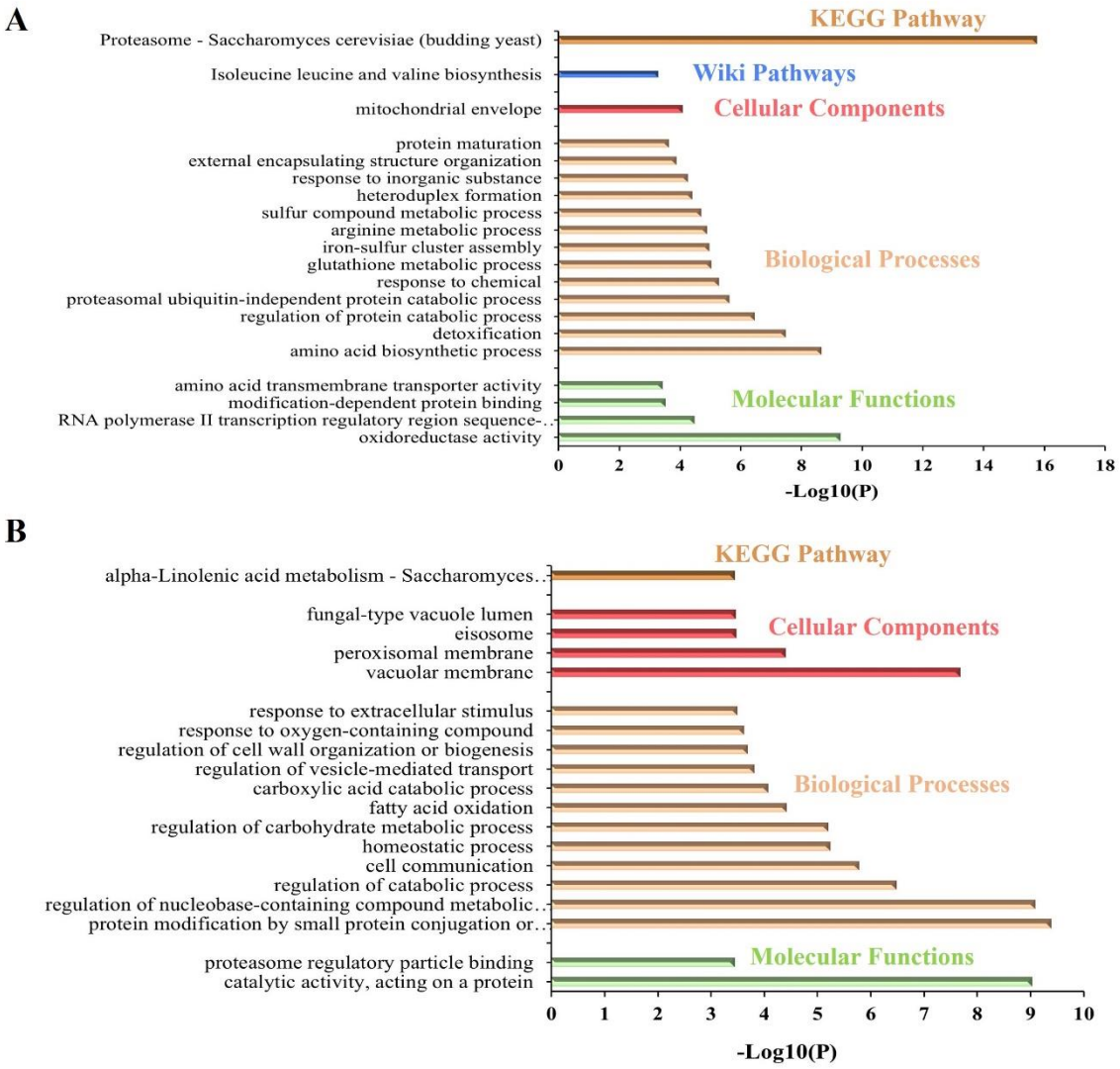

Figure 5.20: Gene Ontology analysis of genes up-regulated in *hmo1*Δ and *hho1*Δ compared to wt in quiescent cells. The significant GO terms from the molecular function category are represented by the light green, biological process category is depicted by the light orange, and the dull red represents significant GO terms from the Cellular Component category according to the Metascape. The X-axis shows the - Log (corrected P-value< 0.05); higher values indicate more statistical significance, and the Y-axis shows the GO term. **(A)** up-regulated genes of *hho1*Δ **(B),** up-regulated genes of *hmo1*Δ, KEGG pathways: Kyoto Encyclopedia of Genes and Genomes curated biological pathways. Wiki pathways: community-curated pathways on WikiPathways.

5.4.2.2 Identification of genes commonly up-regulated in *hho1*Δ and *hmo1*Δ deletion strains compared to wt in quiescent cells

I next looked to see if there was any overlap in those genes upregulated in the quiescent *hho1*Δ and *hmo1*Δ mutant cells compared to wt (Fig. 5.21A). This might inform us as to whether Hmo1p and Hho1p might overlap in their repressive regulatory roles during quiescence.

Comparing the total number of genes upregulated in the *hho1*Δ mutant (689 genes) with those upregulated in the *hmo1*Δ mutant (863 genes), we find that 269 genes overlapped. This suggests that a significant subset of genes are subject to regulation by both Hmo1p and Hho1p during quiescence.

When the average upregulation levels of the co-repressed genes were compared in each mutant, those genes in *hho1*Δ were upregulated the most. This suggests these genes are subject to more repression by *HHO1* than by *HMO1* in quiescent cells (Fig. 5.21B).

When I looked at the 269 genes subject to negative regulation by both *HMO1* and *HHO1* during quiescence, I found these genes to be involved in a wide variety of cellular functions such as amino acid metabolism (*AAD10, KGD1, LEU1, MET4, SAM1*), carbohydrate metabolism (*CHO2 GAS4, HXT1, HXT5, NPR1*), cell cycle and DNA processing (*CDC27, DDI1, DSK2, MSH3, SSM4*), cell wall and membrane biosynthesis *(BGL2, FKS1, MNN10, PMR1, SUR1)*, lipid metabolism (*AIM46, IPT1, LPP1, PHM8, PHS1*), protein biosynthesis and degradation (*AIM46, CAF40, DRE2, MCH1, MCT1*), stress response and defence *(DSE1, GRE1, GRX3,HAP2, HOG1)* and transporters (*ATO2, BTN2, DAL4, HNM1, JEN1)* (Table 5.6).

Overall, these co-repressed genes were enriched for essential cellular functions relevant to quiescence such as metabolism, the cell cycle and DNA Processing, protein turn-over (biosynthesis and degradation) and stress response. Examples of genes in quiescent cells subject to repression by *HHO1* only, by both *HHO1* and *HMO1*, and by *HMO* only, are shown in (Fig. 5.21C, D and E, respectively).

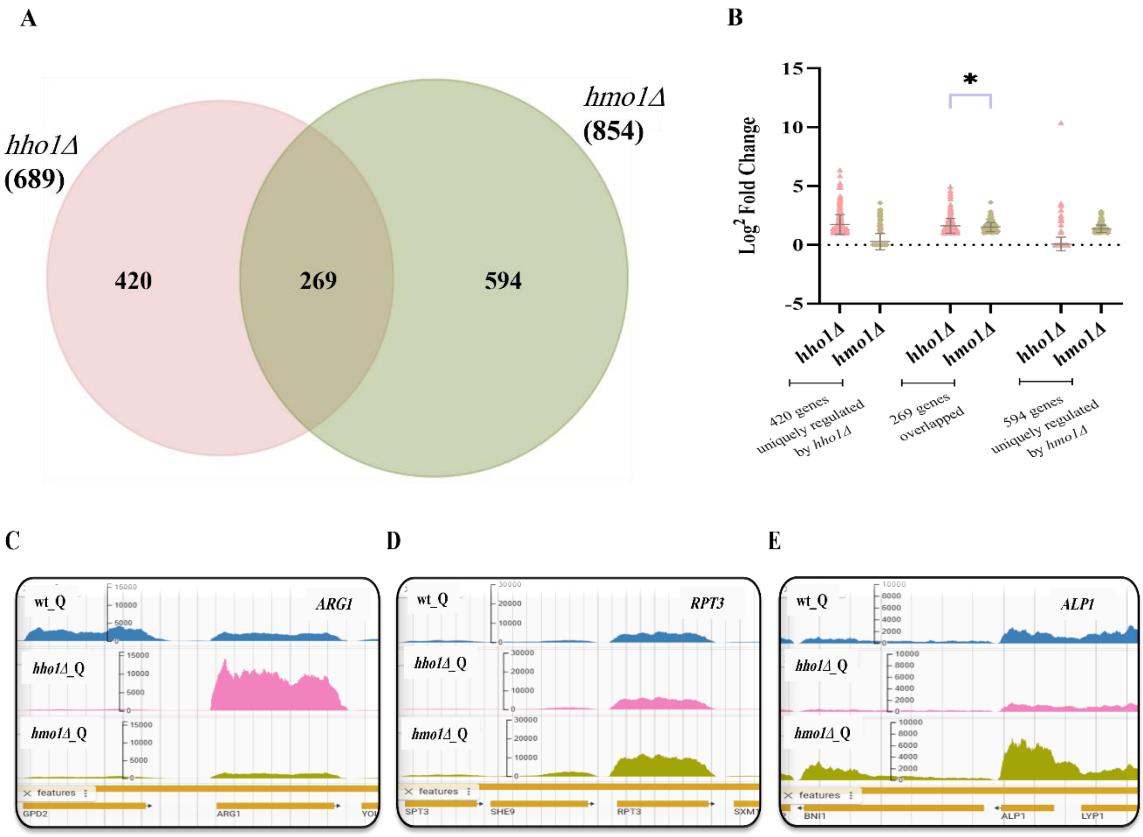

Figure 5.21: Identification of shared and uniquely up-regulated genes in day 7 quiescent cells of *hmo1*Δ and *hho1*Δ mutants. (A) Venn diagram of genes more than 2-fold up-regulated in *hho1*Δ and *hmo1*Δ vs wt in day 7 quiescent cells. **(B)** Scatterplot to show transcription levels of genes commonly and uniquely regulated by *HHO1* and *HMO1*. Significance using T-test analysis (* p = 0.05, ** p = 0.01, **** p = <0.0001). Examples of genes subject to repression by **(C)** *HHO1* only, **(D)** both *HMO1* and *HHO1* together, and **(E)** *HMO1* only.

Amino Acid Metabolism	Carbohydrate Metabolism	Cell Cycle and DNA Processing	Cell Wall and Membrane Biosynthesis	Lipid Metabolism	Protein Biosynthesis and Degradation	Stress Response and Defense	Transporters
AAD10	*CHO2*	*CDC27*	*BGL2*	*AIM46*	*AIM46*	*DSE1*	*ATO2*
ARO3	*GAS4*	*CDC34*	*FKS1*	*IPT1*	*CAF40*	*GRE1*	*BTN2*
ARO7	*HXT1*	*DDI1*	*MNN10*	*LPP1*	*DRE2*	*GRX3*	*DAL4*
ARO9	*HXT5*	*DIN7*	*PMR1*	*PHM8*	*MCH1*	*HAP2*	*HNM1*
AUR1	*NPR1*	*DSK2*	*SUR1*	*PHS1*	*MCT1*	*HOG1*	*JEN1*
ASN2	*PGA3*	*MSH3*	*YRO2*	*PSD1*	*MGR3*	*HSP12*	*MUP1*
ATG10	*RAM1*	*MSH6*		*SUR4*	*MOT2*	*IZH3*	*NCE102*
KGD1	*RGT1*	*RAD51*		*TGL3*	*MRX16*	*OAZ1*	*OAC1*
KGD2	*SFA1*	*RAD54*		*TGL5*	*MUB1*	*SKN7*	*PDR15*
KIC1	*STL1*	*RAD57*			*PDR1*	*YAP1*	*PHO90*
LEU1	*TPS2*	*RAD6*			*PDR12*		*SPS19*
LEU4	*TPS3*	*RIM4*			*RPN1*		*TPO2*
MET4	*URA2*	*RPH1*			*RPN12*		*TPO3*
ILV5	*VID22*	*RPN1*			*RPN3*		*VBA5*
SAM1		*RPN12*			*RPN8*		*VHT1*
YHK8		*RPN3*			*RPO21*		*YDR508C*
		RPN8			*RPT3*		
		RPO21			*RPT6*		
		RPT3			*YTA7*		
		RPT6					

Table 5.6: The 269 genes commonly up-regulated in quiescent *hho1*Δ and *hmo1*Δ mutants relative to wt day 7 quiescent cells.

5.4.2.3 Summary

This section identified and analysed the genes upregulated in the quiescent phase *hmo1*Δ and *hho1*Δ mutants compared to wt. These are the genes at which *HHO1* and *HMO1* are having a negative (repressive) effect upon transcription.

The analysis showed that *HMO1* repressed more genes (863 genes) than *HHO1* did (689 genes). However, those genes repressed by *HHO1* were, on average, subject to greater repression than that exerted by *HMO1*. Gene ontology analysis of these genes revealed a diverse array of types of genes subject to *HMO1* and *HHO1* repression. Interestingly, some key genes involved in apoptosis were shown to be repressed via *HHO1*, suggesting a role for Hho1p in repressing apoptosis in wt quiescent cells.

The overlap analysis of upregulated genes in both mutants revealed that 269 genes are co-regulated by *HMO1* and *HHO1* during quiescence, affecting various cellular functions such as metabolism, cell cycle, and stress response.

This suggests a shared regulatory role for *HMO1* and *HHO1* in repressing gene expression during the quiescent phase. Interestingly, at these commonly negatively regulated genes, the data suggests that, on average, *HHO1* was exerting the greater negative effect upon transcription.

5.4.3 Analysing genes down-regulated in each mutant strain compared to wt in purified day 7 quiescent cells

I next examined the genes that were downregulated by at least twofold in the quiescent mutant strains compared to quiescent wild type (wt). These are the genes at which we can infer that Hho1p and Hmo1p were necessary for promoting their transcription (Fig. 5.22). The results indicated that in the quiescent *hmo1*Δ mutant, 1238 genes were downregulated compared to wt. In contrast, in the quiescent *hho1*Δ mutant, 854 genes were downregulated compared to wt (Table 5.8). Thus, *HMO1* has a greater role upon promoting gene transcription in quiescent cells compared to *HHO1*, at least in terms of the number of genes subject to positive regulation.

When I compared the average levels of the genes downregulated in the quiescent *hho1*Δ and *hmo1*Δ mutant cells, downregulation of the genes in the *hmo1*Δ mutant were significantly greater than the average downregulation of the genes in the *hho1*Δ mutant (Fig. 5.22). This suggests that *HMO1* has a greater influence upon activating target gene transcription in quiescent cells than *HHO1*.

Thus, overall, *HMO1* plays the dominant role in promoting gene transcription during quiescence; *HMO1* positively regulates more genes than *HHO1* during quiescence and regulates these genes to a greater extent than the positive impact of *HHO1* upon its target genes.

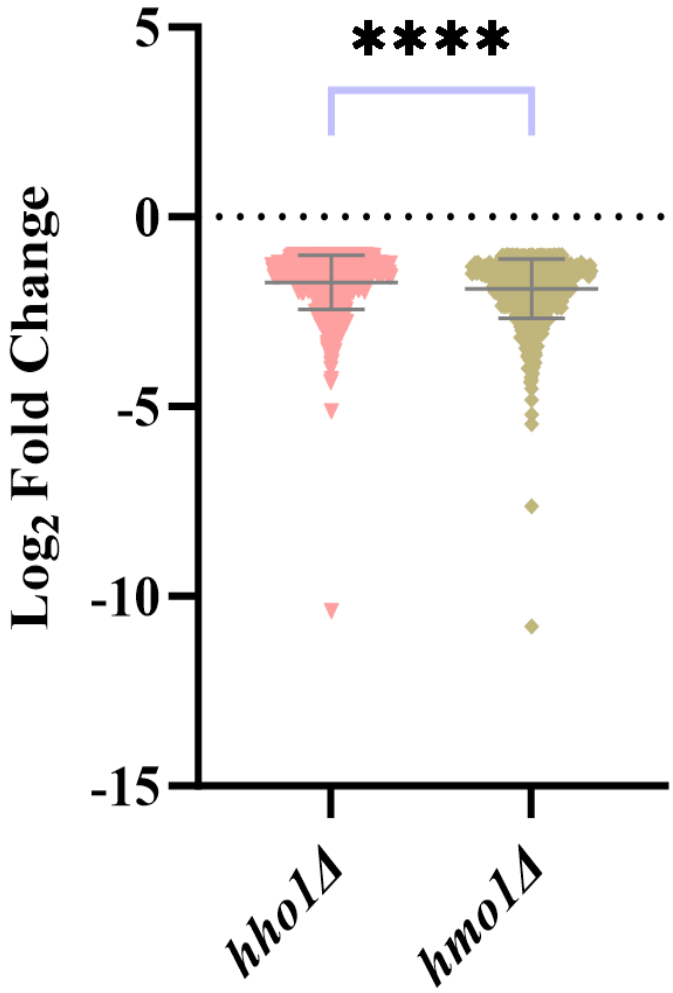

Figure 5.22: Total down-regulated genes in each mutant compared to wt in purified day 7 quiescent cells. A scatter graph is presented which displays the Log2-fold change values of the genes that are at least two-fold down-regulated (Log2 ≥1, adjusted p-value of p≤0.05) in each strain (*hho1*Δ (854 genes) and *hmo1*Δ (1238 genes)) compared to wt. The graph also indicates the mean and standard deviation. Significance using T-test analysis (* p = 0.05, ** p = 0.01, **** p = <0.0001).

5.4.3.1 Gene ontology analysis of genes down-regulated in each mutant compared to wt during quiescence cell (Q)

Gene ontology analysis of the 854 genes downregulated in the *hho1*Δ strain unveiled 306 genes implicated in ribosome biogenesis (Fig. 5.23A). Notable members of this category included *RPS6B* and *RPS9B*, encoding components of the small (40S) ribosomal subunit, and RPS*17B* encoding a ribosomal protein (rp51) responsive to DNA replication stress.

In the molecular functions, 174 genes were associated with 'peptide metabolic process'. Key genes in this class include *RPL22A*, encoding a ribosomal 60S subunit protein *L22A* crucial for the oxidative stress response, alongside *RPS6B*, *RPS9B*, and *RPS17B*.

In the *hmo1*Δ mutant, gene ontology analysis revealed downregulation of 1238 genes, with the most substantial subset (240 genes) involved in the 'small molecule metabolic process' (Fig. 5.23B). This group includes genes such as *ALD6*, an aldehyde dehydrogenase crucial for acetate biosynthesis, *ENO1* and *ENO2*, which are responsible for converting 2-phosphoglycerate to phosphoenolpyruvate and vice versa, and *TPI1*, a triose phosphoisomerase involved in converting carbohydrates to pyruvate during glycolysis. Additionally, 215 genes were categorized within the 'preribosome' category including *RPS17B*, *RPS0A*, *PWP1*, and *RPS21B*.

In the Molecular Function domain, 147 genes were linked to 'structural molecule activity' also included many genes involved in ribosomal structure and function. Noteworthy genes in this category include *RPL22A*, which encodes the ribosomal 60S subunit protein *L22A*, essential for the oxidative stress response and *RPS17B*, encoding the ribosomal protein 51 (rp51) of the small (40S) subunit, which responds to DNA replication stress.

Furthermore, in the Molecular Functions category, 117 genes were associated with 'structural molecule activity' (GO:0005198). Prominent genes here included more genes involved in ribosomal structure and function such as *RPL22A*, *RPS17B*, and *RPS29A*, which are part of the cytosolic small ribosomal subunit involved in translation and *RPS0A*, also part of the small ribosomal subunit, involved in rRNA processing, export from the nucleus, assembly of the small ribosomal subunit, and ultimately translation.

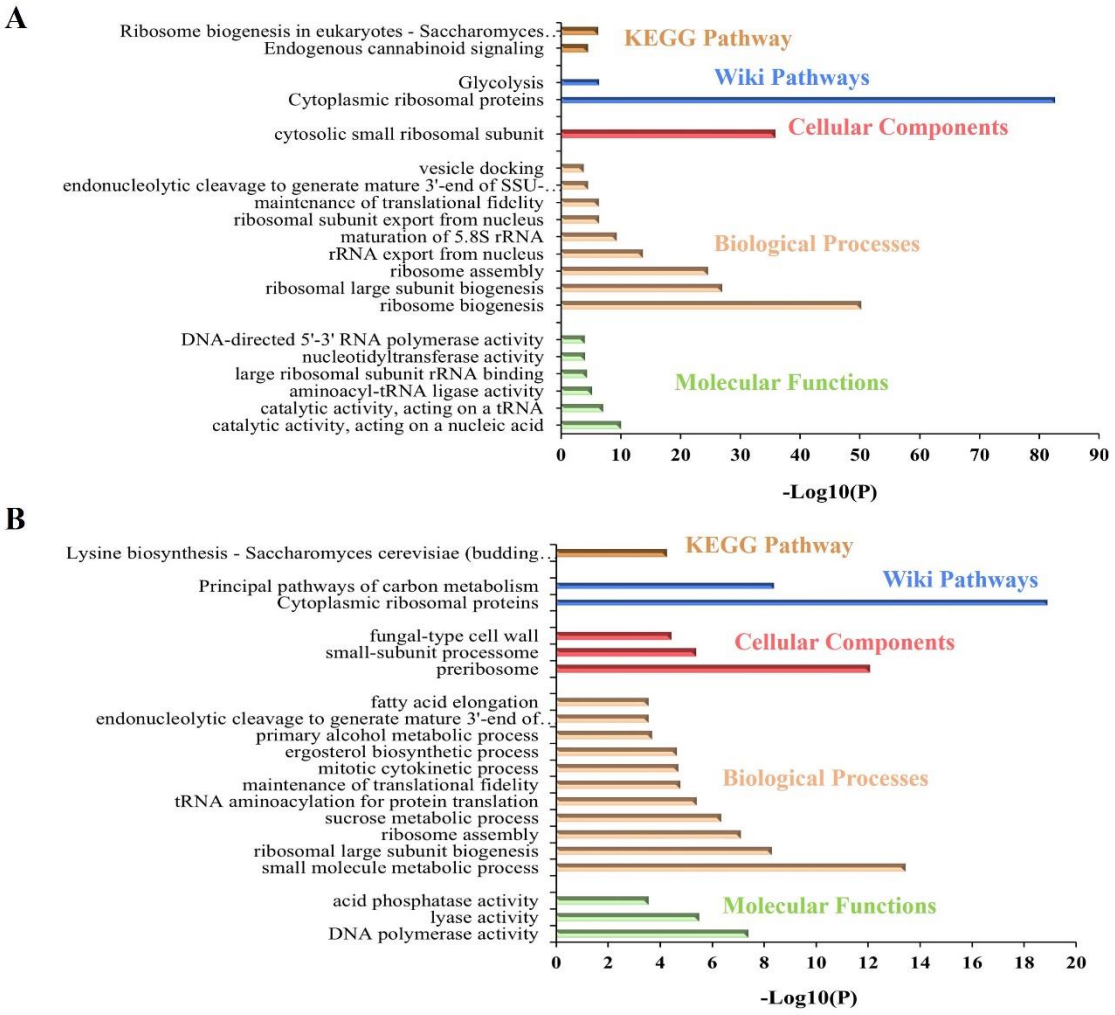

Figure 5.23: Gene Ontology analysis of genes down-regulated in the mutants compared to wt in day 7 quiescent cells. The significant GO terms from the molecular function category are represented by the light green, biological process category is depicted by the light orange, and the dull red represents significant GO terms from the Cellular Component category according to the Metascape. The X-axis shows the - Log (corrected P-value< 0.05); higher values indicate more statistical significance, and the Y-axis shows the GO term. **(A)** genes down-regulated in *hho1*Δ, **(B)** genes down-regulated in *hmo1*Δ, KEGG pathways: Kyoto Encyclopedia of Genes and Genomes curated biological pathways. Wiki pathways: community-curated pathways on WikiPathways.

5.4.3.2 Identification of genes commonly down-regulated in *hho1*Δ and *hmo1*Δ quiescent cells compared to wt

I next looked to see if there was any overlap in those genes downregulated in the *hho1*Δ and *hmo1*Δ mutants during quiescence compared to wt (Fig. 5.24A). This analysis showed that 553 genes overlapped which suggest that these genes are subject to activation by both Hmo1p and Hho1p in quiescent cells.

Upon comparing the average fold downregulation of the regulated genes in both *hmo1*Δ and *hho1*Δ mutants, it became evident that the downregulation was more pronounced in the *hmo1*Δ mutant (Fig. 5.24B). This implies that while both *HMO1* and *HHO1* can positively influence transcription of these genes during quiescence, *HMO1* exerts the greatest impact on this positive regulation.

When I looked at the 553 genes potentially activated by both Hmo1p and Hho1p, I found these genes to be involved in variety of cellular functions such as enzymatic reaction (*ATP19, ARO8, PFK2, URA1*), structural component (*ACT1, VMA22*), metabolite transporters (*ANT1, HXT2*), regulatory proteins (*CDC5, GCR1, SPT4*), chaperones and folding proteins (*HSP90, HSP70, HSP60),* signal transduction (*GPA1, STE20*), ribosomal biogenesis (*RPL11A, RPS2*), DNA/RNA binding (*RPA12, PRP19*), metabolism (*ENO1, PGI1*) and vesicle trafficking (*SEC31, VPS51*).

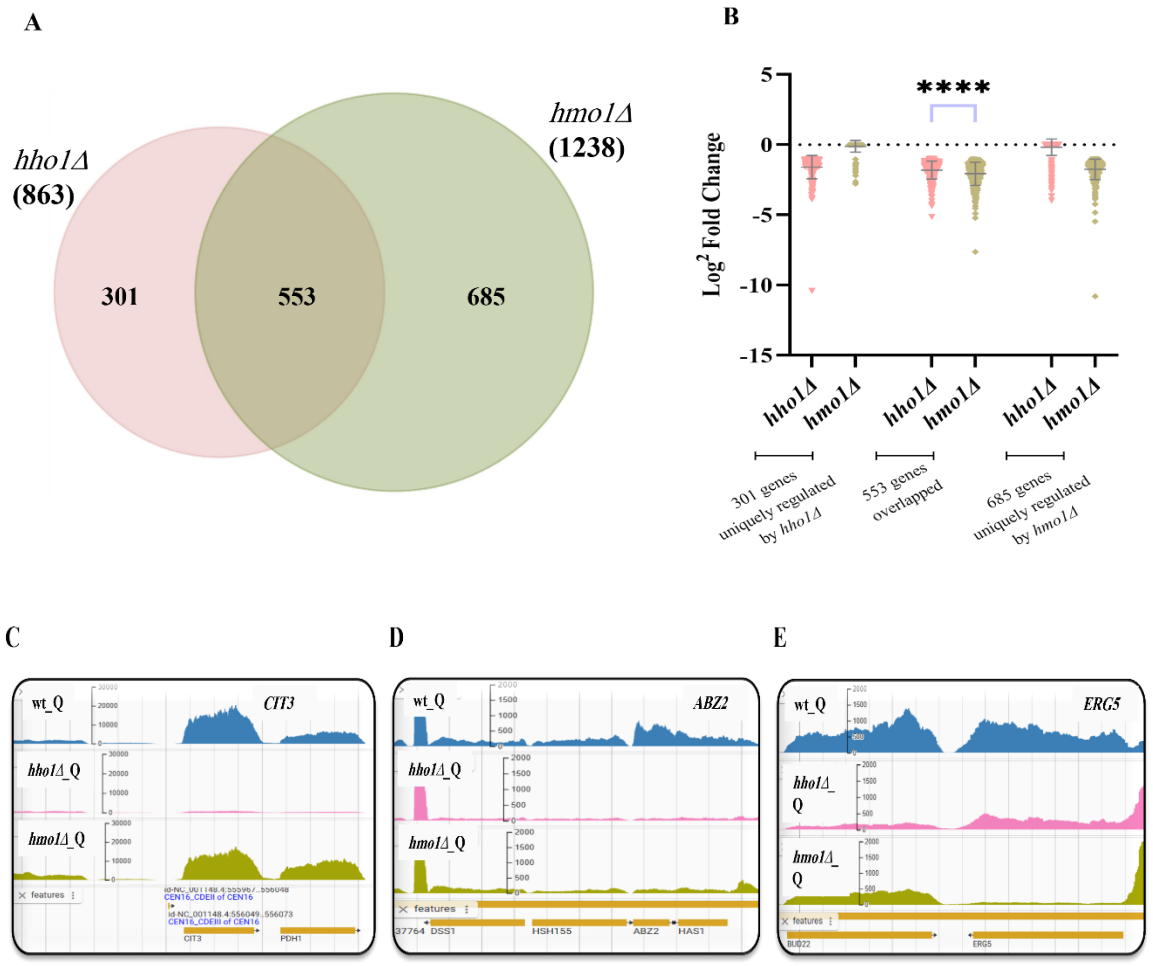

Figure 5.24: Analysis of commonly and uniquely down-regulated genes in quiescent cells. (A) Venn diagram **(B)** scatterplot of transcription levels of shared and uniquely down-regulated genes; the graph also indicates the mean and standard deviation. Significance using T-test analysis (* p = 0.05, ** p = 0.01, **** p = <0.0001) genes examples of genes subject to significant activation by **(C)** *HHO1* only, **(D)** both *HMO1* and *HHO1*, and **(E)** by *HMO1* only.

5.4.3.3 Summary

Each mutant strain exhibited a distinct pattern of gene downregulation during cellular quiescence compared to the wild type; 1238 genes were downregulated in *hmo1*Δ and 863 genes were downregulated in *hho1*Δ. Interestingly, the genes downregulated in the *hmo1*Δ mutant encoded some key metabolic genes which would be required to potentially drive cellular respiration. A cohort of 553 genes were commonly downregulated in both mutant strains during quiescence compared to wt. These 553 genes overlapped genes were downregulated, on average, to the greatest extent in the *hmo1*Δ mutant.

Together, *HMO1* plays the dominant role in the positive regulation of genes during cellular quiescence. However, there was a significant number of genes subject to positive regulation by both *HMO1* and *HHO1*, suggesting a potential cooperation between Hmo1p and Hho1p to promote transcription of these genes during quiescence. Many of these commonly activated genes were involved in ribosome synthesis, structure, and function.

5.5 Time-course analysis of transcription during quiescent cell development

In the previous sections of this chapter, I analysed gene-specific differences in *hho1*Δ and *hmo1*Δ mutants during exponential phase, at the diauxic shift, and in purified day 7 quiescent cells by comparing the transcriptomes of each mutant to wt, at each time point (Fig. 5.25A). Although this analysis gives insight into how the mutant behaves relative to wt at each time point, the comparisons only offer a 'snapshot' of transcription in each mutant at each time point.

In this section, I wanted to determine more clearly how the gene transcription profiles in wt and each mutant change over time during quiescent cell development. I therefore analysed the gene transcription profiles of wt, *hho1*Δ and *hmo1*Δ mutants at diauxie and in day 7 Q cells, but compared the results at these time points to the transcription profile of when each strain was gowing exponentially (Fig. 5.25B).

The main goal was to uncover more clearly the role of Hho1p and Hmo1p in the development of quiescent cells formed during stationary phase.

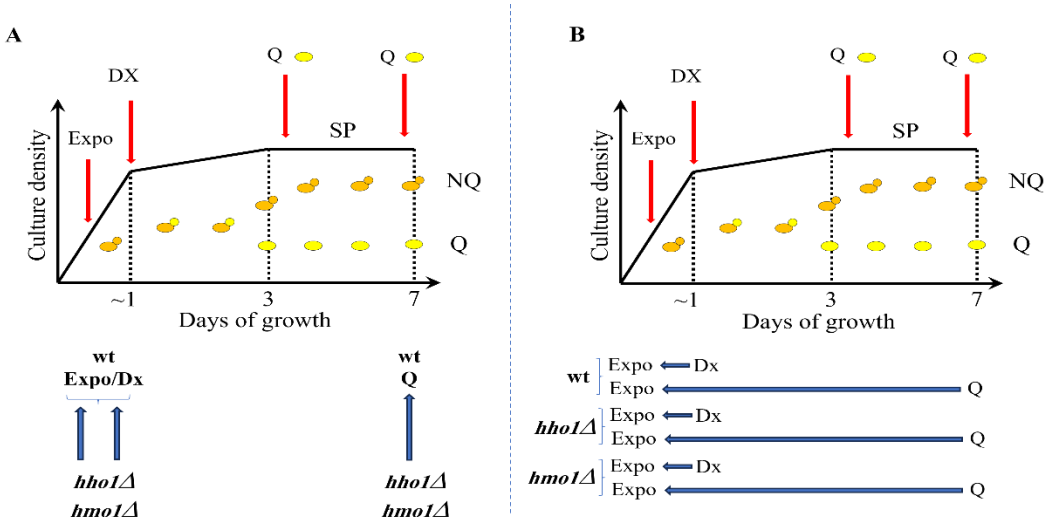

Figure 5.25: Different RNA-seq analysis strategies. **(A)** Comparison of RNA-seq data at exponential phase, at diauxie and in day 7 quiescent (Q) mutant cells compared to wt at each time point. **(B)** Time-course analysis of RNA-seq data; RNA-seq data at diauxie and in day 7 quiescent wt and mutant cells are compared to their own exponential phase RNase-seq data.

5.5.1 Results of analysis of gene expression in wt, *hho1*Δ and *hmo1*Δ at the diauxic shift (DX) compared to transcription during exponential phase

In an effort to elucidate the transcriptional response during quiescent cell development, transcription at diauxie and in day 7 Q cells in wt and the mutants was compared to their own exponential phase transcription profiles (Fig. 5.25B). The wild-type (wt) strain exhibited a significant change in gene expression at diauxie compared to exponential phase, with 1243 genes up-regulated and 1406 genes down-regulated (Table 5.7, wt). This suggests a robust transcriptional response to glucose depletion occurred in wt, as would be expected.

In contrast, the *hho1*Δ strain demonstrated a slightly attenuated response, with 981 genes up-regulated and 1202 genes down-regulated (Table 5.7, *hho1*Δ). This reduction in differentially expressed genes at diauxie compared to wt, may indicate a positive role for the *HHO1* gene in the response to glucose depletion. In the *hmo1*Δ strain, 1319 genes were up-regulated and 1457 were genes down-regulated: a response similar in number to that seen in wt (Table 5.7, *hmo1*Δ).

Strain	The number of genes up-regulated	Number of genes down-regulated
wt Expo vs wt DX	1243	1406
*hho1*Δ Expo vs *hho1*Δ DX	981	1202
*hmo1*Δ Expo vs *hmo1*Δ DX	1319	1457

Table 5.7: Table to show the numbers of genes more than 2-fold up- and down-regulated in each strain at diauxie compared to transcription at exponential phase.

However, visualisation of these transcription changes in each strain via a heat map showed that the heat map of the *hho1*Δ mutant looked most similar to wt; the variations in colour gradients were subtle suggesting only minor changes in gene expression (Fig. 5.26, compare B to A). Conversely, the *hmo1*Δ heat map looked the most different compared to the wt and the *hho1*Δ heat maps (Fig. 5.26, compare C to A). This suggests that despite the number of genes up and down regulated in the *hmo1*Δ mutant being similar to that seen in wt at diauxie, a stronger transcriptional response is occurring in the *hmo1*Δ mutant as compared to the *hho1*Δ mutant, as cells are exhausted of glucose.

In summary, the results provide a numerical and visual comparison of gene expression level changes occurring in response to glucose depletion in wt and the mutants, highlighting the dynamic nature of transcription during this key nutritional shift. The data also suggests that the *hmo1*Δ mutant shows the greatest difference in transcriptional changes at diauxie compared to that seen in wt and the *hho1*Δ mutant.

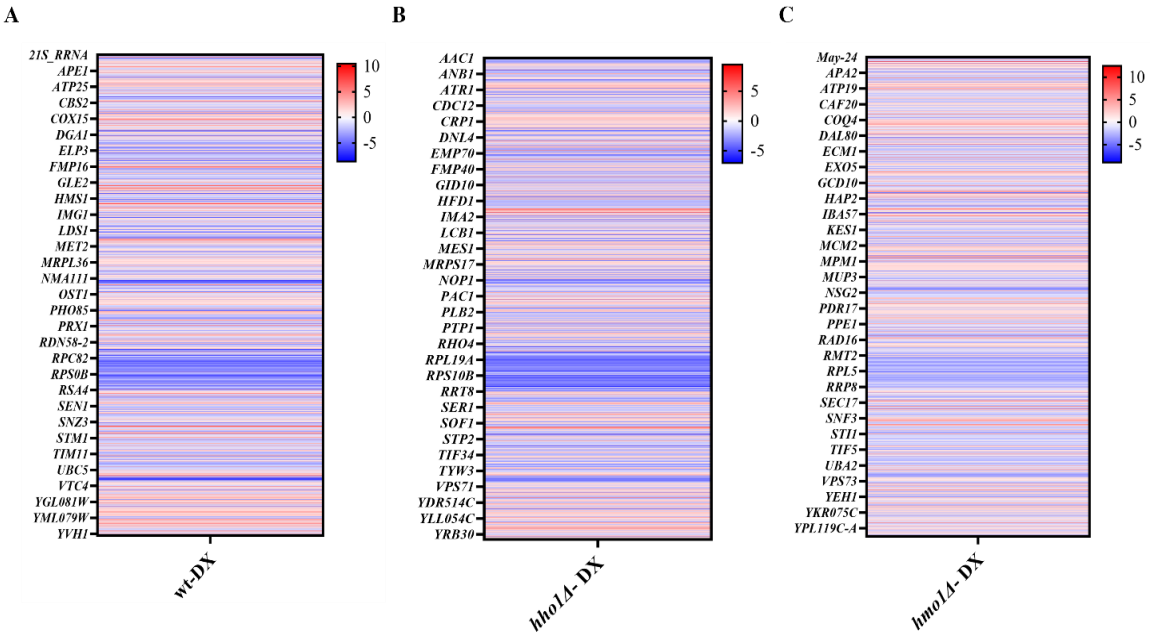

Figure 5.26: Heat map analysis of the total numbers of genes and up- and down-regulated more than 2-fold in each strain at diauxie (DX) compared to their levels at exponential phase. (A-C) A cluster heat map in the total number of genes up- and down-regulated in each strain at diauxie compared to exponential phase. The rows represent genes, and the columns represent mutants. Each cell is colourised based on the comparative level of expression (>2-fold change up (red)/down (blue) and FDR of <0.05) in the strains indicated. The top 30 up- and downregulated genes within each analysis are selectively indicated to the left-hand side of each heat map**.**

5.5.1.1 Analysing transcription levels of the total number of genes up-regulated at the diauxic shift relative to exponential phase levels of transcription in wt, *hho1*Δ and *hmo1*Δ

I next compared the average fold changes of the genes specifically upregulated in each yeast strain during the diauxic shift compared to the exponential growth phase (Fig. 5.27).

The wild-type results served as a baseline of the average gene upregulation occurring during the shift from the exponential phase to post-diauxie. The *hho1*Δ strain exhibited significantly less average upregulation of gene transcription as these mutant cells were starved of glucose compared to wt cells as they transitioned into the stationary phase. Conversely, the *hmo1*Δ strain demonstrated a higher average upregulation of gene transcription as these cells were starved of glucose.

In summary, these data revealed differing impacts of the *hmo1*Δ and *hho1*Δ mutants upon upregulation of gene transcription during the diauxic shift. The data suggests *HMO1* exerts a greater negative role upon transcription during the diauxic shift whereas *HHO1* exerts less of a repressive effect upon gene transcription during the shift from exponential phase to glucose exhaustion.

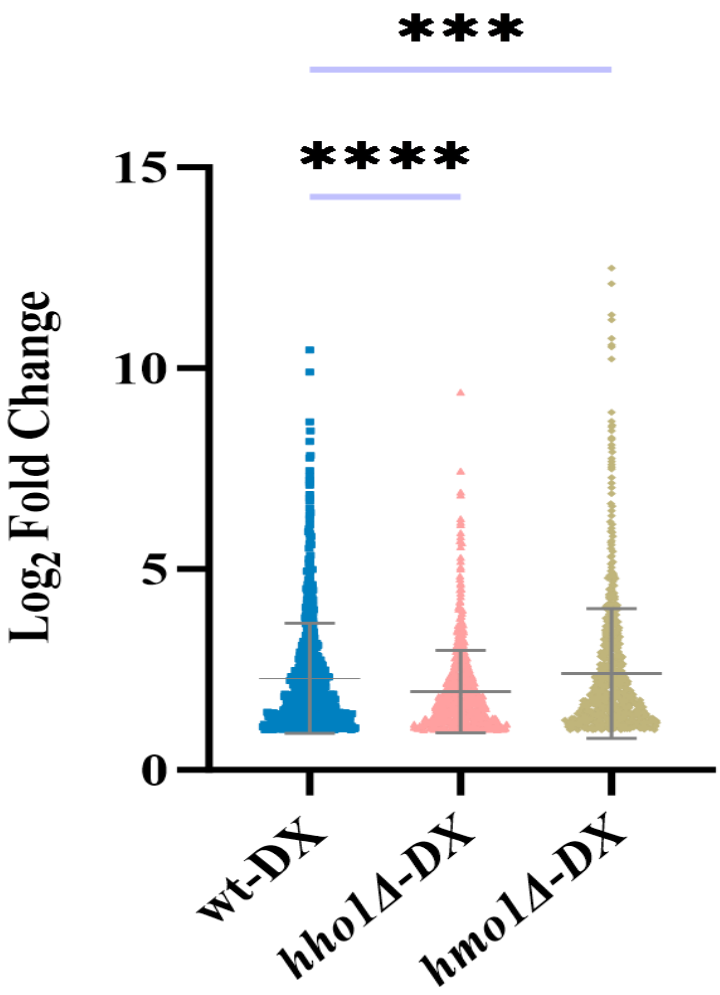

Figure 5.27: Average fold changes in transcription of the total number of genes significantly up-regulated in each strain at the diauxic shift compared to transcription during exponential growth. Scatter graph showing the Log 2-fold change values of all genes at least two-fold up-regulated (Log 2 ≥1, adjusted p-value of p≤0.05) in wt (1243 genes), *hho1*Δ (981 genes) and *hmo1*Δ (1319 genes) compared to their own exponential phase levels of transcription; mean and standard deviation are indicated. Significance using Two-way ANOVA analysis (* p = 0.05, ** p = 0.01, **** p = <0.0001).

5.5.1.2 Variation in the genes up-regulated during the diauxic shift (DX) in each strain compared to exponential phase transcription levels

Figure. 5.28 presents a Venn diagram that illustrates the overlap of the genes at least two-fold upregulated (Log 2 ≥1, adjusted p-value of p≤0.05) during the diauxic shift in wt, *hho1*Δ, and *hmo1*Δ, compared to transcription levels during exponential growth phase (Expo) in each strain. The diagram reveals unique sets of genes upregulated in each strain, with some genes being commonly upregulated across two or more strains, indicating a shared response to the diauxic shift at these genes.

Specifically, the wt strain shows a distinct set of 177 uniquely upregulated genes. The *hho1*Δ strain exhibits a subset of 76 genes that were uniquely upregulated, whilst the *hmo1*Δ mutant has 374 genes that were uniquely upregulated at the diauxic shift compared to exponential phase. The intersection of all three strains highlights a core set of 676 genes that were upregulated in all strains at the diauxic shift compared to exponential phase, suggesting upregulation of these genes was unaffected by loss of either *HMO1* or *HHO1*.

Overall, the deletion of the *HMO1* gene upregulates the most unique subset of genes during the diauxic shift, suggesting a wider role for Hmo1p in negatively regulating gene transcription at diauxie.

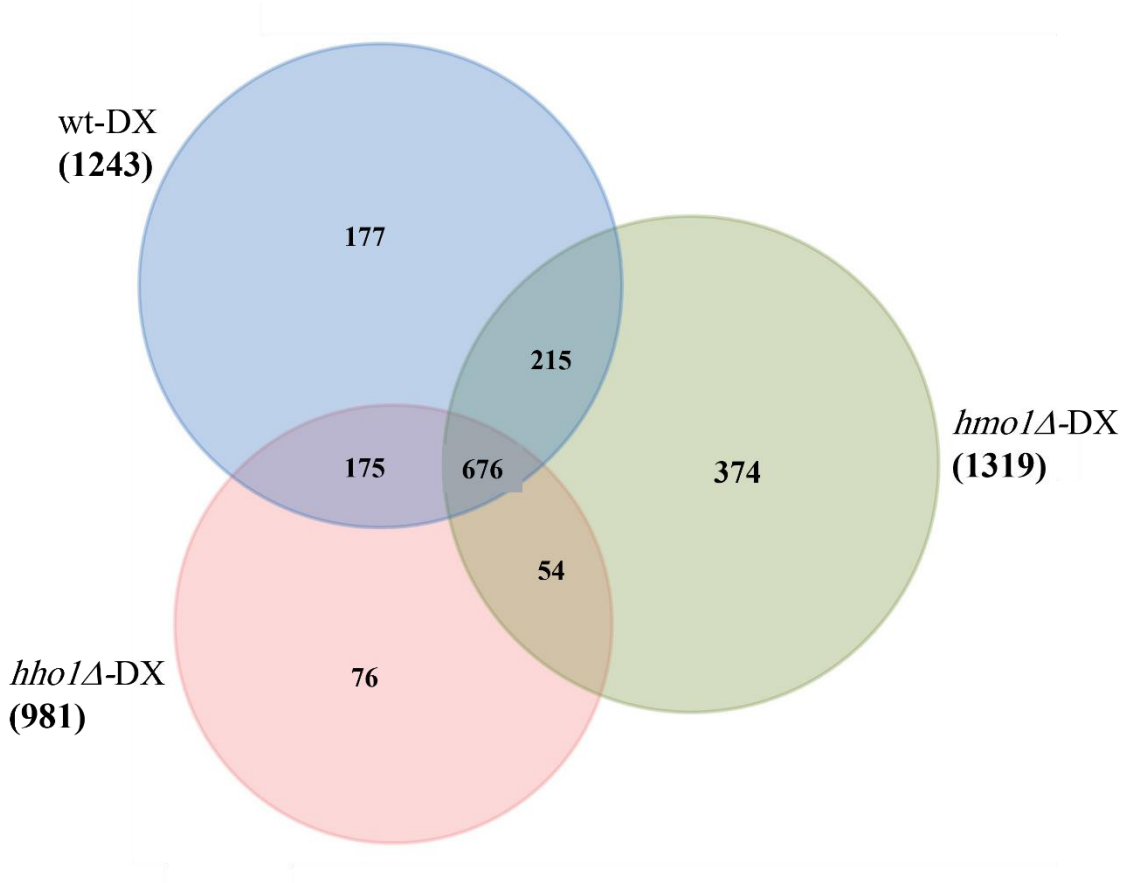

Figure 5.28: Different gene cohorts are up-regulated in each strain during the diauxic shift. Venn diagram of all genes that are at least two-fold up-regulated (Log 2 ≥1, adjusted p-value of p≤0.05) in the wt, *hho1*Δ, and *hmo1*Δ deletion strains compared to the expo.

5.5.1.3 Identification of the genes uniquely up-regulated during the diauxic shift compared to the exponential phase in the *hho1*Δ and *hmo1*Δ deletion strains

The previous venn diagram suggested *HMO1* and *HHO1* have a complex influence upon gene transcription during the diauxic shift. In an effort to clarify the transcriptional alterations induced by the deletion of *HHO1* and *HMO1* at diauxie, I separated out the previous venn diagram to individually view the genes upregulated in the *hho1*Δ and *hmo1*Δ mutants at diauxie compared to exponential phase and compared to events in the wild type (wt) (Fig. 5.29).

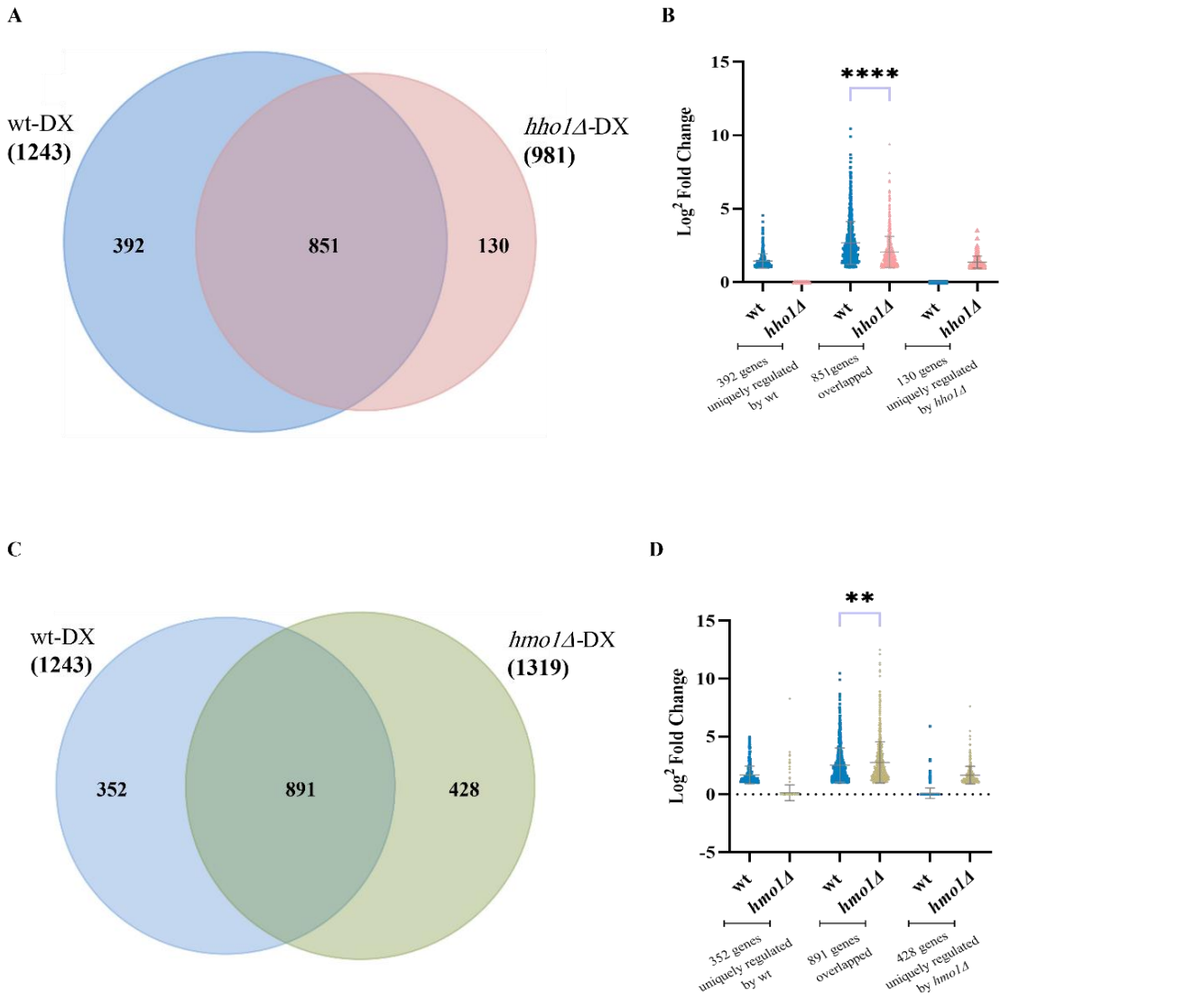

Figure 5.29: Unique and shared transcriptional profiles in yeast deletion mutants during diauxic the diauxic shift compared to events in wt cells. (**A)** Venn diagram depicting the overlap of genes up-regulated in wild-type (wt-DX) and *hho1*Δ *(hho1*Δ-DX) cells at diauxie compared to exponential phase. **(B)** Scatter plot illustrating the average transcription fold changes of the genes up-regulated in *hho1*Δ and wt at diauxie vs exponential phase. **(C)** Venn diagram depicting the overlap of genes up-regulated in wild-type (wt-DX) and *hmo1*Δ *(hmo1*Δ-DX) cells at diauxie compared to exponential phase**. (D)** Scatter plot illustrating the average transcription fold changes of the genes up-regulated in *hmo1*Δ and wt at diauxie vs exponential phase. Significance is indicated by **, corresponding to a p-value of < 0.01. Statistical significance was assessed using T-test analysis, with * representing a p-value of 0.05, ** indicating a p-value < 0.01, and **** denoting a p-value of < 0.0001. The fold changes are presented as log2 values.

I first compared the genes upregulated as the *hho1*Δ mutant shifts from exponential phase to diauxie to those that were upregulated in the wt as it shifts from exponential phase to diauxie (Fig. 5.29A). The Venn diagram illustrates that only 130 genes were uniquely up-regulated in the *hho1*Δ mutant whilst 851 genes were commonly upregulated in the *hho1*Δ mutant and wt as both cells undergo the diauxic shift. This suggests that the lack of *HHO1* only has a minimal impact upon the numbers of genes upregulated as cells shift from exponential growth to post-diuaxie.

Interestingly however, the scatter plot of the 851 genes commonly upregulated in the wt and *hho1*Δ mutant cells as they shift to post-diaxie shows that, on average, the upregulation of these genes was significantly less in the *hho1*Δ mutant than that seen for the upregulation of these genes in wt (Fig. 5.29B). This suggests that, even where the list of genes upregulated in both wt and the *hho1*Δ mutant overlaps (851 genes), the *HHO1* gene is having a generally positive effect upon their transcription and is required for these genes to be fully transcribed in wt at diauxie.

These results suggest that the *hho1*Δ mutation leads to a decrease in the transcription levels of the majority of genes normally upregulated as cells shift from exponential phase to diauxie, which may have downstream effects on the cell's physiological state and function.

The comparison of transcription upregulation in the wt and *hmo1*Δ mutant as they transition from exponential phase to diauxie, also revealed significant alterations (Fig. 5.29C). The Venn diagram revealed that 428 genes were uniquely upregulated in the *hmo1*Δ mutant, whereas wt and the *hmo1Δ* mutant shared a cohort of 891 genes that were upregulated in both strains during this transition. This suggests that *HMO1* is required for the correct repression of a relatively large cohort of genes (428) that should not normally be activated upon the diauxic shift. Furthermore, at the 891 genes commonly upregulated in both the wt and *hmo1Δ* mutant, these genes were upregulated to a greater extent in the *hmo1Δ* mutant than that seen for these genes in wt. This suggests that *HMO1* is acting to 'dampen down' transcription of the genes normally upregulated during the diauxic shift.

Overall, these results suggest that *HMO1* plays the greater role in regulating the gene transcription profile of genes upregulated during the diauxic shift. However, there are also subtle and largely opposing roles for *HMO1* and *HHO1* at the gene cohort normally upregulated in cells as they transition from exponential phase to diauxie; *HMO1* is acting to negatively influence these genes, whilst *HHO1* is having a positive influence upon transcription of these genes.

5.5.1.4 Analysing transcription levels of the total number of genes down-regulated at the diauxic shift relative to exponential phase levels of transcription in wt, *hho1*Δ and *hmo1*Δ

My results showed similar numbers of genes were downregulated in wt and *hmo1*Δ (1406 and 1457, respectively), whilst less genes were downregulated in *hho1*Δ (1202) (Table 5.9). I therefore compared the average fold changes of the genes specifically downregulated in each yeast strain during the diauxic shift compared to the exponential growth phase (Fig. 5.30). The wild-type result served as a baseline of the average gene downregulation occurring during the shift from the exponential phase to post-diauxie. The analysis revealed that the average extent of the genes downregulated in both mutants was significantly less than that seen in wt. This shows that the genes normally downregulated during the diauxic shift were subject to negative regulation by *HHO1* and *HMO1* such that in the absence of *HMO1* and *HHO1*, these genes were not being 'shut down' to the extent that they are in wt.

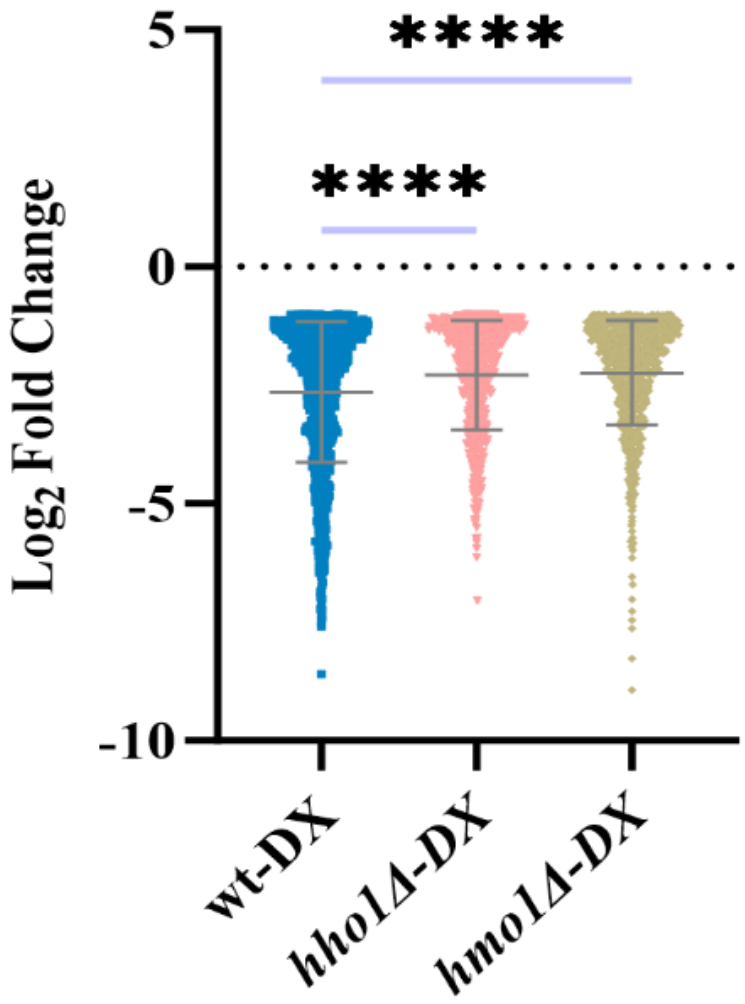

Figure 5.30: Average fold changes in transcription of the total number of genes significantly down-regulated in each strain at the diauxic shift compared to transcription during exponential growth. Scatter graph showing the Log 2-fold change values of all genes at least two-fold down-regulated (Log 2 ≥1, adjusted p-value of p≤0.05) in each strain (wt, *hho1*Δ *and hmo1*Δ) compared to wt, mean and standard deviation are indicated. Significance using Two-way ANOVA analysis (* p = 0.05, ** p = 0.01, **** p = <0.0001).

5.5.1.5 Variation in the genes down-regulated during the diauxic shift in each strain compared to exponential phase transcription levels

I prepared a Venn diagram of the genes downregulated during the diauxic shift across wt, *hho1*Δ, and *hmo1*Δ in comparison to the exponential growth phase (Fig. 5.31).

Notably, the wt strain exhibits 152 uniquely down-regulated genes, providing a baseline for transcriptional behaviour during the diauxic shift. The *hho1*Δ strain revealed 82 uniquely downregulated genes, whilst the *hmo1*Δ strain presents 413 uniquely downregulated genes.

A core group of 834 genes were downregulated in all strains suggesting these genes are not subject to regulation by either *HHO1* or *HMO1*.

Thus, overall, *HMO1* has the greatest influence upon regulating the correct repression of gene transcription during the diauxic shift.

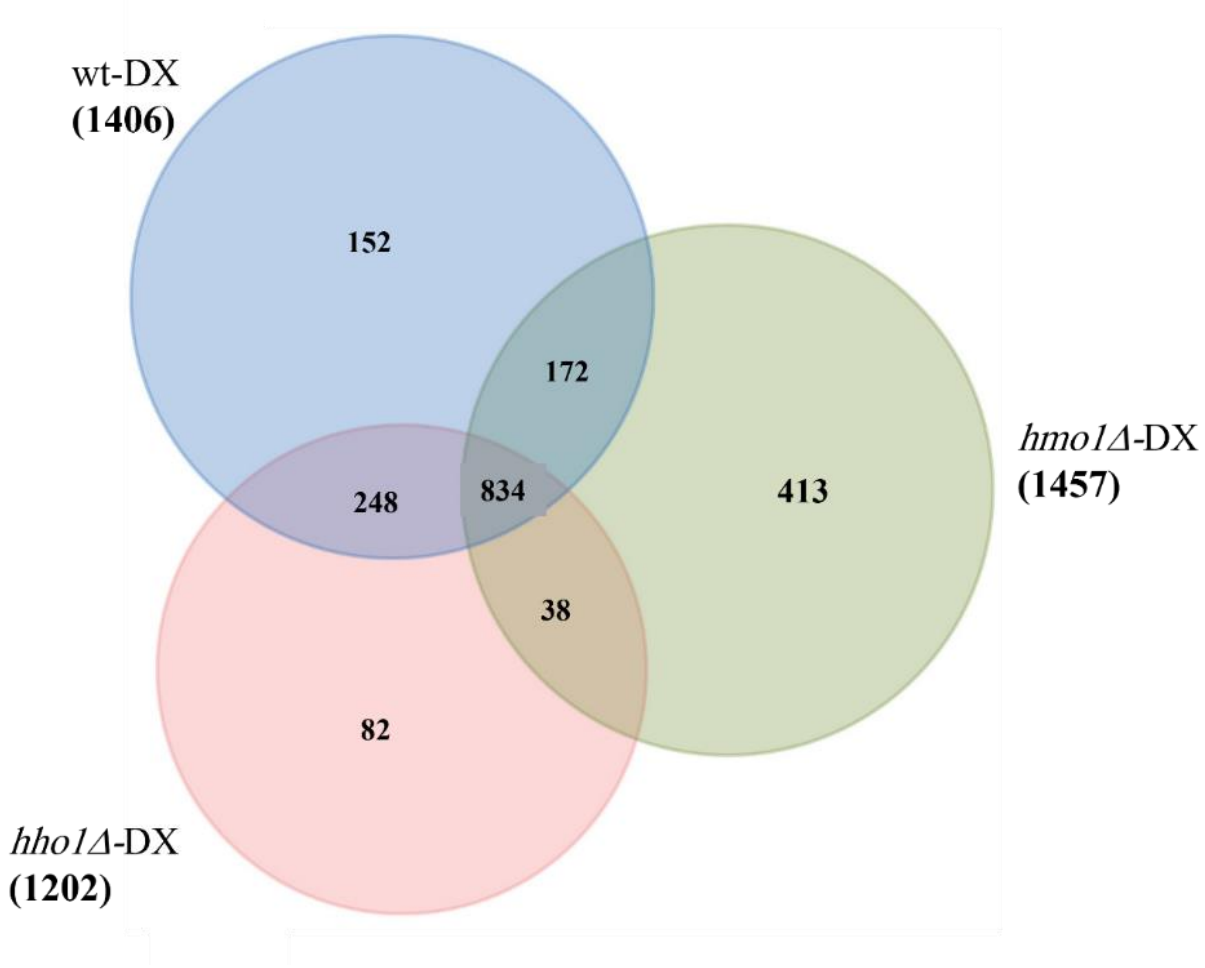

Figure 5.31: Different gene cohorts are down-regulated in each strain during the diauxic shift. Venn diagram of all genes that are at least two-fold down-regulated (Log 2 ≥1, adjusted p-value of p≤0.05) in the wt, *hho1*Δ, and *hmo1*Δ deletion strains compared to their transcription levels at exponential phase.

5.5.1.6 Identification of the genes uniquely down-regulated during the diauxic shift compared to the exponential phase in the *hho1*Δ and *hmo1*Δ deletion strains

In order to clarify the role of *HMO1* and *HHO1* upon gene downregulation during the diauxic shift, I prepared venn diagrams to individually view the genes downregulated in the *hho1*Δ and *hmo1*Δ mutants at diauxie compared to exponential phase and compared to events in the wild type (wt).

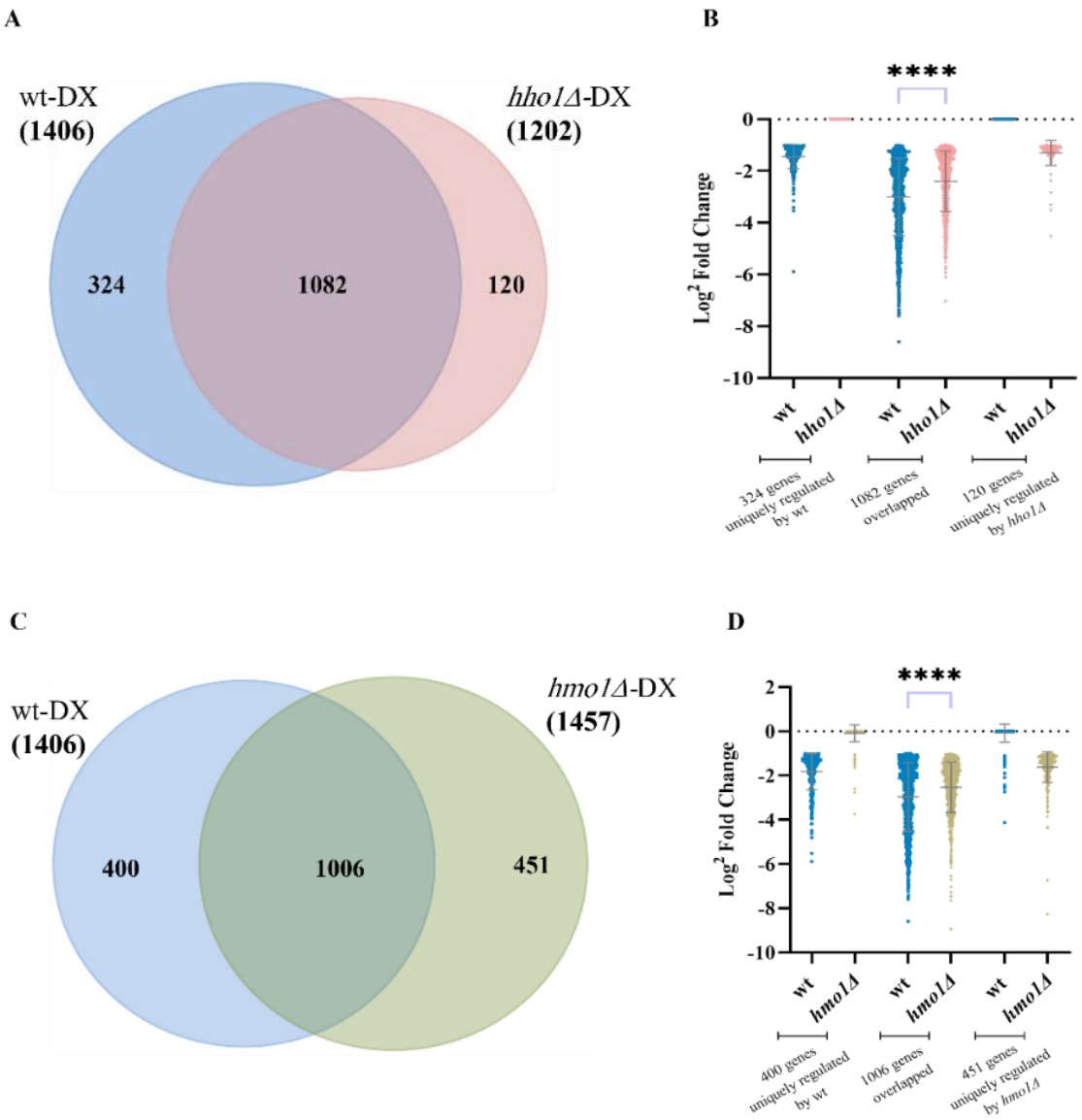

Figure 5.32: Differential gene expression analysis, u**nique and shared transcriptional profiles in yeast deletion mutants during the diauxic shift**. **(A)** Venn diagram depicting the overlap of genes down-regulated in wild-type (wt-DX) and *hho1*Δ *(hho1*Δ-DX) cells at diauxie compared to their exponential phase levels. **(B)** Scatter plot illustrating the average transcription fold changes of the genes down-regulated in *hho1*Δ and wt at diauxie versus exponential phase. **(C)** Venn diagram of genes down-regulated in wt-DX and *hmo1*Δ-DX conditions. **(D)** Scatter plot presenting the average transcription fold changes of the genes down-regulated in *hmo1*Δ and wt diauxic cells. In C and D, significant transcriptional changes are marked with asterisks. Statistical significance was assessed using T-test analysis, with * representing a p-value of 0.05, ** indicating a p-value < 0.01, and **** denoting a p-value of < 0.0001. The fold changes are presented as log2 values.

The Venn diagram illustrated only 120 genes were uniquely downregulated in the *hho1*Δ mutant, whilst 1082 genes were downregulated in both wt and *hho1*Δ (Fig. 5.32A). This suggests that the lack of *HHO1* only has a minimal impact upon the numbers of genes downregulated as cells shift from exponential growth to post-diuaxie.

However, the scatter plot of the 1082 genes commonly downregulated in the wt and *hho1*Δ mutant cells as they shift to post-diaxie shows that, on average, the downregulation of these genes was significantly less in the *hho1*Δ mutant than that seen for the downregulation of these genes in wt (Fig. 5.32B). This suggests that, even where the list of genes downregulated in both wt and the *hho1*Δ mutant overlaps (1082 genes), the *HHO1* gene is having a generally negative effect upon their transcription and is contributing to their full repression. This suggests that in the absence of *HHO1*, the correct full gene downregulation required during the diauxic shift might not be achieved.

The comparison of transcription downregulation in the wt and *hmo1*Δ mutant as they transition from exponential phase to diauxie, also revealed significant alterations (Fig. 5.32C). The Venn diagram revealed that 451 genes were uniquely downregulated in the *hmo1*Δ mutant, whereas wt and the *hmo1*Δ mutant shared a cohort of 1006 genes that were downregulated in both strains during this transition. This suggests that *HMO1* is required for the activation of a relatively large cohort of genes (451) that should not normally be repressed upon the diauxic shift.

Similar to what was seen for *HHO1*, at the 1006 genes commonly downregulated in both the wt and *hmo1*Δ mutant, these genes were downregulated to a lesser extent in the *hmo1*Δ mutant than that seen for these genes in wt (Fig. 5.32D). This suggests that *HMO1* is required to fully negatively influence transcription of the genes normally downregulated during the diauxic shift.

Overall, these results suggest that *HMO1* plays the greater role in regulating the gene transcription profile of genes downregulated during the diauxic shift. However, both *HHO1* and *HMO1* contribute to the full repression of those genes normally downregulated as cells shift from exponential phase to diauxie.

5.5.2 Analysis of gene expression in wt, *hho1*Δ and *hmo1*Δ in day 7 quiescent cells compared to transcription during the exponential phase

RNA sequencing analysis revealed distinct transcriptional regulation patterns among the wild-type (wt), *hho1*Δ, and *hmo1*Δ mutants in quiescent cells compared to exponential (Expo) phase cells (Table 5.8). In wt cells, 1473 genes were upregulated, and 1702 genes were downregulated. In the *hmo1*Δ mutant, 1837 genes were upregulated, and 1937 genes were downregulated. Finally, in the *hho1*Δ mutant, 1673 genes were upregulated, and 1881 genes were downregulated. Thus, as wt cells move from exponential phase to quiescence, there is a change in transcription of a large number of genes. However, in terms of the numbers of genes up and down-regulated in wt, *hmo1*Δ and *hho1*Δ day 7 Q cells compared to transcription in exponential cells, there were no large differences between the strains.

Strain	The number of genes up-regulated	Number of genes down-regulated
wt expo vs Q	1473	1702
*hho1*Δ expo vs Q	1673	1881
*hmo1*Δ expo vs Q	1837	1937

Table 5.8: Genes up-regulated and down-regulated in quiescent cells compared to exponential phase. Only genes significantly (more than 2-fold) up or down regulated are shown**.**

Visualisation of the total global changes in transcription (genes up and down regulated) in the Q cells of each strain compared to the transcription in wt cells, did reveal differences. In the wild-type (WT) strain, a significant down-regulation of genes was observed, with a predominant blue hue across the heat map (Fig. 5.33A). On the contrary, the *hho1*Δ and *hmo1*Δ mutants demonstrated a more distinct transcriptional landscape to wt but showed profiles similar to each other (Fig. 5.33B and C). Overall, the mutants showed a prevalent white/blue coloration, denoting a more widespread and robust, down-regulation of gene transcription.

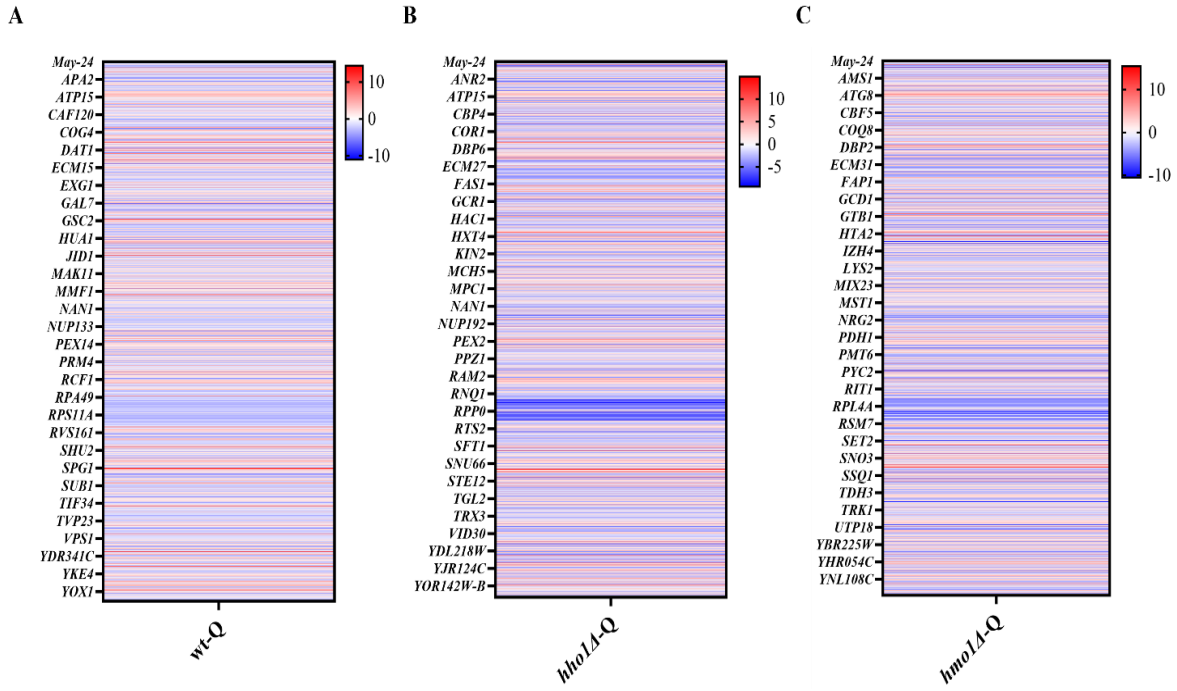

Figure 5.33: Heat map analysis of the total numbers of genes and up- and down-regulated more than 2-fold in day-7 quiescent cells compared to levels at exponential phase. (A-C) Each cell is colour-coded based on the comparative expression level, with red indicating >2-fold change up, and blue indicating >2-fold change down, and a p-value of <0.05 for the strains mentioned. The top 30 up and down regulated genes in each strain are indicated to the left of each heat map.

5.5.2.1 Total genes up-regulated in wt, *hho1*Δ and *hmo1*Δ quiescent cells (Q) compared with exponential phase

I first focussed my analysis of gene transcription changes in Q cells upon those genes specifically upregulated in the three strains at this stage compared to exponential levels (Fig. 5.34). The comparative analysis of average gene upregulation levels revealed that the average fold upregulation of genes in the *hho1*Δ mutant was significantly greater than wt and that the average upregulation of genes in the *hmo1*Δ mutant was similarly higher than wt. Thus, there is significant gene upregulation of transcription in Q cells due to the *hmo1*Δ and *hho1*Δ deletions, with both mutants showing similar levels of upregulation. This suggests a negative role for both *HHO1* and *HMO1* in regulation of gene transcription during Q cell development.

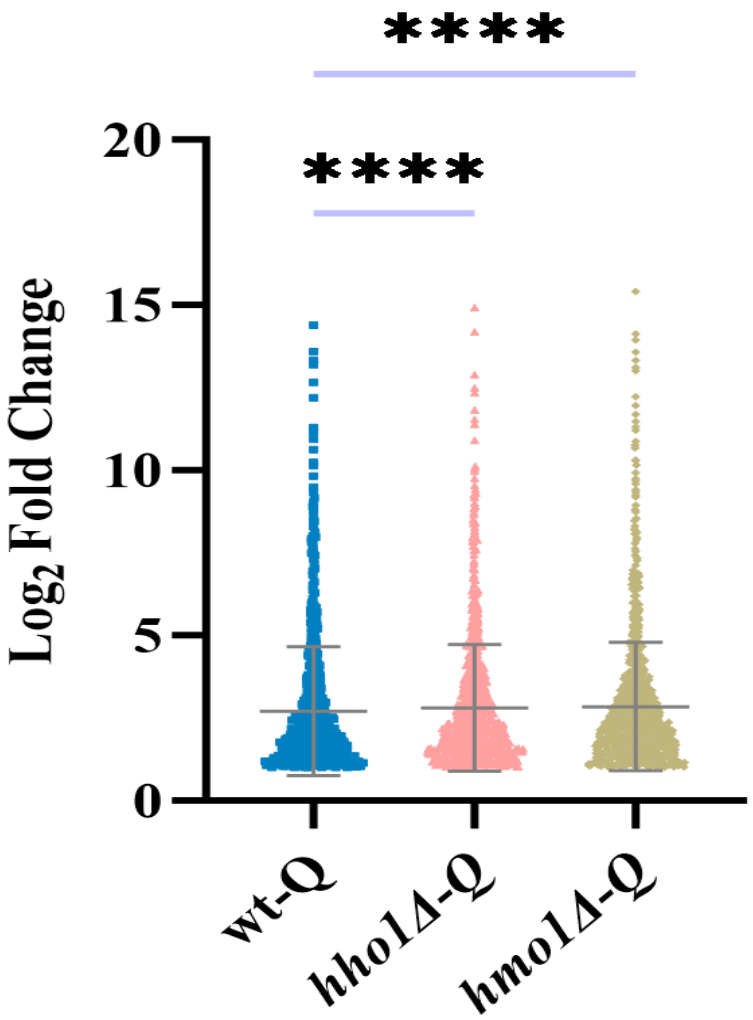

Figure 5.34: Average fold changes in transcription of the total number of genes significantly up-regulated in Quiescent cells of each strain compared to transcription during exponential growth. A scatter graph which displays the Log2-fold change values of the genes that are at least two-fold up-regulated (Log2 ≥1, adjusted p-value of p≤0.05) in the day 7 Quiescent wt (1473 genes), *hho1*Δ (1673 genes), and *hmo1*Δ (1837 genes) cells as compared to transcription levels during exponential phase. The graph also indicates the mean and standard deviation. Significance using Two-way ANOVA analysis (**** p = <0.0001).

5.5.2.2 Variation in the genes up-regulated in quiescent cells (Q) of each strain

The genes upregulated in the wt, *hho1*Δ and *hmo1*Δ mutant Q cells relative to exponential phase transcription levels were analysed (Fig. 5.35). The results showed that 94 genes were uniquely upregulated in the wt Q cells, 144 genes were uniquely upregulated in the *hho1*Δ mutant Q cells, and 295 genes were uniquely upregulated in the *hmo1*Δ mutant Q cells.

This finding suggests an alteration in gene upregulation in Q cells attributable to the *hho1*Δ mutation, and an even larger alteration in the gene upregulation profile due to the *hmo1*Δ mutation.

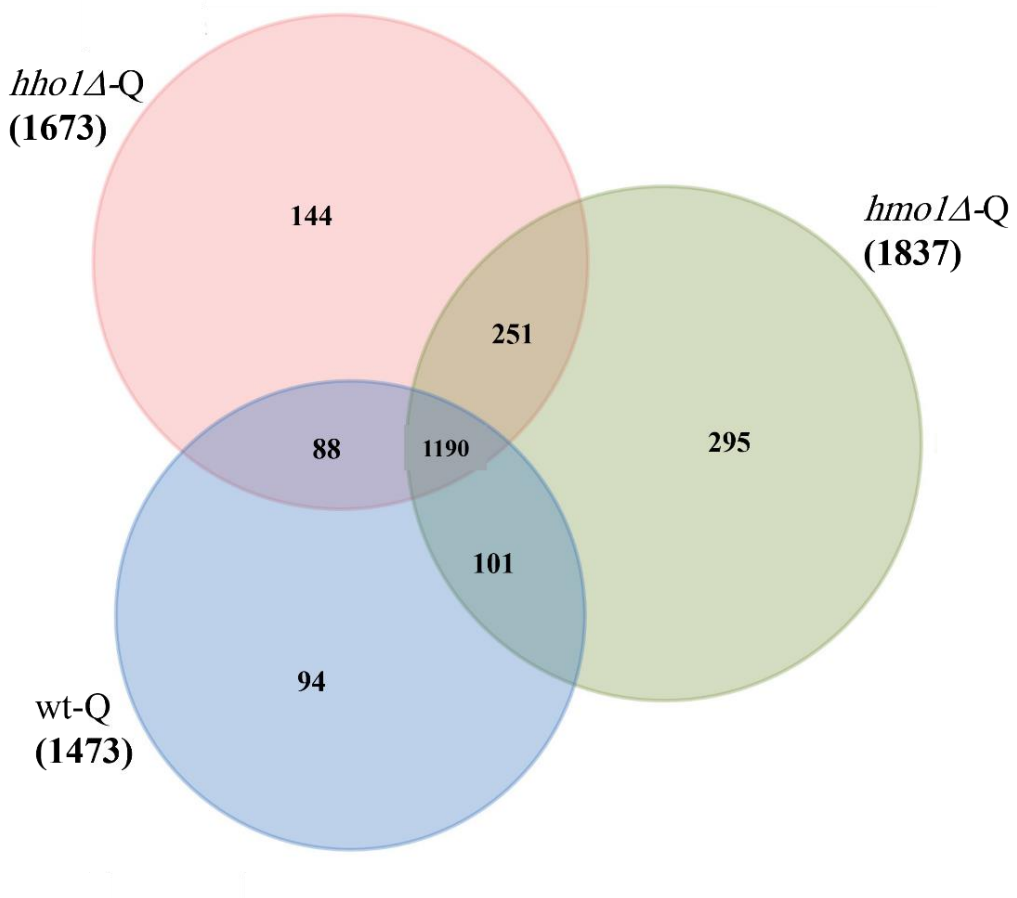

Figure 5.35: Different gene cohorts are upregulated in each strain during quiescence. The Venn diagram displays a set of genes up-regulated at least two-fold (Log 2 ≥1, adjusted p-value of p≤0.05) in quiescent cells of each strain compared to their exponential levels.

5.5.2.3 Differential gene regulation in *hho1*Δ and *hmo1*Δ mutants

In an effort to further elucidate the regulatory landscape of gene expression in quiescent cells, a comparative analysis of gene upregulation in each quiescent mutant was independently compared to the genes upregulated in the wt quiescent cells (Fig. 5.36).

The results showed that 395 genes were uniquely upregulated in the *hho1*Δ mutant quiescent cells compared to wt, whereas 546 genes were exclusively upregulated in the *hmo1*Δ mutant Q cells compared to the wt (Fig. 5.36A and C). Thus, the *hmo1*Δ mutant causes the aberrant upregulation of almost twice as many genes in Q cells compared to the *hho1*Δ mutant.

When I analysed the average upregulation levels of those genes upregulated in both the wt and *hho1*Δ (1278 genes), the results showed that these genes were upregulated to a significantly higher extent in the *hho1*Δ mutant (Fig. 5.36B). A similar result was seen when the genes shown to be upregulated in both wt and *hmo1*Δ mutant Q cells were analysed (1291 genes). Thus, both *HHO1* and *HMO1* act to further negatively influence those genes normally upregulated in quiescent cells.

These findings suggest that the deletion of *HHO1* and *HMO1* genes leads to differing cohorts of genes being aberrantly upregulated in quiescent cells and suggests a role for both *HMO1* and *HHO1* in ‘damping down’ those genes normally upregulated in quiescent cells.

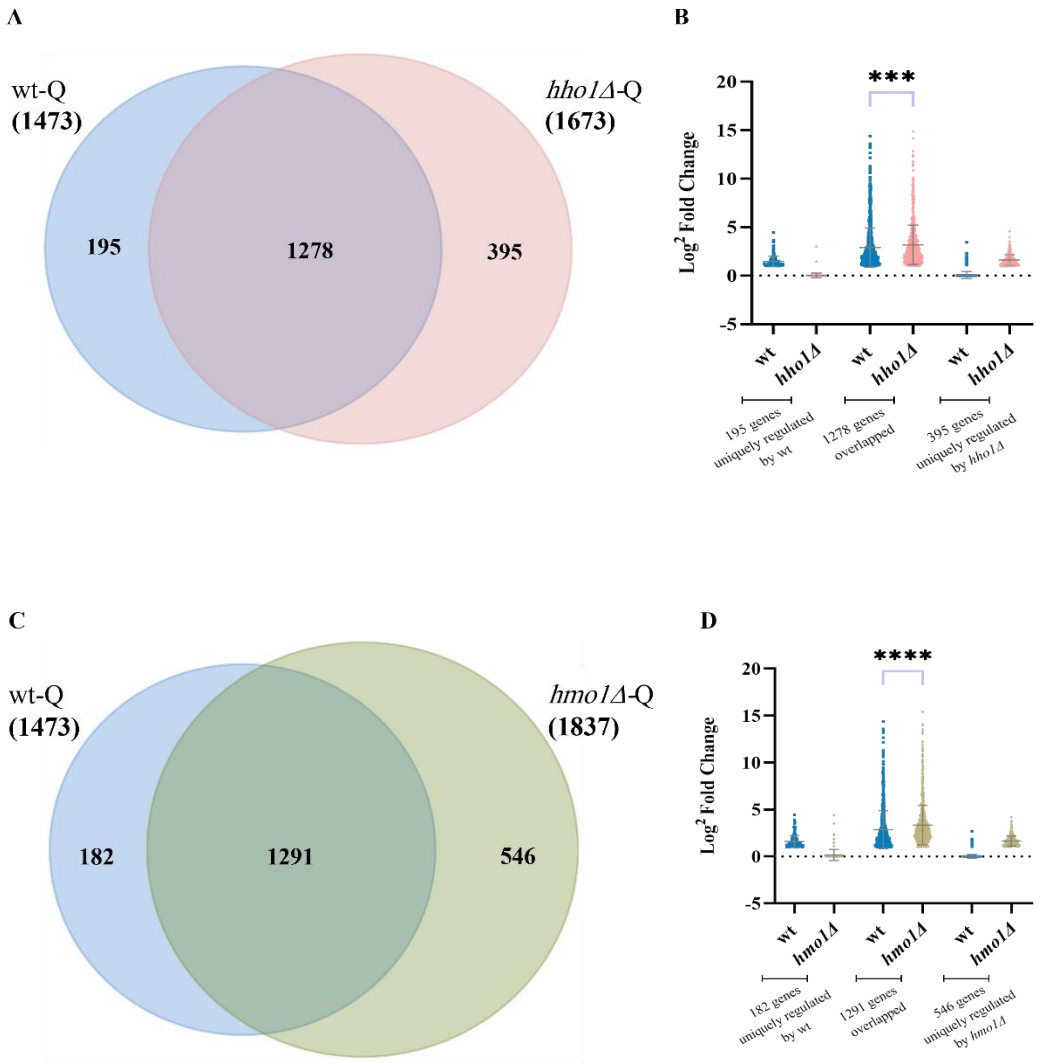

Figure 5.36: Differential up-regulation of genes in wild-type and yeast deletion mutants in quiescent cells. (A) Venn diagram illustrating the unique and shared up-regulated genes between wild-type (wt-Q) and *hho1*Δ-Q conditions. **(B)** Scatter plot presenting the average transcription fold changes of genes up-regulated in *hho1*Δ compared to wt. **(C)** Venn diagram showing the unique and shared up-regulated genes between wt-Q and *hmo1*Δ-Q conditions. **(D)** Scatter plot depicting the average transcription fold changes of genes up-regulated in *hmo1*Δ versus wt. In C and D, Significant transcriptional changes are marked with asterisks. Statistical significance was determined using T-test analysis, with * representing a p-value of <0.05, ** indicating a p-value of <0.01, and **** denoting a p-value of <0.0001. The transcription fold changes are represented as log-fold changes.

5.5.2.4 Analysing transcription levels of the total number of genes down-regulated in wt, *hho1*Δ and *hmo1*Δ quiescent cells relative to exponential phase levels of transcription

The results showed similar numbers of genes were downregulated in the quiescent wt (1702), *hmo1*Δ (1937), and *hho1*Δ mutant cells (1881) (Table 5.10). I next compared the average fold changes of the genes specifically downregulated in each quiescent yeast strain (Fig. 5.37). The wild-type result served as a baseline of the average gene downregulation occurring during the shift from exponential phase to quiescence. Interestingly, the average extent of downregulation of the genes downregulated in the *hho1*Δ mutant was greater than that the extent of gene downregulation in wt quiescent cells. Average downregulation of the genes downregulated in the *hmo1*Δ mutant Q cells was greater still. This suggests that both *HMO1* and *HHO1* were required to restrict the downregulation of the gene transcription that occurs during Q cell development, with *HMO1* playing the greatest role in this behaviour. This means that in the *hmo1*Δ and *hho1*Δ mutants, transcription of genes are being aberrantly further downregulated.

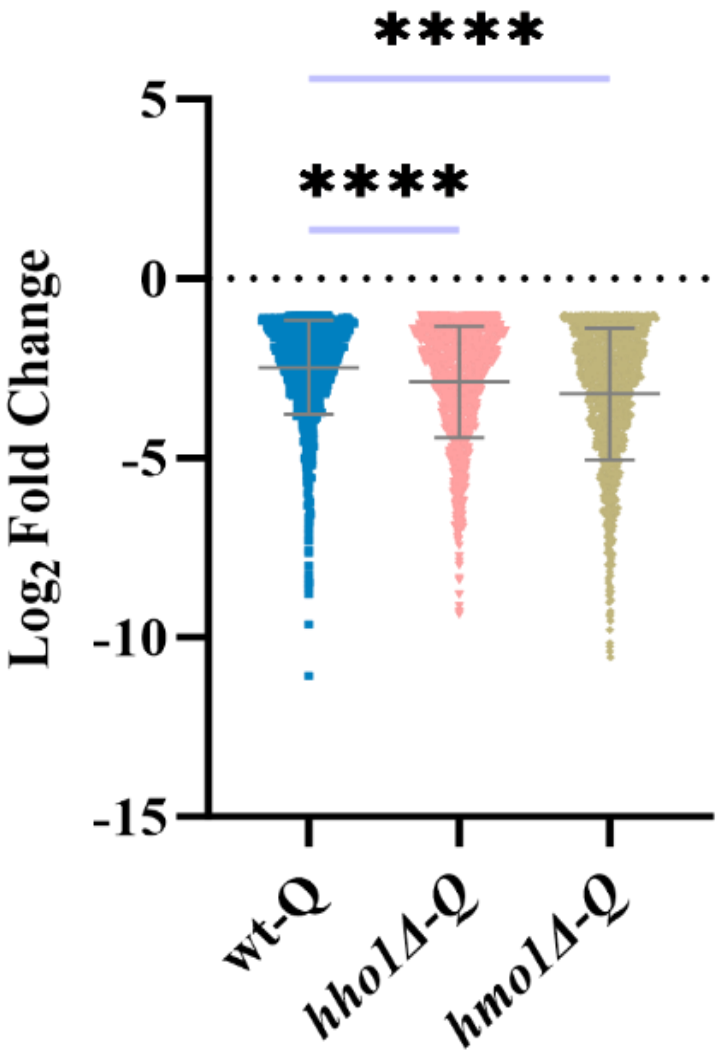

Figure 5. 37: Total number of genes down-regulated in wt, *hho1*Δ and *hmo1*Δ Q cells compared to exponential phase levels of transcription. A scatter plot showing log2-fold change values for all genes down-regulated by at least 2-fold (log2 ≥ 1, an adjusted p-value of p ≤ 0.05) in wt (1702), *hho1*Δ (1881), and *hmo1*Δ (1937) Q cells was compared to transcription in exponential cells. The mean and standard deviation are given as. Significance using Two-way ANOVA analysis (**** p = <0.0001).

5.5.2.5 Variation in the genes down-regulated quiescent cells (Q) in each strain compared to the exponential phase

I created a Venn diagram to investigate whether the genes downregulated in the wt, and mutant Q cells were the same in each strain and overlapped (Fig. 5.38). The results showed an overlap of 1375 genes that were significantly downregulated in all three quiescent cells, accounting for 60.2% of the total genes downregulated in Q cells. Conversely, only 153 genes were uniquely downregulated in the *hho1*Δ deletion strain and only 175 genes were uniquely downregulated in the *hmo1*Δ deletion strain. Thus, *HMO1* and *HHO1* are regulating the majority of the normal cohort of genes downregulated during development of quiescence and act to restrict their downregulation.

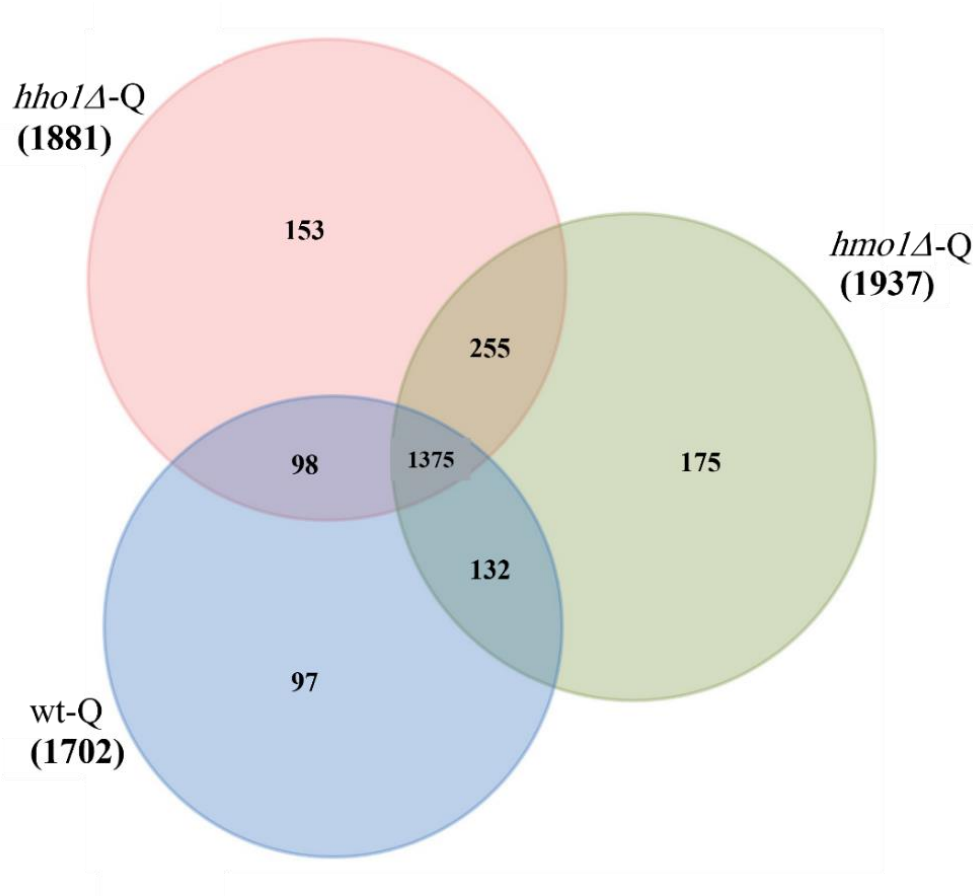

Figure 5.38: Venn diagram showing the overlap of genes significantly down-regulated in quiescent cells of each strain compared to exponential phase cells. All of the genes down-regulated at least 2-fold in wt (log 2 ≥ 1, adjusted p-value p ≤ 0.05), *hho1*Δ and *hmo1*Δ deletion strains compared to exponential phase cells.

5.5.2.6 Identification of uniquely down-regulated genes in wt, *hho1*Δ, and *hmo1*Δ deletion strains during quiescence

As the 3-way Venn diagram presented previously was complicated, it was deconstructed to show individual Venn diagrams comparing those genes downregulated in the *hho1*Δ and *hmo1*Δ mutant Q cells compared to wt Q cells (Fig. 5.39A-B). This analysis more clearly shows the significant overlap in the genes commonly downregulated in wt and *hho1*Δ Q cells (Fig. 5.39A) and in wt and *hmo1*Δ mutant Q cells (Fig. 5.39C). Most interestingly, the scatter plot analysis showed that the average fold change of the genes commonly downregulated in the Q cells of each mutant and wt, was significantly greater in each mutant than in wt (Fig. 5.39B and D). This suggests a significant role for both *HHO1* and *HMO1* in restricting the downregulation of the gene cohort normally downregulated during the development of Q cells. Thus, gene transcription levels of the gene cohort normally downregulated in wt Q cells will be aberrantly low in both of the mutant Q cells.

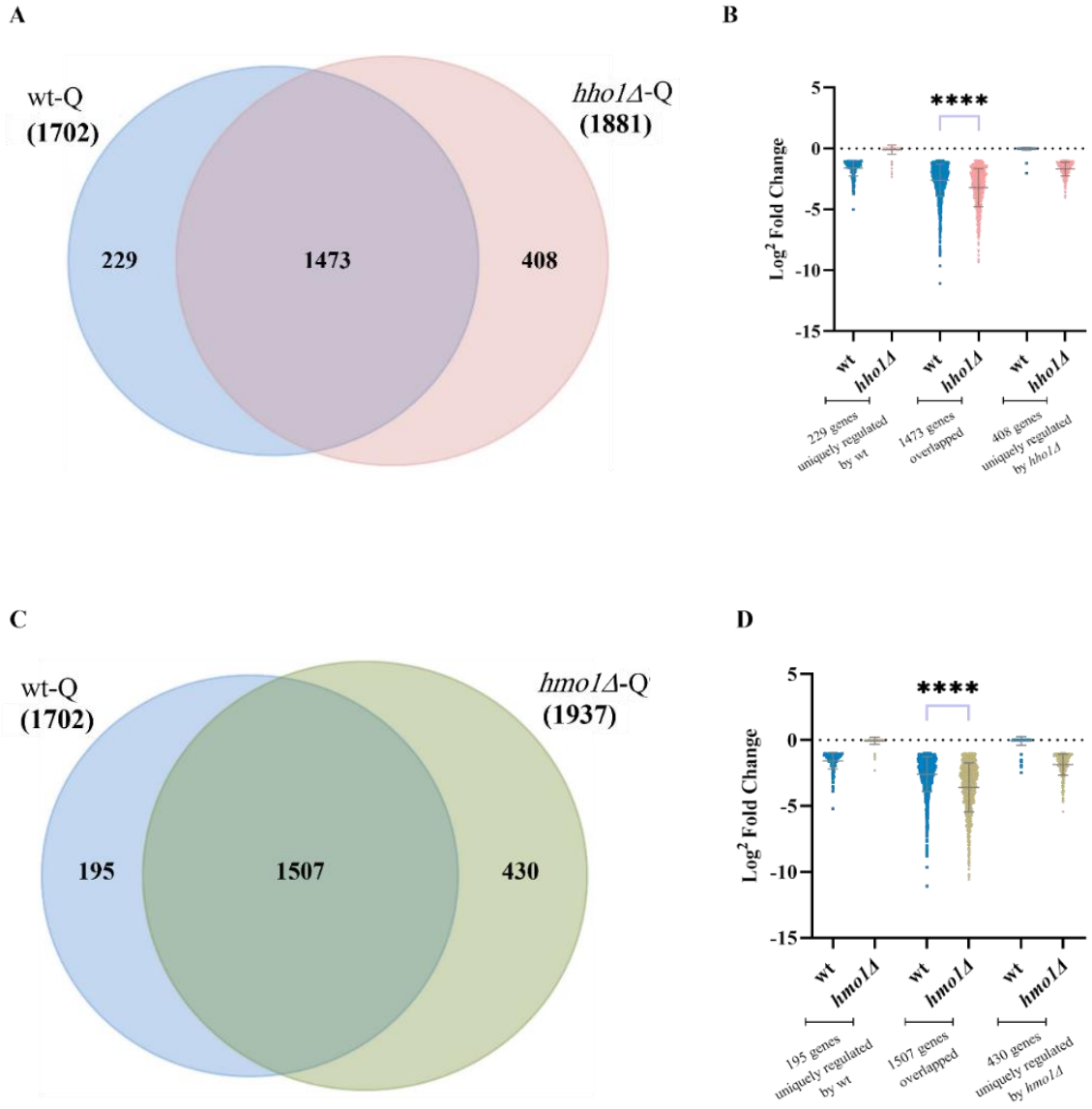

Figure 5.39: Analysis of down-regulated genes in quiescent cells of each mutant versus wt. (A, B) *hho1*Δ vs wt, and **(C, D)** *hmo1*Δ vs wt. Significance using T-test analysis (* p = 0.05, ** p = 0.01, **** p = <0.0001).

5.5.3 Side-by-side visualisation of gene expression changes during development of quiescence

(Figure 5.40) summarizes the overall changes in gene expression over time as quiescence develops in wt and the two mutants. The heat map showing a side-by-side comparison of all genes up and down regulated compared to exponential phase in wt, *hho1*Δ and *hmo1*Δ mutants at diauxie and in quiescent cells confirms a very visible difference in transcription of a large cohort of genes in wt and the mutants as cellular quiescence develops.

The heterogeneity of changes visible in the mutants highlights the intricate changes occurring in gene transcription during Q cell development in the absence of *HHO1* and *HMO1*.

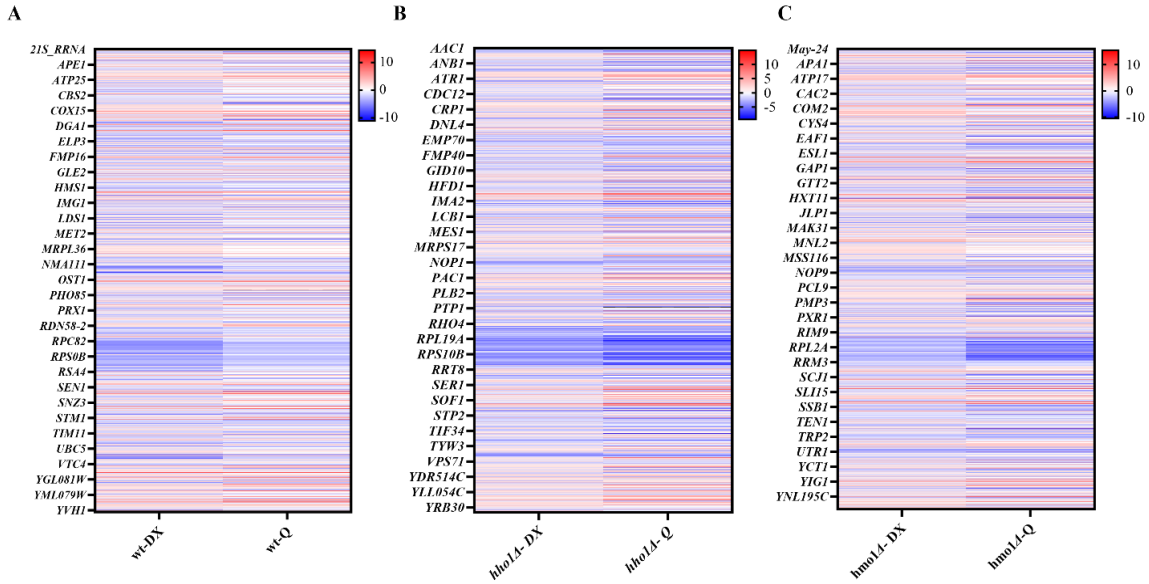

Figure 5.40: Genes up- and down-regulated in each strain at diauxie and in quiescent cells compared to transcription in exponential phase. **(A-C)** A cluster heat map in which the rows represent genes, and the columns represent strain and growth condition. Each cell is colourised based on the comparative level of expression (>2-fold change up (red)/down (blue) and FDR of <0.05) in the strains indicated. Only the top 30 up/down regulated genes are indicated to the left of each heat map for each strain.

5.6 Summary of key findings

• *HHO1* does not influence transcription widely in exponential phase cells.

• The influence of *HHO1* upon transcription increases during growth into SP.

• Gene repression by both *HMO1* and *HHO1* increases during quiescent cell development.

• Co-repression by *HMO1* and *HHO1* increases over time.

• The *hmo1*Δ mutant has the greatest defect in gene activation in day 7 quiescent cells (more genes downregulated).

5.7 Discussion

The RNA-seq analysis of *hmo1*Δ and *hho1*Δ mutants during the exponential growth phase has provided valuable insights into the transcriptional regulation by Hmo1p and Hho1p. The high reproducibility among biological replicates and the quality of mapped reads emphasise the reliability of data (Conesa *et al.*, 2016; Wang *et al.*, 2018). The lack of cross-regulation between *HMO1* and *HHO1* gene transcription during exponential phase suggests the proteins do not regulate other's transcription in actively growing cells, which is in agreement with findings by previous research (Dolinski and Heitman, 1999).

The differential gene expression analysis highlighted a significant disparity in the number of genes affected by each deletion. The *hmo1*Δ mutant exhibited an extensive alteration in gene transcription, with 395 genes significantly up or downregulated, compared to only 67 in the *hho1*Δ mutant, supporting a broader regulatory role for Hmo1p in exponential cells (Dolinski and Heitman, 1999). The balanced distribution of up and downregulated genes in the *hmo1*Δ mutant versus the predominant upregulation of genes in the *hho1*Δ mutant supports a repressive function of both proteins acting as possible linker histones (Panday and Grove, 2016). The heat map visualization further delineates the differential transcription levels, corroborating the roles of *HMO1* and *HHO1* in gene repression during the exponential phase.

Gene ontology analysis of upregulated genes in the *hho1*Δ mutant revealed involvement in 'monoatomic cation transport' and 'glucosidase activity' which is consistent with the regulatory role of Hho1p in sugar transport and metabolism described earlier (Chen *et al.*, 2021). Similarly, the *hmo1*Δ mutant affected genes related to 'cell communication' and 'peroxidase activity', highlighting the diverse cellular functions under Hmo1p's

regulation. The minimal subset of 14 genes commonly upregulated in both mutants indicates distinct regulatory roles for Hmo1p and Hho1p, supporting the hypothesis of their independent pathways in gene repression during the exponential phase (Panday and Grove, 2016).

The substantial number of genes downregulated in the *hmo1*Δ mutant (218 genes) compared to the *hho1*Δ mutant (21 genes) suggests a more extensive role for Hmo1p in transcriptional activation. This finding is consistent with the proposed dual functionality of linker histones in gene regulation, acting as both repressors and activators of transcription (Panday and Grove, 2016).

Gene ontology analysis revealed that the downregulated genes in the *hho1*Δ mutant were significantly involved in vacuolar transport and polyphosphate metabolism, including *VTC1* and *VTC3*, which are crucial for polyphosphate transport into the vacuole (Austin and Mayer, 2020). This aligns with previous studies highlighting the role of Hho1p in vacuolar processes (Wleklik and Borek, 2023). Additionally, genes such as *PHO12*, *PHO11*, and *PHO5*, involved in phosphoric monoester hydrolysis, were also downregulated, further supporting a role for Hho1p in phosphate metabolism. In contrast, the *hmo1*Δ mutant affected a diverse array of genes, with a significant number involved in small molecule metabolic processes (46 genes), which also included the *PHO* family responsible for phosphate transport and metabolism. This broad impact on metabolic genes underscores the multifaceted role of Hmo1p in cellular metabolism, as previously suggested (Wagner, 2024).

The overlap analysis of commonly downregulated genes in both mutants revealed only eight genes, indicating distinct regulatory roles for Hmo1p and Hho1p in gene activation during exponential phase. However, these shared genes, which include those involved in siderophore transport and fungal-type cell wall organization, suggest a coordinated regulation by both proteins in important pathways governing cell structure and sequestration of metal ions (Alliance of Genome Resources, 2022). The data presented here in confirm the significant role of Hmo1p, and to a lesser extent Hho1p, in the activation of gene transcription during the exponential phase

The RNA-seq analysis of *hmo1*Δ and *hho1*Δ yeast mutants at the diauxic shift (DX) has provided a detailed view of the transcriptional changes associated with the deletion of these genes at this important stage of growth. Importantly, the data again revealed a lack of cross-regulation between *HMO1* and *HHO1* gene transcription at this stage of growth (Wang *et al.*, 2023).

A total of (1457) genes were significantly up or downregulated in the *hmo1*Δ mutant compared to the wild type, while only (409) genes were affected in the *hho1*Δ mutant. This disparity highlights the broader impact of Hmo1p on gene transcription at the diauxic shift, which aligns with previous findings on the extensive role of Hmo1p in transcriptional regulation (Geistlinger *et al.*, 2013). The heat map visualization further illustrates the differential transcription levels, with a greater number of genes upregulated in the *hho1*Δ mutant, suggesting a predominantly repressive role for Hho1p at the diauxic shift. This observation is consistent with the known repressive functions of linker histones (Schlossarek *et al.*, 2022).

Gene ontology analysis of upregulated genes in the *hho1*Δ mutant revealed significant involvement in ribosome biogenesis and RNA metabolism (Fig. 5.12A), which is in line with the established role of Hho1p in these processes (Levy *et al.*, 2008). Similarly, the *hmo1*Δ mutant showed a large number of genes associated with ribonucleoprotein complex structure and RNA metabolism confirming the multifaceted role of Hmo1p in cellular metabolism (Gadal *et al.*, 2002).

The identification of 139 genes commonly upregulated in both mutants suggests an overlapping role for Hmo1p and Hho1p in gene regulation during the diauxic shift. These genes are involved in various cellular functions, including ribosomal biogenesis, DNA replication, and repair, as well as metabolism and stress response (Geistlinger *et al.*, 2013).

The transcriptional regulation by the linker histones Hho1p and Hmo1p during the diauxic shift in yeast has been a subject of considerable interest. The results of this study indicates that Hmo1p plays a more significant role in gene activation during this metabolic transition than Hho1p. Specifically, a greater number of genes were downregulated in the *hmo1*Δ mutant compared to the *hho1*Δ mutant, suggesting that Hmo1p may be required for the activation of a broader range of genes.

This finding is consistent with previous studies that have highlighted the diverse roles of Hmo1p in gene regulation (Dolinski and Heitman, 1999).

Despite the differences in the number of downregulated genes, the Log2 mean fold change values between the deletion mutant strains did not differ significantly, suggesting that both Hmo1p and Hho1p exert similar levels of activation at the target genes they positively regulate at the diauxic phase. This observation supports the hypothesis that these histones may function to maintain essential gene expression during this metabolic shift (Galdieri *et al.*, 2010).

Gene ontology analysis revealed that in the *hho1*Δ mutant, genes involved in small molecule metabolic processes, carbohydrate metabolic processes, and response to oxidative stress were notably downregulated. This includes genes such as *CHA1*, *AGX1*, and *NGK1*, which are integral to various metabolic pathways (Ma and Liu, 2010). In contrast, the *hmo1*Δ mutant exhibited downregulation in genes associated with DNA integration, phosphorus metabolic processes, and plasma membrane components, highlighting the diverse roles of Hmo1p in cellular processes (Dolinski and Heitman, 1999).

Only (43) genes were commonly downregulated in both mutants, indicating specific and unique regulatory roles for Hmo1p and Hho1p. The genes subject to activation by both proteins showed the most robust activation by Hmo1p, suggesting a greater role for Hmo1p in positive gene regulation at diauxie.

As described for the exponential phase and diauxie data, the high level of reproducibility was also observed in the RNA-Seq analysis of quiescent cells from wt, *hmo1*Δ, and *hho1*Δ mutant strains (Fig. 5.17A). However, a regulatory interplay between *HMO1* and *HHO1* during quiescence was uncovered in which they were seen to influence each other's transcription (Fig. 5.17). Indeed, there was an upregulation of *HHO1* in *hmo1*Δ quiescent cells and transcription of *HMO1* in *hho1*Δ cells was downregulated suggesting *HMO1* negatively regulates *HHO1* transcription in quiescent cells, whilst *HHO1* positively regulates *HMO1* transcription.

The differential expression analysis revealed a substantial number of genes with altered transcription levels in the *hmo1*Δ and *hho1*Δ mutants compared to wt quiescent cells (Table 5.6). The *hmo1*Δ mutant exhibited a more pronounced effect on gene transcription, which is consistent with the broader regulatory roles of *HMO1* identified in previous study (Panday and Grove, 2016). The heat map visualization (Fig. 5.18A-B) provides a clear representation of the genes differentially expressed in each mutant strain. The distinct clusters of downregulated genes in the *hho1*Δ mutant and the varied expression pattern in the *hmo1*Δ mutant suggest that *HMO1* and *HHO1* may have different roles or regulatory mechanisms during quiescence.

The gene ontology analysis further elucidates the roles of *HMO1* and *HHO1* in quiescent cells. The upregulated genes in the *hho1*Δ mutant were predominantly associated with proteasome-mediated ubiquitin-dependent protein catabolic processes, while those in the *hmo1*Δ mutant were linked to protein modification (Fig. 5.20A-B). These results are in agreement with the functional categorizations reported by (Panday and Grove, 2016) highlighting the significance of these processes in quiescent cells.

Lastly, the identification of genes commonly upregulated in both *hho1*Δ and *hmo1*Δ deletion strains compared to wt during quiescence (Fig. 5.21A) suggests a shared regulatory role for Hmo1p and Hho1p. This overlap in gene regulation of quiescent cells has not been previously observed.

In the quest to understand the regulatory mechanisms governing gene transcription during cellular quiescence, the comparative analysis of mutant strains deficient in Hho1p and Hmo1p has provided insightful revelations. The downregulation of a significant number of genes in the *hmo1*Δ mutant, compared to the *hho1*Δ mutant, underscores the pivotal role of *HMO1* in promoting gene transcription during quiescence. This finding aligns with previous research indicating that *HMO1* is intricately involved in chromatin organization and transcriptional regulation (Wang *et al.*, 2023).

The gene ontology analysis further delineates the functional categories impacted by the absence of these proteins. The substantial number of genes associated with ribosome biogenesis and peptide metabolic processes in the *hho1*Δ mutant, including critical components such as *RPS6B* and *RPS9B*, echoes the importance of *HHO1* in ribosomal DNA transcription and assembly (Levy *et al.*, 2008). Conversely, the *hmo1*Δ mutant's pronounced effect on genes involved in small molecule metabolic processes, such as *ALD6* and *ENO1*, reflects *HMO1*'s broader regulatory scope, impacting pathways essential for cellular metabolism and energy production.

The overlap of 553 genes downregulated in both mutants during quiescence suggests a possible relationship between Hho1p and Hmo1p in maintaining gene expression levels for a variety of cellular functions. This observation is consistent with the notion that these proteins may collaborate to ensure the stability of the transcriptional landscape during periods of cellular dormancy (Sideri *et al.*, 2015).

Moreover, the more pronounced gene downregulation in the *hmo1*Δ mutant indicates that *HMO1* may have a dominant influence over *HHO1* in positively regulating gene transcription during quiescence. This is in line with studies suggesting that *HMO1* has a more extensive interaction network within the genome, potentially facilitating a more significant impact on transcriptional regulation.

We also delved into the transcriptional dynamics of *Saccharomyces cerevisiae* mediated by Hho1p and Hmo1p during the development of quiescent cells. Our time-course analysis has uncovered significant transcriptional changes as cells transition from exponential growth through diauxie to day 7 quiescent (Q) cells.

The wild-type strain demonstrated a robust transcriptional response to glucose depletion at diauxie, marked by a substantial up-regulation and down-regulation of numerous genes. This aligns with the anticipated metabolic adjustments as cells adapt to the shifting nutrient availability, as previously described in similar yeast studies (Livas *et al.*, 2011; Apweiler *et al.*, 2012; Alfatah *et al.*, 2021).

The *hho1*Δ mutant displayed a ‘muted’ response, suggesting that Hho1p plays a pivotal role in managing the transcriptional adaptation to glucose depletion. In contrast, the *hmo1*Δ mutant exhibited a transcriptional response comparable in magnitude to the wild-type but with distinct gene-specific alterations, indicating a more pronounced role for Hmo1p in this process.

Heat map analysis provided a visual representation of the transcriptional changes, underscoring the stability of gene expression in the *hho1*Δ mutant and the pronounced differences in the *hmo1*Δ mutant compared to the wild-type. This suggests that Hho1p contributes to the stability of gene expression during glucose depletion, while Hmo1p may be involved in the activation or repression of specific genes during this transition (Livas *et al.*, 2011).

The deletion of *HMO1* affected a unique subset of genes during the diauxic shift, highlighting its significant role in regulating gene transcription at this stage. The core set of genes upregulated in all strains, regardless of the deletion of *HMO1* or *HHO1*, points to a shared transcriptional program essential for quiescent cell development.

The diauxic shift in *Saccharomyces cerevisiae* represents a critical metabolic transition from fermentative to oxidative growth, necessitating a complex reprogramming of gene expression. From the results obtained, we dissected the transcriptional regulatory roles of the *HHO1* and *HMO1* during this shift. Our findings reveal a nuanced interplay between these proteins in orchestrating the yeast's adaptive response. Initially, we quantified the transcriptional changes across the genome during the diauxic shift. We observed that approximately (1400) genes were downregulated in both wild-type (wt) and *hmo1*Δ strains. This downregulation is consistent with the metabolic shift from rapid fermentation to the more energy-efficient but slower process of respiration, as previously described (Gasmi *et al.*, 2014). In contrast, the *hho1*Δ strain showed a reduced number of downregulated genes (~1200), suggesting a differential regulatory landscape in the absence of *HHO1*. This aligns with the work of (Li *et al.*, 2021), who noted the specificity of *HHO1* in gene silencing during stress responses (Li *et al.*, 2021).

Further analysis of the average fold changes of genes specifically downregulated in each strain highlighted that the mutants exhibited a less pronounced downregulation compared to wt. This indicates that both *HHO1* and *HMO1* are integral to the repression of genes during the diauxic shift, supporting the findings of (Debasree *et al.*, 2018), who emphasized the importance of linker histone in gene regulation.

Our Venn diagram analysis provided a visual representation of the transcriptional overlap and uniqueness between the strains. Remarkably, *HMO1* appeared to exert a more dominant influence on gene regulation, with 413 uniquely downregulated genes in the *hmo1*Δ strain. This observation is in line with the regulatory scope of *HMO1* elucidated by (Nordin *et al.*, 2024), who mapped the genome-wide binding sites of *HMO1*, correlating them with transcriptional changes (Nordin *et al.*, 2024). Conversely, a core set of 834 genes consistently downregulated across all strains points to a regulatory mechanism independent of *HHO1* and *HMO1*. This core gene set likely reflects essential cellular functions that are downregulated in response to the diauxic shift, as suggested by (Galdieri *et al.*, 2010), who explored the conserved transcriptional responses in yeast. In summary, our study highlights the distinct and overlapping roles of *HHO1* and *HMO1* in gene repression during the diauxic shift. *HMO1*, in particular, emerges as a pivotal factor in the transcriptional reprogramming of yeast, ensuring the appropriate downregulation of a significant subset of genes.

In the study of yeast quiescence, the transcriptional regulation patterns of wild-type (wt), *hho1*Δ, and *hmo1*Δ mutants were carefully analysed. The RNA sequencing analysis provided a comprehensive view of the genes' behaviour as the cells transitioned from the exponential phase to the quiescent phase. The wt cells exhibited a significant shift in gene expression, with 1473 genes upregulated and 1702 genes downregulated. This change highlights the dynamic nature of yeast cells adapting to the quiescent state (Greenlaw *et al.*, 2024).

Both *hho1*Δ and *hmo1*Δ mutants showed similar patterns of gene expression, with *hho1*Δ having 1673 upregulated and 1881 downregulated genes and *hmo1*Δ with 1837 upregulated and 1937 downregulated genes. These figures suggest that the deletion of *HHO1* and *HMO1* does not drastically alter the number of genes regulated but does affect specific gene cohorts. A closer look at the genes specifically upregulated in quiescent cells revealed that *hho1*Δ and *hmo1*Δ mutants had higher average fold upregulation compared to wt. This indicates a significant upregulation of transcription in Q cells due to the deletions, with both mutants showing similar levels of upregulation.

The downregulation of genes in the mutants was more pronounced than in wt, suggesting that *HMO1* and *HHO1* play roles in restricting the downregulation of gene transcription during Q cell development. The *hmo1*Δ mutant, in particular, showed the greatest extent of downregulation, indicating its prominent role in this regulatory process.

In conclusion, the deletion of *HHO1* and *HMO1* leads to distinct cohorts of genes being aberrantly regulated in quiescent cells. The study highlights the complex interplay of genetic factors that govern the quiescent state in yeast and opens avenues for further research into the mechanisms of cellular quiescence.

In summary, the RNA-seq analysis of yeast mutants lacking Hmo1p and Hho1p has provided significant insights into their roles in transcriptional regulation. The study found that Hmo1p has a broader regulatory impact than Hho1p, affecting a larger number of genes. Both proteins appear to function largely independently from one another, with Hmo1p acting as both a repressor and activator of transcription, while Hho1p mainly exhibits repressive functions. Together, these findings contribute to a better understanding of the complex genetic regulation occurring at the diauxic shift and during cellular quiescence.

Chapter 6

ChIP-Seq analysis of Hho1p and Hmo1p occupancy

6.1 Introduction

Chromatin Immunoprecipitation (ChIP) is a useful method to identify specific DNA-protein interactions along the genome. Combining ChIP and DNA sequencing technology by using ChIP-Seq means that it is now possible to determine genome wide enrichment of a protein of interest (Lefrançois *et al.*, 2014). Advantages over traditional ChIP qPCR methods not only include the ability to scan for regions of protein binding over the entire genome, but also to identify previously unknown regions of protein enrichment, or peaks of protein binding (Fig. 6.1)

In this chapter, the location of Hho1-myc and Hmo1-myc have been mapped across the yeast genome during exponential growth, at the diauxic shift, and in stationary phase (SP) separated day 7 quiescent (Q) cells. Firstly, this was to identify where the proteins bind in actively growing cells and to determine if the proteins redistribute during quiescent cell development. The prediction would be that the proteins will occupy different sites at different stages of growth. Secondly, the occupancy profiles were to be correlated with the transcription profiles in the two mutants to determine the genes under direct and indirect Hmo1p and Hho1p regulation. Biological duplicate samples of input (in) and immunoprecipitated (IP) DNA were prepared and sequenced from each time point.

However, prior to analyzing my data, I first analyzed previously published Hho1p and Hmo1p occupancy profiles in actively growing cells generated using the ChIP-exo technique (Rossi *et al.*, 2021).

Traditional ChIP-Seq methods often face issues such as low resolution and high background noise, which can make it difficult to accurately determine protein binding locations. ChIP-exo addresses these issues by adding an exonuclease digestion step, enhancing the precision of binding site localization (Park, 2009).

In ChIP-exo, after the immunoprecipitation of protein-DNA complexes, exonucleases digest DNA fragments that extend beyond the protein binding sites, producing well-defined endpoints that accurately mark protein-DNA interaction sites. This digestion step greatly reduces background noise and improves the resolution of binding site identification.

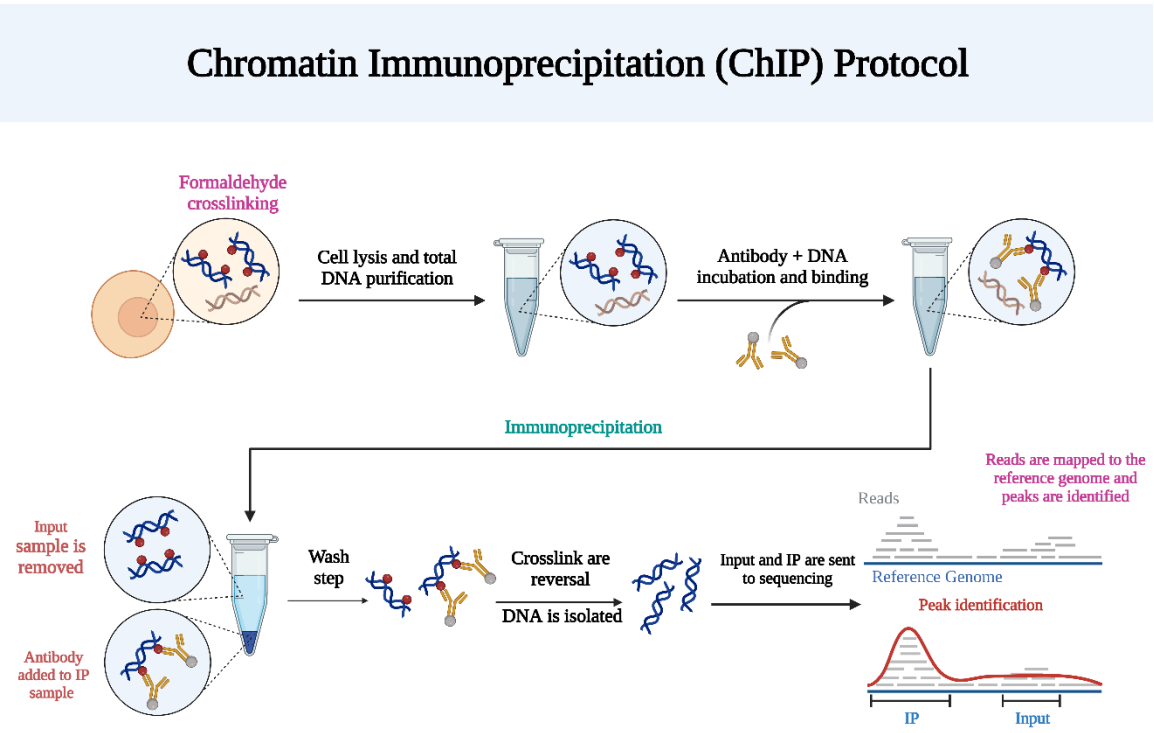

Figure 6.1: Schematic to illustrate the ChIP-Seq protocol. The genomic DNA is treated with formaldehyde to cross-link proteins to the DNA. Following lysis of the cells, the DNA is fragmented using sonication to give DNA fragments ~500 bp in length. The Input (IN) sample is removed, and the antibody specific to the protein of interest is added to the IP sample. The protein-bound fragments are purified from the IP sample. DNA is purified from both the IN and IP samples, which involves reversing the cross-links and degrading any proteins. The purified DNA is then sequenced. Following sequencing, the reads are mapped to the reference genome and regions of enrichment of the protein of interest, peaks, are identified.

6.2 Results

6.2.1 Confirming Hmo1-myc and Hho1-myc strains

I tagged Hmo1p in wt and *hho1*Δ mutant strains and tagged Hho1p in wt and *hmo1*Δ. Successful construction yielded an Hmo1p protein containing a 9x myc-tag at its C-terminal end (Fig. 6.2). Appropriate phenotypic analysis was used to ensure Hmo1p functionality was maintained (Fig. 6.3). It is evident from the lack of an elongation cell morphology typical of *hmo1*Δ mutant cells that Hmo1-9myc remained functional in the wt and *hho1*Δ mutant cells. Tagging of Hho1p was also confirmed by western blot and did not impair Hho1p function (Fig. 6.4A and B).

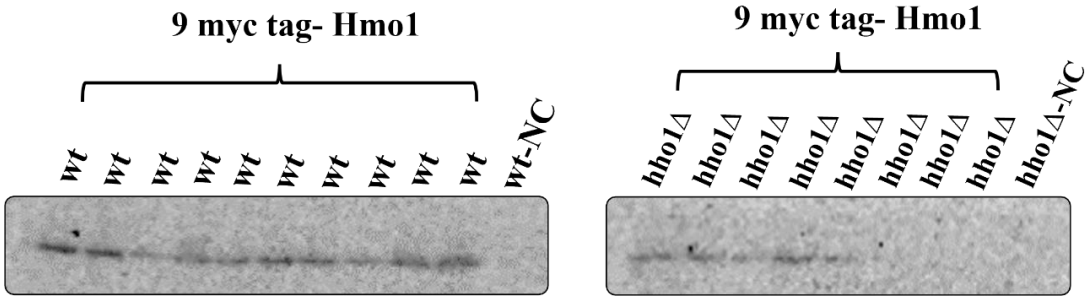

Figure 6.2: Western Blot analysis to confirm Hmo1-myc in wt and *hho1*Δ mutant cells. Anti-myc antibodies was used to detect Hmo1-9myc in lysates from wt and *hho1*Δ mutant cells. Lysates were prepared from cells in exponential phase containing anti-myc, NC (Negative Control). The tagged Hmo1-myc protein was of the expected size.

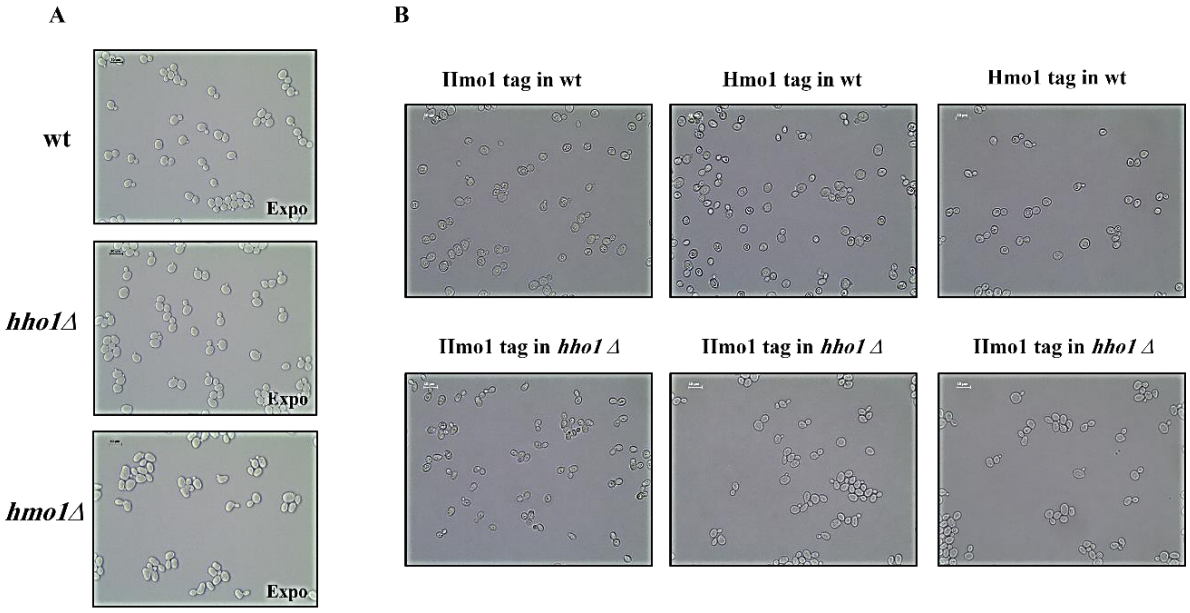

Figure 6.3: wt, *hho1*Δ, and *hmo1*Δ mutant cell morphology. **(A)** The mutant strains shown were grown on YPD and examined under the microscope as they grew exponentially. **(B)** Anti-myc strains were grown on YPD and examined under the microscope from exponentially growing cultures. Microscopy was performed on the oil under a magnification of 100x. Triplicate images for Hmo1-myc in wt and in *hho1*Δ are shown. Black and white scale bars are 10μm.

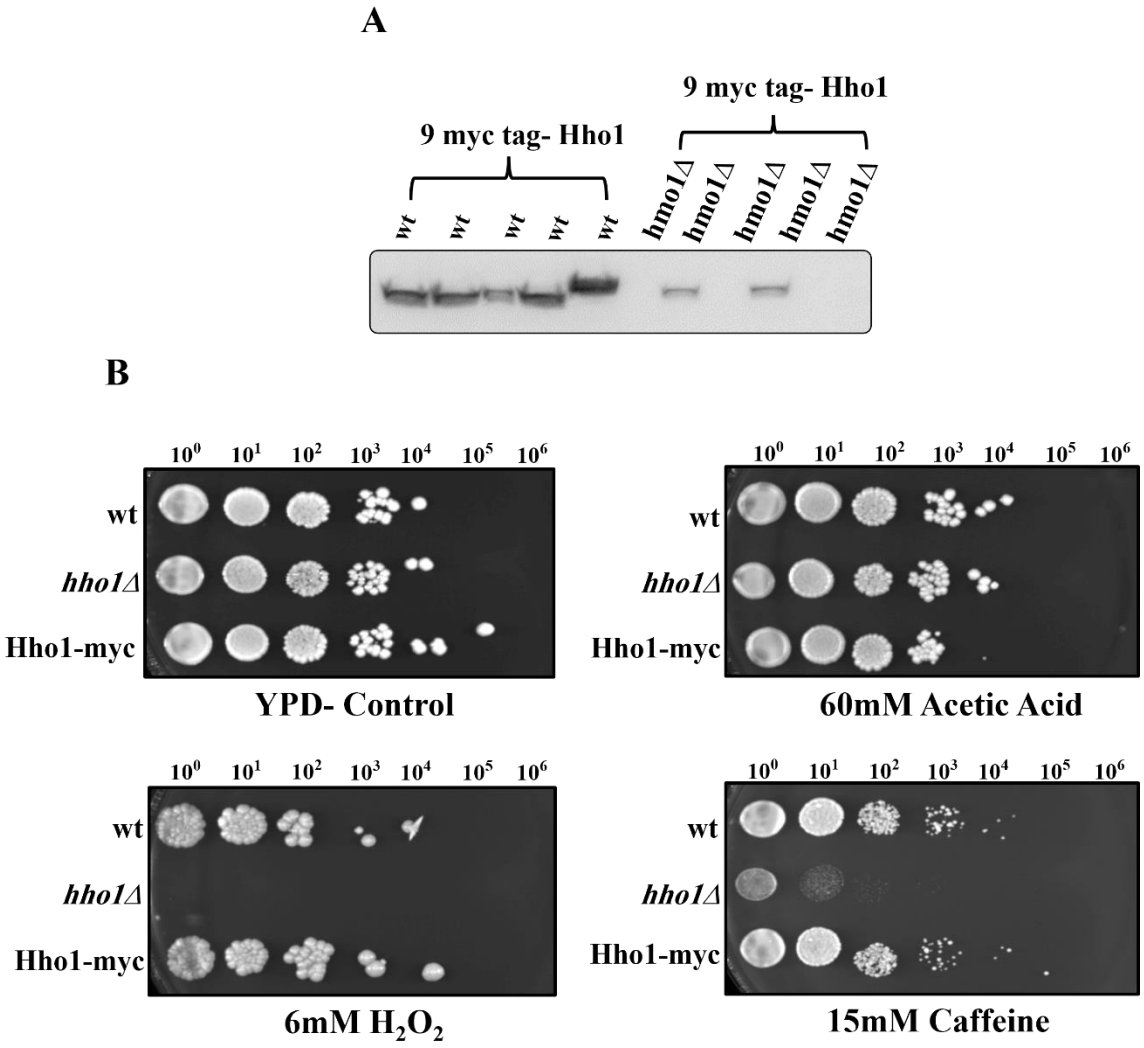

Figure 6.4: Confirmation of Hho1-myc in wt and *hmo1*Δ mutant cells. (A) Western blot to confirm presence of myc tag on Hho1p. The tagged Hho1-myc protein was of the expected size. **(B) Assay to confirm Hho1-myc is functional.** Sensitivity to hydrogen peroxide (H_2O_2) of exponentially growing wt, *hho1*Δ and Hho1-myc cultures was tested to confirm absence of *hho1*Δ phenotypes in the Hho1-myc strain, 10-fold serial dilution starting from $1x10^7$cells/ml were spotted onto YPD and Hydrogen Peroxide plates (YPD-H_2O_2 2%) and photographed following 48hour of growth at 30℃.

6.2.2 Analysis of Hho1p and Hmo1p occupancy in exponential phase cells using published ChIP-exo data

Using published ChIP-exo data from Rossi et al., the occupancy of Hmo1p and Hho1p in exponential phase cells was analysed (Rossi *et al.*, 2021). Their findings revealed that Hmo1p exhibits a total of 253 binding sites, compared to 8 binding sites for Hho1p (Table 6.1).

Further investigation into the occupancy sites of Hmo1p showed it is associated with 145 genes, whereas Hho1p was linked to 4 genes, mirroring its lower overall occupancy. These gene numbers represent where each protein was found either associated on a gene coding region (ORF) or was found within a region 1Kb up or downstream of that gene.

We next explored the distribution of Hho1p and Hmo1p across various other chromosomal features, including cryptic unstable transcripts (CUTs), stable unannotated transcripts (SUTs), and sensitive unstable transcripts (XUTs). The distribution pattern of occupancy largely reflected the overall occupancy numbers for each protein. Specifically, Hho1p was only found at 4 orphan TFIIB peaks. In contrast, Hmo1p was found at more diverse chromosomal features including 9 CUTs, 13 SUTs, 20 XUTs, and 56 orphan TFIIB peaks.

Thus, Hho1p is found associated with only a handful (4) of ORFs in exponentially growing cells, whilst Hmo1p is associated with 145 ORFs.

Protein	Total peak's	Genes	CUT	SUT	XUT	snR	Orphan TFIIB	ncRNA	tRNA	TY1 LTR	ACS
Hho1p	8	4	0	0	0	0	4	0	0	0	0
Hmo1p	253	145	9	13	20	4	56	2	1	1	2

Table 6.1: Peaks of Hho1p and Hmo1p occupancy in exponential phase cells. 1- First column total number of occupancy sites (peaks), **2-** Gene (mapped to a protein encoding gene (ORF) +/- 1Kb up and downstream). **3-** CUTs (Cryptic unstable transcripts are short RNA transcripts that arise from non-coding regions of the genome). **4-** SUTs (Stable unannotated transcripts). **5-** XUTs (sensitive unstable transcripts). **6-** snR peaks of protein-DNA binding associated with small nuclear RNAs (snRNAs) or their binding sites.**7-** Orphan TFIIB peak TFIIB a peak of TFIIB (Transcription Factor IIB) binding that does not coincide with annotated transcription start sites (TSS) or known gene promoters TFIIB is a general transcription factor involved in the initiation of transcription by RNA polymerase II. **8-** ncRNA Non-coding RNAs are RNA molecules that are transcribed from DNA but do not encode proteins. **9-** tRNA is an essential component of protein synthesis.**10-** long terminal repeat (LTR) typically refers to peaks of protein-DNA binding associated with the long terminal repeat regions of retrotransposons or retroviruses. **11-** ACS peaks of protein-DNA binding associated with the origin of DNA replication known as the ARS consensus sequence (ACS), The ACS is a specific DNA sequence recognized by the origin recognition complex (ORC) (Rossi *et al.*, 2021).

6.2.3 Analysis of Hho1p and Hmo1p distribution at genes

I next analyzed more closely the distribution of each protein that had been associated with a gene to determine if the protein was found at a promoter, at the gene coding region (ORF), or was found downstream of the associated gene (Table 6.2). Hmo1p was predominantly found at gene promoters, with a total of 110 sites mapped to the promoters of the 145 genes it had been associated with. In contrast, only 35 sites of Hmo1p occupancy mapped to the open reading frames (ORFs) of its associated genes. Examples of genes showing peaks of Hmo1p at the promoter (*RPL12A*) and ORF (*CDC19*) are shown in (Fig. 6.5).

Conversely, of the 4 genes that had been associated with the peaks of Hho1p, all 4 Hho1p peaks mapped to their ORFs.

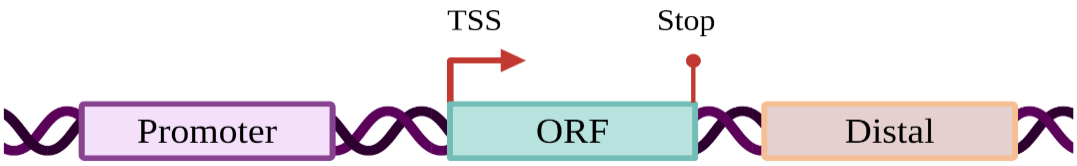

Proteins	Number of associated genes	Promoter	ORF	Distal
Hho1p	4	0	4	0
Hmo1p	145	110	35	0

Table 6.2: The distribution of Hmo1p and Hho1p peaks identified at each associated gene; numbers of sites of occupancy at the gene promoter, across the gene coding region (open reading frame, ORF), or at sites downstream (distal) of the associated ORF. TSS is the transcription start site, indicated by arrow. Stop represents the stop codon.

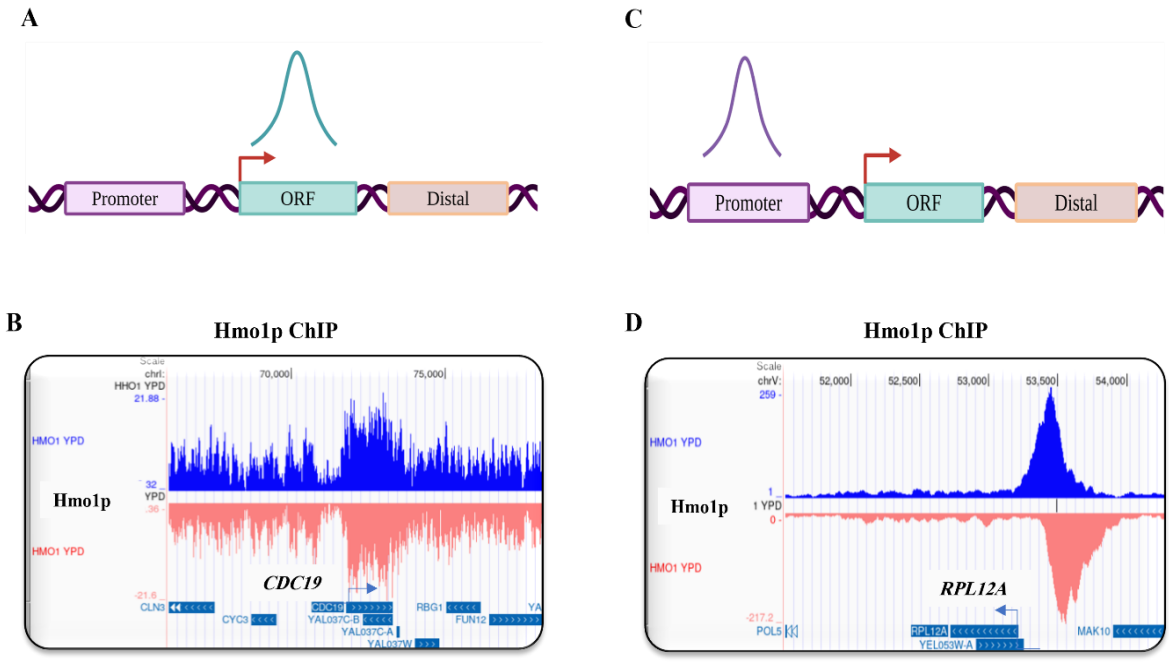

Figure 6.5: Hmo1p can be found on ORFs and at gene promoters. **(A, C)** Schematic to demonstrate characterisation of a peak located at promoters and ORFs (protein coding). An arrow represents the transcription start site**. (B)** J-browse screen-shot to show an example of Hmo1p located at an ORFs (*CDC19)* **(D)** J-browse screen-shot depicting Hmo1p peak located at the promoter region of *RPL12A.*

6.2.3.1 Hmo1p peaks located on divergent promoters

Interestingly, I found 24 peaks of Hmo1p in promoter regions between divergently expressed genes (Fig. 6.6A). An example of one such shared promoter region is between the *TEM1* and *RPS1B* genes (Fig. 6.6B). Correlation of the transcription profiles in the *hmo1*Δ mutant of the pairs of genes which share a peak of Hmo1p in the divergent promoters revealed only 5 of the pairs of genes showed any significant up or downregulation in the absence of Hmo1p (Table 6.3). In all of these cases, transcription of only one gene in each pair was upregulated in the *hmo1*Δ mutant compared to wt. Thus, the data suggest that where Hmo1p is found at divergent promoters in exponential phase cells, it acts to repress only one gene in the pair.

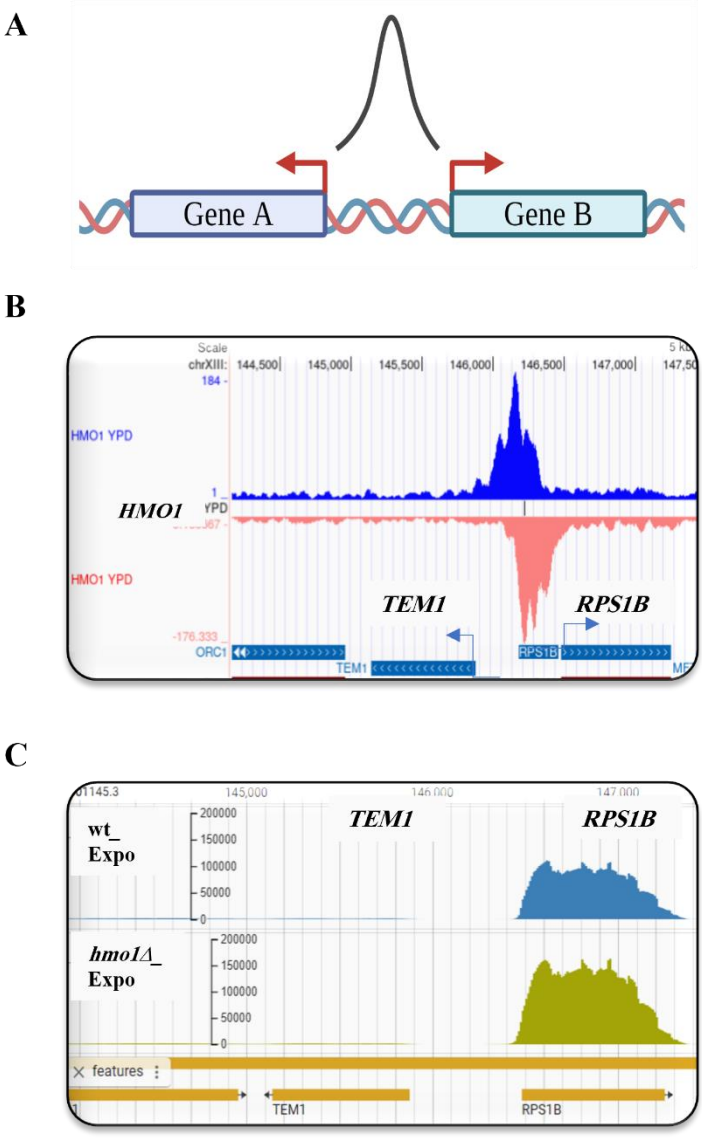

Figure 6.6: Peaks located in Hmo1p. (A) Schematic to demonstrate Hmo1p peaks located between divergent promoters. **(B)** Hmo1p located between the divergent promoters of *TEM1* and *RPS1B*. **(C)** Transcriptional response of *TEM1* and *RPS1B* in an *hmo1*Δ mutant vs wt, showing only *RPS1B* is more than 2-fold upregulated compared to wt.

Divergent gene pairs	Transcription in *hmo1*Δ vs wt	Divergent gene pairs	Transcription in *hmo1*Δ vs wt
TEM1* and *RPS1B	*TEM1:* no change *RPS1B:* up-regulated	***RPL42B* and *CHS7***	Both: no change
YBL071C-B* and *KTI11	Both: no change	***RPL40A* and *MLP2***	Both: no change
RPL32* and *ROX3	Both: no change	***RPL17B* and *ATG27***	Both: no change
RPL19A* and *AAC3	Both: no change	***RPL39* and *RPS22A***	Both: no change
TPS1* and *MEO1(YBR126W-A)	*TPS1:* up-regulated *MEO1:* no change	***RSM7* and *YJR115W***	*RSM7:* no change *YJA115W:* up-regulated
RPL31A* and *RXT3	*RPL31A:* up-regulated *RXT3:* no change	***RPS17A* and *YML6***	Both: no change
RPL13A* and *RPS16B	Both: no change	***RPL13B* and *RPS16A***	Both: no change
UGO1* and *RPL27B	Both: no change	***RPP2A* and *RPS15***	Both: no change
RPL30* and *RPL24A	Both: no change	***RPL33B* and *DFR1***	Both: no change
YGR117C* and *RPS23A	Both: no change	***YOR292C* and *RPS10A***	Both: no change
RPL24B* and *GPC1(YGR149W)	Both: no change	***NAT3* and *RPS23B***	Both: no change
TDA3(YHR009C)* and *RPL27A	Both: no change	***RPS17B* and *ADA2***	*RPS17B:* up-regulated *ADA2:* no change

Table 6.3: Hmo1p occupancy at genes with divergent promoters and their transcriptional regulation in *hmo1*Δ. Table shows pairs of genes sharing a divergent promoter at which Hmo1p was mapped by ChIP-exo. Gene transcription changes (up-regulated (highlighted in yellow), down-regulated, or show no change in expression) are indicated of the genes in the *hmo1*Δ mutant compared to wt.

6.2.3.2 Correlation between Hho1p occupancy and gene transcription in *hho1*Δ mutant during exponential phase

To elucidate the relationship between Hho1p binding and gene expression during exponential phase, we examined the transcription levels of the 4 ORFs (*TEF1*, *TEF2*, *ENA2*, and *PDC1*) at which Hho1p had been found by Rossi et al., with the transcription of these genes in the exponentially growing *hho1*Δ mutant (Fig 6.7). Interestingly our analysis revealed that even though there was a strong peak of Hho1p that spanned the open reading frames (ORFs) of these genes in exponential phase cells, there was no impact upon transcription of these genes in the *hho1*Δ mutant when Hho1p was absent.

Thus, at the 4 genes at which Hho1p is present during exponential phase, the data suggests that Hho1p does not have a regulatory role upon that gene's transcription, at least during exponential phase.

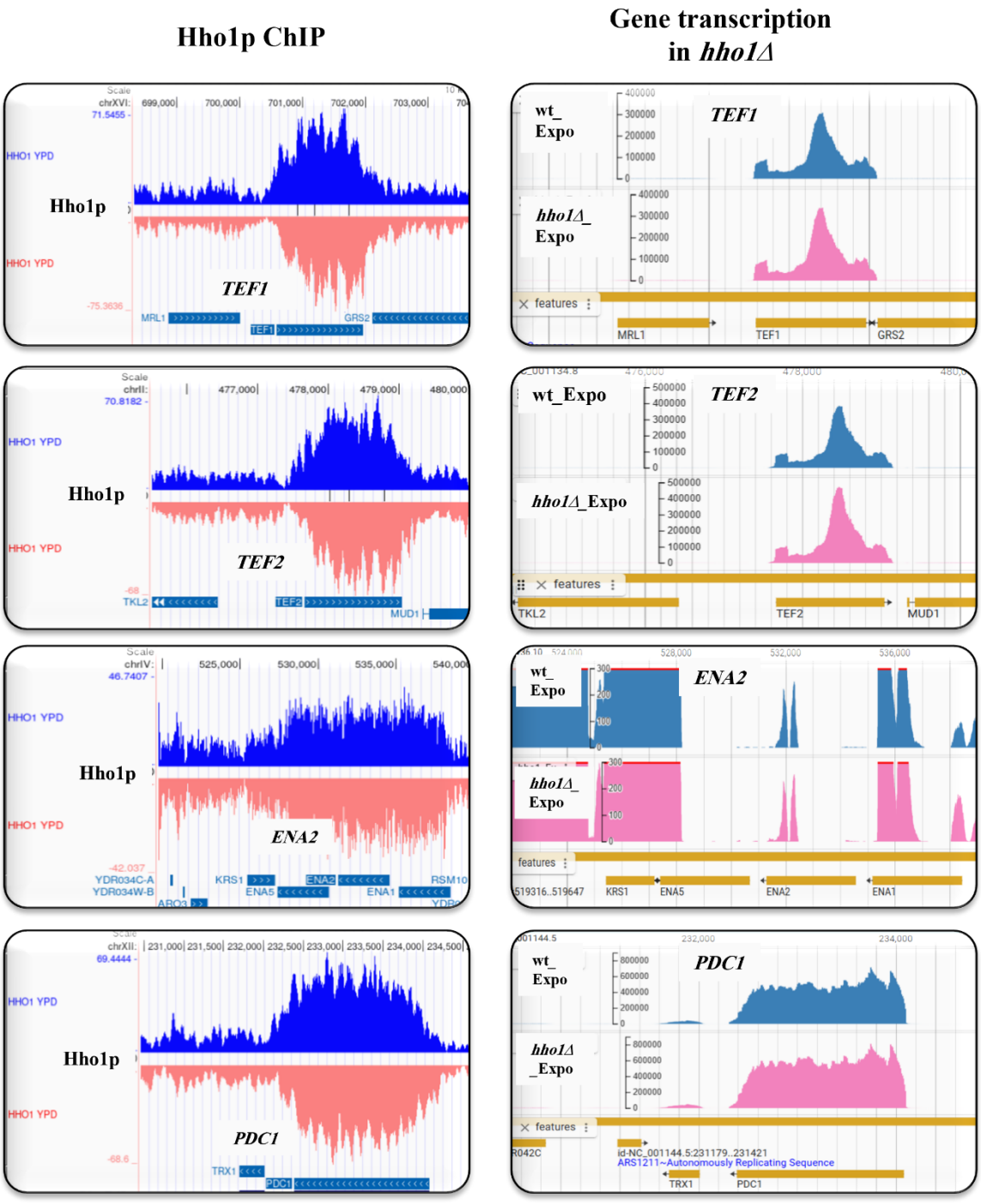

Figure 6.7: Correlation between Hho1p occupancy and transcription levels in the *hho1*Δ mutant. Screenshots from J-browse of Hho1p ChIP-exo data in exponential phase cells (Rossi *et al.*, 2021) and RNA-seq data from exponentially growing cells (this study).

6.2.3.3 Correlation between Hmo1p occupancy and gene transcription in *hmo1*Δ mutant during exponential phase

To investigate the relationship between Hmo1p binding and transcriptional regulation in exponential phase cells we correlated the Hmo1p gene occupancy data with our data of global transcription from the exponential *hmo1*Δ mutant (Rossi *et al.*, 2021) (see Chapter 5, Table 5.1).

We first correlated the 145 sites of Hmo1p occupancy at genes, with the 177 genes we found that were upregulated in the *hmo1*Δ strain compared to wt during exponential phase (Fig 6.8A). The data showed that only 8 genes bound by Hmo1p were upregulated upon deletion of *HMO1*. These 8 genes might represent the genes subject to direct repression by Hmo1p in exponentially growing cells. An example of one potentially directly repressed gene is *TPS1* (Fig. 6.8B). The data showed that the eight Hmo1p occupied genes that were upregulated in the *hmo1*Δ strain, (*TPS1*, *RPL13A*, *RPL35A*, *RPS17B*, *RPS24A*, *YJR115W*, *RPS25B*, and *RPL21B)*, all contained Hmo1p at their promoter regions (Table 6.8C).

When the analysis was repeated for Hmo1p occupancy at those genes downregulated in the *hmo1*Δ strain (218 genes), only 6 genes bound by Hmo1p were downregulated in the *hmo1*Δ strain (Fig 6.8D). These 6 genes might represent the genes subject to direct activation by Hmo1p in exponentially growing cells. An example of one potentially directly activated gene is *TDH2* (Fig. 6.6E). Of these six genes that were downregulated in the *hmo1*Δ strain that harbored a site of Hmo1p (*PGK1*, *HMO1*, *RPL8A*, *TDH2*, *PHO84*, and *ADH1)*, Hmo1p binds at the ORFs of these genes (Fig. 6.8F). The exception was of course for *HMO1*, where Hmo1p binds at the promoter (Table 6.6F), and which is aberrantly listed as being downregulated in the *hmo1*Δ mutant due the gene itself having been deleted in this strain.

Overall, the correlation between Hmo1p occupancy and the genes under their positive and negative transcriptional control in exponential phase cells is poor. However, these data could suggest that Hmo1p exerts its repressive role at the promoter, possibly via inhibiting transcription initiation. Conversely, Hmo1p might exert its activating role in the gene coding region by promoting transcription elongation. Furthermore, we might predict from the above analysis that the regulatory role of Hmo1p upon its own transcription might be a repressive role, such that Hmo1p might act to downregulate its own transcription during exponential phase. The use of a conditional *HMO1* depletion mutant might help uncover its role in regulating its own transcription.

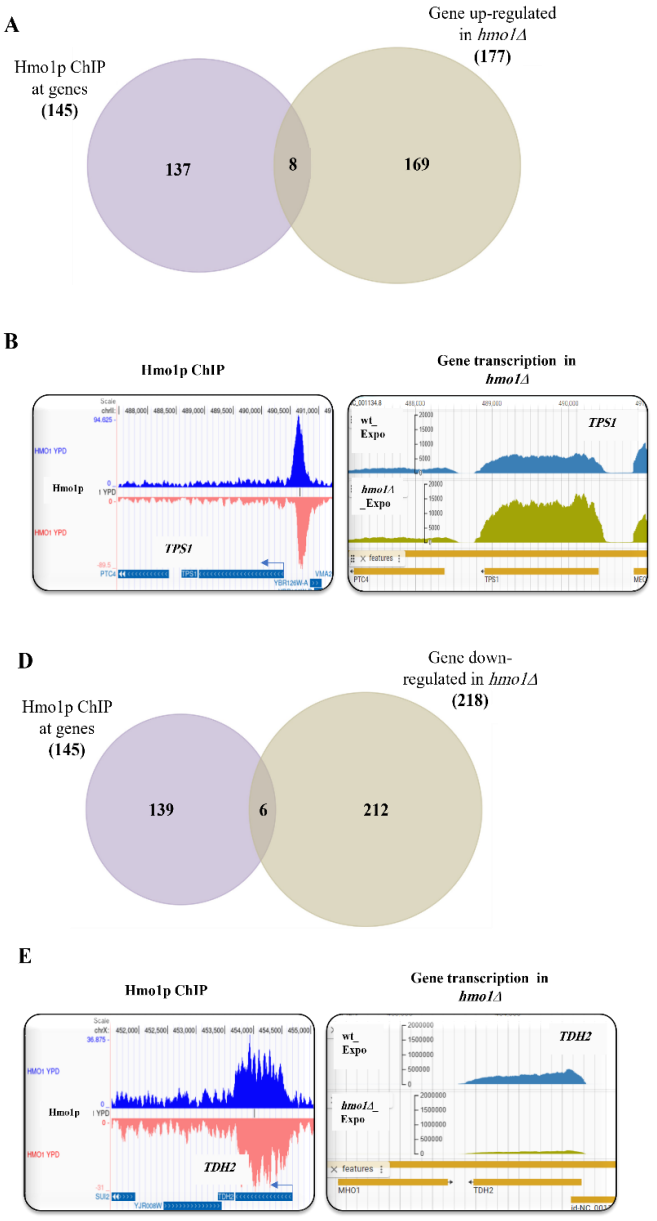

C

Directly repressor genes	Hmo1p location
TPS1	promoter
RPL13A	promoter
RPL35A	promoter
RPS17B	promoter
RPS24A	promoter
YJR115W	promoter
RPS25B	promoter
RPL21B	promoter

F

Directly activator genes	Hmo1p location
PGK1	ORF's
HMO1	promoter
RPL8A	ORF's
TDH2	ORF's
PHO84	ORF's
ADH1	ORF's

Figure 6.8: Correlation of Hmo1p occupancy with transcription in the exponential phase *hmo1*Δ mutant. (A) Venn diagram to identify the genes containing a peak of Hmo1p (Rossi et al., 2021) that showed up-regulation in the *hmo1*Δ mutant. **(B)** Example of a gene 'directly' repressed by Hmo1p (*TPS1*); J-browse screen-shot to show the peak of Hmo1p at *TPS1* (Rossi *et al.*, 2021) and RNA-seq transcriptional of *TPS1* in *hmo1*Δ. **(C)** Location of Hmo1p at the 8 'directly' repressed genes. **(D)** Venn diagram to identify the genes containing a peak of Hmo1p that showed down-regulation in the *hmo1*Δ mutant**. (E)** Example of a gene 'directly' activated by Hmo1p (*TDH2*); J-browse screen-shot to show the peak of Hmo1p at *TDH2* (Rossi *et al.*, 2021) and RNA-seq transcriptional of *TDH2* in *hmo1*Δ. **(F)** Location of Hmo1p at the 6 'directly' activated genes.

6.2.4 Summary

The ChIP-exo analysis revealed that Hmo1p has a significantly higher genomic occupancy than Hho1p. Hmo1p binds to 253 sites, whereas Hho1p binds to only 8. Hmo1p is associated with a larger number of ORFs, indicating its extensive role in genomic organization and function.

The data showed that Hmo1p binding sites correspond to regions with high transcriptional activity. Hmo1p occupied genes upregulated in the *hmo1*Δ strain, such as *TPS1*, highlighting Hmo1p's direct role in transcriptional repression. Conversely, *TDH2* was an example of a gene subject to direct activation by Hmo1p.

The other genes directly bound by Hmo1p that were significantly upregulated in *hmo1*Δ include *RPL13A*, *RPL35A*, *RPS17B*, *RPS24A*, *YJR115W*, *RPS25B*, and *RPL21B*. These genes are involved in diverse cellular processes including metabolism and ribosome biogenesis. Conversely, the data showed that genes such as *PGK1*, *RPL8A*, *TDH2*, *PHO84*, and *ADH1* were subject to direct activation by Hmo1p.

These data suggest that Hmo1p plays a critical role in directly maintaining normal transcriptional levels of specific genes. The differential binding and resulting transcriptional changes in *hmo1*Δ indicate that Hmo1p may act as a transcriptional activator or repressor, depending on the context of its binding sites.

In conclusion, the extensive binding of Hmo1p across the genome and its significant impact on gene transcription in *hmo1*Δ reveal its essential role in gene regulation. This study provides crucial insights into the functional dynamics of Hmo1p in yeast and its broader implications in genomic organization and transcriptional control.

6.2.5 ChIP-seq analysis to show Hho1p and Hmo1p occupancy during exponential phase, at diauxie, and in day 7 quiescent cells

I next performed ChIP-seq to identify Hho1p and Hmo1p occupancy in exponential phase cells, at the diauxic shift, and in purified day 7 quiescent cells. The total number of peaks identified for Hho1p was 490 in the exponential phase, 590 at the diauxic shift, and 1829 peaks in quiescent cells. In contrast, Hmo1p had 671 peaks in the exponential phase, 269 peaks at the diauxic shift, and 639 peaks in the quiescent cells. (Fig 6.9A). This differential occupancy pattern suggests a dynamic role of Hho1p and Hmo1p in chromatin remodeling and gene regulation as cells enter into stationary phase and form quiescent cells. (Fig 6.9B). Notably, Hho1p shows a marked increase in binding sites during the transition into quiescent cells.

A

Total number of Peak's	Exponential Phase (Expo)	Diauxic Shift (DX)	Quiescent cell (Q)
Hho1p	490	590	1829
Hmo1p	671	269	639

B

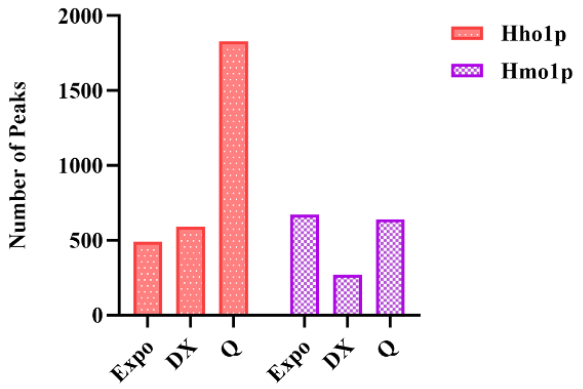

Figure 6.9: Hho1p and Hmo1p occupancy sites determined by ChIP-seq. (A) Table to show Hho1p (Hho1-myc) and Hmo1p (Hmo1-myc) occupancy sites during exponential phase (Expo), at diauxie (DX) and in day 7 quiescent cells (Q) as determined by ChIP-seq. **(B)** Plotting the number of sites of Hmo1p and Hho1p occupancy shown above at different times.

6.2.5.1 ChIP-seq analysis of Hho1-myc in exponential phase cells

Following our ChIP-seq analysis, the total number of peaks observed for Hho1p in exponential phase cells was 490. This was a much greater number of sites than the 8 sites revealed by the ChIP-exo analysis from Rossi et al., discussed previously.

It has been shown that there are regions in the yeast genome which show a false positive ChIP signal for most proteins analyzed (Teytelman *et al.*, 2013). These regions are termed 'hyper-ChIPable' sites and are considered to be regions of open chromatin to which proteins will transiently and non-specifically bind to give a false positive ChIP signal.

We therefore subtracted any of these hyper-ChIPable regions which overlapped with the 490 sites detected for Hho1p occupancy in our analyses to yield a revised number of 385 Hho1p sites of occupancy in exponential phase cells (Table 6.4). Of these 385 peaks of Hho1p, 263 mapped to genes, 100 mapped to tRNAs, whilst 18 sites were found at snoRNAs.

Strain	Total Peaks	Genes	tRNA	snRNA	snoRNA	ncRNA	transposable element	rRNA
Hho1p	385	263	100	1	18	2	1	0

Table 6.4: Hho1p occupancy in exponential phase cells. 1- First column; total number of Hho1p occupancy sites following subtraction of the 'hyperChIPable' sites (Teytelman *et al.*, 2013) **2-** Genes (mapped to a protein encoding gene (ORF) +/- 1Kb up and downstream) . **3-** tRNA is an essential component of protein synthesis. **4-** snRNA peaks of protein-DNA binding associated with small nuclear RNAs (snRNAs) or their binding sites. **5-** snoRNAs peaks of protein-DNA binding associated with small nucleolar RNAs, a type of non-coding RNA, are widely present in the nucleoli of eukaryotic cells and play an important role in rRNA modification **6-** ncRNA Non-coding RNAs are RNA molecules that are transcribed from DNA but do not encode proteins. **7-** transposable elements is a nucleic acid sequence in DNA that can change its position within a genome. **8-** rRNA peaks of protein-DNA binding associated with ribosomal RNA.

I next investigated the relationship between Hho1p occupancy and gene transcription in exponential phase cells by comparing the 263 Hho1p occupancy sites at genes with the genes upregulated in the *hho1*Δ mutant (Fig. 6.10A). This revealed that only 1 gene (*SER3*) that was occupied by Hho1p was upregulated in the *hho1*Δ mutant. This suggests that this gene was directly repressed by Hho1p in exponentially growing cells. When I compared the Hho1p occupancy at genes to the genes downregulated in the *hho1*Δ mutant, none of the genes occupied by Hho1p were downregulated suggesting no genes in exponential phase cells are directly positively regulated by Hho1p (Fig. 6.10B). Thus, consistent with the Rossi et al data, this analysis suggests that there is only a minor direct role for Hho1p in regulating gene transcription in exponentially growing cells.

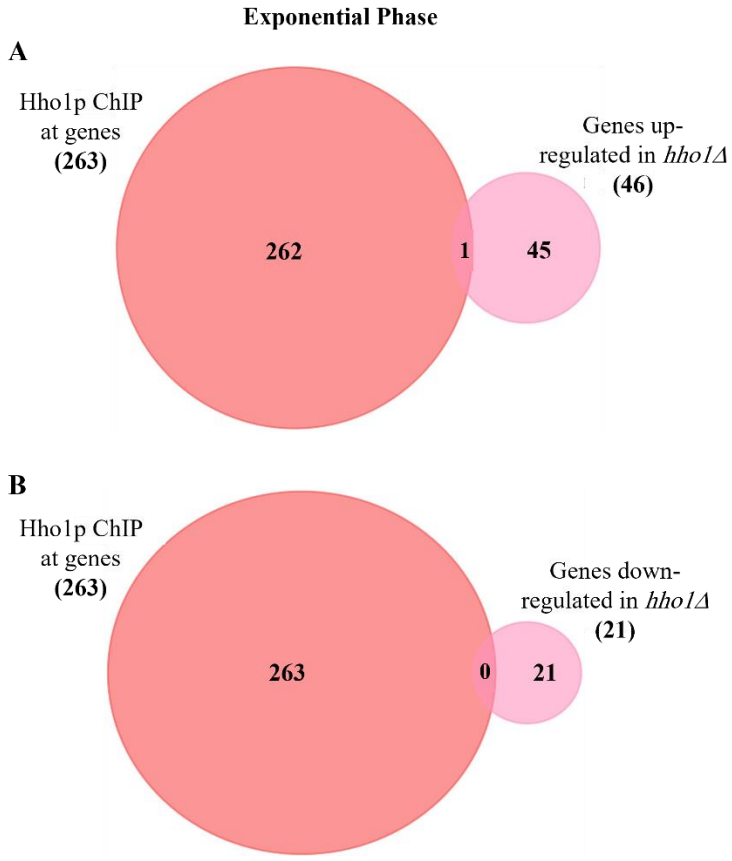

Figure 6.10: Comparing Hho1p occupancy in exponential phase wt cells with the number of genes down- and up-regulated in the exponential phase *hho1*Δ mutant. (A) Venn diagram to show 1 gene shared between Hho1p and up-regulated genes in a *hho1*Δ deletion mutant **(B)** Venn diagram to identify the shared peaks in the Hho1p occupancy data and *hho1*Δ mutant transcription of down-regulated.

6.2.5.2 Hho1p occupancy during the diauxic shift

I next investigated the distribution of Hho1p peaks during the diauxic shift (DX) and found a total of 590 sites associated with Hho1p (Table 6.5). For these peaks of Hho1p, the hyper ChIP able sites previously described were not subtracted since the hyper ChIP able study was only performed in exponential phase cells (Teytelman *et al.*, 2013). Of the 590 peaks of Hho1p, 578 peaks were located within open reading frames (ORFs), suggesting a strong correlation between Hho1p and gene expression during the diauxic shift. Additionally, 10 peaks were observed at tRNAs, indicating a potential role in translation regulation. Consistent with previously published data, a single peak was detected at the rRNA genes (Teytelman *et al.*, 2013).

Strain	Total peaks	Genes	tRNA	snRNA	snoRNA	ncRNA	transposable element	rRNA
Hho1p	590	578	10	0	0	0	1	1

Table 6.5: Hho1p occupancy at the diauxic shift. 1-First column; total number of Hho1p occupancy sites (peaks), **2-** Genes (mapped to a protein encoding gene (ORF) +/- 1Kb up and downstream). **3-** tRNA is an essential component of protein synthesis. **4-** snRNA peaks of protein-DNA binding associated with small nuclear RNAs (snRNAs) or their binding sites. **5-** snoRNAs peaks of protein-DNA binding associated with small nucleolar RNAs, a type of non-coding RNA, are widely present in the nucleoli of eukaryotic cells and play an important role in rRNA modification **6-** ncRNA Non-coding RNAs are RNA molecules that are transcribed from DNA but do not encode proteins. **7-** transposable elements is a nucleic acid sequence in DNA that can change its position within a genome **8-** rRNA peaks of protein-DNA binding associated with ribosomal RNA.

In order to investigate the relationship between Hho1p occupancy and gene transcription at diauxie, the 578 Hho1p occupancy sites genes and the genes upregulated in a *hho1*Δ mutant at diauxie were compared (Fig. 6.11A). This revealed 40 genes occupied by Hho1p that were upregulated in the *hho1*Δ mutant suggesting these genes are directly repressed by Hho1p at diauxie. Conversely, 30 of the genes occupied by Hho1p at diauxie were shown to be downregulated in the *hho1*Δ mutant, suggesting this gene cohort is directly activated by Hho1p at diauxie (Fig. 6. 11B).

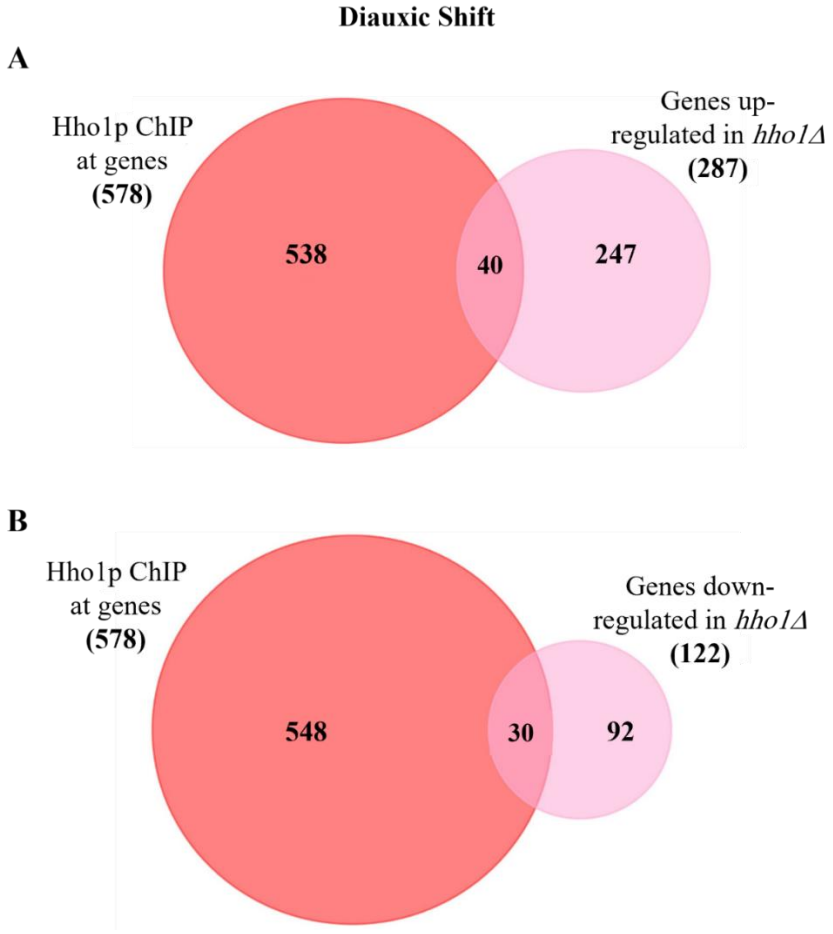

Figure 6.11: Hho1p occupancy at genes in diauxic cells compared with the total number of genes down- and up-regulated in the *hho1*Δ mutant strain at diauxie. (A) Venn diagram to show 40 genes shared between Hho1p and up-regulated genes in a *hho1*Δ deletion mutant **(B)** Venn diagram to show 30 genes shared of the down-regulated genes with Hho1p**.**

Gene ontology analysis of the 40 genes directly repressed by Hho1p at diauxie (upregulated in *hho1*Δ) revealed an enrichment of genes involved in the cell wall and in ribosome biogenesis (Fig. 6.12). Conversely, the 30 genes potentially directly activated by Hho1p at diauxie (downregulated in *hho1*Δ) were enriched for genes involved in metabolism and the cell membrane.

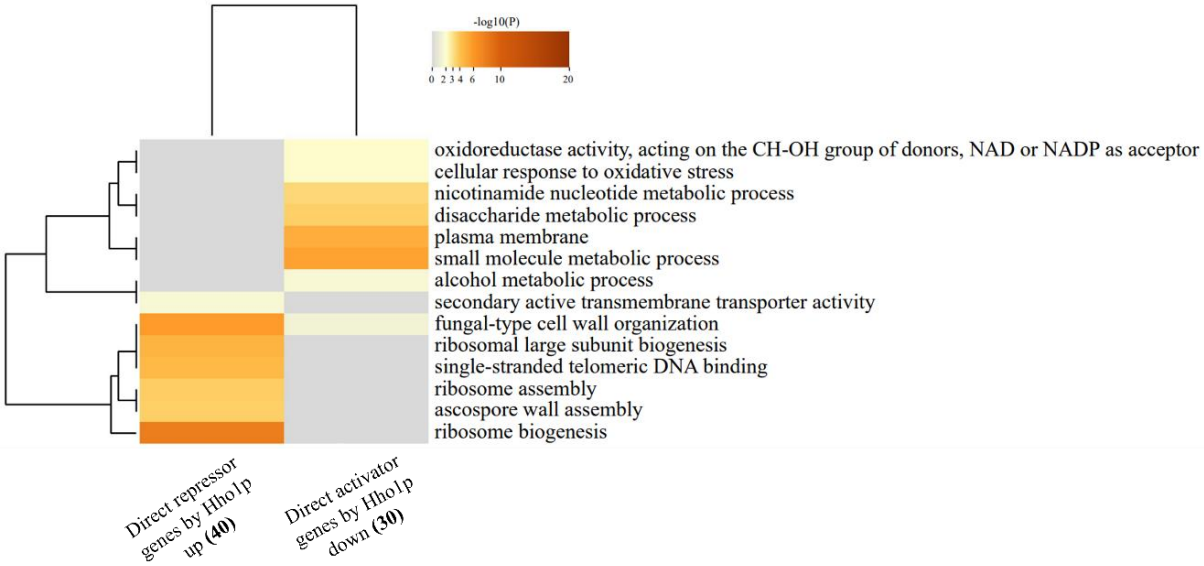

Figure 6.12: Gene Ontology for genes directly regulated by Hho1p at diauxie. The heat map and dendrogram represent the hierarchical clustering of gene ontology terms of the genes subject to direct Hho1p regulation. The color gradient in the heat map indicates the strength of association, with orange representing higher association. The dendrogram shows the relationship between these terms in biological processes.

6.2.5.3 Hho1p occupancy in quiescent cells

Our analysis of Hho1p occupancy in separated day 7 quiescent cells showed a total number of 1829 peaks (Table 6.6). Of these sites of occupancy, 1774 were associated with ORFs and 41 sites mapped to tRNAs. The analysis also showed peaks of Hho1p at other elements such as snRNAs (2), snoRNAs (7), ncRNAs (3) and transposable elements (2).

strain	Total Peaks	Genes	tRNA	snRNA	snoRNA	ncRNA	transposable element	rRNA	Pseudogene
Hho1p	1829	1774	41	2	7	3	2	0	0

Table 6.6: Hho1p occupancy in quiescent cells. 1-First column; total number of Hho1p occupancy sites (peaks), **2-** Genes (mapped to a protein encoding gene (ORF) +/- 1Kb up and downstream). **3-** tRNA is an essential component of protein synthesis. **4-** snRNA peaks of protein-DNA binding associated with small nuclear RNAs (snRNAs) or their binding sites. **5-** snoRNAs peaks of protein-DNA binding associated with small nucleolar RNAs, a type of non-coding RNA, are widely present in the nucleoli of eukaryotic cells and play an important role in rRNA modification **6-** ncRNA Non-coding RNAs are RNA molecules that are transcribed from DNA but do not encode proteins.**7-** transposable elements is a nucleic acid sequence in DNA that can change its position within a genome **8-** rRNA peaks of protein-DNA binding associated with ribosomal RNA. 9- Pseudogene is a segment of DNA that structurally resembles a gene but is not capable of coding for a protein.

When the sites of Hho1p occupancy at the ORFs in quiescent cells were compared to the genes upregulated in *hho1*Δ mutant quiescent cells, 156 of these occupied genes showed upregulation (Fig. 6.13A). This suggests that this cohort of genes is directly repressed by Hho1p in quiescent cells. On the other hand, 313 of the sites occupied by Hho1p in Q cells were downregulated in the *hho1*Δ mutant Q cells, suggesting these genes are directly activated by Hho1p in the Q cells (Fig. 6.13B). Thus, in quiescent cells, Hho1p directly positively regulates almost twice as many genes as the data suggests are directly negatively regulated by Hho1p.

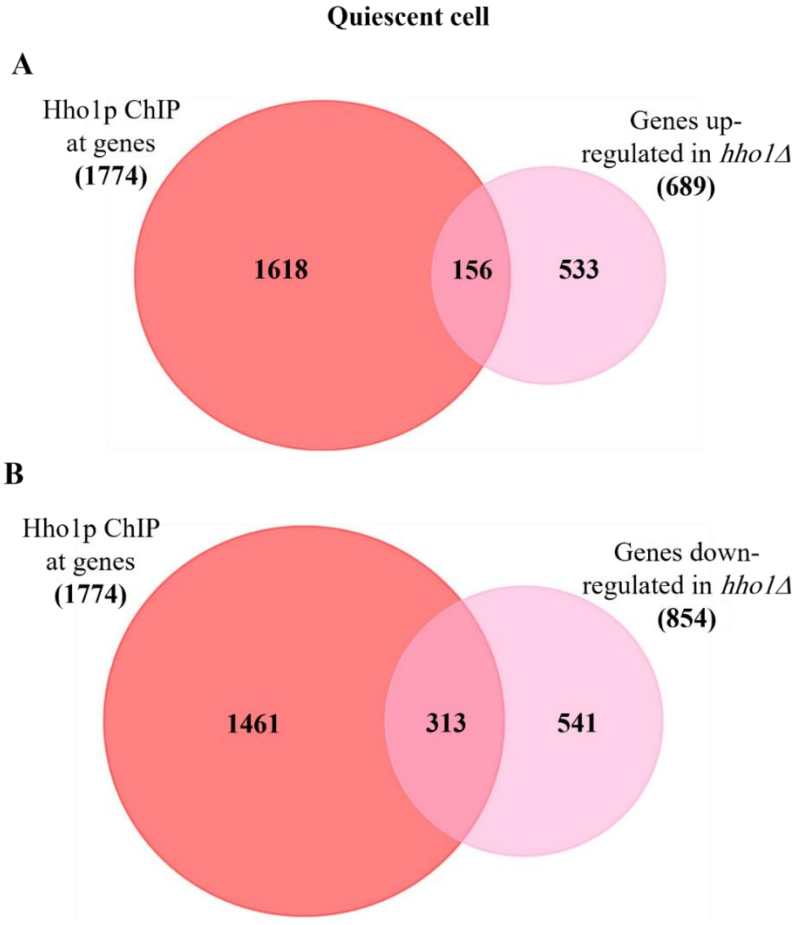

Figure 6.13: Comparing Hho1p occupancy and the total number of genes down- and up-regulated in the *hho1*Δ mutant strain in quiescent cells. **(A)** Venn diagram to show 156 genes shared between Hho1p and up-regulated genes in a *hho1*Δ deletion mutant **(B)** Venn diagram to show 313 genes shared of the down-regulated genes with Hho1p**.**

GO analysis of the 156 genes directly repressed by Hho1p in quiescent cells (upregulated in *hho1*Δ) showed an enrichment for genes involved in ribosome synthesis and function and translation. Of the 313 genes directly activated by Hho1p in Q cells (downregulated in *hho1*Δ), genes involved in detoxification were most significant. Together, this suggests a that in quiescent cells, Hho1p plays the most significant direct role in shutting down protein synthesis and coping with cell toxicity; two key properties of quiescent cells (Fig. 6.14).

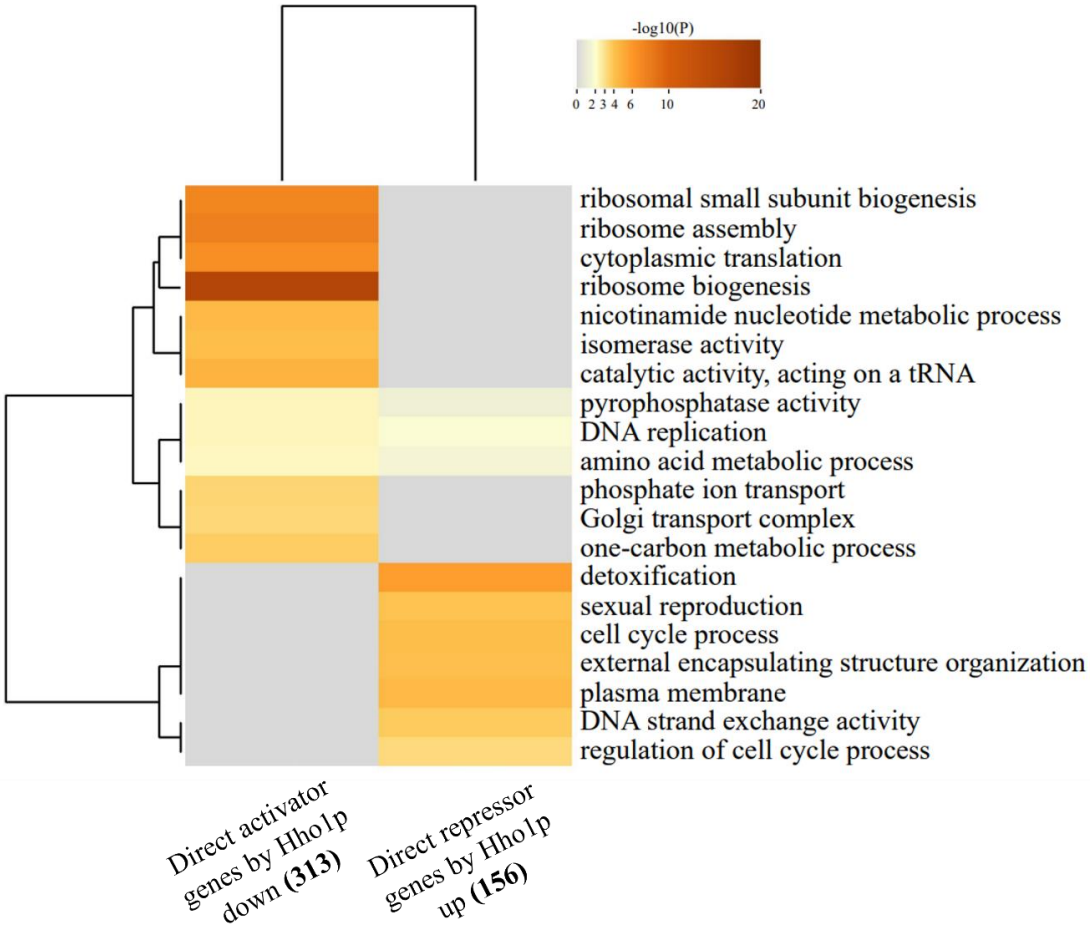

Figure 6.14: Gene Ontology Terms for genes directly regulated by Hho1p in day-7 quiescent cells. The heat map and dendrogram represent the hierarchical clustering of gene ontology terms for the genes directly regulated by Hho1p in day-7 quiescent cells. The color gradient in the heat map indicates the strength of association, with orange representing higher association. The dendrogram shows the relationship between these terms in biological processes.

6.2.5.4 Hmo1p occupancy in exponential phase cells

I also performed ChIP-seq analysis of Hmo1p in exponential phase cells, cells at diauxie and in separated day 7 quiescent cells. The results for the occupancy of Hmo1p in exponential phase cells revealed a total of 671 peaks of Hmo1p binding (Fig. 6.6A). However, prior to analysis of these peaks we first removed any sites that overlapped with the previously discussed 'hyper-ChIP able' regions (Teytelman *et al.*, 2013). This resulted in a revised list of 558 peaks of Hmo1p binding in exponential phase cells (Table 6.7). Of these 558 peaks, 415 were associated with genes, and 118 were associated with tRNA genes.

Strain	Total Peaks	Genes	tRNA	snRNA	snoRNA	ncRNA	transposable element	rRNA
Hmo1p	558	415	118	1	17	4	1	2

Table 6.7: Hmo1p occupancy in exponential phase cells. 1-First column; revised total number of Hmo1p occupancy sites (peaks) from which the 'hyper-chippable' sites have been subtracted (Teytelman *et al.*, 2013) **2-** Genes (mapped to a protein encoding gene (ORF) +/- 1Kb up and downstream). **3-** tRNA is an essential component of protein synthesis**. 4-** snRNA peaks of protein-DNA binding associated with small nuclear RNAs (snRNAs) or their binding sites. **5-** snoRNAs peaks of protein-DNA binding associated with small nucleolar RNAs, a type of non-coding RNA, are widely present in the nucleoli of eukaryotic cells and play an important role in rRNA modification **6-** ncRNA Non-coding RNAs are RNA molecules that are transcribed from DNA but do not encode proteins**.7-** transposable elements is a nucleic acid sequence in DNA that can change its position within a genome **8-** rRNA peaks of protein-DNA binding associated with ribosomal RNA.

We then examined the overlap of the 415 genes associated with peaks of Hmo1p and the 177 genes that were upregulated in the exponential *hmo1*Δ mutant cells (Fig. 6.15A). This revealed 32 genes occupied by Hmo1p that were upregulated in the absence of Hmo1p indicating that these genes were subject to direct repression by Hmo1p in exponential phase.

The analysis was then repeated for those genes that contained a peak of Hmo1p that were downregulated in *hmo1*Δ mutant exponential cells (Fig. 6.15B). This revealed 21 genes occupied by Hmo1p that were downregulated in the *hmo1*Δ mutant suggesting these are the genes subject to direct positive regulation by Hmo1p in exponential phase.

Figure 6.15: Comparing Hmo1p occupied genes in exponential phase cells with the number of genes down- and up-regulated in exponential *hmo1*Δ mutant strain. (A) Venn diagram to show 35 genes overlapped in the *hmo1*Δ up-regulated and Hmo1p **(B)** 24 genes shared in the *hmo1*Δ down-regulated with Hmo1p.

GO analysis of the 32 potentially directly repressed genes revealed genes involved in protein synthesis, response to external stress and trehalose synthesis. Conversely the 21 genes subject to direct activation by Hmo1p in exponential cells were enriched for genes involved in gluconeogenesis (Fig. 6.16)

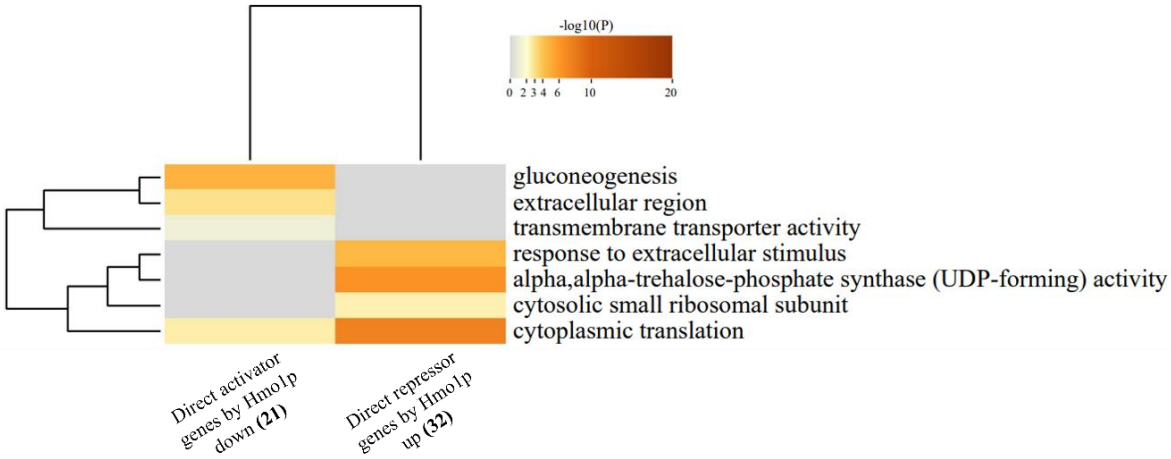

Figure 6.16: Gene Ontology Terms of genes directly regulated by Hmo1p in exponential phase. The heat map and dendrogram represent the hierarchical clustering of gene ontology terms of the genes subject to direct regulation (positive (activator) and negative (repressor)) by Hmo1p in exponential phase cells. The color gradient in the heat map indicates the strength of association, with orange representing higher association. The dendrogram shows the relationship between these terms in biological processes.

6.2.5.5 Hmo1p occupancy at the diauxic shift

ChIP analysis revealed a total of 269 sites of occupancy for Hmo1p in cells at the diauxic shift (Table 6.8). Of these 269 sites, 254 sites were associated with ORFs. However, Hmo1p was also found at 10 tRNAs, 3 ncRNA and 1 RNA, suggesting a potential role in the adaptive response during the diauxic shift.

Strain	Total peaks	Genes	tRNA	snRNA	snoRNA	ncRNA	transposable element	rRNA
Hmo1p	269	254	10	0	1	3	0	1

Table 6.8: Hmo1p occupancy in cells at diauxie. 1-First column; total number of Hmo1p occupancy sites (peaks), **2-** Genes (mapped to a protein encoding gene (ORF) +/- 1Kb up and downstream). **3-** tRNA is an essential component of protein synthesis. **4-** snRNA peaks of protein-DNA binding associated with small nuclear RNAs (snRNAs) or their binding sites. **5-** snoRNAs peaks of protein-DNA binding associated with small nucleolar RNAs, a type of non-coding RNA, are widely present in the nucleoli of eukaryotic cells and play an important role in rRNA modification **6-** ncRNA Non-coding RNAs are RNA molecules that are transcribed from DNA but do not encode proteins.**7-** transposable elements is a nucleic acid sequence in DNA that can change its position within a genome **8-** rRNA peaks of protein-DNA binding associated with ribosomal RNA.

In order to investigate the relationship between Hmo1p occupancy and gene transcription at diauxie, the 254 Hmo1p occupancy sites located at ORFs, and the 859 genes up regulated in a *hmo1*Δ mutant at diauxie were compared (Fig. 6.17A). This revealed 78 genes occupied by Hho1p that were upregulated in the *hmo1*Δ mutant suggesting these genes are directly repressed by Hmo1p at diauxie. Conversely, 14 of the genes occupied by Hmo1p at diauxie were shown to be downregulated in the *hmo1*Δ mutant, suggesting this gene cohort is directly activated by Hmo1p at diauxie (Fig. 6. 17B).

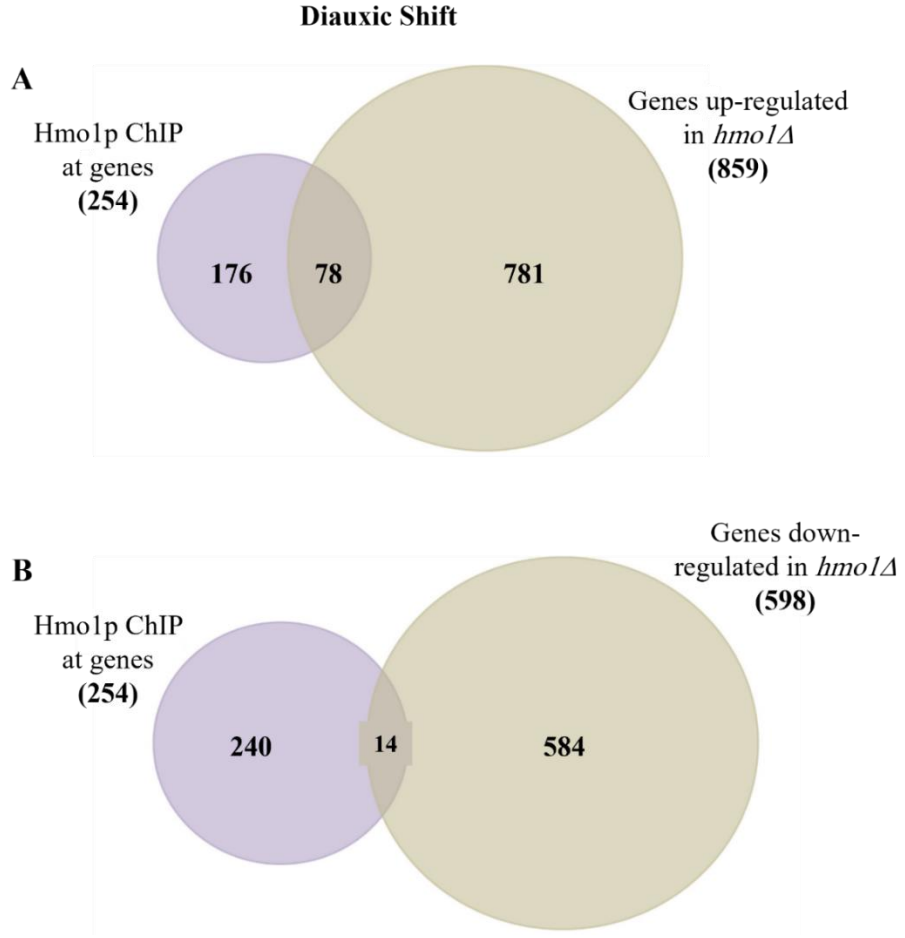

Figure 6.17: Comparing Hmo1p occupancy at genes with the number of genes down- and up-regulated in the *hmo1*Δ mutant strain at diauxie. (A) Venn diagram to show 78 of the genes occupied by Hmo1p at diauxie were up-regulated at diauxie and **(B)** 14 genes occupied by Hmo1p at diauxie were down-regulated at diauxie.

GO analysis of the 78 genes directly repressed by Hmo1p during diauxie showed an enrichment of genes involved in ribosome synthesis and function. Conversely, of the 14 genes activated by Hmo1p at diauxie, most genes were involved in carbohydrate synthesis. Together, this suggest and important role for Hmo1p in repressing protein synthesis and potentially activating synthesis of carbohydrates required for storage, metabolism or the cell wall (Fig. 6.18).

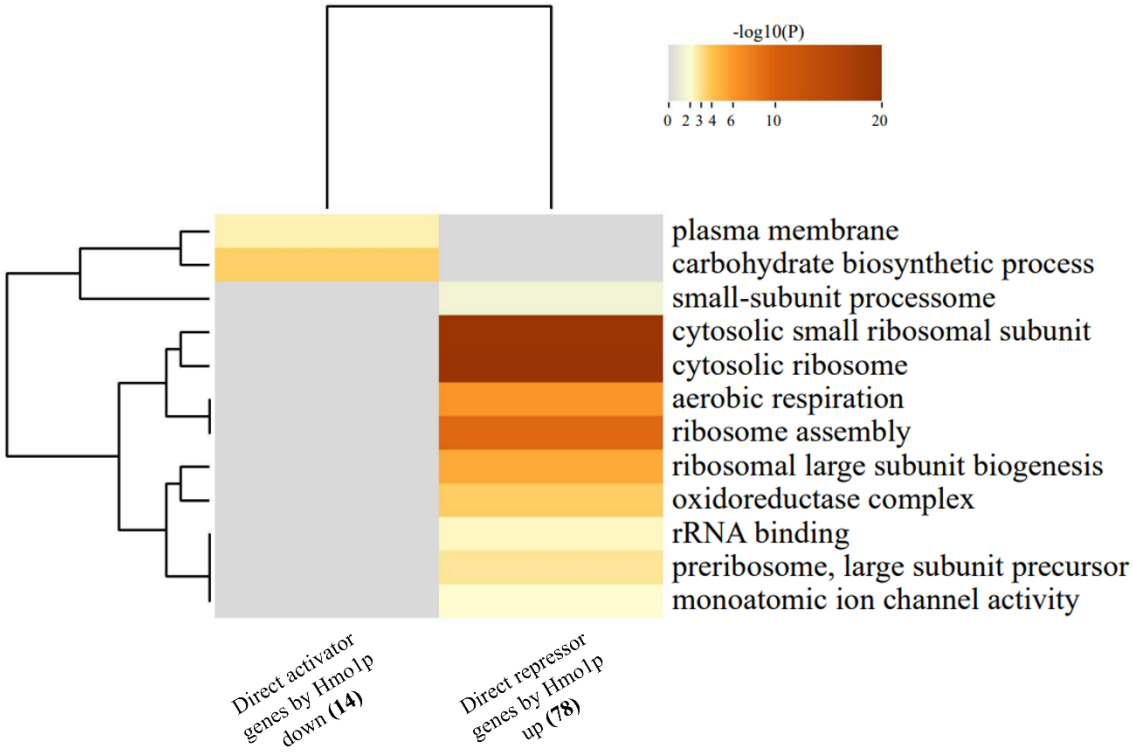

Figure 6.18: Gene Ontology terms of genes directly regulated by Hmo1p at diauxie. The heat map and dendrogram represent the hierarchical clustering of gene ontology terms of those genes directly regulated by Hmo1p at diauxie. The color gradient in the heat map indicates the strength of association, with orange representing higher association. The dendrogram shows the relationship between these terms in biological processes.

6.2.5.6 Hmo1p occupancy in quiescent cells

The ChIP-seq data revealed a total of 639 sites of Hmo1p occupancy across the genome of purified day 7 quiescent cells. Of these 639 sites, 617 were associated with genes, 11 sites with tRNAs, 3 sites with snoRNAs, 5 sites with ncRNAs, and 2 sites were found at rRNA gene sequence (Table 6.9).

Strain	Total Peaks	Genes	tRNA	SnRNA	snoRNA	ncRNA	transposable element	rRNA	Pseudogene
Hmo1p	639	617	11	0	3	5	0	2	1

Table 6.9: The total number of peaks in Hmo1p occupancy in quiescent phase. 1-First column; total number of Hmo1p occupancy sites (peaks), **2-** Genes (mapped to a protein encoding gene (ORF) +/- 1Kb up and downstream). **3-** tRNA is an essential component of protein synthesis. **4-** snRNA peaks of protein-DNA binding associated with small nuclear RNAs (snRNAs) or their binding sites. **5-** snoRNAs peaks of protein-DNA binding associated with small nucleolar RNAs, a type of non-coding RNA, are widely present in the nucleoli of eukaryotic cells and play an important role in rRNA modification **6-** ncRNA Non-coding RNAs are RNA molecules that are transcribed from DNA but do not encode proteins.**7-** transposable elements is a nucleic acid sequence in DNA that can change its position within a genome **8-** rRNA peaks of protein-DNA binding associated with ribosomal RNA. **9-** Pseudogene is a segment of DNA that structurally resembles a gene but is not capable of coding for a protein**.**

Further analysis revealed that of the 617 sites of Hmo1p found at genes, 100 of these genes were upregulated in the *hmo1*Δ mutant quiescent cells suggesting these genes are subject to direct Hmo1p-mediated repression in Q cells. Conversely, 96 of the genes occupied by Hmo1p in Q cells were down regulated in *hmo1*Δ mutant Q cells. This suggests that these 96 genes are directly activated by Hmo1p in Q cells (Fig. 6.19A and B).

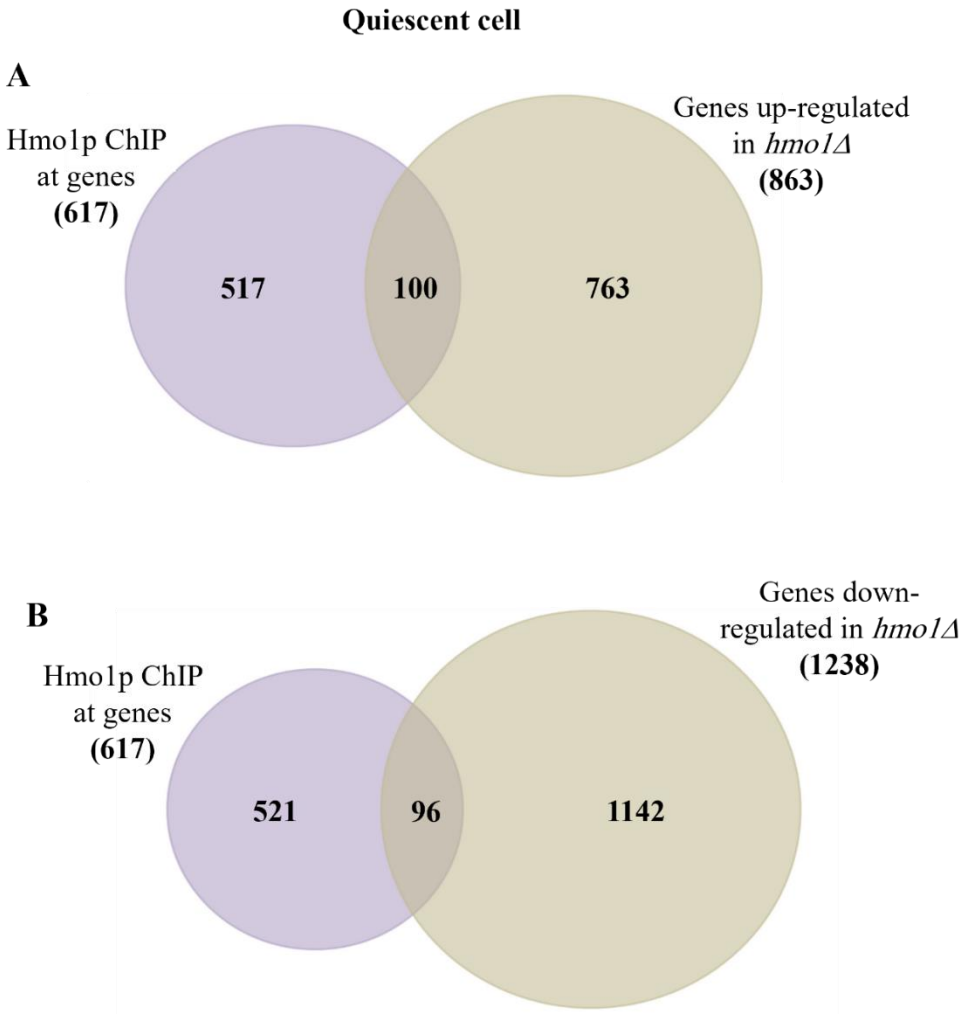

Figure 6.19: Comparing Hmo1p occupancy in quiescent cells with genes that are down- and upregulated in the quiescent cells of the *hmo1*Δ mutant strain. (A) Venn diagram of genes occupied by Hmo1p in Q cells with those genes up-regulated in *hmo1*Δ mutant Q cells. **(B)** Venn diagram of genes occupied by Hmo1p in Q cells with those genes down-regulated in *hmo1*Δ mutant Q cells.

GO analysis of the 617 genes directly repressed by Hmo1p in quiescent cells revealed and enrichment for genes involved in cell signaling, transport across them membrane and metabolism. On the other hand, the 69 genes directly activated by Hmo1p in quiescent cells were involved in cytosolic ribosome structure and function (Fig. 6.20).

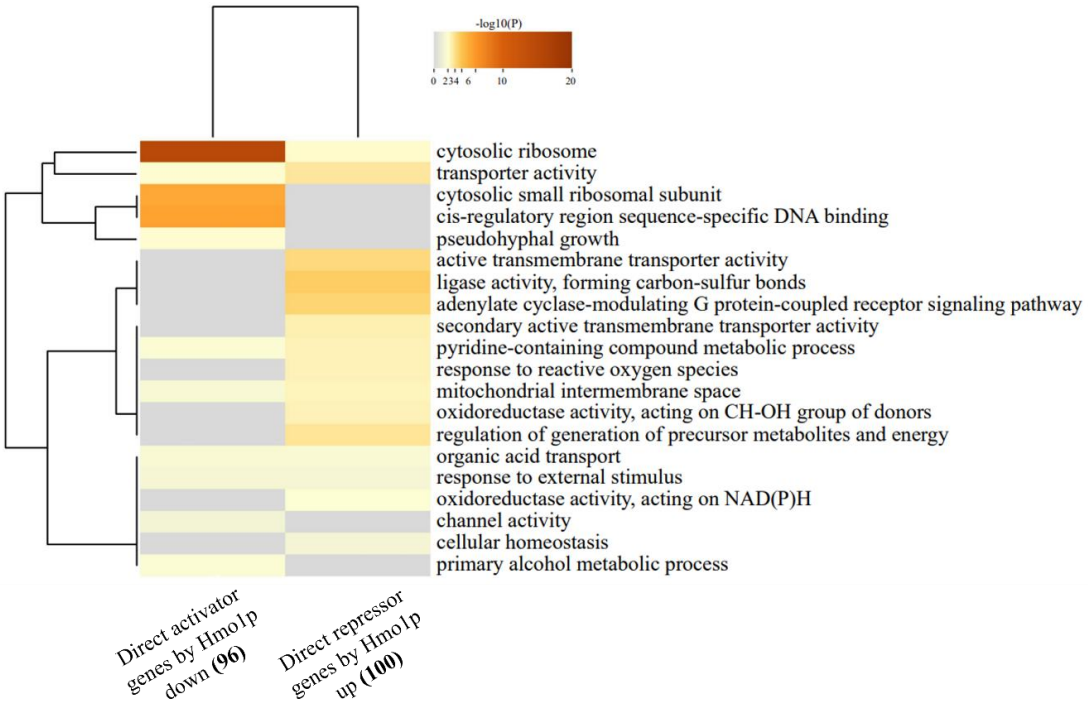

Figure 6.20: Gene Ontology (GO) term enrichment analysis of genes directly regulated by Hmo1p in day-7 quiescent cells. The heatmap displays the -log10(p) values of enriched GO terms for genes occupied by Hmo1p in quiescent cells that are up-regulated (Up) and down-regulated (Down) in *hmo1*Δ quiescent cells. The color gradient from yellow to dark brown shows the level of significance, with darker shades demonstrating.

6.2.6 Identification of genes potentially directly co-regulated by Hmo1p and Hho1p

To understand the extent of the overlap of gene regulation by Hmo1p and Hho1p at the different growth phases, I compared the genes previously shown to be directly regulated (positively and negatively) by Hmo1p and Hho1p at exponential phase, at diauxie and in the quiescent cells (Fig. 6.21).

The data revealed only 1 gene was potentially subject to direct co-regulation by both Hmo1p and Hho1p in exponential phase cells. However, 9 genes were shown to be co-regulated by Hmo1p and Hho1p at the diauxic shift and 21 genes were indicated as being directly co-regulated in quiescent cells. Although the numbers are small, this does show a greater contribution to gene regulation by both Hmo1p and Hho1p acting together occurs in quiescent cells.

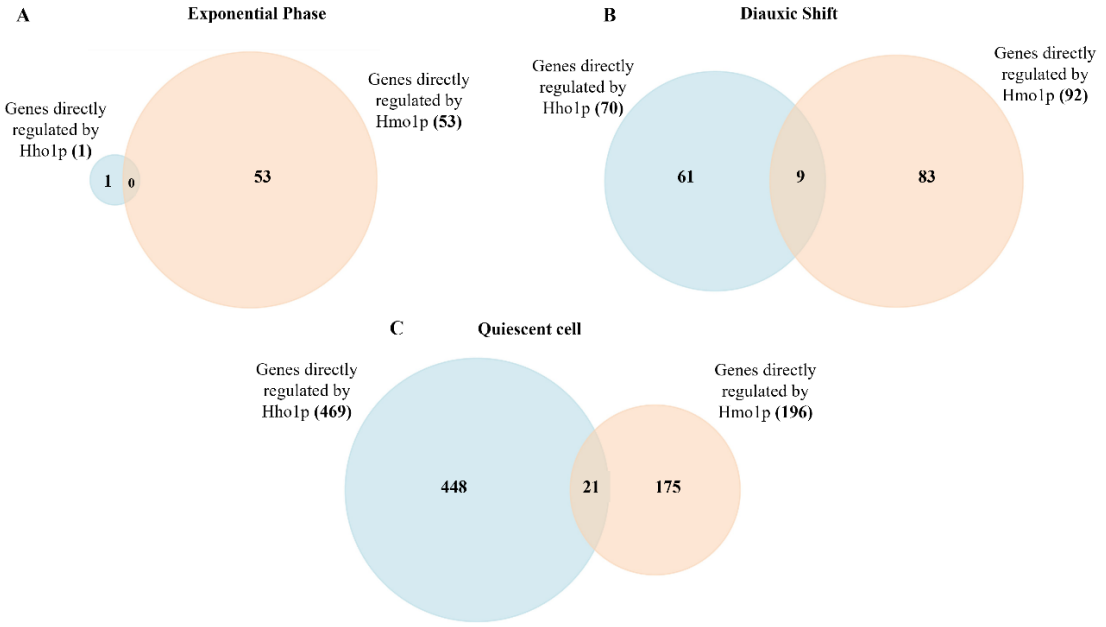

Figure 6.21: Analysis to show genes subject to direct co-regulation by both Hho1p and Hmo1p. **(A)** Venn diagram of those genes directly regulated (positively and negatively) by Hmo1p and Hho1p in exponential phase cells. **(B)** Venn diagram of those genes directly regulated (positively and negatively) by Hmo1p and Hho1p at the diauxic shift. **(C)** Venn diagram of those genes directly regulated (positively and negatively) by Hmo1p and Hho1p in day-7 quiescent cells.

6.3 Summary of main findings

- Occupancy by Hho1p increases as cells grow into stationary phase.
- Hho1p occupancy is greater than Hmo1p occupancy in Q cells.
- Genes directly repressed by Hmo1p and Hho1p increase during Q cell development
- The direct repression of genes by Hmo1p and Hho1p are largely independent of each other.
- However, a few genes are subject to direct co-repression by both Hmo1p and Hho1p.

6.4 Discussion

This chapter investigates the occupancy and regulatory roles of Hho1p and Hmo1p during quiescent cell formation. During the exponential phase, my ChIP-seq data showed Hho1p occupied 385 sites, which increases to 1829 in the quiescent cells. Conversely, the 671 peaks of Hmo1p in exponential phase peaks decrease to 269 at diauxie and rise to 639 in the quiescent cells. Both Hho1p and Hmo1p predominantly occupy ORFs and tRNA genes, suggesting their involvement in transcription of protein and tRNA encoding genes.

Interestingly, correlating the occupancy of Hho1p in exponential phase cells from my ChIP-seq data with the transcription changes in exponential phase *hho1*Δ mutants showed evidence of only 1 gene in exponential phase cells being directly regulated by Hho1p. This is consistent with previous studies which have shown little evidence of a role for Hho1p in regulating gene transcription during exponential growth (Teytelman *et al.*, 2013; Rossi *et al.*, 2021). This therefore raises the question as to what the other 384 sites of Hho1p occupancy are doing in exponential phase cells. It could be that my ChIP-seq data is picking up numerous non-specific binding sites for Hho1p, which would be consistent with the fact that the ChIP-exo study revealed only 8 sites of Hho1p occupancy in exponential phase cells (Rossi *et al.*, 2021). Conversely, it could mean that Hho1p is having a transcription-independent role in exponential phase cells such as acting to maintain chromatin structure and / or mediating DNA damage. Indeed, the fact that the *hho1*Δ mutant displays a greater level of H2A-serine 129 phosphorylation in SP cells does suggest a role for Hho1p in the DNA damage response. Furthermore, the comet assay in the *hho1*Δ mutant supports a role for Hho1p in regulating chromatin structure during exponential phase.

When Hho1p occupancy was correlated with gene transcription in the *hho1*Δ mutant at diauxie and in the quiescent cells, the data suggested an increase in Hho1p acting directly to regulate transcription occurred over time. Indeed, the data suggested Hho1p was directly repressing 156 genes in quiescent cells and was directly activating 313 genes. Thus, contrary to expectation, Hho1p was having a predominantly positive role upon gene transcription in quiescent cells as opposed to it having the greatest predicted role in gene repression.

Analysis of the Hmo1p ChIP-seq data in exponential phase cells showed evidence for 32 genes being directly repressed by Hmo1p and 21 genes being subject to direct activation. In cells at diauxie, there was evidence for 78 genes being directly repressed by Hmo1p and only 14 genes boing subject to direct activation. In quiescent cells, the data revealed 100 genes were subject to direct repression by Hmo1p and 96 genes were being directly activated by Hmo1p. Thus, Hmo1p plays a largely negative role upon transcription in exponential phase cells and cells at diauxie. However, Hmo1p plays an almost equal role in gene activation and repression in the quiescent cells.

The data also revealed an increase in the cooperation between Hho1p and Hmo1p for direct gene regulation as quiescent cells develop.

The dynamic binding patterns and regulatory roles of Hho1p and Hmo1p contribute to the ongoing discourse on the complexity of chromatin-mediated gene regulation. These findings underscore the importance of temporal dynamics in chromatin biology, a theme that has been extensively explored in recent studies (George and Conway-Campbell, 2016; Cui *et al.*, 2022; Han *et al.*, 2024).

In summary, our genome-wide analysis of Hho1p and Hmo1p occupancy and their consequent impact on gene expression enriches the current understanding of the regulatory mechanisms of these chromatin-associated proteins during the development of cellular quiescence. The dynamic binding patterns and dual regulatory roles highlight the intricate nature of chromatin remodeling and gene regulation, reinforcing themes that are well-established in the field.

Future research will aim to further elucidate the molecular mechanisms underlying the interactions between Hho1p, Hmo1p, and other chromatin modifiers, as well as their interplay with other regulatory pathways. This will provide a more integrated view of the cellular processes governing chromatin dynamics and gene expression involved in regulating yeast cellular quiescence, potentially enhancing our ability to manipulate quiescence in human cells for therapeutic purposes.

Chapter 7

Final Discussion

7.1 Discussion

In the yeast *Saccharomyces cerevisiae*, the *HHO1* gene has been proposed to encode the yeast linker histone H1, with Hmo1p, a high-mobility group protein, suggested to have overlapping roles with Hho1p (Syed *et al.*, 2010a; Brush, 2015). The research in this thesis investigates the phenotypic, physiological, and transcriptional features of *hho1*Δ and *hmo1*Δ gene deletion mutants to determine more precisely whether either Hho1p or Hmo1p can be considered the true linker histone H1 of yeast.

7.1.1 Gene deletion confirmation

The deletions of *HHO1* and *HMO1* genes were attained by means of homologous recombination, with the coding regions substituted by the KAN gene, which provides resistance to kanamycin. PCR analysis and Western blot analysis confirmed the efficacy of the gene deletions (Allen *et al.*, 2006; Bryant *et al.*, 2012b).

7.1.2 Growth and viability analysis (exponential growth phase)

During the exponential growth phase in glucose-containing media, the *hho1*Δ mutant did not display substantial growth defects as compared to the wild type (wt), indicating that Hho1p is not important for basic cell proliferation during these conditions. On the contrary, the *hmo1*Δ mutant exhibited a late onset of growth and a decreased maximum cell density, highlighting towards a notable growth defect (Gadal *et al.*, 2002; Bermejo *et al.*, 2009). These findings were further supported by reduced cell viability in the *hmo1*Δ mutant after 24 hours of growth, highlighting the significance of Hmo1p in maintaining cellular viability during active cell division. The difference in growth characteristics observed between *hho1*Δ and *hmo1*Δ mutants during the exponential phase signifies the distinctive roles played by these proteins. While Hho1p may not be necessary for rapid cell division and accumulation of biomass, Hmo1p seems to be essential to these processes. The growth delay and reduction in cell density in the *hmo1*Δ mutant suggest that Hmo1p influences pathways crucial for cellular metabolism and proliferation.

7.1.3 Stationary growth phase

In the stationary phase, both mutants demonstrated distinctive phenotypes from those seen during the exponential phase. The *hho1*Δ mutant displayed no substantial difference in growth or viability when compared to wt, while the *hmo1*Δ mutant continued to display growth defects and reduced cell viability (7). This suggests that while Hho1p may not be critical for cell survival during exponential growth, Hmo1p plays an important role in sustaining cell viability through both growth phases. The stationary phase denotes a period of nutrient constraint and cellular quiescence, where cells undergo metabolic reprogramming to survive sustained periods of nutrient shortage. The absence of significant growth or viability differences in the *hho1*Δ mutant during this phase signifies that Hho1p is not essential for the metabolic shifts necessary for stationary phase survival. In contrast, the persistent growth defects in the *hmo1*Δ mutant during this phase suggest that Hmo1p is vital for the cellular adaptations required for survival under nutrient-limited conditions.

7.1.4 Cell morphology

Microscopic analysis showed that the *hmo1*Δ mutant displayed an elongated cell morphology during exponential growth, a phenotype not seen in the *hho1*Δ mutant. Hmo1p is vital for maintaining normal cellular architecture throughout active division, which is indicated by this atypical cell shape (8). The absence of such morphological defects in the *hho1*Δ mutant suggests that Hho1p's role may be subtler and context-dependent, possibly influencing chromatin structure rather than directly impacting cell shape. Cellular functions such as division, differentiation, and response to environmental stimuli are closely associated to cellular morphology. The elongated morphology seen in *hmo1*Δ mutants might indicate towards defects in cell wall synthesis, cytoskeleton organization, or cell cycle regulation. Hmo1p absence might lead to mis-regulation of genes involved in these crucial processes, leading to an abnormal cell shape, as it is known to be is associated to transcriptional regulation.

7.1.5 Stress responses (response to acetic acid and hydrogen peroxide)

The differential sensitivities of the mutants to external stressors, such as acetic acid and hydrogen peroxide, underline the different roles that Hho1p and Hmo1p play in mechanisms related to stress response. Though the *hho1*Δ mutant became sensitive to acetic acid and hydrogen peroxide upon entry into exponential growth, it was as resistant as wt in the stationary phase (Brush, 2015). On the other hand, an *hmo1*Δ mutant exhibited enhanced growth on acetic acid in exponential phase but retained a reduced growth capacity at stationary phase (Syed *et al.*, 2010a). This variability of responses could be easily perceived to mean that Hho1p and Hmo1p contribute toward various inputs to cellular stress responses, probably through their functions in chromatin structure and modulations of gene expression. The fact that the *hho1*Δ mutant showed increased sensitivity to acetic acid and hydrogen peroxide at the exponential phase means that Hho1p can have a defensive role against oxidative and metabolic stresses. This might point to a more general function in maintaining chromatin structure and integrity, important for proper expression of stress response genes. By contrast, improved growth of the *hmo1*Δ mutant in the presence of acetic acid might be indicative of a compensatory metabolic adaptation that mitigates the harmful outcomes from acetic acid stress. Still, the stationary-phase growth deficiency recurrently reflects the wider role of Hmo1p in adaptation to stress and cellular metabolism.

7.1.6 Chromatin structure and compaction

Also, chromatin sensitivity to a micrococcal nuclease assay revealed that both *hho1*Δ and *hmo1*Δ mutants were more sensitive than wt. Increased sensitivity to Mnase itself indicated that Hho1p and Hmo1p are involved in promoting chromatin compaction (Patterton *et al.*, 1998). The role of Hho1p in chromatin compaction was further evidenced by increased phosphorylation of histone H2A at Ser129 in the *hho1*Δ mutant during stationary phase, which could be taken as indicator of higher levels of DNA damage according to several studies. Therefore, it is deduced that Hho1p also guards chromatin integrity and thus is involved in facilitating DNA damage repair processes. Chromatin compaction is thus an important principle of genome organization, which has implications for gene expression, DNA replication, and repair processes. For the *hho1*Δ and *hmo1*Δ mutants, the heightened Mnase sensitivity is interpreted to mean a more open chromatin structure and therefore implies a role for Hho1p and Hmo1p in higher-order chromatin organization.

This increased Mnase sensitivity in these deletion mutants is thus interpreted to mean that chromatin is more open in organization. It does, however, expose the DNA to damage and destabilizes the genome, which is evidenced by increase in H2A phosphorylation in *hho1*Δ mutant.

7.1.7 DNA damage repair

High levels of H2A Ser129 phosphorylation are maintained in the *hho1*Δ mutant during the stationary phase, suggesting that Hho1p may play a critical role in DNA damage repair (Schäfer *et al.*, 2008). Even in the absence of Hho1p in this instance, it can be noticed that there is an accumulation of DNA damage with heightened phosphorylation of H2A serving as a marker for DNA double-strand breaks. The findings thus imply that Hho1p is required for genome stability and are compatible with a role in counteracting genome instability in response to DNA-damage-inducing conditions, such as oxidative stress and nutrient deprivation. Probably due to its role in chromatin compaction, which may protect the genetic material from damage and facilitate recruitment of repair machinery to sites of damage, the *hho1*Δ mutation generated more DNA damage in this phase. These observations bring out the role of chromatin structure on the maintenance of the genome and that of Hho1p in the process.

7.1.8 Thermotolerance

In particular, neither the deletion of *HHO1* nor of *HMO1* substantially affected the acquired thermotolerance that is characteristic for quiescent cells. Compared with wt, both the *hho1*Δand *hmo1*Δ mutants were similarly resistant against high temperatures, indicating that the primary mechanisms providing thermotolerance are not substantially influenced by the loss of either one of these proteins (Allen *et al.*, 2006; Bryant *et al.*, 2012a). However, overexpression studies with Hho1p and Hmo1p showed that these proteins might contribute to thermotolerance by promoting compaction and stability of chromatin under stress conditions (Schäfer *et al.*, 2008). One of the important adaptive responses that enables cells to survive high temperatures is thermotolerance. The similar thermotolerance exhibited by *hho1*Δ and *hmo1*Δ mutants as compared to wt could be an indication that other factors or pathways are compensating for the deficiency of these proteins in resistance to heat stress.

Overexpression studies showing enhanced thermotolerance indicated subsidiary roles for Hho1p and Hmo1p in protecting cells from heat stresses, probably through chromatin stabilization and prevention from heat-induced DNA damage.

7.1.9 Transcriptional regulation by RNA polymerase II

The possible role of Hho1p and Hmo1p in regulating transcription during the transition from exponential to stationary phase was examined, as RNA polymerase II levels and activity were measured throughout the transition from exponential to stationary phase. A positive role of Hho1p was discovered in controlling Pol II levels in stationary phase cells. During the stationary phase, Pol II ser-5 phosphorylation, a marker of active transcription, was maintained for a longer period of time in the *hho1*Δ mutant compared to wt, indicating that Hho1p acts as a general transcriptional regulator on passage to quiescence, likely through the regulation of chromatin structure and accessibility (Allen *et al.,* 2006). Modulation of Pol II activity and recruitment to gene promoters are achieved through a complex interplay of factors. The persistence of phosphorylated Pol II in the *hho1*Δ mutant during the stationary phase suggests that the normal transcriptional shut-down which occurs as cells differentiate into quiescent states is disrupted. From the results obtained it can be assumed that Hho1p is involved in promoting this transition by facilitating chromatin compaction and transcriptional repression, hence conserving cellular resources under conditions of nutrient scarcity.

7.1.10 Functional overlap and distinct roles for Hmo1p and Hho1p.

Both distinct and overlapping functions of Hho1p and Hmo1p in yeast were revealed by characterization of the *hho1*Δ and *hmo1*Δ mutants. More specifically, Hmo1p is required for cell morphology maintenance and growth during exponential phase and Hho1p is involved mainly in the DNA damage repair process and chromatin stabilization under stress. However, in a recent study, it was observed that both proteins participate in chromatin compaction, which influences a wide range of cellular events comprising transcription factors, stress response, and genome stability (Gadal *et al.,* 2002; Ray and Grove, 2009a).This means that, despite their interaction, Hho1p and Hmo1p exhibit differential cellular physiology with respect to growth, morphology, and stress responses.

The role of Hho1p in DNA damage repair and chromatin stability at this level definitely places it at the forefront of genome maintenance in cells, particularly under stressed conditions. In contrast, the involvement of Hmo1p in the morphology and growth of exponential phase cells highlights its important role in cell division and proliferation. The redundancy of functions discussed above provides evidence that both proteins mediate higher order chromatin compaction and therefore modulate cellular processes.

7.1.11 Impact on gene transcription

Using global transcriptomic analyses differential outcome of Hho1p and Hmo1p on gene expression was further investigated. Deletion of *HHO1* and *HMO1* clearly showed very different changes in gene expression profiles, therefore pointing toward the specific and redundant roles of these factors in transcriptional regulation. It was found that Hho1p regulated genes involved in DNA repair and stress response, while Hmo1p influenced genes related to cell cycle and morphogenesis (Gadal *et al.*, 2002; Bryant *et al.*, 2012a). These findings highlight the complex regulatory networks governed by Hho1p and Hmo1p and their contributions to cellular adaptation under different growth conditions. Global transcriptomic analysis explained the broader effect of Hho1p and Hmo1p on gene expression. The specific genes and pathways that became influenced by their deletion highlight the fact that they play different regulatory roles. More specifically, Hho1p regulates DNA repair and stress response genes along with its role in genomic maintenance, while Hmo1p modulates genes involved in cell-cycle and morphogenesis consistent with its role in the process of cell proliferation and architecture.

In summary, the results obtained in the thorough characterization of the *hho1*Δ and *hmo1*Δ mutants highlight both redundant and specific roles of Hho1p and Hmo1p in *Saccharomyces cerevisiae*. Hho1p participates more in DNA repair processes and chromatin stability during stressful cell conditions, whereas high requirements for Hmo1p were established for cell morphology maintenance and cell growth in the exponential phase.

Both proteins compact chromatin, modulating cellular events like transcription, response to stress, and genome stability. These data highlight how Hho1p and Hmo1p complexly regulate chromatin organization and are required for proper cellular adaptation and survival upon diverse environmental fluctuations.

7.1.12 Occupancy and regulatory roles of Hho1p and Hmo1p in *Saccharomyces cerevisiae*

This study focused into the occupancy and corresponding regulatory roles of chromatin-associated Hho1p and Hmo1p proteins across different growth phases in *Saccharomyces cerevisiae*. Their dynamic binding patterns are imperative for chromatin restructuring and gene regulation. For example, Hho1p exhibits 490 peaks in the exponential phase that increase to 1829 in quiescence, highlighting its prominent role in chromatin organization. In contrast, Hmo1p peaks decrease from 671 in exponential phase to 269 in diauxic phase, reflecting the adaptability of regulatory roles under varying metabolic conditions before their rise again at 639 in quiescent phase. In particular, it utilizes methodologies given by (Xu *et al.*, 2020) chromatin immunoprecipitation followed by high-throughput sequencing to map genome-wide binding patterns. The results regarding the dynamics of binding are consistent with the literature on chromatin restructuring. For example, (Hu *et al.*, 2024) revealed considerable changes in nucleosome spacing in allopolyploid cotton. These findings highlight Hho1p and Hmo1p's significant functions in chromatin accessibility and transcriptional regulation.

Transcriptional analysis of the *hho1*Δ and *hmo1*Δ strains showed that the deletion of Hho1p up-regulates 46 genes and down-regulates 21 genes of the Hho1p ORFs, hence showing a role for this gene product in regulation. Hho1p and Hmo1p have contacts mostly with ORFs and with tRNA genes, thus perhaps being part of the regulation of coding regions and tRNA genes. Hho1p minor peaks, along with minimal binding of Hmo1p to transposable elements and rRNA, in snRNA, snoRNA, and ncRNA categories, highlight specific regulatory functions. The direct role of Hmo1p as a repressor at loci such as *TPS1* and *TDH2* aligns with published data on chromatin modifiers and transcription factors. Our data now demonstrate that repression of genes by Hmo1p also functions through mechanisms similar to other chromatin remodellers and histone modifications.

In conclusion, this study improves our knowledge of the intricate interplay between chromatin-associated proteins during different cellular growth phases. The dynamic regulatory functions of Hho1p and Hmo1p, as shown through ChIP-Seq analysis, offered valuable insights into their roles in chromatin biology and transcriptional regulation.

These findings not only align with but also extend the existing body of research on chromatin dynamics and gene regulation, offering a comprehensive view of the functional versatility of Hho1p and Hmo1p in *Saccharomyces cerevisiae*.

Conclusion

- Hmo1p and Hho1p can function together and independently to regulate transcription to ensure correct Q cell development.

7.2 Key insights from our research include

- Hho1p is mainly implicated in DNA damage repair and chromatin stability, whereas Hmo1p is important for cell morphology and growth during the exponential phase.
- Both Hho1p and Hmo1p results in compaction of chromatin, affecting cellular processes such as transcription and stress response.
- *hho1*Δ and *hmo1*Δ mutants display differential sensitivities to stressors like acetic acid and hydrogen peroxide, highlighting distinct roles in stress response mechanisms.
- Deletion of *HHO1* or *HMO1* does not significantly impact thermotolerance in stationary phase cells.
- Hho1p influences RNA polymerase II levels and activity during the transition to stationary phase, indicating a role in transcriptional regulation.
- The deletion of *HHO1* and *HMO1* results in distinct changes in gene expression, reflecting their unique roles in transcriptional regulation.
- Hmo1p is essential for maintaining cell viability during active cell division, while Hho1p's role becomes more prominent under stress conditions.
- *hmo1*Δ mutants exhibit elongated cell morphology during exponential growth, indicating Hmo1p's role in maintaining normal cell architecture.
- Hho1p is crucial for DNA damage repair, particularly under stress conditions.
- The distinct and overlapping roles of Hho1p and Hmo1p in chromatin compaction and gene expression highlight their importance in regulating complex cellular processes essential for adaptation and survival.

Appendix

Table S.1: List of gene directly co-regulated by Hho1p occupancy at genes in diauxic cells, upregulated (Up) and downregulated (Down)

Hho1p -up DX (40 genes)			
AAC3	*AIR1*	*NSR1*	*PUT1*
DTR1	*FAF1*	*RPL8A*	*EMG1*
PHO89	*YVH1*	*IPI1*	*ERB1*
SPS22	*TIR1*	*CPS1*	*EMW1*
PWP2	*PUG1*	*HCA4*	*TOS6*
RSA4	*HXK2*	*RPA12*	*POL1*
NOP14	*VRG4*	*DAN1*	*IMP4*
PRM7	*SUA5*	*PRY2*	*LDS2*
RRP8	*THI4*	*SOF1*	*TIR2*
UPC2	*RSR1*	*YPS3*	*YTM1*

Hho1p-down DX (30 genes)		
BDH2	*OM45*	*NNR2*
ACH1	*YAT2*	*UGP1*
CHA1	*SIP2*	*MSC1*
HSP30	*NQM1*	*CAT2*
HBT1	*GND2*	*TDA1*
FMP45	*YHR033W*	*YNL195C*
YDL124W	*REE1*	*YNR014W*
NDE2	*IMA5*	*CIN5*
TPS2	*JEN1*	*USV1*
POT1	*FAT3*	*AQY1*

Table S.2: List of gene directly co-regulated by Hho1p occupancy at genes in quiescent cells, upregulated

Hho1p- Q up (156 genes)									
LDS1	*DTR1*	*LDB17*	*YDR222W*	*SAM2*	*HOM3*	*CDC20*	*TDA3*	*GAS1*	*SKM1*
SHE1	*YPC1*	*YDL114W*	*RKM4*	*LPP1*	*RNR1*	*CTT1*	*YNG2*	*RFA2*	*YOL029C*
SCT1	*GPX2*	*SNU23*	*DIN7*	*SPS1*	*ILV1*	*TEL2*	*OYE2*	*SSU72*	*RCL1*
ALK2	*SPS22*	*NUR1*	*SRP101*	*BNR1*	*RAD51*	*FHN1*	*INO1*	*YNL193W*	*CIN5*
DSF2	*FUS1*	*RPN4*	*GIC2*	*VHS2*	*DDI1*	*RSR1*	*NCA3*	*YGP1*	*RSB1*
UBC4	*HSP30*	*RAD57*	*TRR1*	*AGE2*	*YFL040W*	*AMA1*	*ARG3*	*CUZ1*	*VPS21*
AAC3	*SLM5*	*SNQ2*	*TRP4*	*PRM2*	*YPI1*	*SMI1*	*BIT61*	*MEP2*	*SRL1*
AGP2	*PTP1*	*MRH1*	*PHO92*	*MCM3*	*CSS2*	*NAS6*	*CCT3*	*YNL134C*	*RAX1*
SLI15	*GLT1*	*PST1*	*TSA2*	*YND1*	*RTG2*	*SCW4*	*CCT8*	*NMA111*	*ALA1*
EHT1	*SFA1*	*CTH1*	*VPS52*	*TPA1*	*SAP4*	*MUP3*	*ILV3*	*AVT4*	*AMF1*
TAH11	*FAT3*	*YKR045C*	*YCT1*	*CLB4*	*TUB1*	*KAR5*	*SPT21*	*RAS2*	*USV1*
PXP2	*MDH1*	*OMA1*	*TPO1*	*ECM38*	*RAD52*	*UBX4*	*YMR187C*	*YNL058C*	*MMT2*
TDA4	*GPX1*	*PCK1*	*YEH2*	*CTF3*	*YOX1*	*ILV2*	*SGS1*	*EFM6*	*AFT2*
YJR149W	*CCE1*	*MHT1*	*IZH3*	*REH1*	*YAP1*	*DLT1*	*CLN1*	*GAS4*	*COX10*
DAN1	*GAP1*	*GTT2*	*HOG1*	*YML131W*	*HOF1*	*MMT1*	*GAS3*	*HRP1*	*PEP4*
RAD53	*GLR1*	*PDR12*	*ARL3*	*RDS3*	*FHL1*				

Table S.3: List of gene directly co-regulated by Hho1p occupancy at genes in quiescent cells, downregulated

Hho1p- Down Q (313 genes)										
BOL1	*CHS2*	*STE50*	*QRI7*	*KEI1*	*YVH1*	*IOC3*	*AGA2*	*RBG2*	*RTT107*	*SDS22*
GCV3	*ORC2*	*RNQ1*	*RPP1A*	*RPS17B*	*DAL7*	*BNA6*	*ATE1*	*OKP1*	*STB5*	*TPO5*
CLN3	*MIS1*	*PGK1*	*TSR1*	*RMT2*	*GTT1*	*RAI1*	*COG7*	*HGH1*	*CTF8*	*GPM1*
CDC19	*RPL19A*	*CTO1*	*MBP1*	*PUF6*	*NPR2*	*GUS1*	*EFM5*	*ELP2*	*PPX1*	*TGL1*
POP5	*RFC5*	*RIM1*	*PSA1*	*MET18*	*SDD1*	*KAP114*	*ERG25*	*CIR1*	*PHO90*	*RPS3*
MYO4	*EXO84*	*CTR86*	*BSC1*	*AYR1*	*POL5*	*TAN1*	*ADE6*	*GND2*	*RPL17B*	*TTI1*
MAK16	*ALG1*	*PWP2*	*GPM2*	*SHQ1*	*YEL023C*	*OST5*	*PEX8*	*EFG1*	*ERG20*	*URA6*
BUD14	*BMT2*	*RAD18*	*GCV1*	*LYS12*	*GEA2*	*CHC1*	*PDC6*	*DIA4*	*NUP192*	*HCS1*
PRS4	*CSH1*	*RSA4*	*TPI1*	*UTP25*	*WBP1*	*ARO8*	*SRB5*	*ARD1*	*VPS53*	*URB1*
PTH2	*ARL1*	*ABP1*	*TVP23*	*AIR1*	*TMA20*	*GCN1*	*COG2*	*MYO1*	*RPC17*	*ECM9*
NCL1	*PGI1*	*YCR090C*	*SWI5*	*RPS24B*	*SAH1*	*YGL159W*	*UTP8*	*RRM3*	*MRX12*	*BCH2*
GAL7	*MCX1*	*YBR238C*	*MSW1*	*BAR1*	*NSA2*	*NUT1*	*RPL24B*	*BCD1*	*CBF1*	*TRZ1*
POA1	*ROT2*	*CWC2*	*BFR2*	*YIL014C-A*	*RPS26B*	*PRP43*	*MTR3*	*RPP1*	*ACF4*	*SKG1*
OLA1	*MSH3*	*RBS1*	*CPR5*	*YIL001W*	*PEA2*	*VPS73*	*NSR1*	*SSZ1*	*BUD4*	*JLP1*
ETR1	*PHO89*	*NOP14*	*SRB7*	*SQT1*	*RPL22B*	*LSG1*	*PSD2*	*IPI1*	*RPS5*	*IRC19*
RKM3	*POF1*	*NUP84*	*PEP7*	*MRS1*	*SPB4*	*MAD1*	*MSM1*	*CDC12*	*PEX1*	*DPS1*
UTP13	*LIP2*	*YNL035C*	*UBC12*	*RPS29A*	*DUS3*	*IMD3*	*RPS1A*	*GTR1*	*SEC65*	*DRS1*
BNA5	*RPS28B*	*GSP1*	*RPP0*	*STE23*	*UTP21*	*SEC39*	*FPR4*	*URA5*	*MDM1*	*SDS22*
COG8	*PIF1*	*CGI121*	*TRM9*	*HXT2*	*SEC59*	*BUD22*	*CSI1*	*ERB1*	*CTF18*	*YKU80*
GCV2	*EFR3*	*RPS10B*	*YHM2*	*PPA2*	*ECM16*	*WRS1*	*RPS7A*	*PUS7*	*YOR338W*	*PPT2*
ABZ2	*TOF1*	*IPI3*	*RPL16B*	*PHO91*	*BIO4*	*MDM20*	*GCY1*	*PAC1*	*RPA43*	*GDE1*
HER2	*POL2*	*YKL050C*	*GCD10*	*ATP23*	*YNR066C*	*ERP4*	*SPP2*	*YTM1*	*RPS12*	*GPI2*
ADH2	*GIS2*	*RPL42A*	*LAP2*	*CPR8*	*ENB1*	*DBP5*	*MTR10*	*FSH3*	*YPL257W*	*TIM50*
PSE1	*TEX1*	*FPR1*	*COG6*	*ALG12*	*NOP8*	*ATX2*	*SYC1*	*RRP36*	*NEW1*	*SVL3*
PHA2	*YTP1*	*KRE33*	*NNT1*	*DBP6*	*RPL25*	*CMR2*	*NPT1*	*SNU66*	*RTT10*	*REC8*
LMO1	*NOC3*	*LOT6*	*SDO1*	*ERG3*	*SHM2*	*RPL22A*	*SPC3*	*EMP70*	*SMC4*	*IOC2*
ERG24	*POP1*	*RPS7B*	*IDP3*	*ZRG17*	*RPL18A*	*RKI1*	*RPL33B*	*RPL20B*	*SPT14*	*SUT2*
ACF2	*NCA2*	*MMS1*	*SEC10*	*EMG1*	*PWP1*	*RPA135*	*YOP1*	*MRI1*		
TIS11	*NOC4*	*THI22*	*CBF5*	*NMT1*	*ADE17*	*YPR015C*	*HOS1*			

Table S.4: List of gene directly co-regulated by Hmo1p occupancy in exponential phase cells, upregulated (Up) and downregulated (Down)

Hmo1p -up Expo (32 genes)		
TEC1	*RPS24A*	*MSN4*
YBR085C-A	*RPL9A*	*RPL40B*
TPS1	*TOS8*	*RPL8B*
COS111	*STF2*	*YLR257W*
RPL35A	*RPL26B*	*RPS1A*
RPL35B	*CTT1*	*TSL1*
NRG1	*RIM4*	*YNL144C*
SNF11	*YJL107C*	*HPF1*
TPS2	*YJR115W*	*TPO4*
RPS17B	*HAP4*	*PUT4*
USV1	*ULA1*	

Hmo1p -down Expo (21 genes)	
HIS4	*CIS3*
PGK1	*TDH2*
LYS20	*GPM1*
PDR15	*TOS4*
TIR1	*TUB4*
VTC1	*RPS22B*
FTR1	*RPL31B*
RPL8A	*YGP1*
WSC4	*AQR1*
SPL2	*FIT2*
RPL7B	

Table S.5: List of gene directly co-regulated by Hmo1p occupancy in diauxic shift, upregulated (Up)

Hmo1p-up-DX (78 genes)							
ATP1	*RPL31A*	*RPL34A*	*NSR1*	*SOD1*	*TOS4*	*RPL16B*	*RPL33B*
RPL32	*KGD2*	*RPS24A*	*RPS0A*	*ATP2*	*ACO1*	*POR1*	*RPS10A*
COR1	*RPL27B*	*RPS8B*	*GUT1*	*RPS5*	*NDI1*	*CIT1*	*RPL20B*
RPL19B	*RPL40A*	*RPL23B*	*RPL27A*	*RPS4A*	*RPL6A*	*RPL25*	*GAL4*
ACH1	*OM45*	*FTR1*	*RPS27B*	*JEN1*	*RPS1B*	*IRA2*	*RPL33A*
BAP2	*RPL16A*	*ACT1*	*HXT5*	*RPL17A*	*RPS18B*	*RPP2A*	*RPS6A*
RPL19A	*KGD1*	*HAC1*	*RPL42B*	*HOT13*	*RPS17A*	*CYT1*	*HST2*
RPS6B	*RPL34B*	*PUS2*	*RPS4B*	*RPL14A*	*AAC1*	*LPX1*	*SPO24*
HSP30	*RPL2B*	*RPL30*	*RPL17B*	*RPS0B*	*RPS19B*	*RPS7A*	
RPS16B	*GTT3*	*RPL24B*	*RPS21B*	*CCW12*	*RPL42A*	*LSC1*	

Table S.6: List of gene directly co-regulated by Hmo1p occupancy in diauxic shift, downregulated (Down)

Hmo1p-down-DX (14 genes)	
CHA1	*YLR177W*
TPS2	*YNR014W*
HPM1	*MDH2*
DLD3	*PNS1*
SSA4	*PTR2*
AIM17	*HOG1*
PTK2	*UGP1*

Table S.7: List of gene directly co-regulated by Hmo1p occupancy in quiescent cells, upregulated (Up)

Hmo1p-up-Q (100 genes)						
ACS1	*DLD1*	*PIG2*	*YOR1*	*TRK2*	*YNL193W*	*SSO1*
RPL32	*YDL124W*	*FAA3*	*YHL008C*	*CCP1*	*YNL144C*	*USV1*
HEK2	*NDE2*	*GLC3*	*LAM4*	*IRC20*	*YNL134C*	*FMP40*
RPL19B	*MRK1*	*GPA2*	*HXT5*	*PDR8*	*MET4*	*HHO1*
HHF1	*RTK1*	*GIP2*	*CPS1*	*VID22*	*EOS1*	*PDR12*
YBR016W	*FMP16*	*DOT6*	*YAK1*	*RSC9*	*FRE4*	*ULA1*
REB1	*SND1*	*SLX8*	*MDV1*	*CYB2*	*RPL25*	*CCL1*
SLM4	*UME6*	*BCK2*	*MEF2*	*RPS17A*	*RRT8*	*YPR127W*
RAD16	*MSN5*	*IGD1*	*MHP1*	*AAC1*	*YOR019W*	*NCE102*
IRA1	*YRA1*	*ATG1*	*SOD1*	*ALD3*	*CRC1*	*SUE1*
TBS1	*PHO8*	*NQM1*	*RPS5*	*FAA4*	*RGS2*	
OM14	*ITR1*	*PIL1*	*RPS4A*	*GTO3*	*DCI1*	
PHO89	*PSP1*	*MEP1*	*BAT2*	*YMR253C*	*PDR10*	
ADY2	*GUT2*	*RPL24B*	*MTR2*	*YME2*	*DIP5*	
CPR4	*RPL40A*	*YGR201C*	*GAP1*	*ZWF1*	*VMA11*	

Table S.8: List of gene directly co-regulated by Hmo1p occupancy in quiescent cells, downregulated (Down)

Hmo1p-down-Q (96 genes)					
FUI1	*RPL13A*	*PEA2*	*CYC1*	*TOS4*	*GPD2*
ACH1	*RPL31A*	*RPL29*	*RPL43B*	*EXG1*	*RPP2A*
RPS11B	*KNH1*	*HXK1*	*RSF2*	*RPL26A*	*HMS1*
RFS1	*STP4*	*TOS3*	*HAP4*	*RPS29A*	*SLD7*
NRG2	*BAP3*	*YGR050C*	*MDH1*	*RPL31B*	*RKI1*
TIP1	*AFR1*	*BTN2*	*MSN4*	*DIF1*	*BAG7*
TEC1	*HSP42*	*RPS0A*	*RPL14A*	*NDE1*	*RPS30B*
MIS1	*HXT7*	*MGA1*	*SRP40*	*YMR244W*	*YOR186W*
RPL19A	*TRR1*	*ENO1*	*PCK1*	*FET4*	*STE4*
TEF2	*RPL37B*	*TIM10*	*TPO1*	*RPS3*	*RPL20B*
RPS6B	*GRH1*	*SRB2*	*RPS0B*	*DCP2*	*TYE7*
THI2	*POR2*	*MPC2*	*GAL2*	*PBI2*	*SAM3*
GGC1	*MIG3*	*RPS4B*	*CCW12*	*ATO2*	*RPL36B*
RPL35A	*SPO73*	*HSP150*	*SLS1*	*YNR014W*	*CUP9*
RPP1B	*ALD5*	*ASF1*	*YLR179C*	*TRM13*	*RPL5*
PMA2	*YPR015C*	*SPO24*	*YPR063C*	*NAT3*	*AQY1*

References

Albert, B., Colleran, C., Leger-Silvestre, I., Berger, A.B., Dez, C., Normand, C., *et al.* (2013) Structure-function analysis of Hmo1P unveils an ancestral organization of HMG-Box factors involved in ribosomal DNA transcription from yeast to human. *Nucleic acids research* **41**: 10135–10149.

Alexander, B.D., and Perfect, J.R. (1997) Antifungal Resistance Trends Towards the Year 2000. *Drugs* **54**: 657–678.

Alfatah, M., Wong, J.H., Krishnan, V.G., Lee, Y.C., Sin, Q.F., Goh, C.J.H., *et al.* (2021) TORC1 regulates the transcriptional response to glucose and developmental cycle via the Tap42-Sit4-Rrd1/2 pathway in Saccharomyces cerevisiae. *BMC biology* **19**: 95.

Allan, J., Hartman, P., Crane-Robinson, C., and Aviles, F. (1980) The structure of histone H1 and its location in chromatin. *Nature* **288**: 675–679.

Allard, S., Utley, R.T., Savard, J., Clarke, A., Grant, P., Brandl, C.J., *et al.* (1999) NuA4, an essential transcription adaptor/histone H4 acetyltransferase complex containing Esa1p and the ATM-related cofactor Tra1p. *The EMBO journal* **18**: 5108–5119.

Allen, B.L., and Taatjes, D.J. (2015) The Mediator complex: a central integrator of transcription. *Nature reviews Molecular cell biology* **16**: 155–166.

Allen, C., Büttner, S., Aragon, A.D., Thomas, J.A., Meirelles, O., Jaetao, J.E., *et al.* (2006) Isolation of quiescent and nonquiescent cells from yeast stationary-phase cultures. *The Journal of cell biology* **174**: 89–100.

Amigo, R., Farkas, C., Gidi, C., Hepp, M.I., Cartes, N., Tarifeño, E., *et al.* (2022) The linker histone Hho1p modulates the activity of ATP-dependent chromatin remodeling complexes. *Biochimica et Biophysica Acta (BBA)-Gene Regulatory Mechanisms* **1865**: 194781.

An, W., Holde, K. van, and Zlatanova, J. (1998a) The non-histone chromatin protein HMG1 protects linker DNA on the side opposite to that protected by linker histones. *Journal of Biological Chemistry* **273**: 26289–26291.

An, W., Holde, K. van, and Zlatanova, J. (1998b) The Non-histone Chromatin Protein HMG1 Protects Linker DNA on the Side Opposite to That Protected by Linker Histones *. *Journal of Biological Chemistry* **273**: 26289–26291.

Andrews, A.J., and Luger, K. (2011) Nucleosome structure (s) and stability: variations on a theme. *Annual review of biophysics* **40**: 99–117.

Apweiler, E., Sameith, K., Margaritis, T., Brabers, N., Pasch, L. van de, Bakker, L.V., *et al.* (2012) Yeast glucose pathways converge on the transcriptional regulation of trehalose biosynthesis. *BMC genomics* **13**: 1–14.

Aragon, A.D., Rodriguez, A.L., Meirelles, O., Roy, S., Davidson, G.S., Tapia, P.H., *et al.* (2008) Characterization of differentiated quiescent and nonquiescent cells in yeast stationary-phase cultures. *Molecular biology of the cell* **19**: 1271–1280.

Austin, S., and Mayer, A. (2020) Phosphate homeostasis− a vital metabolic equilibrium maintained through the INPHORS signaling pathway. *Frontiers in Microbiology* **11**: 539723.

Bailey, T.B., Whitty, P.A., Selker, E.U., McKnight, J.N., and McKnight, L.E. (2022) Tup1 is critical for transcriptional repression in Quiescence in S. cerevisiae. *PLoS Genetics* **18**: e1010559.

Baker Brachmann, C., Davies, A., Cost, G.J., Caputo, E., Li, J., Hieter, P., and Boeke, J.D. (1998) Designer deletion strains derived from Saccharomyces cerevisiae S288C: a useful set of strains and plasmids for PCR-mediated gene disruption and other applications. *Yeast* **14**: 115–132.

Baker, M. (2011) Making sense of chromatin states. *Nat Methods* **8**: 717–722.

Bauerle, K.T., Kamau, E., and Grove, A. (2006) Interactions between N- and C-Terminal Domains of the Saccharomyces cerevisiae High-Mobility Group Protein *HMO1* Are Required for DNA Bending. *Biochemistry* **45**: 3635–3645.

Baxevanis, A.D., and Landsman, D. (1998) Histone Sequence Database: new histone fold family members. *Nucleic acids research* **26**: 372–375.

Becker, P.B., and Hörz, W. (2002) ATP-dependent nucleosome remodeling. *Annual review of biochemistry* **71**: 247–273.

Bednar, J., Hamiche, A., and Dimitrov, S. (2016a) H1–nucleosome interactions and their functional implications. *Biochimica et Biophysica Acta (BBA)-Gene Regulatory Mechanisms* **1859**: 436–443.

Bednar, J., Hamiche, A., and Dimitrov, S. (2016b) H1–nucleosome interactions and their functional implications. *Biochimica et Biophysica Acta (BBA) - Gene Regulatory Mechanisms* **1859**: 436–443.

Bendandi, A., Dante, S., Zia, S.R., Diaspro, A., and Rocchia, W. (2020) Chromatin compaction multiscale modeling: a complex synergy between theory, simulation, and experiment. *Frontiers in Molecular Biosciences* **7**: 15.

Bermejo, R., Capra, T., Gonzalez-Huici, V., Fachinetti, D., Cocito, A., Natoli, G., *et al.* (2009) Genome-organizing factors Top2 and Hmo1P prevent chromosome fragility at sites of S phase transcription. *Cell* **138**: 870–884.

Boles, E., and Hollenberg, C.P. (1997) The molecular genetics of hexose transport in yeasts. *FEMS microbiology reviews* **21**: 85–111.

Brush, G.S. (2015) Evidence that histone H1 is dispensable for proper meiotic recombination in budding yeast. *BMC research notes* **8**: 1–6.

Bryant, J.M., Govin, J., Zhang, L., Donahue, G., Pugh, B.F., and Berger, S.L. (2012a) The linker histone plays a dual role during gametogenesis in Saccharomyces cerevisiae. *Molecular and cellular biology* **32**: 2771–2783.

Bryant, J.M., Govin, J., Zhang, L., Donahue, G., Pugh, B.F., and Berger, S.L. (2012b) The linker histone plays a dual role during gametogenesis in Saccharomyces cerevisiae. *Molecular and cellular biology* **32**: 2771–2783.

Chen, B.-C., and Lin, H.-Y. (2022) Deletion of NTH1 and HSP12 increases the freeze–thaw resistance of baker's yeast in bread dough. *Microbial Cell Factories* **21**: 149.

Chen, T., Zhang, Z., Li, B., Qin, G., and Tian, S. (2021) Molecular basis for optimizing sugar metabolism and transport during fruit development. *Abiotech* 1–11.

Choder, M. (1991) A general topoisomerase I-dependent transcriptional repression in the stationary phase in yeast. *Genes & development* **5**: 2315–2326.

Christianson, T.W., Sikorski, R.S., Dante, M., Shero, J.H., and Hieter, P. (1992) Multifunctional yeast high-copy-number shuttle vectors. *Gene* **110**: 119–122.

Clapier, C.R., Iwasa, J., Cairns, B.R., and Peterson, C.L. (2017) Mechanisms of action and regulation of ATP-dependent chromatin-remodelling complexes. *Nature reviews Molecular cell biology* **18**: 407–422.

Collart, M.A., and Oliviero, S. (1993) Preparation of yeast RNA. *Current protocols in molecular biology* **23**: 13–12.

Conesa, A., Madrigal, P., Tarazona, S., Gomez-Cabrero, D., Cervera, A., McPherson, A., *et al.* (2016) A survey of best practices for RNA-seq data analysis. *Genome biology* **17**: 1–19.

Cui, G., Dong, Q., Gai, K., and Qi, S. (2022) Chromatin dynamics: Chromatin remodeler, epigenetic modification and diseases. *Epigenetics-Regulation and New Perspectives* .

Dang, W., Steffen, K.K., Perry, R., Dorsey, J.A., Johnson, F.B., Shilatifard, A., *et al.* (2009) Histone H4 lysine 16 acetylation regulates cellular lifespan. *Nature* **459**: 802–807.

Davidson, G.S., Joe, R.M., Roy, S., Meirelles, O., Allen, C.P., Wilson, M.R., *et al.* (2011a) The proteomics of quiescent and nonquiescent cell differentiation in yeast stationary-phase cultures. *Molecular biology of the cell* **22**: 988–998.

Davidson, G.S., Joe, R.M., Roy, S., Meirelles, O., Allen, C.P., Wilson, M.R., *et al.* (2011b) The proteomics of quiescent and nonquiescent cell differentiation in yeast stationary-phase cultures. *Molecular biology of the cell* **22**: 988–998.

Debasree, D., Khaja, M.S., and Ananda, M. (2018) Histone Chaperones Regulate Mammalian Gene Expression. *Gene Expression and Regulation in Mammalian Cells* .

Dever, T.E., Kinzy, T.G., and Pavitt, G.D. (2016) Mechanism and regulation of protein synthesis in Saccharomyces cerevisiae. *Genetics* **203**: 65–107.

Dolinski, K.J., and Heitman, J. (1999) Hmo1p, a high mobility group 1/2 homolog, genetically and physically interacts with the yeast FKBP12 prolyl isomerase. *Genetics* **151**: 935–944.

Dong, L., and Xu, C.W. (2004) Carbohydrates induce mono-ubiquitination of H2B in yeast. *Journal of Biological Chemistry* **279**: 1577–1580.

Downs, J.A., Lowndes, N.F., and Jackson, S.P. (2000) A role for Saccharomyces cerevisiae histone H2A in DNA repair. *Nature* **408**: 1001–1004.

Flanagan, T.W., and Brown, D.T. (2016) Molecular dynamics of histone H1. *Biochimica et Biophysica Acta (BBA) - Gene Regulatory Mechanisms* **1859**: 468–475.

Fleming, A.B., Kao, C.-F., Hillyer, C., Pikaart, M., and Osley, M.A. (2008a) H2B ubiquitylation plays a role in nucleosome dynamics during transcription elongation. *Molecular cell* **31**: 57–66.

Fleming, A.B., Kao, C.-F., Hillyer, C., Pikaart, M., and Osley, M.A. (2008b) H2B ubiquitylation plays a role in nucleosome dynamics during transcription elongation. *Molecular cell* **31**: 57–66.

Fuchs, S.M., Laribee, R.N., and Strahl, B.D. (2009) Protein modifications in transcription elongation. *Biochimica et Biophysica Acta (BBA)-Gene Regulatory Mechanisms* **1789**: 26–36.

Fuge, E.K., Braun, E.L., and Werner-Washburne, M. (1994) Protein synthesis in long-term stationary-phase cultures of Saccharomyces cerevisiae. *Journal of bacteriology* **176**: 5802–5813.

Gadal, O., Labarre, S., Boschiero, C., and Thuriaux, P. (2002) Hmo1p, an HMG-box protein, belongs to the yeast ribosomal DNA transcription system. *The EMBO journal* **21**: 5498–5507.

Galdieri, L., Mehrotra, S., Yu, S., and Vancura, A. (2010) Transcriptional regulation in yeast during diauxic shift and stationary phase. *Omics: a journal of integrative biology* **14**: 629–638.

Galili, T., O'Callaghan, A., Sidi, J., and Sievert, C. (2018) heatmaply: an R package for creating interactive cluster heatmaps for online publishing. *Bioinformatics* **34**: 1600–1602.

Gallagher, S., Winston, S.E., Fuller, S.A., and Hurrell, J.G. (2011) Immunoblotting and immunodetection. *Current protocols in cell biology* **52**: 6–2.

Garay, E., Campos, S.E., Gonzalez de la Cruz, J., Gaspar, A.P., Jinich, A., and DeLuna, A. (2014) High-resolution profiling of stationary-phase survival reveals yeast longevity factors and their genetic interactions. *PLoS genetics* **10**: e1004168.

Gasmi, N., Jacques, P.-E., Klimova, N., Guo, X., Ricciardi, A., Robert, F., and Turcotte, B. (2014) The switch from fermentation to respiration in Saccharomyces cerevisiae is regulated by the Ert1 transcriptional activator/repressor. *Genetics* **198**: 547–560.

Geistlinger, L., Csaba, G., Dirmeier, S., Küffner, R., and Zimmer, R. (2013) A comprehensive gene regulatory network for the diauxic shift in Saccharomyces cerevisiae. *Nucleic acids research* **41**: 8452–8463.

George, C.L., and Conway-Campbell, B.L. (2016) Dynamic Regulation of Chromatin Modification and Transcription by GR and the Steroid Receptors. *Epigenetics and Neuroendocrinology: Clinical Focus on Psychiatry, Volume 1* 49–71.

Georgieva, M., Roguev, A., Balashev, K., Zlatanova, J., and Miloshev, G. (2012) Hho1p, the linker histone of Saccharomyces cerevisiae, is important for the proper chromatin organization in vivo. *Biochimica Et Biophysica Acta (BBA)-Gene Regulatory Mechanisms* **1819**: 366–374.

Ghaemmaghami, S., Huh, W.-K., Bower, K., Howson, R.W., Belle, A., Dephoure, N., *et al.* (2003) Global analysis of protein expression in yeast. *Nature* **425**: 737–741.

Gietz, R.D., and Schiestl, R.H. (2007) High-efficiency yeast transformation using the LiAc/SS carrier DNA/PEG method. *Nature protocols* **2**: 31–34.

Giménez-Barcons, M., and Díez, J. (2011) Yeast processing bodies and stress granules: self-assembly ribonucleoprotein particles. *Microbial cell factories* **10**: 1–3.

Grant, P.A., Duggan, L., Côté, J., Roberts, S.M., Brownell, J.E., Candau, R., *et al.* (1997) Yeast Gcn5 functions in two multisubunit complexes to acetylate nucleosomal histones: characterization of an Ada complex and the SAGA (Spt/Ada) complex. *Genes & development* **11**: 1640–1650.

Gray, J.V., Petsko, G.A., Johnston, G.C., Ringe, D., Singer, R.A., and Werner-Washburne, M. (2004) "Sleeping beauty": quiescence in Saccharomyces cerevisiae. *Microbiology and molecular biology reviews* **68**: 187–206.

Greenlaw, A.C., Alavattam, K.G., and Tsukiyama, T. (2024) Post-transcriptional regulation shapes the transcriptome of quiescent budding yeast. *Nucleic Acids Research* **52**: 1043–1063.

Haar, T. von der (2008) A quantitative estimation of the global translational activity in logarithmically growing yeast cells. *BMC systems biology* **2**: 1–14.

Han, M.-H., Park, J., and Park, M. (2024) Advances in the multimodal analysis of the 3D chromatin structure and gene regulation. *Experimental & Molecular Medicine* 1–9.

Harmonizing model organism data in the Alliance of Genome Resources (2022) *Genetics* **220**: iyac022.

Henry, K.W., Wyce, A., Lo, W.-S., Duggan, L.J., Emre, N.T., Kao, C.-F., *et al.* (2003) Transcriptional activation via sequential histone H2B ubiquitylation and deubiquitylation, mediated by SAGA-associated Ubp8. *Genes & development* **17**: 2648–2663.

Herman, P.K. (2002a) Stationary phase in yeast. *Current opinion in microbiology* **5**: 602–607.

Herman, P.K. (2002b) Stationary phase in yeast. *Current opinion in microbiology* **5**: 602–607.

Hsu, J.-Y., Sun, Z.-W., Li, X., Reuben, M., Tatchell, K., Bishop, D.K., *et al.* (2000) Mitotic phosphorylation of histone H3 is governed by Ipl1/aurora kinase and Glc7/PP1 phosphatase in budding yeast and nematodes. *Cell* **102**: 279–291.

Hu, G., Grover, C.E., Vera, D.L., Lung, P.-Y., Girimurugan, S.B., Miller, E.R., *et al.* (2024) Evolutionary dynamics of chromatin structure and duplicate gene expression in diploid and allopolyploid cotton. *Molecular Biology and Evolution* msae095.

Janke, C., Magiera, M.M., Rathfelder, N., Taxis, C., Reber, S., Maekawa, H., *et al.* (2004) A versatile toolbox for PCR-based tagging of yeast genes: new fluorescent proteins, more markers and promoter substitution cassettes. *Yeast* **21**: 947–962.

Jazwinski, S., and Kim, S. (2019) Examination of the dimensions of biological age. Front Genet. 2019; 10: 263. .

Jenuwein, T., and Allis, C.D. (2001) Translating the histone code. *Science* **293**: 1074–1080.

Jezek, M., Jacques, A., Jaiswal, D., and Green, E.M. (2017) Chromatin immunoprecipitation (ChIP) of histone modifications from Saccharomyces cerevisiae. *JoVE (Journal of Visualized Experiments)* e57080.

Johnston, M. (1987) A model fungal gene regulatory mechanism: the GAL genes of Saccharomyces cerevisiae. *Microbiological reviews* **51**: 458–476.

Juven-Gershon, T., and Kadonaga, J.T. (2010) Regulation of gene expression via the core promoter and the basal transcriptional machinery. *Developmental biology* **339**: 225–229.

Kamau, E., Bauerle, K.T., and Grove, A. (2004) The Saccharomyces cerevisiae high mobility group box protein *HMO1* contains two functional DNA binding domains. *Journal of Biological Chemistry* **279**: 55234–55240.

Karmodiya, K., Krebs, A.R., Oulad-Abdelghani, M., Kimura, H., and Tora, L. (2012) H3K9 and H3K14 acetylation co-occur at many gene regulatory elements, while H3K14ac marks a subset of inactive inducible promoters in mouse embryonic stem cells. *BMC genomics* **13**: 1–18.

KASINSKY, H.E., LEWIS, J.D., DACKS, J.B., and AUSLÓ, J. (2001) Origin of H1 linker histones. *The FASEB journal* **15**: 34–42.

Keogh, M.-C., Mennella, T.A., Sawa, C., Berthelet, S., Krogan, N.J., Wolek, A., *et al.* (2006) The Saccharomyces cerevisiae histone H2A variant Htz1 is acetylated by NuA4. *Genes & development* **20**: 660.

Kobor, M.S., Venkatasubrahmanyam, S., Meneghini, M.D., Gin, J.W., Jennings, J.L., Link, A.J., *et al.* (2004) A protein complex containing the conserved Swi2/Snf2-related ATPase Swr1p deposits histone variant H2A. Z into euchromatin. *PLoS biology* **2**: e131.

Koç, A., Wheeler, L.J., Mathews, C.K., and Merrill, G.F. (2004) Hydroxyurea Arrests DNA Replication by a Mechanism That Preserves Basal dNTP Pools. *Journal of Biological Chemistry* **279**: 223–230.

Kouzarides, T. (2007) Chromatin modifications and their function. *Cell* **128**: 693–705.

Kulak, N.A., Pichler, G., Paron, I., Nagaraj, N., and Mann, M. (2014) Minimal, encapsulated proteomic-sample processing applied to copy-number estimation in eukaryotic cells. *Nature Methods* **11**: 319–324.

Kulakovskaya, T.V., Andreeva, N.A., Ledova, L.A., Ryazanova, L.P., Trilisenko, L.V., and Eldarov, M.A. (2021) Enzymes of polyphosphate metabolism in yeast: Properties, functions, practical significance. *Biochemistry (Moscow)* **86**: S96–S108.

Kuo, M.-H., Brownell, J.E., Sobel, R.E., Ranalli, T.A., Cook, R.G., Edmondson, D.G., *et al.* (1996) Transcription-linked acetylation by Gcn5p of histones H3 and H4 at specific lysines. *Nature* **383**: 269–272.

Kuranda, K., Leberre, V., Sokol, S., Palamarczyk, G., and François, J. (2006) Investigating the caffeine effects in the yeast *Saccharomyces cerevisiae* brings new insights into the connection between TOR, PKC and Ras/cAMP signalling pathways. *Molecular Microbiology* **61**: 1147–1166.

Lam, U.T.F., Tan, B.K.Y., Poh, J.J.X., and Chen, E.S. (2022) Structural and functional specificity of H3K36 methylation. *Epigenetics & Chromatin* **15**: 17.

Landsman, D. (1996) Histone H1 in Saccharomyces cerevisiae: a double mystery solved? *Trends in biochemical sciences* **21**: 287–288.

Lee, K.-B., and Thomas, J.O. (2000) The effect of the acidic tail on the DNA-binding properties of the HMG1,2 class of proteins: insights from tail switching and tail removal11Edited by T. Richmond. *Journal of Molecular Biology* **304**: 135–149.

Lefrançois, P., Gallagher, J.E., and Snyder, M. (2014) Global analysis of transcription factor-binding sites in yeast using ChIP-Seq. *Yeast Genetics: Methods and Protocols* 231–255.

Lever, M.A., Th'ng, J.P.H., Sun, X., and Hendzel, M.J. (2000) Rapid exchange of histone H1.1 on chromatin in living human cells. *Nature* **408**: 873–876.

Levin, D.E. (2005) Cell Wall Integrity Signaling in *Saccharomyces cerevisiae*. *Microbiol Mol Biol Rev* **69**: 262–291.

Levy, A., Eyal, M., Hershkovits, G., Salmon-Divon, M., Klutstein, M., and Katcoff, D.J. (2008) Yeast linker histone Hho1p is required for efficient RNA polymerase I processivity and transcriptional silencing at the ribosomal DNA. *Proceedings of the National Academy of Sciences* **105**: 11703–11708.

Li, B., Carey, M., and Workman, J.L. (2007) The role of chromatin during transcription. *Cell* **128**: 707–719.

Li, Q., Zhou, H., Wurtele, H., Davies, B., Horazdovsky, B., Verreault, A., and Zhang, Z. (2008a) Acetylation of histone H3 lysine 56 regulates replication-coupled nucleosome assembly. *Cell* **134**: 244–255.

Li, Q., Zhou, H., Wurtele, H., Davies, B., Horazdovsky, B., Verreault, A., and Zhang, Z. (2008b) Acetylation of histone H3 lysine 56 regulates replication-coupled nucleosome assembly. *Cell* **134**: 244–255.

Li, Q., Zhou, L., Li, Y., Zhang, D., and Gao, Y. (2021) Plant NIGT1/HRS1/HHO transcription factors: key regulators with multiple roles in plant growth, development, and stress responses. *International Journal of Molecular Sciences* **22**: 8685.

Liu, C.L., Kaplan, T., Kim, M., Buratowski, S., Schreiber, S.L., Friedman, N., and Rando, O.J. (2005) Single-nucleosome mapping of histone modifications in S. cerevisiae. *PLoS biology* **3**: e328.

Liu, R., Wu, J., Guo, H., Yao, W., Li, S., Lu, Y., *et al.* (2023) Post-translational modifications of histones: Mechanisms, biological functions, and therapeutic targets. *MedComm* **4**: e292.

Livas, D., Almering, M.J., Daran, J.-M., Pronk, J.T., and Gancedo, J.M. (2011) Transcriptional responses to glucose in Saccharomyces cerevisiae strains lacking a functional protein kinase A. *BMC genomics* **12**: 1–12.

Lo, W., Duggan, L., Tolga, N., and Emre, B. R., Lane, WS, Shiekhattar, R. and Berger, SL (2001) Snf1—a histone kinase that works in concert with the histone acetyltransferase Gcn5 to regulate transcription. *Science* **293**: 1142–1146.

Longtine, M.S., Mckenzie III, A., Demarini, D.J., Shah, N.G., Wach, A., Brachat, A., *et al.* (1998) Additional modules for versatile and economical PCR-based gene deletion and modification in Saccharomyces cerevisiae. *Yeast* **14**: 953–961.

Lu, J., Kobayashi, R., and Brill, S.J. (1996) Characterization of a high mobility group 1/2 homolog in yeast. *Journal of Biological Chemistry* **271**: 33678–33685.

Luger, K., Mäder, A.W., Richmond, R.K., Sargent, D.F., and Richmond, T.J. (1997) Crystal structure of the nucleosome core particle at 2.8 Å resolution. *Nature* **389**: 251–260.

Lundin, C., North, M., Erixon, K., Walters, K., Jenssen, D., Goldman, A.S.H., and Helleday, T. (2005) Methyl methanesulfonate (MMS) produces heat-labile DNA damage but no detectable in vivo DNA double-strand breaks. *Nucleic Acids Research* **33**: 3799–3811.

Ma, M., and Liu, Z.L. (2010) Comparative transcriptome profiling analyses during the lag phase uncover YAP1, PDR1, PDR3, RPN4, and HSF1 as key regulatory genes in genomic adaptation to the lignocellulose derived inhibitor HMF for Saccharomyces cerevisiae. *BMC genomics* **11**: 1–19.

Magalhães, R.S., Popova, B., Braus, G.H., Outeiro, T.F., and Eleutherio, E.C. (2018) The trehalose protective mechanism during thermal stress in Saccharomyces cerevisiae: the roles of Ath1 and Agt1. *FEMS yeast research* **18**: foy066.

McKnight, J.N., Boerma, J.W., Breeden, L.L., and Tsukiyama, T. (2015) Global Promoter Targeting of a Conserved Lysine Deacetylase for Transcriptional Shutoff during Quiescence Entry. *Molecular Cell* **59**: 732–743.

Mell, J.C., and Burgess, S.M. (2001) Yeast as a model genetic organism. *e LS* .

Meluh, P.B., Yang, P., Glowczewski, L., Koshland, D., and Smith, M.M. (1998) Cse4p is a component of the core centromere of Saccharomyces cerevisiae. *Cell* **94**: 607–613.

Miles, S., Li, L., Davison, J., and Breeden, L.L. (2013) Xbp1 directs global repression of budding yeast transcription during the transition to quiescence and is important for the longevity and reversibility of the quiescent state. *PLoS genetics* **9**: e1003854.

Millán-Ariño, L., Izquierdo-Bouldstridge, A., and Jordan, A. (2016) Specificities and genomic distribution of somatic mammalian histone H1 subtypes. *Biochimica et Biophysica Acta (BBA) - Gene Regulatory Mechanisms* **1859**: 510–519.

Millar, C.B., Xu, F., Zhang, K., and Grunstein, M. (2006) Acetylation of H2AZ Lys 14 is associated with genome-wide gene activity in yeast. *Genes & development* **20**: 711–722.

Miloshev, G., Staneva, D., Uzunova, K., Vasileva, B., Draganova-Filipova, M., Zagorchev, P., and Georgieva, M. (2019) Linker histones and chromatin remodelling complexes maintain genome stability and control cellular ageing. *Mechanisms of Ageing and Development* **177**: 55–65.

Misteli, T., Gunjan, A., Hock, R., Bustin, M., and Brown, D.T. (2000) Dynamic binding of histone H1 to chromatin in living cells. *Nature* **408**: 877–881.

Mohrmann, L., and Verrijzer, C.P. (2005) Composition and functional specificity of SWI2/SNF2 class chromatin remodeling complexes. *Biochimica et Biophysica Acta (BBA)-Gene Structure and Expression* **1681**: 59–73.

Moore, J.D., Yazgan, O., Ataian, Y., and Krebs, J.E. (2007) Diverse roles for histone H2A modifications in DNA damage response pathways in yeast. *Genetics* **176**: 15–25.

Nagy, Z., and Tora, L. (2007) Distinct GCN5/PCAF-containing complexes function as co-activators and are involved in transcription factor and global histone acetylation. *Oncogene* **26**: 5341–5357.

Nakanishi, S., Lee, J.S., Gardner, K.E., Gardner, J.M., Takahashi, Y., Chandrasekharan, M.B., *et al.* (2009) Histone H2BK123 monoubiquitination is the critical determinant for H3K4 and H3K79 trimethylation by COMPASS and Dot1. *Journal of Cell Biology* **186**: 371–377.

Nalabothula, N., McVicker, G., Maiorano, J., Martin, R., Pritchard, J.K., and Fondufe-Mittendorf, Y.N. (2014) The chromatin architectural proteins HMGD1 and H1 bind reciprocally and have opposite effects on chromatin structure and gene regulation. *BMC Genomics* **15**: 92.

Nathan, D., Ingvarsdottir, K., Sterner, D.E., Bylebyl, G.R., Dokmanovic, M., Dorsey, J.A., *et al.* (2006) Histone sumoylation is a negative regulator in Saccharomyces cerevisiae and shows dynamic interplay with positive-acting histone modifications. *Genes & development* **20**: 966–976.

Nechaev, S., and Adelman, K. (2011) Pol II waiting in the starting gates: Regulating the transition from transcription initiation into productive elongation. *Biochimica et Biophysica Acta (BBA)-Gene Regulatory Mechanisms* **1809**: 34–45.

Nordin, A., Pagella, P., Zambanini, G., and Cantù, C. (2024) Exhaustive identification of genome-wide binding events of transcriptional regulators. *Nucleic Acids Research* **52**: e40–e40.

Olive, P.L., and Banánth, J.P. (1993) Induction and rejoining of radiation-induced DNA single-strand breaks:“tail moment” as a function of position in the cell cycle. *Mutation Research/DNA Repair* **294**: 275–283.

Olive, P.L., Banáth, J.P., and Durand, R.E. (1990) Heterogeneity in radiation-induced DNA damage and repair in tumor and normal cells measured using the" comet" assay. *Radiation research* **122**: 86–94.

Oliveira, A.P., and Sauer, U. (2012) The importance of post-translational modifications in regulating Saccharomyces cerevisiae metabolism. *FEMS yeast research* **12**: 104–117.

Orikasa, Y., Mikumo, D., and Ohwada, T. (2018) A 2-Deoxyglucose-resistant mutant of Saccharomyces cerevisiae shows enhanced maltose fermentative ability by the activation of MAL genes. *Foods* **7**: 52.

Panday, A., and Grove, A. (2016) The high mobility group protein *HMO1* functions as a linker histone in yeast. *Epigenetics & Chromatin* **9**: 1–12.

Panday, A., and Grove, A. (2017) Yeast *HMO1*: linker histone reinvented. *Microbiology and Molecular Biology Reviews* **81**: 10–1128.

Park, P.J. (2009) ChIP–seq: advantages and challenges of a maturing technology. *Nature reviews genetics* **10**: 669–680.

Parrish, N.M., Dick, J.D., and Bishai, W.R. (1998) Mechanisms of latency in Mycobacterium tuberculosis. *Trends in Microbiology* **6**: 107–112.

Patterton, H.G., Landel, C.C., Landsman, D., Peterson, C.L., and Simpson, R.T. (1998) The biochemical and phenotypic characterization of Hho1p, the putative linker histone H1 of Saccharomyces cerevisiae. *Journal of Biological Chemistry* **273**: 7268–7276.

Peppel, J. van de, Kemmeren, P., Bakel, H. van, Radonjic, M., Leenen, D. van, and Holstege, F.C. (2003) Monitoring global messenger RNA changes in externally controlled microarray experiments. *EMBO reports* **4**: 387–393.

Pi∼ non, R. (1978) Folded chromosomes in non-cycling yeast cells: evidence for a characteristic g 0 form. *Chromosoma* **67**: 263–274.

Pokholok, D.K., Harbison, C.T., Levine, S., Cole, M., Hannett, N.M., Lee, T.I., *et al.* (2005) Genome-wide map of nucleosome acetylation and methylation in yeast. *Cell* **122**: 517–527.

Rando, O.J. (2007) Global patterns of histone modifications. *Current opinion in genetics & development* **17**: 94–99.

Ray, S., and Grove, A. (2009a) The yeast high mobility group protein HMO2, a subunit of the chromatin-remodeling complex INO80, binds DNA ends. *Nucleic acids research* **37**: 6389–6399.

Ray, S., and Grove, A. (2009b) The yeast high mobility group protein HMO2, a subunit of the chromatin-remodeling complex INO80, binds DNA ends. *Nucleic Acids Res* **37**: 6389–6399.

Redon, C., Pilch, D., Rogakou, E., Sedelnikova, O., Newrock, K., and Bonner, W. (2002) Histone H2a variants H2AX and H2AZ. *Current opinion in genetics & development* **12**: 162–169.

Robert, F., Pokholok, D.K., Hannett, N.M., Rinaldi, N.J., Chandy, M., Rolfe, A., *et al.* (2004) Global position and recruitment of HATs and HDACs in the yeast genome. *Molecular cell* **16**: 199–209.

Roberts, C.W., and Orkin, S.H. (2004) The SWI/SNF complex—chromatin and cancer. *Nature Reviews Cancer* **4**: 133–142.

Robzyk, K., Recht, J., and Osley, M.A. (2000) Rad6-dependent ubiquitination of histone H2B in yeast. *Science* **287**: 501–504.

Rossi, M.J., Kuntala, P.K., Lai, W.K., Yamada, N., Badjatia, N., Mittal, C., *et al.* (2021) A high-resolution protein architecture of the budding yeast genome. *Nature* **592**: 309–314.

Schäfer, G., McEvoy, C.R., and Patterton, H.-G. (2008) The Saccharomyces cerevisiae linker histone Hho1p is essential for chromatin compaction in stationary phase and is displaced by transcription. *Proceedings of the National Academy of Sciences* **105**: 14838–14843.

Schlossarek, D., Luzarowski, M., Sokołowska, E.M., Thirumalaikumar, V.P., Dengler, L., Willmitzer, L., *et al.* (2022) Rewiring of the protein–protein–metabolite interactome during the diauxic shift in yeast. *Cellular and Molecular Life Sciences* **79**: 550.

Sekinger, E.A., Moqtaderi, Z., and Struhl, K. (2005) Intrinsic histone-DNA interactions and low nucleosome density are important for preferential accessibility of promoter regions in yeast. *Molecular cell* **18**: 735–748.

Separovich, R.J., and Wilkins, M.R. (2021) Ready, SET, Go: Post-translational regulation of the histone lysine methylation network in budding yeast. *Journal of Biological Chemistry* **297**.

Shah, K.H., Zhang, B., Ramachandran, V., and Herman, P.K. (2013) Processing body and stress granule assembly occur by independent and differentially regulated pathways in Saccharomyces cerevisiae. *Genetics* **193**: 109–123.

Shilatifard, A. (2006) Chromatin modifications by methylation and ubiquitination: implications in the regulation of gene expression. *Annu Rev Biochem* **75**: 243–269.

Sideri, T., Rallis, C., Bitton, D.A., Lages, B.M., Suo, F., Rodríguez-López, M., *et al.* (2015) Parallel profiling of fission yeast deletion mutants for proliferation and for lifespan during long-term quiescence. *G3: Genes, Genomes, Genetics* **5**: 145–155.

Sivolob, A., and Prunell, A. (2003a) Linker histone-dependent organization and dynamics of nucleosome entry/exit DNAs. *Journal of molecular biology* **331**: 1025–1040.

Sivolob, A., and Prunell, A. (2003b) Linker Histone-dependent Organization and Dynamics of Nucleosome Entry/Exit DNAs. *Journal of Molecular Biology* **331**: 1025–1040.

Smolle, M., and Workman, J.L. (2013) Transcription-associated histone modifications and cryptic transcription. *Biochimica et Biophysica Acta (BBA)-Gene Regulatory Mechanisms* **1829**: 84–97.

Sokolova, V., Miratsky, J., Svetlov, V., Brenowitz, M., Vant, J., Lewis, T.S., *et al.* (2023) Structural mechanism of HP1α-dependent transcriptional repression and chromatin compaction. *Biorxiv* 2023–11.

Spitz, F., and Furlong, E.E. (2012) Transcription factors: from enhancer binding to developmental control. *Nature reviews genetics* **13**: 613–626.

Stark, R., Grzelak, M., and Hadfield, J. (2019) RNA sequencing: the teenage years. *Nature Reviews Genetics* **20**: 631–656.

Stoler, S., Keith, K.C., Curnick, K.E., and Fitzgerald-Hayes, M. (1995) A mutation in CSE4, an essential gene encoding a novel chromatin-associated protein in yeast, causes chromosome nondisjunction and cell cycle arrest at mitosis. *Genes & development* **9**: 573–586.

Suda, T., Arai, F., and Hirao, A. (2005) Hematopoietic stem cells and their niche. *Trends in immunology* **26**: 426–433.

Suh, H., Hazelbaker, D.Z., Soares, L.M., and Buratowski, S. (2013) The C-terminal domain of Rpb1 functions on other RNA polymerase II subunits. *Molecular cell* **51**: 850–858.

Suka, N., Luo, K., and Grunstein, M. (2002) Sir2p and Sas2p opposingly regulate acetylation of yeast histone H4 lysine16 and spreading of heterochromatin. *Nature genetics* **32**: 378–383.

Svenkrtova, A., Belicova, L., Volejnikova, A., Sigler, K., Jazwinski, S.M., and Pichova, A. (2016) Stratification of Yeast Cells during Chronological Aging by Size Points to the Role of Trehalose in Cell Vitality. *Biogerontology* **17**: 395–408.

Syed, S.H., Goutte-Gattat, D., Becker, N., Meyer, S., Shukla, M.S., Hayes, J.J., *et al.* (2010a) Single-base resolution mapping of H1–nucleosome interactions and 3D organization of the nucleosome. *Proceedings of the National Academy of Sciences* **107**: 9620–9625.

Syed, S.H., Goutte-Gattat, D., Becker, N., Meyer, S., Shukla, M.S., Hayes, J.J., *et al.* (2010b) Single-base resolution mapping of H1–nucleosome interactions and 3D organization of the nucleosome. *Proc Natl Acad Sci U S A* **107**: 9620–9625.

Szymanski, E.P., and Kerscher, O. (2013) Budding yeast protein extraction and purification for the study of function, interactions, and post-translational modifications. *JoVE (Journal of Visualized Experiments)* e50921.

Teytelman, L., Thurtle, D.M., Rine, J., and Oudenaarden, A. van (2013) Highly expressed loci are vulnerable to misleading ChIP localization of multiple unrelated proteins. *Proceedings of the National Academy of Sciences* **110**: 18602–18607.

Thomas, J.O., and Stott, K. (2012) H1 and HMGB1: modulators of chromatin structure. *Biochemical Society Transactions* **40**: 341–346.

Thomas, M.C., and Chiang, C.-M. (2006) The general transcription machinery and general cofactors. *Critical reviews in biochemistry and molecular biology* **41**: 105–178.

Ueda, T., Chou, H., Kawase, T., Shirakawa, H., and Yoshida, M. (2004) Acidic C-Tail of HMGB1 Is Required for Its Target Binding to Nucleosome Linker DNA and Transcription Stimulation. *Biochemistry* **43**: 9901–9908.

Ushinsky, S., Bussey, H., Ahmed, A., Wang, Y., Friesen, J., Williams, B., and Storms, R. (1997) Histone H1 in Saccharomyces cerevisiae. *Yeast* **13**: 151–161.

Uzunova, K., Georgieva, M., and Miloshev, G. (2013) Saccharomyces cerevisiae Linker Histone—Hho1p Maintains Chromatin Loop Organization during Ageing. *Oxidative Medicine and Cellular Longevity* **2013**: 437146.

Venkatesh, S., and Workman, J.L. (2015) Histone exchange, chromatin structure and the regulation of transcription. *Nature reviews Molecular cell biology* **16**: 178–189.

Vinayachandran, V., Reja, R., Rossi, M.J., Park, B., Rieber, L., Mittal, C., *et al.* (2018) Widespread and precise reprogramming of yeast protein–genome interactions in response to heat shock. *Genome research* **28**: 357–366.

Wach, A., Brachat, A., Alberti-Segui, C., Rebischung, C., and Philippsen, P. (1997) Heterologous HIS3 marker and GFP reporter modules for PCR-targeting in Saccharomyces cerevisiae. *Yeast* **13**: 1065–1075.

Wagner, C.A. (2024) The basics of phosphate metabolism. *Nephrology Dialysis Transplantation* **39**: 190–201.

Wang, L., Xi, Y., Sung, S., and Qiao, H. (2018) RNA-seq assistant: machine learning based methods to identify more transcriptional regulated genes. *BMC genomics* **19**: 1–13.

Wang, M., Li, J., Wang, Y., Fu, H., Qiu, H., Li, Y., *et al.* (2023) Single-molecule study reveals Hmo1p, not Hho1p, promotes chromatin assembly in budding yeast. *Mbio* **14**: e00993-23.

Wang, W., Xue, Y., Zhou, S., Kuo, A., Cairns, B.R., and Crabtree, G.R. (1996) Diversity and specialization of mammalian SWI/SNF complexes. *Genes & development* **10**: 2117–2130.

Watson, M., Stott, K., Fischl, H., Cato, L., and Thomas, J.O. (2014) Characterization of the interaction between HMGB1 and H3—a possible means of positioning HMGB1 in chromatin. *Nucleic Acids Research* **42**: 848–859.

Weinberger, M., Feng, L., Paul, A., Smith Jr, D.L., Hontz, R.D., Smith, J.S., *et al.* (2007) DNA replication stress is a determinant of chronological lifespan in budding yeast. *PloS one* **2**: e748.

Werner-Washburne, M., Braun, E., Johnston, G.C., and Singer, R.A. (1993) Stationary phase in the yeast Saccharomyces cerevisiae. *Microbiological reviews* **57**: 383–401.

Wickham, H. (2009) *ggplot2*. Springer New York, New York, NY.

Wleklik, K., and Borek, S. (2023) Vacuolar processing enzymes in plant programmed cell death and autophagy. *International Journal of Molecular Sciences* **24**: 1198.

Woodcock, C.L., Skoultchi, A.I., and Fan, Y. (2006) Role of linker histone in chromatin structure and function: H1 stoichiometry and nucleosome repeat length. *Chromosome Res* **14**: 17–25.

Wu, M., Zhang, C., Sun, X., Wang, G., Liu, Y., and Xiao, D. (2014) Effects of NTH1 Gene Deletion and Overexpressing TPS1 Gene on Freeze Tolerance in Baker's Yeast. Springer, pp. 447–454.

Xiao, L., Kamau, E., Donze, D., and Grove, A. (2011a) Expression of yeast high mobility group protein *HMO1* is regulated by TOR signaling. *Gene* **489**: 55–62.

Xiao, L., Kamau, E., Donze, D., and Grove, A. (2011b) Expression of yeast high mobility group protein *HMO1* is regulated by TOR signaling. *Gene* **489**: 55–62.

Xiao, L., Williams, A.M., and Grove, A. (2010) The C-Terminal Domain of Yeast High Mobility Group Protein *HMO1* Mediates Lateral Protein Accretion and In-Phase DNA Bending. *Biochemistry* **49**: 4051–4059.

Xiao, T., Kao, C.-F., Krogan, N.J., Sun, Z.-W., Greenblatt, J.F., Osley, M.A., and Strahl, B.D. (2005) Histone H2B ubiquitylation is associated with elongating RNA polymerase II. *Molecular and cellular biology* **25**: 637–651.

Xu, H., Wang, J., Liang, Y., Fu, Y., Li, S., Huang, J., *et al.* (2020) TriTag: an integrative tool to correlate chromatin dynamics and gene expression in living cells. *Nucleic acids research* **48**: e127–e127.

Young, C.P., Hillyer, C., Hokamp, K., Fitzpatrick, D.J., Konstantinov, N.K., Welty, J.S., *et al.* (2017) Distinct histone methylation and transcription profiles are established during the development of cellular quiescence in yeast. *BMC genomics* **18**: 1–18.

Zhang, H., Roberts, D.N., and Cairns, B.R. (2005) Genome-wide dynamics of Htz1, a histone H2A variant that poises repressed/basal promoters for activation through histone loss. *Cell* **123**: 219–231.

Zhang, Y., and Reinberg, D. (2001) Transcription regulation by histone methylation: interplay between different covalent modifications of the core histone tails. *Genes & development* **15**: 2343–2360.

Zhou, B.-R., Jiang, J., Feng, H., Ghirlando, R., Xiao, T.S., and Bai, Y. (2015) Structural Mechanisms of Nucleosome Recognition by Linker Histones. *Mol Cell* **59**: 628–638.